Semi-leptonic B decays and QED effects

A thesis submitted in partial fulfillment of

the requirements for the degree of

Doctor of Philosophy

by

Dayanand Mishra

(Roll No. 18330007)

Under the supervision of

Dr. Namit Mahajan

Professor

Theoretical Physics

Physical Research Laboratory, Ahmedabad, India.

DEPARTMENT OF PHYSICS

INDIAN INSTITUTE OF TECHNOLOGY GANDHINAGAR

2023

to

my family

DECLARATION

I declare that this written submission represents my ideas in my own words and where others' ideas or words have been included, I have adequately cited and referenced the original sources. I also declare that I have adhered to all principles of academic honesty and integrity and have not misrepresented or fabricated or falsified any idea/data/fact/source in my submission. I understand that any violation of the above will be cause for disciplinary action by the Institute and can also evoke penal action from the sources which have thus not been properly cited or from whom proper permission has not been taken when needed.

(Name: Dayanand Mishra)

(Roll No: 18330007)

Date: 28 June 2023

CERTIFICATE

It is certified that the work contained in the thesis titled **"Semi-leptonic B decays and QED effects"** by **Dayanand Mishra** (Roll no: 18330007), has been carried out under my supervision and that this work has not been submitted elsewhere for degree.

I have read this dissertation and in my opinion, it is fully adequate in scope and quality as a dissertation for the degree of Doctor of Philosophy.

Prof. Namit Mahajan
(Thesis Supervisor)
Professor
Theoretical Physics Division
Physical Research Laboratory
Navarangpura, Ahmedabad, India

Contents

Abstract **v**

List of Publications **vii**

List of Figures **ix**

List of Figures **ix**

List of Tables **xiii**

List of Tables **xiii**

1 Introduction **1**

1.1 The Standard Model 3

1.1.1 Strong sector 4

1.1.2 Electroweak Sector 7

1.1.2.1 Spontaneous Symmetry Breaking 8

1.1.2.2 Yukawa interaction 10

1.2 Flavor Physics 11

1.3 B decays 13

1.4 Effective Field Theories (EFTs) 17

1.5 Era of Precision 18

1.6 Organisation of thesis 20

2 Tools and techniques: Infrared divergences and EFTs **21**

2.1 Infrared Divergences 21

2.1.1 Understanding IR 22

2.1.2 Physical implications: first perspective 25
2.1.3 Example: $e^+e^- \to hadrons$ at high energy 28
2.1.4 Physical implications: second perspective 36
2.1.5 IR problems beyond point-like 39
2.2 Effective Field Theories (EFTs) 40
2.2.1 An example 41
2.2.2 EFT I: Fermi theory for weak decays of mesons 44
2.2.3 EFT II: Heavy Quark Effective Theory 50
2.2.3.1 Quantum Mechanics of heavy particles 50
2.2.3.2 QFT of heavy particles 53

3 Soft photon effects in $B \to K\ell\ell$ 59
3.1 Introduction 59
3.2 Non-radiative $B \to K\ell^+\ell^-$ 62
3.3 QED Corrections to $B \to K\ell\ell$ 64
3.3.1 Contact Term 66
3.3.2 Real Photon Emission 68
3.3.3 Virtual Photon Corrections 70
3.3.4 Sommerfeld factor 74
3.3.5 Total $\mathcal{O}(\alpha_{em})$ QED corrections 74
3.4 Results 76
3.5 Discussion and Conclusions 78

4 A Novel observable: $\frac{|V_{ub}|}{|V_{cb}|}$ 81
4.1 Introduction 81
4.2 Non-radiative $B \to P\ell\nu_\ell$ $(P = D, \pi)$ 84
4.2.1 Form factors for $B \to P(= D, \pi)\ell\nu_\ell$ 86
4.3 Soft photon QED corrections to $B \to P\ell\nu_\ell$ 88
4.3.1 Real photon emissions 88
4.3.1.1 Photon inclusive case 90
4.3.1.2 Photon exclusive case 92
4.3.2 Virtual Photon Corrections 93
4.3.3 Total $\mathcal{O}(\alpha_{em})$ QED corrections 95

4.4 Results 98
4.4.1 Phenomenological application of R_V 102
4.5 Discussion and Conclusions 105

5 Radiative Inclusive B decays 109
5.1 Introduction 109
5.2 Non-perturbative parameters: λ_1 and λ_2 111
5.3 An example: $B \to X_u \ell \nu_\ell$ 113
5.4 Differential rate of $B \to X_u \ell \nu_\ell \gamma$ 116
5.5 Results 140
5.5.1 Determination of non-perturbative parameters 143
5.6 Discussion and Conclusion 144

6 Summary and Future Work 147
6.1 Summary 147
6.2 Future Work 150

A Essential definitions and Identities 153
A.1 Essential definitions 153
A.2 Essential Identities 154

B Useful Integrals 157
B.1 Real photon emission 157
B.2 Virtual Corrections 159

C Kinematics of decay rate 161
C.1 Three body kinematics 161
C.1.1 Exclusive decay modes 161
C.1.2 Inclusive decay modes 162
C.2 Four body kinematics 163
C.2.1 Exclusive decay modes: 163
C.2.2 Inclusive decay modes: 164

Acknowledgements

I would like to express my heartfelt gratitude and appreciation to the following individuals and institutions who have played a significant role in the completion of this Ph.D. thesis:

First and foremost, I would like to extend my deepest gratitude to my supervisor, Prof. Namit Mahajan. His guidance, expertise, and unwavering support throughout this journey have been invaluable. His profound knowledge and dedication to research have shaped me into the researcher I am today. I am truly grateful for your mentorship.

I am also immensely grateful to Prof. Srubabati Goswami, Dr. Ketan Patel, and Prof. Ramitendranath Bhattacharya for their valuable contributions as members of my Doctoral Supervisory Committee (DSC). Their insights, suggestions, and constructive criticisms have greatly enhanced the quality of this thesis. Their expertise and scholarly guidance have been instrumental in shaping my research.

I would like to extend my sincere thanks to the esteemed faculty members of the Theoretical Physics division Prof. Shubendra Mohanty, Prof. Hiranmaya Mishra, Prof. Jitesh Bhatt, Prof. Dilip Angom, Prof. Partha Konar, Prof. Srubabati Goswami, Prof. Navindar Singh, Prof. Ketan Patel, Prof. Satyajit Seth, and Prof. Paramita Datta. Their expertise, guidance, and teachings during the coursework have laid a strong foundation of knowledge and understanding in theoretical physics. Their lectures, discussions, and insightful explanations have broadened my horizons and shaped my perspective in the field.

I would like to express my sincere appreciation to Dr. Anshika Bansal, who has been more than a senior, but also a supportive sister, friend, and collaborator. Her encouragement, intellectual discussions, and constant belief in my abilities have been a constant source of inspiration.

I extend my heartfelt thanks to Dr. Shireen Gangal for engaging in physics discussions, which have greatly enriched my understanding of the subject matter.

I am grateful to Anju Rani, Deepak Gaur, Namita Uppal, Naval Kishor, Sunil Kumar, Vikas Soni, Yash Srivastava, and Yogesh for their friendship and positive support throughout my Ph.D. journey. Their companionship, encouragement, and understanding have made this experience more enjoyable and fulfilling.

I would like to extend my appreciation to Pranav Bharadwaj for the *countless stimulating physics and philosophical discussions that have broadened my perspectives and challenged my intellect.*

To Dr. Sana Ahmed, Meghna Soni, Supriya Pan, Anupam Ghosh, Deepak Kumar Rai, Tanya Sharma, and Monika Devi, I express my gratitude for being wonderful friends who have provided unwavering support and shared many memorable moments.

I would like to acknowledge Madhusudhan P and Vinitha Nimma, and all my batchmates of PRL for the pleasant meals we shared, which provided a much-needed break and a chance to unwind during the course of this research.

My sincere thanks go to the entire Theoretical Physics group of PRL, the Director of PRL, and the Dean of PRL for creating a conducive research environment. I express my appreciation to the PRL Library, Academic Services, and Administration Services for their valuable resources and assistance throughout my research.

I am grateful to the IITGn academics for their support, which has enriched my academic experience.

To my beloved wife, Priya Mishra, I owe an immeasurable debt of gratitude. Her unwavering support, understanding, and patience during the ups and downs of this journey have been my anchor. Her love and encouragement have given me the strength to persevere.

I would also like to thank my daughter, Yalinee Mishra, and my entire family, including my parents, sisters, grandparents, and in-laws, for their unconditional love, support, and understanding throughout my academic pursuits. Their belief in me has been a constant source of motivation.

I would like to express my heartfelt thanks to the anonymous reviewer(s) of my thesis. Your critical evaluation, insightful feedback, and constructive suggestions have been instrumental in improving the quality of this work. Your expertise and careful scrutiny have contributed significantly to the refinement of my research. I am truly grateful for your time, dedication, and valuable contributions as a reviewer.

Last but certainly not least, I would like to extend my sincere thanks to all those individuals whom I may have inadvertently omitted from this acknowledgment. Your contributions, support, and positive impact on my journey have been truly invaluable. Please know that your involvement and assistance have played a significant role in shaping the successful completion of this Ph.D. thesis.

Thank you all for your invaluable contributions and for being part of this significant milestone in my academic career.

(Dayanand Mishra)

Abstract

The study of semi-leptonic B meson decays plays a crucial role in testing the Standard Model (SM) of particle physics and exploring potential New Physics (NP) effects. B meson consists of a heavy quark, b, and a light anti-quark, $\bar{q}$ $(q = u, d, s)$. The heaviness of the b quark allows us to consider the inverse of its mass, $1/m_b$, as a perturbative expansion parameter. The framework that incorporates these $1/m_b$ corrections treating the b quark as a heavy quark is known as the Heavy Quark Effective Theory (HQET). Theoretical calculations of B meson decay rates involve the effective weak Hamiltonian, combining short-distance physics encoded in the Wilson coefficients with long-distance physics captured in the matrix elements of operators. These matrix elements of operators are parametrized in terms of non-perturbative parameters like form factors, which introduces theoretical uncertainties. Various observables have been constructed such as Lepton Flavor Universality (LFU) ratios ($R_{K^{(*)}}$, $R_{D^{(*)}}$) and angular variables like P_i', aiming to minimize theoretical uncertainties and provide cleaner tests of the SM. While these observables exhibit deviations from SM predictions, it is premature to attribute them to NP effects. Hence, it is crucial to investigate possible overlooked theoretical contributions, like QED effects.

The thesis, devoted to a better understanding of the QED effects in semi-leptonic B decays, is divided into three major parts. Firstly, the effects of soft photon corrections on $B \to K\ell\ell$ are studied. The decay rate and the ratio R_K are found to depend on the maximum energy of the soft photon, $k_{\max}$. Extending such analysis to charged current modes, lead us to construct an observable, $R_V = \frac{|V_{ub}|}{|V_{cb}|}$, that is theoretically clean and independent of $k_{\max}$, which is the second part of the thesis. Equality of R_V calculated using inclusive and exclusive measurements of CKM matrix elements establishes a correlation between the coefficients of two distinct sectors: $b \to u$ and $b \to c$. In the third part, the possibility of computing the non-perturbative parameters, λ_1 and λ_2, is explored focusing on the inclusive decays of the B meson. The decay width of $B \to X_u \ell \nu_\ell \gamma$ is calculated in the framework of HQET employing the Cutkosky cut method. The total decay rate for radiative mode is cast into a linear com-

bination of non-perturbative parameters λ_1 and λ_2 similar to the non-radiative one, which allows for the simultaneous determination of these parameters in a definitive manner. This approach offers a complementary avenue for computing the non-perturbative parameters in inclusive decays.

This then firmly establishes the importance of QED effects which are often neglected or overlooked, and motivates inclusion of such effects in other modes as well.

Keywords: B decays, QED effects, HQET,

List of Publications

Publications included in thesis

1. **Dayanand Mishra** and Namit Mahajan, "Impact of soft photons on $B \to K\ell^+\ell^-$", Phys. Rev. D 103 (2021) 5, 056022 [arXiv:2010.10853]

2. Anshika Bansal, Namit Mahajan, and **Dayanand Mishra** "$\frac{|V_{ub}|}{|V_{cb}|}$ and quest for new physics", JHEP 02 (2022) 130 [arXiv:2112.00363]

3. Namit Mahajan, and **Dayanand Mishra**, "$B \to X_u\ell\nu_\ell\gamma$ and determination of non-perturbative parameters", [arXiv: 2303.17372] [under review in JHEP]

Other publications (not included in the thesis):

1. Anshika Bansal, Namit Mahajan and **Dayanand Mishra**, "More on Denominator Regularization in Quantum Field Theory", [arXiv:2211.12284] [under review in PRD]

Conference proceedings

1. **Dayanand Mishra** and Namit Mahajan, "Impact of Soft photons on $B \to K\ell\ell$", $PoS, LHCP2021, 205$.

List of Figures

1.1 The matter content of the Standard Model [https://en.wikipedia.org/wiki/Elementary_particle]. 4
1.2 $qq \to qq$ scattering: lowest order (left), quark loop (middle), and gluon loop (right). 6
1.3 Qualitative behaviour of effective coupling strengths for QED (α_{em}) and QCD (α_s). 7
1.4 The unitarity triangle (db). 13

2.1 Representative diagram for a single photon emission 25
2.2 Virtual correction due to a single photon 27
2.3 Real emissions 29
2.4 Virtual corrections: (a) Vertex correction, (b) self-energy corrections to one fermion, and (c) self-energy corrections to another fermion 29
2.5 Real emission of n soft photons in any possible order 34
2.6 Virtual corrections due to n soft photons 34
2.7 Feynman diagrams for $q_1 \to q_2q_3q_4$ with QCD corrections in full theory. 45
2.8 Feynman diagrams for effective theory of the process $q_1 \to q_2q_3q_4$. 46
2.9 Feynman diagrams for penguin operators. 48

3.1 Feynaman diagrams of $B \to K\ell^+\ell^-$ for two different topologies: (a) penguin (b) box. 60
3.2 Representative diagram for real photon emission 65
3.3 Representative diagrams contributing to virtual corrections 65

3.4 Two photon Contact Term. (Left) real emission (Right) Virtual correction 72
3.5 $\mathcal{O}(\alpha_e m)$ corrections to neutral and charged $B \to K\ell\ell$ modes. Left: electrons, Right: muons 77
3.6 Behaviour of $\ln(m_l)$ terms 78
3.7 Shift in $R_K^{\mu e}$ due to $\mathcal{O}(\alpha_{em})$ QED effects 78

4.1 Feynman diagram for $B \to D(\pi)\ell\nu_\ell$. 85
4.2 (a) Diagram illustrating real photon emission from one of the external charged particles (denoted by $\times$). (b) Diagram representing the Contact Term (CT) contribution. 88
4.3 (a) Dalitz plot displaying the phase space boundaries for the energies of the muon (magenta) and the D^0 meson (blue) in the decay $B^- \to D^0\mu^-\nu_\mu$. (b) Dalitz plot illustrating the phase space boundaries for the energies of the muon (magenta) and the π^0 meson (blue) in the decay $B^- \to \pi^0\mu^-\nu_\mu$. 90
4.4 (a) self-energy correction to the lepton (a similar diagram for the self-energy correction to the B meson), (b) vertex correction, and (c) virtual correction due to the contact term (a similar diagram where the photon originates from the contact term and interacts with the B meson). 93
4.5 Radiative corrections to the CKM elements $|V_{cb}|$ and $|V_{ub}|$, represented by the dashed line ($\delta^{\text{QED}}V_{cb}$) and solid line ($\delta^{\text{QED}}V_{ub}$) respectively. These corrections are plotted for different thresholds on the photon energy, k_{max}, in the context of the decays (a) $B^0 \to P^+$ (where P^+ can be D^+ or π^+) and (b) $B^- \to P^0$ (where P^0 can be D^0 or π^0) involving a muon (μ^-) and a neutrino (ν_μ). 99
4.6 Radiative corrections to the CKM elements $|V_{cb}|$ and $|V_{ub}|$ (i.e., $\delta^{\text{QED}}Vcb$ (dashed) and $\delta^{\text{QED}}Vub$ (solid)) for $k_{\text{max}} = 100$ MeV in the decay process $B^0 \to P^+(= D^+, \pi^+)\mu^-\nu_\mu$, considering the inclusion of the extra Coulomb factor from the final-state charged particles (red) and not considering it (magenta). 100

4.7 Radiative corrections to V_{ub}/V_{cb} (i.e. ΔR_V) as a function of lepton energy for the different tsoft photon maximum energy, k_{max} for (a) $B^0 \to P^+(= D^+, \pi^+)\mu^-\nu_\mu$ and (b) $B^- \to P^0(= D^0, \pi^0)\mu^-\nu_\mu$. 101

4.8 Effects of radiative corrections on the ratio R_P (with $P = D$ represented by the dashed line and $P = \pi$ represented by the solid line) are shown for various thresholds on the photon energy, k_{max}, in the decays (a) $B^0 \to P^+(= D^+, \pi^+)\ell^-\nu_\ell$ and (b) $B^- \to P^0(= D^0, \pi^0)\ell^-\nu_\ell$. 102

5.1 Representative Diagram of forward scattering for $b \to u\ell\nu_\ell$ 113

5.2 Feynman diagrams for $B \to X_u\ell\nu_\ell\gamma$. 117

5.3 Representative diagram with explicit cut 119

5.4 (a) Differential decay width of $B \to X_u\mu\nu_\mu\gamma$ as a function of normalized lepton energy, y, for various values of normalized photon energy, x. (b) Differential decay width of $B \to X_u\mu\nu_\mu\gamma$ as a function of normalized lepton energy (y) for a specific normalized photon energy ($x_{\min} = 0.3$). 141

5.5 Forward-backward asymmetry (A_{FB}) as a function of lepton energy, y. 142

5.6 Differential decay rate of the $B \to X_u\mu\nu_\mu\gamma$ decay mode as a function of the photon energy (x). 142

List of Tables

1.1 Transformation properties of the particle content of the SM 5

4.1 Comparison of the QED shifts (%) in the decay rate (for both tau and muon modes) at $k_{\mathrm{max}} = 100$ MeV with Ref. [23], considering the inclusion (exclusion) of the extra Coulomb factor arising from the final-state charged particles (as considered in Ref. [23]). . . . 100

4.2 The ratio, R_V obtained with the different choice of $f^{(A)}_{B\to\pi}$ and $f^{(A)}_{B\to D}$ for the corresponding form factors. 101

4.3 V_{qb}^{NP} for various exclusive and inclusive B decay modes 104

4.4 Ratio of R_V in the NP to R_V in the SM for inclusive $B \to X_u/X_c$ modes and four different combination of exclusive $B \to \pi/D/\rho/D^*$ modes 104

Chapter 1

Introduction

The fundamental goal of high-energy particle physics is to answer the question: What are we made of at the very fundamental level? To address this question, lots of experiments have been performed, and are being done currently and several high-precision experiments are planned. The basic idea we have now is that all the experiments of particle physics we have done can be explained by looking at groups of particles interacting with each other through different forces. The theory which ties all of this is known as the Standard Model (SM) of particle physics (to be discussed in detail in Section-1.1). The SM describes the properties of all the elementary particles and three fundamental forces of nature namely the strong, weak, and electromagnetic forces [1–3] (see also [4–6]). It does not include the gravitational force. Though the SM has achieved great success in explaining various experimentally observed phenomena, it is unable to explain some of the phenomena of nature like dark matter and dark energy [7, 8], matter antimatter asymmetry [9, 10], unification of forces [11, 12], neutrino masses [13, 14], stabilization of the electroweak scale [15–17], etc. Hence, it is clear that the SM is not the end of the story.

It further leads to the question: How to look for new particles and interactions which lie Beyond the Standard Model (BSM)? In principle, there are two ways to detect BSM signatures, namely Direct Detection and Indirect Detection.

Direct Detection: In collider experiments such as the Large Hadron

Collider (LHC), new particles may be produced and detected. However, the limiting factor is the center of mass (c.o.m.) energy. If the particle's mass is higher than the c.o.m. energy, it can not be produced as a real particle. However, it can exist as a virtual particle. The direct detection of Higgs is one such example [18, 19].

Indirect Detection: In this scenario, the new particles appear as quantum fluctuations at low energy due to microphysics at high energies. This requires high accuracy from both theories as well as experiments. Experiments such as LHCb follow this way to find new particles. The prediction of the top quark at the B factory DORIS with ARGUS experiment is one such example [20]. Theoretically, the rare decays of leptons and hadrons, as well as the related observables such as asymmetries provide access to look for these indirect searches with the help of Effective Field Theories (EFTs) [21] (discussed in Section-1.4). Hence, precise theoretical predictions of physical observables are required for the comparison between experimental measurements and the SM predictions.

In the pursuit of precise theoretical predictions, it is crucial to address the theoretical uncertainties that arise from non-perturbative quantities in the SM. Observables such as decay rates and physical parameters of the SM contain these uncertainties, stemming from quantities like form factors and decay constants that are difficult to compute precisely. To mitigate the impact of non-perturbative uncertainties, alternative observables are constructed by combining different measurable quantities. These include ratios of decay rates, such as Lepton Flavor Universality (LFU) ratios ($R_K^{(*)}, R_D^{(*)}$) as discussed in Chapter-3. These ratios exhibit reduced sensitivity to form factors.

However, it is important to note that while LFU ratios and similar observables are less affected by hadronic uncertainties, they may still be subject to the effects of QED, particularly those arising from soft photon emissions [22–27]. Soft photon effects can have a significant impact on precision calculations, as they encompass enhancements from both low-energy and collinear photons emitted by high-energy relativistic particles (Further details are provided in Chapter-2). In particular, the collinear logs can produce corrections up to $\mathcal{O}(10\%)$ [25].

This thesis delves into the significance of the soft photon corrections to the exclusive semi-leptonic processes through an analysis of IR properties of the soft photon, and the radiative inclusive mode (where the photon is hard) via the implementation of Effective Field Theory techniques (as outlined in Section-2). To begin our exploration, we review the Standard Model of particle physics and the theory of weak interactions in B physics, addressing the existing challenges and proposing potential solutions.

1.1 The Standard Model

The Standard Model (SM) is a renormalizable Quantum Field Theory (QFT) that describes elementary fields and their interactions through local gauge groups, $SU(3)_C \times SU(2)_L \times U(1)_Y$. The $SU(3)_C$ gauge group describes the strong interactions, while the $SU(2)_L \times U(1)_Y$ gauge group describes the ElectroWeak (EW) part of the SM.

The particle content of the SM consists of fermions with half-integer spin and bosons with integer spin. Fermions are divided into quarks and leptons. Quarks, carrying color charge, are organized into doublets of up-type (up (u), charm (c), top (t)) and down-type (down (d), strange (s), bottom (b)) quarks referred as generations. This organization is based on their increasing order of masses. Quarks have electric charge, with up-type quarks having $Q = 2/3$ and down-type quarks having $Q = -1/3$. Leptons include charged leptons (electron (e), muon (μ), tau (τ) with $Q = -1$ and neutrinos (electron-neutrino (ν_e), muon-neutrino (ν_μ), tau-neutrino (ν_τ)) that are electrically neutral. Neutrino masses, although confirmed by experiments, are not present in the SM. For more information refer to[14, 28]. Figure (1.1) which displays the SM particles with their mass, charge, and spin.

In the SM, $SU(2)_L \times U(1)_Y$ gauge group exhibits the chiral nature which plays an important role in describing the fundamental phenomena of Strong and EW interactions, Spontaneous Symmetry Breaking (SSB), and Flavor Physics (see [5, 29, 30] for more details). This chiral symmetry arises from the different ways in which fields transform under the fundamental representations of $SU(2)_L$. Only fermions exhibit chirality, and they are classified as either left-handed or

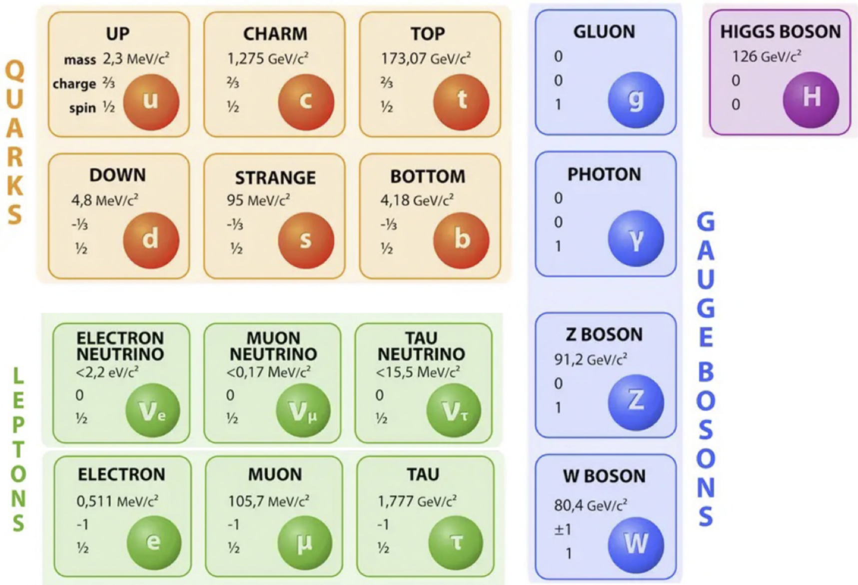

Figure 1.1: The matter content of the Standard Model [https://en.wikipedia.org/wiki/Elementary_particle].

right-handed fields based on their transformations under $SU(2)_L$. The process of localizing a global symmetry and gauging it is a standard procedure in QFT[4, 31, 32]. It is used to introduce gauge fields and couplings in the Standard Model, as well as interpret the interaction terms in the Lagrangian. Table-(1.1) provides a detailed description of how the SM matter contents transform under each group. Now, let us delve into the various sectors of the SM.

1.1.1 Strong sector

We will start by constructing the QCD Lagrangian, which is a result of localising the global $SU(3)_C$ symmetry in the quark sector of the SM. The QCD Lagrangian density is given by

$$\mathcal{L}_{QCD} = -\frac{1}{4} G^a_{\mu\nu} G^{\mu\nu\ a} + \sum_f \bar{\psi}_f (i\not{D} - m_f)\psi_f, \tag{1.1}$$

where

$$\begin{aligned} G^a_{\mu\nu} &= \partial_\mu G^a_\nu - \partial_\nu G^a_\mu + g_s f^{abc} G^b_\mu G^c_\nu, \text{ and} && (1.2) \\ D_\mu &= \partial_\mu + i g_s \frac{\lambda_a}{2} G^a_\mu && (1.3) \end{aligned}$$

The SM particles	$(SU(3)_C, SU(2)_L, U(1)_Y)$
Fermions	
e_R	$(\mathbf{1}, \mathbf{1}, -1)$
L_L	$(\mathbf{1}, \mathbf{2}, -1/2)$
u_R	$(\mathbf{3}, \mathbf{1}, 2/3)$
d_R	$(\mathbf{3}, \mathbf{1}, -1/3)$
Q_L	$(\mathbf{3}, \mathbf{2}, 1/6)$
Gauge bosons	
G^a_μ	$(\mathbf{8}, \mathbf{1}, 0)$
W^i_μ	$(\mathbf{1}, \mathbf{3}, 0)$
B_μ	$(\mathbf{1}, \mathbf{1}, 0)$
Higgs	
ϕ	$(\mathbf{1}, \mathbf{2}, 1/2)$

Table 1.1: Transformation properties of the particle content of the SM

are the gluon field strength tensor and covariant derivative, respectively. The index a denotes the eight gluon fields, m_f is the mass parameters, and f represents the quark flavors. Moreover, g_s and λ_a are gauge coupling and Gell-Mann matrices (explicit structures are provided in Appendix-A), respectively. The non-Abelian nature of $SU(3)_C$ results in self-interactions between gluons, which leads to both triple and quartic gluon terms that are absent in Abelian theories like QED. Hence, the QED Lagrangian is analogous to the QCD Lagrangian, except for the color indices and self-interactions among the photon fields. $f^{abc} = 0$ in QED.

Let us understand the behavior of coupling strength for QCD at high energy. For illustration, consider the $qq \to qq$ scattering in the increasing order of $\alpha_s = g_s^2/4\pi$ (analogous to $\alpha_{em} = e^2/4\pi$, the coupling strength in QED). The Feynman diagrams to the leading and first sub-leading order in α_s are shown in Fig.(1.2). Other diagrams have been left since we are after the understanding of the variation of coupling strength with scale; detailed calculations of these diagrams and others can be seen in any textbook of QCD, such as [33]. The loop

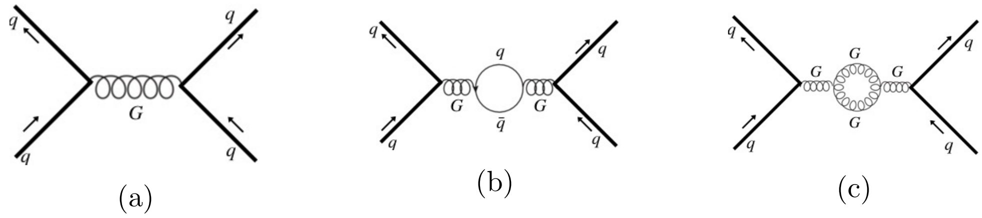

Figure 1.2: $qq \to qq$ scattering: lowest order (left), quark loop (middle), and gluon loop (right).

diagrams, due to integration up to infinite loop momenta, cause ultraviolet (UV) divergences. However, QCD, like QED, is a renormalizable QFT. Therefore, all UV divergences of the loop diagrams can be effectively removed by a redefinition of the quark fields ($\psi_f(x)$) and gluon fields ($G^a_\mu(x)$) in the Lagrangian, simultaneously redefining the coupling g_s and quark masses m_f. The residual finite contributions introduce an additional dependence on scale μ (defined as renormalization scale), with respect to lowest order α_s. The final outcome, adding loops to lowest order diagram, is given by

$$\alpha_s(\mu) = \frac{\alpha_s(\mu_0)}{1 + \frac{\alpha_s(\mu_0)}{2\pi}\beta_0 \ln \frac{\mu}{\mu_0}} \tag{1.4}$$

The coefficient β_0 is given by

$$\beta_0 = 11 - \frac{2}{3}n_f \tag{1.5}$$

where n_f represents the number of quark flavors considered in quark loops having the masses smaller than the scales μ, & μ_0 involved in Eq.(1.4). It is noted that the gluon loop dominates. Further, since n_f is at max 6, β_0 is positive in the SM, and therefore $\alpha_s(\mu)$ in Eq.(1.4) logarithmically decreases with growing energy scale. It has dramatic consequences for the high-energy behaviors of perturbative QCD (pQCD) which leads to the phenomena of asymptotic freedom.

Unlike QCD, QED predicts negative β_0, which leads to the phenomena of asymptotic sickness. Fig.(1.3) shows the qualitative picture of the running of QCD and QED coupling strengths with energy. Further, at low energy around $\mu = \Lambda_{QCD}$, denominator vanishes and, consequently $\alpha_s(\mu) \to \infty$. It is found that pQCD breaks down at small energies. For example $\alpha_s(M_Z^2) \sim 0.12$ whereas

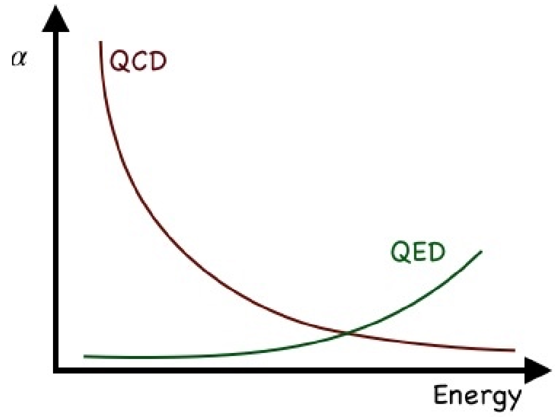

Figure 1.3: Qualitative behaviour of effective coupling strengths for QED (α_{em}) and QCD (α_s).

$\alpha_s(1\,GeV^2) \sim 0.5(\pm 0.1)$ and further below $\alpha_s(0.5\,GeV^2) \sim 0.6$ to 1.2. Hence, the quarks and gluons make transition to the nonperturbative region at $\mu = \Lambda_{QCD}$ due to confinement and form color-neutral bound states called hadrons. Note that the experiments of particle physics (detectors) only see hadrons together with leptons and photons. Hence the above qualitative picture can be formalized by writing the S matrix for a decay rate. The probability amplitude for a decay $i \to f$ is

$$\mathcal{M}(i \to f) \sim \langle f|\hat{S}|i\rangle \tag{1.6}$$

The final states i and f are hadrons. The operator $\hat{S}$ contains the interactions vertices from the QCD lagrangian. This probability amplitude is an example of a hadronic matrix element. This amplitude is then parametrized into combination of non perturbative objects such as form factors. Currently, the only first principle method available to calculate these non-perturbative objects is lattice QCD[34, 35]. The other available methods are chiral perturbation theory[36, 37], Light cone sum rules[38, 39], etc. Further details on form factors are provided in Section-1.3.

1.1.2 Electroweak Sector

Next we consider the electroweak (EW) sector (described by $SU(2)_L \times U(1)_Y$ gauge group) of the SM. This sector includes all fermions (leptons and quarks) in the SM, and they transform non-trivially under $SU(2)_L \times U(1)_Y$. The fermions can be grouped as isospin-doublets (left-handed), ψ_L, which include all fermions in the SM, and singlets (right handed), ψ_R, which include all the fermions except neutrinos in the SM. The Lagrangian density of the EW sector is

$$\begin{aligned}\mathcal{L}_{EW} &= -\frac{1}{4}W^a_{\mu\nu}W^{\mu\nu\ a} - \frac{1}{4}B_{\mu\nu}B^{\mu\nu} + \sum_i \Big(\bar{Q}^i_L i\not{D} Q^i_L + \bar{L}^i_L i\not{D} L^i_L + \bar{u}^i_R i\not{D} u^i_R \\ &\quad + \bar{d}^i_R i\not{D} d^i_R + \bar{e}^i_R i\not{D} e^i_R\Big) \qquad (1.7)\end{aligned}$$

where,

$$W^a_{\mu\nu} = \partial_\mu W^a_\nu - \partial_\nu W^a_\mu - g\epsilon^{abc}W^b_\mu W^c_\nu, \qquad (1.8)$$

$$B_{\mu\nu} = \partial_\mu B_\nu - \partial_\nu B_\mu, \qquad (1.9)$$

$$D_\mu \psi_L = (\partial_\mu + ig\frac{\sigma_a}{2}W^a_\mu + ig'YB_\mu)\psi_L, \qquad (1.10)$$

$$D_\mu \psi_R = (\partial_\mu + ig'YB_\mu)\psi_R \qquad (1.11)$$

where the index a represents three gauge fields, σ^a: Pauli matrices. The fermionic part of above Lagrangian is invariant under $[U(3)]^5$ symmetry, and contains terms describing the interactions between the gauge fields and the fermions. Unlike QCD, there are no fermionic mass terms in the EW sector. Including such terms would break gauge invariance and thus the SM fermions are massless unless there is another mechanism at play to finally provide masses to the fermions.

1.1.2.1 Spontaneous Symmetry Breaking

Spontaneous Symmetry Breaking (SSB) is a key concept in the SM that addresses the absence of massless matter fields observed in nature. The $SU(2)_L \times U(1)_Y$ symmetry of the SM is spontaneously broken into $U(1)_Q$ through the introduction of a Higgs doublet, represented by the field $\phi(x) = (\phi^+, \phi^0)^T$. This SSB mechanism gives mass to the $W^\pm$ and Z bosons. The Higgs doublet plays a crucial role by transforming non-trivially under $SU(2)_L \times U(1)_Y$ with weak hypercharge $Y = 1/2$. The neutral component of the Higgs field develops a Vecuum

Expectation Value (VEV), v such that

$$\langle 0|\phi|0\rangle = v/\sqrt{2},\ v^2 = \frac{\mu^2}{\lambda} \tag{1.12}$$

which minimizes the Higgs potential of the SM, which is given by

$$V(|\phi|^2) \;=\; \mu^2\phi^2 + \lambda\phi^4. \tag{1.13}$$

It is characterized by two parameters, $\mu^2 < 0$ and $\lambda > 0$. Further, the breakdown $SU(2)_L \times U(1)_Y \rightarrow U(1)_Q$ results into the charge operator: $Q = T_3 + Y$, which leaves the Higgs VEV invariant, and thus $U(1)_Q$ remains unbroken.

Now, let us consider scalar part of EW Lagrangian

$$\mathcal{L}_{EW} \;=\; (D_\mu\phi)^\dagger(D^\mu\phi) - V(|\phi|^2) \tag{1.14}$$

$$\text{where, } D_\mu\phi \;=\; (\partial_\mu + ig\frac{\sigma_a}{2}W_\mu^a + ig'YB_\mu)\phi \tag{1.15}$$

The relations between different couplings can be calculated as

$$\tan\theta_w = \frac{g'}{g},\ e = g\sin\theta_w = g'\cos\theta_w. \tag{1.16}$$

where the parameter θ_w is the Weinberg angle. Further, gauge invariant mass terms for the gauge bosons arise from mixed terms in covariant derivative where one picks up a VEV from ϕ. It is given by

$$\left[D_\mu\begin{pmatrix}0\\ \\ v\end{pmatrix}\right]^\dagger D_\mu\begin{pmatrix}0\\ \\ v\end{pmatrix} \sim m_W^2W_\mu^+W_\mu^- + \frac{1}{2}m_Z^2Z_\mu Z^\mu \tag{1.17}$$

it implies $m_W = \frac{gv}{2}$, $m_Z = \frac{gv}{2\cos\theta}$, and $m_\gamma = 0$. The mass of W boson then can be equated to Fermi constant obtained from muon decay experiment to calculate numerical value of VEV v, $v = 246\ GeV$. Hence SSB implies relations between $m_W,\ m_Z,\ e,\ g,\ g'$ which can be tested experimentally. Let us now consider the formalism for fermion mass generation.

1.1.2.2 Yukawa interaction

In the SM, fermions acquire masses through the Yukawa interaction, which involves the coupling of fermions to the Higgs field. The Lagrangian for the Yukawa interaction is given by:

$$\mathcal{L}_Y = -\bar{Q}_L \phi^* Y^u u_R - \bar{Q}_L \phi Y^d d_R - \bar{L}_L \phi Y^e e_R + h.c. \tag{1.18}$$

It contains 3×3 Yukawa matrices, $Y^{u,d,e}$, whose elements determine the strength of the coupling between the Higgs field and the respective fermions. Further, the Yukawa term breaks the $[U(3)]^5$ symmetry of the $\mathcal{L}_{EW}$ to $[U(1)]^4$, resulting into the conservation of accidental symmetries of the SM (which are the Baryon number and three individual lepton numbers). These Yukawa matrices are diagonalized by bi-unitary transformations, which leave one of the matrices non-diagonal. To diagonalize this term, an additional rotation of either of the quarks is performed, resulting in the mass eigenstate basis. This mismatch between the flavor and the mass eigenstates gives rise to the Cabibbo-Kobayashi-Maskawa (CKM) matrix V_{CKM} [40, 41], describing quark flavor mixing[1]. In Wolfenstein parametrization [44], up to order $\mathcal{O}(\lambda^3)$, it is given by

$$V_{CKM} = \begin{pmatrix} 1 & \lambda & A\lambda^3(\rho + i\eta) \\ -\lambda & 1 - \lambda^2/2 & A\lambda^2 \\ A\lambda^3(1 - \rho - i\eta) & -A\lambda^2 & 1 - \lambda^2/2 \end{pmatrix} \tag{1.19}$$

There are other parametrizations as well, such as PDG and others [45]. The basis where all Yukawa couplings are simultaneously diagonal is called mass eigenstate basis.

$$m_q = \frac{v y_q}{\sqrt{2}}, \; m_\ell = \frac{v y_\ell}{\sqrt{2}} \tag{1.20}$$

[1] In the SM, right-handed neutrinos are absent. Hence there is no mixing in the lepton sector. If one considers the right-handed neutrinos as well, it will give rise to a similar flavor rotation matrix known as Pontecorvo–Maki–Nakagawa–Sakata (PMNS) matrix [42, 43] for the leptonic sector.

We now understand the mechanism by which fermions get masses in the SM, which also gives rise to the CKM matrix. The CKM matrix plays a crucial role in processes involving flavor changes, such as weak decays. It represents the basis of flavor physics. So let us understand the flavor structure of the SM.

1.2 Flavor Physics

We focus only on the quark sector of the flavor physics. Understanding the dynamics of quarks and gluons at large distances is essential for accurately predicting weak decays. These decays provide valuable indirect information about the interactions of quarks at a fundamental level. A challenging aspect of studying weak decays is calculating the hadronic matrix elements. When investigating weak decays, a fundamental question arises: "Is there any evidence indicating that the Standard Model is incomplete and requires the addition of new components to explain the experimental data?" This question carries both curiosity and hope. Unfortunately, to date, the answer remains negative. In this scenario, the primary objective is to precisely determine the fundamental parameters involved in these processes.

While the Standard Model encompasses 18 physical parameters[2], the quark flavor structure of the SM contains ten physical parameters (six quark masses, three mixing angles, and one phase). The aim of experimental flavor physics is to measure these parameters through various methods, ensuring consistency and the potential for detecting the signature of new physics. It is worth noting that the presence of a non-zero phase signifies CP violation in the theory, where charge (C) and parity (P) are discrete symmetries of the field theory describing the SM.

To be more explicit, flavor physics consists of two types of processes: flavor-conserving and flavor-changing processes. In the Standard Model, flavor-conserving processes are induced by neutral currents mediated by the Z boson, photon (γ), and gluon (g). On the other hand, flavor-changing processes are

[2]nine fermion masses including quarks and leptons, three couplings, two from the Higgs sector, and four CKM parameters

induced by both charged ($W_{\pm}$) currents at the tree level and neutral currents at the loop level. The explicit form of the neutral current (NC) interaction, which is manifestly flavor diagonal in the Standard Model, is given by

$$J_{\mu}^{NC} = \sum_{i} \bar{f}_i \Big[\frac{e}{\sin^2\theta_w \cos\theta_w} Z_{\mu}(T_{3\ i} - Q_i \sin^2\theta_w) + eA_{\mu}Q_i \Big] f_i. \tag{1.21}$$

It is important to note that the NC interactions induced by the exchange of the Z boson violate parity (P) and charge conjugation (C) but conserve their combination, CP, while, electromagnetic interactions conserve all three symmetries separately: C, P, and CP. On the other hand, the explicit form of the charged current, which only involves left-handed fermions, is given by

$$J_{\mu}^{CC} = \begin{pmatrix} \bar{u} & \bar{c} & \bar{t} \end{pmatrix}_L \gamma_{\mu} V_{CKM} \begin{pmatrix} d \\ s \\ b \end{pmatrix}_L \tag{1.22}$$

The charged current interactions possess a $(V - A)$ structure, which means they maximally violate parity (P) and charge conjugation (C), while conserving electric charge, lepton number, and baryon number separately. Additionally, they violate CP due to the presence of a non-trivial phase in the CKM matrix (V_{CKM}). Moreover, the suppression of Flavor Changing Neutral Current (FCNC) transitions compared to Charged Current (CC) transitions can be understood by simply looking at the branching ratios [45]

$$\mathcal{BR}(B \to D\ell\nu_{\ell}) = 9.1\%, \ \mathcal{BR}(B^0 \to K^0 e^+ e^-) = 1.6 \times 10^{-7} \tag{1.23}$$

The FCNC processes are suppressed both by loop factors and CKM elements. Therefore, they are referred to as rare decays.

Using the unitarity of the CKM matrix, the off-diagonal terms of $V_{CKM}V_{CKM}^{\dagger}$ follow $\sum_{i=1}^{3} V_{id}V_{is}^{\dagger} = 0$. There are six such relations, each representing a triangle in the complex plane known as a Unitarity Triangle (UT). The most significant UT is $\sum_i V_{id}V_{ib}^\dagger = 0$, as each term is approximately of the same order $\mathcal{O}(\lambda^3)$. This triangle is illustrated in Fig.(1.4). The db triangle represents

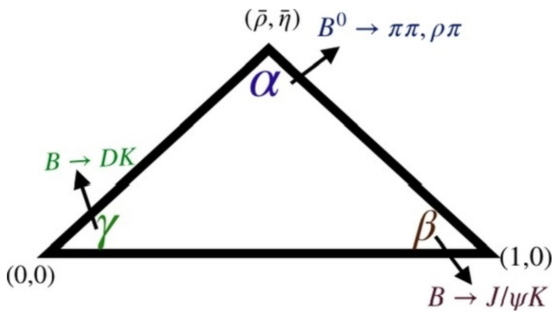

Figure 1.4: The unitarity triangle (db).

the unitarity constraints on $b \to d$ transitions, which are FCNC processes in B_d decays. Examples of such processes include $B_d - \bar{B}_d$ mixing and rare B decays such as $B_d \to K^{(*)}(\omega)\gamma$. These unitarity relations are tested by measuring the angles of the triangle through asymmetries. The sides of the triangle can be determined by studying CC and FCNC B transitions.

Another triangle with sides of similar order is the ut triangle, which can also be measured in FCNC transitions involving $t \to u$. The analogous FCNC processes are $T - \bar{T}$ mixing and decays such as $T \to D^{(*)}\gamma$. However, due to the fast decay top quark, it decays before hadronization [46]. On the other hand, the b quark, being the second heaviest quark in the SM, first hadronizes into a b hadron and then undergoes decay. In this thesis, the focus is on B mesons and therefore, we restrict our reference to these only, though many of the broad arguments apply to baryons containing a b-quark with obvious modifications. Let us understand the B system and its decay briefly.

1.3 B decays

Mesons are composite structures of a quark, anti-quark and gluons. B mesons contain one bottom (b) quark, which is the second heaviest quark observed in nature, after the top (t) quark. The two extreme mass scales present in the flavor sector of the SM are the weak scale, defined by the heaviest particles present in the SM (such as the W, Z, and Higgs bosons, along with the top quark) and

QCD scale ($\sim 1\ GeV$), where non-perturbative picture starts dominating. The charm and the bottom mesons lie between these two extremes. The mass of the charm meson is not too far from $\mu \sim 1$ GeV. Therefore, the non-perturbative physics starts dominating. The mass of the B meson is roughly three times the mass of the charmed meson and hence reasonably far from the QCD scale. On the other hand, it is also far from the weak scale. This separation of scales allows for the perturbative treatment of both weak and short-distance QCD physics, which play a role in the decay processes of B mesons. While non-perturbative physics related to the internal structure of hadrons still remains, it can be separated (using Operator Product Expansion (OPE) [47]) and studied independently from the perturbative physics. Thus, B physics provides a natural laboratory for testing many aspects of the SM.

Due to its relatively large mass, the B meson exhibits a wide range of decay modes, which can be broadly categorized into four types:

1. Pure leptonic decays: In these decays, the final state particles are leptons. For example, $B \to \mu\mu$.

2. Pure hadronic decays: These decays involve final state composed of hadrons. Uncertainties in these decays are primarily due to the dynamics of hadronic interactions. An example is $B \to K\pi$.

3. Semi-leptonic decays: In these decays, the final states consist of both hadrons and leptons. The uncertainties associated with semi-leptonic decays are comparatively lower. Examples include $B \to K\ell\ell$ and $B \to D(\pi)\ell\nu$.

4. Radiative decays: These decays involve radiation of hard photon. Examples include $B \to K^*\gamma$, $B \to X_s\gamma$, and $B \to \mu\mu\gamma$.

By studying these various decay modes, we can gain insights into the properties and interactions of B mesons, providing valuable tests of the Standard Model.

In this thesis, our main focus will be on the semi-leptonic decays of B mesons. These decays include processes mediated by charged current (e.g., $B \to D(\pi)\ell\nu_\ell$), as well as neutral current (e.g., $B \to K(\pi)\ell\ell$). To calculate physical quantities such as decay rates, we employ the weak effective Hamiltonian[48, 49] as a theoretical tool. The relevant piece of the effective Hamiltonian for charged current transitions like $b \to u\ell\nu$ (or $b \to c\ell\nu$) is given by

$$H_{eff}^{CC} = \frac{G_F}{\sqrt{2}} V_{u(c)b} (\bar{u}(\bar{c})\gamma_\mu P_L b)(\bar{\nu}\gamma^\mu P_L \ell). \tag{1.24}$$

To gain a clearer understanding, let us consider an example of a semi-leptonic decay, $B \to \pi\ell\nu_\ell$. The scattering amplitude for this process is given by

$$\mathcal{M}(B \to \pi\ell\nu_\ell) = \frac{G_F}{\sqrt{2}} V_{ub} \left(\bar{\ell}\Gamma^\mu \nu_\ell\right) \langle \pi|\bar{u}\Gamma_\mu b|B\rangle \tag{1.25}$$

where $\Gamma_\mu = \gamma_\mu(1-\gamma_5)$. Notably, only the vector current contributes to the hadronic matrix element, while the axial current vanishes due to the parity invariance of QCD. Thus, the hadronic matrix element can be written as

$$\langle \pi|\bar{u}\Gamma^\mu b|B\rangle = \langle \pi|\bar{u}\gamma^\mu b|B\rangle \tag{1.26}$$

and can be decomposed into two independent kinematical structures multiplied by two scalar invariant functions of q^2 known as form factors:

$$\langle \pi(p_2)|\bar{u}\gamma^\mu b|B(p_1)\rangle = (p_1+p_2)_\mu f^+(q^2) + (p_1-p_2)_\mu f^-(q^2). \tag{1.27}$$

Where f^+ and f^- are scalar quantities representing the form factors (further details are discussed in Chapter-4). The kinematic region for the decay is characterized by the momentum transfer squared, q^2, which varies within the range:

$$m_\ell^2 \leq q^2 \leq (m_B - m_\pi)^2 \tag{1.28}$$

Up until now, we have discussed semi-leptonic decays that occur through flavor-changing weak interactions involving virtual W boson exchange.

However, in addition to these decays, there is another type of semi-leptonic decay, which is induced by flavor-changing neutral currents in the SM. These FCNC decays originated from short-distance loop diagrams. A prominent example of this is the rare decay $B \to K\ell\ell$ which proceeds via $b \to s\ell\ell$ quark level process. The effective Hamiltonian for neutral current-induced processes (for example, $b \to s$ transition) is given by

$$H_{eff} = \frac{G_F}{\sqrt{2}} V_{ts}^* V_{tb} \sum_{i=1}^{10} C_i(\mu)\mathcal{O}_i(\mu) \tag{1.29}$$

where G_F is the Fermi constant. V_{ts}^* and V_{tb} are the CKM elements corresponding to the used operator, C_i are the Wilson coefficients that can be determined using perturbation theory, $\mathcal{O}_i$ are the operators, and μ is the scale that separates long-distance physics from short-distance physics. Similar to the $B \to D(\pi)\ell\nu_\ell$ decay mode, the matrix elements of these operators can be parameterized in terms of non-perturbative parameters such as form factors using Lorentz decomposition, the state of the system, and the relevant operators (for the explicit structure of the operators see Chapter-2, and for the form factor parametrization, see Chapter-3).

Furthermore, it is important to note that the masses of heavy quarks, such as m_b and m_c, are significantly larger than the non-perturbative scale Λ_{QCD}, and they follow the hierarchy $m_b \gg m_c \gg \Lambda_{QCD}$. To understand the implications of these mass inequalities, it is advantageous to separate the heavy quarks from the light quarks and gluons in the QCD Lagrangian. This separation is achieved through the following expression:

$$\mathcal{L}_{QCD} = -\frac{1}{4} G^a_{\mu\nu} G^{\mu\nu\ a} + \mathcal{L}_{u,d,s} + \bar{Q}(i\not{D} - m_Q)Q \tag{1.30}$$

$$= \mathcal{L}_{light} + \bar{Q}(i\not{D} - m_Q)Q \tag{1.31}$$

This formulation is valid in the limit as m_c, m_b approach infinity. Here, the quark field Q represents either the b or c quark. The charm quark c can be called heavy only with some reservations. Hence, when discussing the heavy quark theory, the more appropriate one will be b quark [50]. Therefore, the heaviness of the Q quark proves to be a useful expansion parameter for the description for B meson. The techniques employed to calculate physical observables, such as decay rates for inclusive decay modes, involve the non-relativistic expansion and OPE, together referred to as the Heavy Quark Expansion (HQE) [51, 52]. Further details regarding the HQE and its applications are provided in Chapter-2 and Chapter-5 respectively.

1.4 Effective Field Theories (EFTs)

Effective field theory (EFT) is a powerful tool in physics that simplifies the complexity of a problem by focusing only on the DOF that are relevant to a particular scale. This approach is based on the idea that considering only the relevant DOF makes a problem more manageable. In QFT, this means that we only include operators that are responsible for experimental observables and describe the relevant light DOF. As a result, we can eliminate the degrees of freedom that are not relevant to the problem we are studying, specifically heavy particles with masses that are much larger than the energy scale associated with the problem. This allows us to focus solely on the relevant degrees of freedom, which makes the problem easier to handle (see [53–56]).

The heavy particles are said to be integrated out such that their effects are still present through coupling constants and other parameters that change with scale. By adding more operators to the theory, we can improve its accuracy, but these operators must be guided by symmetry principles. The structure and coefficients of these operators can provide valuable information about the heavy particles that have been integrated out, as they can be fitted with experimental data. This is a useful feature of effective field theories that allows us to make accurate predictions without necessarily needing to know the details of the heavy particles that have been integrated out.

Further, EFTs can be categorized into three types (borrowed from Ref. [54]) based on the DOF included. The first kind involves only the fields that contribute at the energy and momentum scale of the interaction. An example for this is the beta decay which can be explained without mentioning the W-boson, which is a heavy particle with a mass much larger than the energy scale of the beta decay process. The second kind includes fields that no longer participate in the dynamics but are still part of the Fock space. These fields are treated as infinitely heavy and are stationary while lighter DOF bounce off them in elastic collisions. An example of this is the system of heavy mesons, which includes a heavy quark and all light DOF. In this case, the heavy quark acts as the source of a chromomagnetic field, and its recoil can be ignored at leading order and incorporated into subleading terms. The third type of EFT applies the second kind of EFT approach selectively to the relevant components of the field that can generate substantial momentum. In doing so, the momentum say in the z-direction is integrated out, retaining only the components that produce particle motion in the x and y directions. This approach has been effectively applied in various situations, including the Soft Collinear Effective Theory (SCET).

In this thesis, we have explored the first two kinds of EFTs in various phenomenological examples. The detailed methods are provided in Chapter 2.

1.5 Era of Precision

The physical parameters of Flavor Physics within the SM are known. However, it is crucial to recognize the theoretical uncertainties involved, as highlighted in the Introduction of this chapter. Despite our anticipation of discovering NP in the realm of flavor physics, particularly in B physics, no evidence of NP has been found so far. Nevertheless, there have been observations of certain discrepancies in the data. One example is the violation of lepton flavor universality in the charged current-induced decays ($R_{D^{(*)}}$) with a deviation of approximately 3σ from the SM prediction (for details on B physics anomalies, see[57, 58]). Furthermore, inconsistencies exist in the measured values of CKM elements and the angles of the unitarity triangle, including the differences between exclusive and inclusive measurements of V_{ub} and V_{cb}.

The most challenging aspect of some of these measurements lies in the calculation of hadronic matrix elements for the relevant processes. The most reliable methods available to compute the non-perturbative parameters, such as form factors and decay constants, in the B system are Lattice QCD and Light Cone Sum Rules. While there may be discrepancies, it is crucial to ensure that all other sources of uncertainties have been taken into account. Specifically, one needs to consider the QED corrections due to soft photons.

In general, QED corrections can impact decay rate or other observables due to two factors. The first is the soft factor, which includes terms like $\ln k_{\max}$, where $k_{\max}$ represents the maximum energy of the soft photon. The second is the hard collinear factor, which involves terms like $\ln m_f$, where m_f denotes the mass of the charged particle emitting the soft photon. Naively, these factors can lead to both positive and negative modifications of the decay rate. Therefore, it is essential to calculate the decay rate, considering the inclusion of soft photons, before drawing any conclusions. More detailed information on the behaviour of the soft photon and the cancellation mechanism for Infrared (IR) divergences, is provided in Chapter-2.

Next, in the context of inclusive B decays, precise predictions for observable quantities require a first-principle calculation of non-perturbative parameters. However, to date, there is no available first-principle method to calculate these parameters. Therefore, it becomes necessary to compare different predictions for these parameters in order to assess their consistency. Additionally, it is desirable to explore alternative approaches that could simplify the calculation of these parameters.

One approach to achieve this goal is to investigate a process that is fundamentally different from the process under consideration but shares the same non-perturbative parameters. This can be accomplished by studying processes involving hard photons. The inclusion of a hard photon introduces a completely new process and also provides the flexibility to explore various asymmetries. We have used this approach to obtain the non-perturbative parameters λ_1 and λ_2 involved in process $B \to X_u \ell \nu_\ell$. The detailed information are provided in Chapter-5.

Throughout this thesis, our aim will be to investigate the effects of soft and hard photons and their distinct phenomenological implications on various semi-leptonic B decays.

1.6 Organisation of thesis

The organization of this thesis is as follows: In Chapter-2, we provide a detailed discussion on the concept of infrared divergences in QED and an account of effective field theories. We also explore the tools utilized in various problems. In Chapter-3, we examine the impact of soft photons on the branching ratio of $B \to K\ell\ell$ and the Lepton Flavor Universality (LFU) ratio R_K. Chapter-4 introduces a new observable, $R_V = |V_{ub}|/|V_{cb}|$, which demonstrates insensitivity to theoretical uncertainties such as form factors and QED effects. We also observe that despite discrepancies between inclusive and exclusive measurements of individual CKM elements, the formed ratio, R_V, is consistent within a 1σ range. It provides more stringent constraints on the CKM elements. Chapter-5 delves into a new, simple yet efficient, approach for computing non-perturbative parameters in inclusive semileptonic charged current-induced B decays. Finally, in Chapter-6, we conclude our findings and outline future research directions. Additionally, this thesis includes three appendices. In Appendix-A, we collect all the useful identities and definitions. In Appendix-B, we provide all the useful integrals involved in the QED corrections. The Appendix-C covers the kinematics of three and four body decays.

Chapter 2

Tools and techniques: Infrared divergences and Effective Field Theories (EFTs)

In this chapter, we will discuss the important tools and techniques used in this thesis in calculating physical observables. The discussion will begin by considering infrared divergences due to soft photons that arise in the calculation of scattering amplitudes and cross-sections, along with their physical interpretation. The concept of Effective Field Theories (EFTs) will then be introduced as a powerful tool for making predictions at different energy scales. This will include an exploration of the basic principles of EFTs and their application in constructing low-energy effective Lagrangians. Finally, these concepts will be applied to various decay rates of B mesons (see Chapters- 3-5).

2.1 Infrared Divergences

In reality, it is not possible to achieve the ideal conditions of infinite system size and perfect measurement instruments. These limitations pose challenges while using perturbation theory to define observables in particle decays, as they can result in InfraRed (IR) divergences. These divergences can lead to issues in perturbative calculations. IR-divergences are generally associated with massless particles, and there are two known mechanisms for enforcing massless particles. The first is a spontaneously broken global symmetry that gives rise to massless Goldstone bosons. The second is the gauge symmetry that protects the mass of gauge bosons. However, in well-defined observables such as cross-sections or decay rates, these IR divergences can be canceled out [59–61]. These cancellation theorems are based on the first principles, such as unitarity. In the Flavor Physics experiments, QED radiation is usually considered as background, and, therefore can be removed using the Monte-Carlo tools like PHOTOS [62, 63] or PHOTONS++ in SHERPA [64]. QED is also important in other contexts, like initial state radiation in e^+e^- colliders [65]. Like QED, QCD also exhibits IR divergences due to the emission of massless particles, the gluons, and it also requires a cancellation mechanism to ensure that physical observables remain unaffected by these divergences (for further details, see [33, 60, 61, 66]). While we won't go into the details, it is important to note that QCD is different from QED because it has a mass scale parameter for observable hadronic spectrum [33].

2.1.1 Understanding IR

To understand the concept of IR divergences better, we consider a quantity, say $\mathcal{M}$, calculated in perturbation theory using renormalization and effective field theory. The perturbative coefficients in $\mathcal{M}$ have a scale dependence that is controlled by Renormalization Group Equation (RGE). This ensures that physical observables are independent of the artificially introduced boundary set by μ. The general equation for this observable can be written as:

$$\mathcal{M}\Big(\frac{Q}{\mu}, \alpha(\mu)\Big) = \mathcal{M}_0\Big[1 + \frac{\alpha(\mu)}{\pi} C_1\Big(\frac{Q}{\mu}\Big) + \Big(\frac{\alpha(\mu)}{\pi}\Big)^2 C_2\Big(\frac{Q}{\mu}\Big) + ...\Big] \tag{2.1}$$

Here, the scale dependence is denoted by the ratio of the momentum transfer Q to the arbitrary scale μ, $\alpha(\mu)$ is the running coupling constant, $C_k\Big(\frac{Q}{\mu}\Big)$ are the coefficients calculated perturbatively and $\mathcal{M}_0$ is evaluated at tree level. RGE ensures that the physical observables remain finite, preventing the occurrence of UV divergences.

Although renormalization is a powerful technique to handle infinities in QFTs, it is not enough to remove the divergences completely [66, 67]. Particularly, for theories with massless particles, the perturbative coefficients $C_k(\frac{Q}{\mu})$, in Eq.(2.1) describing a physical observable $\mathcal{M}$ may still exhibit integrals that diverge at large distances in coordinate space or low energies in momentum space. This problem is known as the infrared catastrophe [68–70], and also arises when calculating the probability of the emission of massless particles during a hard scattering process. Its signature can be seen long before the development of QFT in the analysis of electron scattering in a Coulomb field with additional photon radiation [68, 71]. It was found that the frequency spectrum of emitted photons exhibits a behavior described by $d\nu/\nu$ and is non-integrable at low frequencies [72, 73].

In Ref.[59], Bloch and Nordsieck proposed a new approximation scheme, now known as the eikonal approximation. The applicability of this approach is limited only to the systems where the energy of the photon is much smaller compared to the other energy scales involved, like the electron's mass, momentum transfer, etc. Additionally, it is assumed that the photon's wavelength is significantly larger compared to the classical radius of the electron, i.e., $R_e = q_e^2/m_e$. Consequently, they proposed that perturbation theory, in powers of $\alpha_{em} \propto e^2$, is no longer valid in the limit of soft photons and must be abandoned. Furthermore, they showed that by employing this semi-classical approximation, i.e., the eikonal approximation, the result obtained for the average radiated energy is the same as one would expect classically. However, this outcome is contingent upon the emission of an infinite number of soft (or low-energy) photons. The two complementary perspectives (following the approach of [66]) are considered to address the underlying issues properly.

1. Well-defined observables

2. Finiteness of S-matrix

Let us briefly understand these two complementary perspectives one by one.

Well-defined Observables

In a theory with massless particles, the first possible explanation for the problem of IR divergences is related to the true definition of an observable. In such theories, scattering processes can yield particles with infinitesimal energy and angular separation. However, all the physical detectors possess finite energy and angular resolutions. It becomes then essential to incorporate the effects that lie below the threshold of the detector to precisely calculate the observables, such as cross-sections or decay rates. Theoretically, this is accomplished by employing Quantum Mechanics (QM), which requires the sum over all unobserved configurations to account for the low energy and small angular resolution effects. Finally, one expects finite results for the physical observable, which, therefore, can be considered to be a measurable quantity.

In QCD, $\ln m_q$ are typically incorporated into hadronic quantities like distribution amplitudes, parton distribution functions, or jets through factorization theorems. If it is not possible to absorb these terms, it indicates that the variable is not infrared-safe for details on the IR problem of QCD, see [33, 66, 74–76]). While in QED, the question: What observables are well-defined for zero lepton masses? led to the development of the Kinoshita-Lee-Nauenberg (KLN) theorem [60, 61] (discussed later). This theorem represents the most inclusive principle regarding the cancellation of infrared (IR) divergences.

Finiteness of S-matrix

The second perspective on the IR problem is that the asymptotic states have been misidentified in constructing the quantum theory. In most S-matrix formulations, it is often assumed that one can adiabatically turn off the interactions at the large times. However, for theories involving massless particles, and infinite-range interactions, the conventional assumption is not realistic. For example, even in the asymptotic regime, high-energy electrons continue to emit and absorb photons. Choosing free Hamiltonian eigenstates as asymptotic states is insufficient since they do not accurately represent the true physical states. Furthermore, the traditional separation of the Hamiltonian into the free term and the interaction term is no longer appropriate as the interactions continue to exist for early as well as late times. It is necessary to include asymptotic interactions as an integral part of the Hamiltonian that will be treated exactly or diagonalized. By acknowledging the importance of asymptotic interactions, choosing appropriate asymptotic states can improve the computation of physical observables, allowing for well-defined scattering amplitudes even in the presence of massless particles. This improvement can, in turn, rescue the S-matrix construction (this idea is discussed in [77–79] in greater detail).

2.1.2 Physical implications: first perspective

To understand the physical implications of the first perspective on IR divergences, we now examine the photon emission from one of the external fermion legs (a similar example can be seen in [32, 33, 73]), as shown in Figure (2.1). The QED

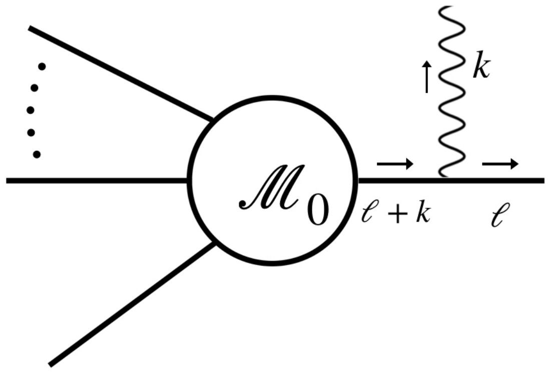

Figure 2.1: Representative diagram for a single photon emission

Feynman rules provide an expression of the form:

$$\mathcal{M}^{\gamma} = Q_{\ell}\bar{u}\gamma^{\mu}\frac{\not{\ell} + \not{k} + m_{\ell}}{(\ell + k)^2 - m_{\ell}^2 + i\eta}\mathcal{M}_0, \tag{2.2}$$

where $\mathcal{M}_0$ accounts for the remaining part of the scattering process, including possible virtual corrections. If the photon is emitted from the final state satisfying $k^2 = 0$ and $\ell^2 = m_{\ell}^2$, the denominator of the fermion propagator is simplified as

$$2\ell.k + i\eta = E_{\ell}E_k(1 - \beta\cos\theta_{\ell k}) + i\eta. \tag{2.3}$$

Here $\beta = |\ell|/E_\ell$, $E_\ell = \sqrt{|\ell|^2 + m_\ell^2}$, $E_k = |k|$, and $\theta_{\ell k}$ is the angle between the charged fermion and photon. While the η prescription prevents a singularity, we still anticipate two sources of enhancement:

- The soft photon limit, i.e., $E_k \to 0$.
- The collinear limit, i.e. $m_\ell/E_\ell \to 0$ and $\theta_{\ell k} \to 0$.

These enhancements are known as soft and collinear divergences, respectively. In $d = 4$ space-time dimensions, they lead to logarithmic singularities of the form $\ln m_\gamma$ (m_γ is the fictitious mass provided to the photon) and $\ln m_\ell$, respectively. In certain regions of phase space, these divergences combine and lead to soft-collinear divergences of the form $\ln m_\gamma \ln m_\ell$. For a finite lepton mass, the collinear logarithm $\ln m_\ell$ is a physical effect. It is referred to as a hard-collinear log. Of course, physical observables have to be free of divergences. This cancellation of divergences is expected to be a consequence of some deep physical principles which separate observable quantities from non-observable ones. Therefore, it is important to understand and study the origin of these divergences and the mechanism behind their cancellation. Now, the question one may ask is: Do these enhancements, the soft and collinear, always turn into actual divergences? It depends upon the observable computed, and the theory considered. The reason behind these enhancements is clear: the fermion propagator approaches the on-shell, i.e., $(\ell + k)^2 = m_\ell^2$, in limits (both soft and collinear) under consideration. Hence, in our theory, The internal fermion carrying momentum $\ell + k$ is treated to be a genuine physical state and can propagate over arbitrary distances and durations.

The IR divergences are fundamentally related to the definition of a particle and the measurement process. It is difficult to distinguish a single electron from an electron that emits a soft photon or a highly relativistic electron that emits a photon at an infinitesimally small angle. The key to resolving this issue lies in a careful assessment of what can be measured. It is related to the idea of infinite space and infinite detector resolution as discussed in Section- 2.1. To understand it in a better way, we may consider a situation where particles emit low-energy photons or photons that travel in nearly the same direction as the emitting particle. The energy loss at the emission point is significantly reduced. As a result, these types of photon emissions can occur over large distances and are difficult to suppress. These phenomena i.e., the soft and the collinear emissions of the photon, lead to what is commonly called the long-distance effects. If we consider only the true IR divergences (only due to the soft emissions), excluding collinear divergences, they can be effectively regulated by introducing an energy scale, m_γ.

Till this point, we have talked only about the real photon emission. We also have to consider the Feynman diagram, where the emitted photon forms a loop attaching to another charged particle. It is shown in Fig.(2.2). In this case,

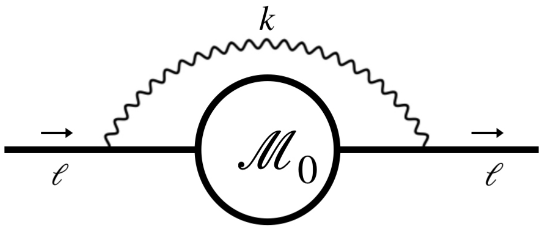

Figure 2.2: Virtual correction due to a single photon

the denominator of the fermion propagator will have an additional k^2 compared to real emission. However, this contribution becomes insignificant compared to $\ell \cdot k$ when all the components of the photon momentum get smaller at the same rate.To evaluate the contributions of loop integral and photon propagator, power counting tools are required. However, even in the case of virtual corrections, the emissions of soft and collinear particles can become significantly enhanced at large distances and times. This enhancement exhibits the same divergence as observed in real emissions. Both virtual corrections and real emissions are required to account for the finite energy due to the soft photons and angle resolutions due to the collinear photons. The incoherent addition of virtual corrections and real emission is performed to construct a properly defined observable, where these divergences cancel against each other.

In summary, the work of Block-Nordsiech puts light on the issue of the infra-red divergences and highlights the mistakes one was making. The presence of massless particles in a theory results in long-range interactions, leading to unsuppressed emissions at late and early times. The traditional perturbation theory, which separates virtual corrections from undetected real emissions, becomes inadequate in such circumstances, rendering individual matrix elements ill-defined. The solution involves introducing an infrared regulator in the form of a particle mass. This regulator will eventually cancel in the physically defined observable, such as decay rates.

It is apparent that the cancellation mechanism for soft divergences given by [59] is effective only for the Abelian theories and is insufficient for QCD. In QCD, summation over degenerate initial states is necessary to achieve a complete cancellation of soft divergences. Further, non-Abelian theories face a more significant challenge compared to Abelian theories when it comes to collinear divergences. In Abelian theories like QED, collinear divergences can be regulated by the masses of matter fields. However, in non-Abelian theories such as QCD, collinear divergences persist even when matter fields have non-zero masses. This is because interactions involving strictly massless particles, such as the three-gluon vertex in QCD, unavoidably lead to collinear difficulties. Hence, it is evident that a straightforward cancellation mechanism like the one in the Bloch-Nordsieck analysis can not work in general. This is because the emission of the collinear particle from the initial state changes the kinematics of the process due to the presence of hard collinear logs, whereas, the virtual corrections do not modify the kinematics. Thus, the cancellation of divergences is inevitably disturbed. To see this properly, let us consider the case of electron scattering off a heavy particle using photon exchange.

2.1.3 Example: $e^+e^- \to hadrons$ at high energy

In this section, we consider an example of an electron scattering off a heavy particle via photon exchange to show the cancellation between the IR divergences coming from the real photon emissions and the virtual corrections. Initially, we examine this cancellation at the lowest order in α_{em} and then generalize it to all orders. Lastly, we demonstrate the exponentiation of the lowest-order outcome. The heavy particle in this scenario acts as a source for an external photon field.

The bremsstrahlung diagrams that contribute to the real emission of the photon are shown in Fig.(2.3), while virtual correction diagrams contributing to

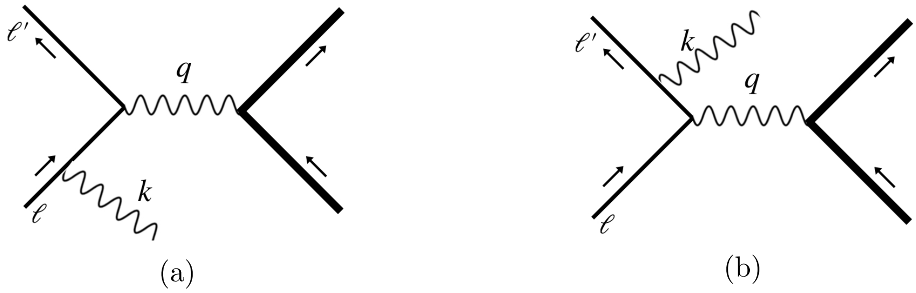

Figure 2.3: Real emissions

this process are shown in Fig.(2.4). First, focusing on the real emission where an

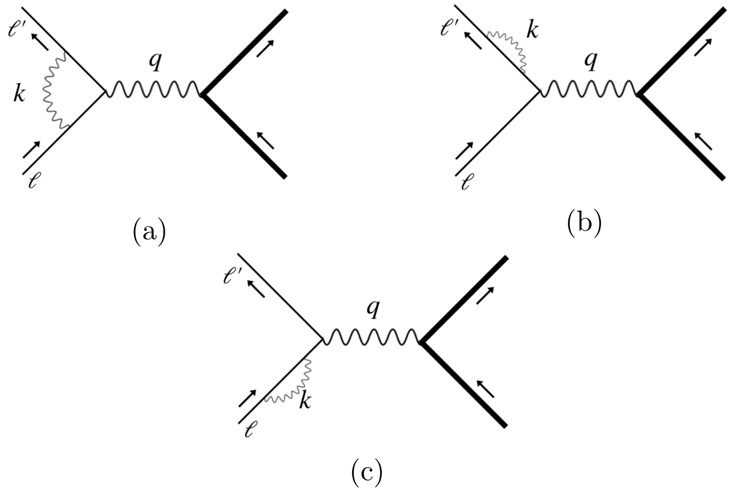

Figure 2.4: Virtual corrections: (a) Vertex correction, (b) self-energy corrections to one fermion, and (c) self-energy corrections to another fermion

electron scatters off from a heavy particle causing its four-momentum to change from ℓ to ℓ' and emits a photon with momentum k. One can write the matrix element as a sum of the Feynman diagrams shown in Fig.(2.3). Here, we will assume that k_μ is much smaller than $q_\mu = (\ell' - \ell)_\mu$. While expanding in powers of k, i.e. the momentum of the soft photon, and considering only the leading term, the matrix element simplifies significantly. At leading power in k, the matrix element is given by

$$\mathcal{M}_\gamma = Q_\ell \Big(\frac{\ell'.\epsilon(k)}{\ell'.k} - \frac{\ell.\epsilon(k)}{\ell.k} \Big) \mathcal{M}_0, \tag{2.4}$$

where $Q_\ell(= -e)$ is the electron charge.

The leading order term for the radiative probability amplitude is gauge-invariant. This property is independent of the spin of the emitting particle. It can be seen that the radiative matrix element is singular for small k. Therefore, the soft approximation for the total radiative cross-section can be formally constructed by factorizing the phase space at leading power in k and summing over polarizations. The cross-section corresponding to the emission of a single soft photon as a real particle is

$$\sigma_{real} = \sigma_0 \mathcal{I}_r\Big(\frac{m_\ell^2}{q^2}, \frac{\mu^2}{E_k^2}\Big). \tag{2.5}$$

Here, σ_0 is the cross-section for the non-radiative process, and $\mathcal{I}_r$, the soft factor, is defined as

$$\mathcal{I}_r\Big(\frac{m_\ell^2}{q^2}, \frac{\mu^2}{E_k^2}\Big) = -Q_\ell^2 \int \frac{d^3\mathbf{k}}{(2\pi)^3 2E_k}\Big(\frac{\ell'^\mu}{\ell'.k} - \frac{\ell^\mu}{\ell.k}\Big)\Big(\frac{\ell'_\mu}{\ell'.k} - \frac{\ell_\mu}{\ell.k}\Big). \tag{2.6}$$

The logarithmic nature of the divergence confirms our previous assumption of retaining only the leading order in the soft expansion. Any higher-order term would contribute to finite corrections. Additionally, we perform an integration over photon energy up to a maximum cutoff k_{max}[1], which represents the maximum energy of the soft photon. Photons having energy, $|\mathbf{k}| < k_{max}$, could not be detected by the detector due to its resolution. Therefore, their effects must be included in the calculation. The integral, in the dimensional regularization (with $D = 4 - 2\epsilon$, and $\epsilon \to 0$), is obtained as

$$\mathcal{I}_r\Big(\frac{m_\ell^2}{q^2}, \frac{\mu^2}{E_k^2}\Big) = -\frac{\alpha_{em}}{\pi}\frac{1}{\epsilon}\Big(\frac{4\pi\mu^2}{k_{max}^2}\Big)^\epsilon\Big[\Big(\frac{1 - 2m_\ell^2/q^2}{\beta}\Big)\ln\Big(\frac{\beta+1}{\beta-1}\Big) - 1\Big] + \mathcal{O}(\epsilon^0) \tag{2.7}$$

where

$$\beta = \sqrt{1 - 4m_\ell^2/q^2} > 1. \tag{2.8}$$

In the limit of large momentum transfer, $-q^2 \to \infty$, Eq.(2.7) can be simplified

[1]It is to be noted that $E_k = k_{max}$

as

$$\mathcal{I}_r\Big(\frac{m_\ell^2}{q^2},\frac{\mu^2}{E_k^2}\Big) = \frac{\alpha_{em}}{\pi}\Big[-\frac{1}{\epsilon}\ln\Big(\frac{-q^2}{m_\ell^2}\Big) + \ln\Big(\frac{k_{max}^2}{4\pi\mu^2}\Big)\ln\Big(\frac{-q^2}{m_\ell^2}\Big)\Big]. \tag{2.9}$$

The second term in the expression exhibits a Sudakov double-logarithmic enhancement. This enhancement arises from two logarithms: one logarithm originates from the soft scale represented by the resolution scale $k_{\max}$, and the other logarithm arises from the collinear scale, which becomes divergent in the limit $m_\ell \to 0$. Now, we will see that these soft poles in ϵ will get canceled with the divergences appearing in the virtual correction.

Virtual corrections pose a more complex challenge due to the presence of ultraviolet divergences that necessitate renormalization. It is imperative to ensure that the counter-terms used in the renormalization process eliminate any residual infrared divergences. One approach to achieve this is through the utilization of a minimal scheme. In QED, it is observed that both Z_ψ and Z_1, i.e., the renormalization constant for the electron field and the vertex, respectively, contain IR divergences in the mass-shell scheme. However, it is important to note that these divergences cancel out in the scattering amplitude. This cancellation is a consequence of the QED Ward identity. Now, we direct our attention to the vertex correction diagrams depicted in Figure (2.4). This diagram will give us the only remaining contribution, which is infrared-singular. A straightforward power-counting analysis reveals that only terms in which the numerator does not contain any powers of the photon momentum can give rise to infrared divergences. These divergences are logarithmic in nature. The mathematical expression for the virtual correction part is

$$a_{soft} = -e^3\mu^{3\epsilon}\int\frac{d^Dk}{(2\pi)^D}\frac{\bar{u}(\ell')\gamma^\alpha(\not{\ell}'+m)\gamma^\mu(\not{\ell}+m)\gamma_\alpha u(\ell)}{(k^2+i\eta)(k^2-2\ell'.k+i\eta)(k^2-2\ell.k+i\eta)}, \tag{2.10}$$

where D is the space-time dimension. To generalize the calculation to higher orders more easily, it is more informative to follow the same steps that were taken for real emission diagrams on the integrand of the integral in Eq.(2.6), instead of directly computing it. This involves neglecting k^2 in the propagator of fermions and also employing the Dirac equation to simplify the numerator, resulting in a single infrared pole in ϵ which could lead to a second infrared catastrophe. Since the lowest-order matrix element factorizes, we can express it as follows.

$$a_{soft} = ie^2\mu^{2\epsilon}\mathcal{M}_0 \int \frac{d^Dk}{(2\pi)^D} \frac{\ell.\ell'}{(k^2+i\eta)(-\ell'.k+i\eta)(-\ell.k+i\eta)} \tag{2.11}$$

It is worth noting that the transition from Eq.(2.10) to Eq.(2.11) seems to have introduced a new challenge: New divergences in the UV region, the region where our approximation fails, seem to appear in the integral of Eq.(2.11). It is important to mention here that these UV divergences do not appear in the original QED calculations, but instead, they are the characteristic divergences appearing in the effective theory at low energy, which describes the IR sector of the QED. We can introduce a UV regulator to deal with this singularity and concentrate on the infrared pole.

In the on-shell scheme, the self-energy counterterm associated with the Feynman diagrams shown in Fig.(2.4 (b)) and (2.4 (c)) is designed in such a way that the combined effect of the diagrams and the counterterm results in zero contribution on-shell. Hence, these graphs do not play any role in our calculation. On the other hand, the vertex counterterm is determined by ensuring that the renormalized vertex correction vanishes at $q^2 = 0$, which corresponds to $\ell' = \ell$ in our case. This condition can be imposed in the soft approximation by expressing the vertex correction as:

$$\begin{aligned}(a + a_{\mathrm{CT}})_{soft} &= \mathcal{M}_0\left(\frac{-iQ_\ell^2\mu^{2\epsilon}}{2}\right) \int \frac{d^Dk}{(2\pi)^D} \left(\frac{\ell'^\mu}{\ell'.k+i\eta} - \frac{\ell^\mu}{\ell.k+i\eta}\right)^2 \frac{1}{k^2+i\eta} &(2.12)\\ &= \mathcal{M}_0\mathcal{I}_v\left(\frac{m_\ell^2}{q^2}, \frac{\mu^2}{q^2}\right) &(2.13)\end{aligned}$$

In the parenthesis, the terms depending on m_ℓ^2 provide the counterterms to the self-energy corrections, whereas the cross term reflecting vertex corrections can be simplified in terms of Eq.(2.11). It is to be noted that the above expression is gauge invariant, and it vanishes if $\ell' = \ell$, which reflects the cancellation of the self-energy and the vertex renormalization.

To directly compare Eq.(2.13) with Eq.(2.6), we observe that the real part of the integral I_v is only significant when the photon is on its mass shell, i.e., $k^2 = 0$. This can be deduced by examining the poles in the complex plane of E_k: The two poles are associated with the fermions lines placed above and below the real axis, respectively. The other two poles are associated with photon propagators placed below the real axis. Consequently, we can evaluate the integral by closing the contour in the lower half-plane and selecting the residue of the photon pole, which corresponds to the photon being on-shell. The resulting expression now precisely matches the form of Eq.(2.9), except for two differences. Firstly, there is an overall factor of $-1/2$ that needs to be accounted for. Secondly, the threshold energy E_k in Eq.(2.9) should be replaced with an ultraviolet cutoff, $\sqrt{-q^2}$.

$$\mathcal{I}_v\Big(\frac{m_\ell^2}{q^2}, \frac{\mu^2}{q^2}\Big) = -\frac{1}{2}\mathcal{I}_r\Big(\frac{m_\ell^2}{q^2}, \frac{\mu^2}{-q^2}\Big). \tag{2.14}$$

The physical cross-section is calculated by combining two contributions. First, we consider the leading-order probability of emitting a soft photon that goes undetected, which is given by the real-emission cross-section in Eq.(2.5). Second, we include the virtual correction to the scattering process. The correction term is directly proportional to the real part of $\mathcal{I}_v$, multiplied by twice the tree-level cross-section. The resulting expression for the observable, i.e., cross-section, is

$$\sigma_{tot} = \sigma_0\Big[1 + I_r\Big(\frac{m_\ell^2}{q^2}, \frac{\mu^2}{E_k^2}\Big) + 2I_v\Big(\frac{m_\ell^2}{q^2}, \frac{\mu^2}{q^2}\Big)\Big] \tag{2.15}$$

Upon utilizing Eq.(2.14), it becomes evident that all singular terms cancel out, as we have previously indicated, resulting in finite logarithmic terms. For $-q^2 \to \infty$, the outcome is

$$\sigma_{tot} \sim \sigma_0\Big[1 - \frac{\alpha}{\pi}\ln\Big(\frac{-q^2}{k_{max}^2}\Big)\ln\Big(\frac{-q^2}{m_\ell^2}\Big) + \mathcal{O}(\alpha^2)\Big] \tag{2.16}$$

The cancellation of all singular terms is evident from this equation. It leaves only finite logarithms. This expression exhibits a combination of a soft logarithm and a collinear logarithm. The cancellation we observed is due to the fact that the divergence in the loop integral arises exclusively from the on-shell configurations of the virtual photon. This is consistent with the qualitative arguments presented in Section-2.1.1, which identify infrared divergences as long-range phenomena.

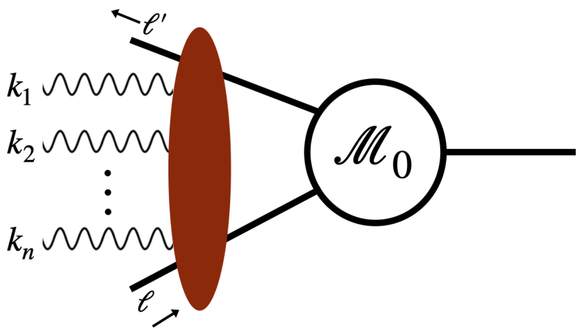

Figure 2.5: Real emission of n soft photons in any possible order

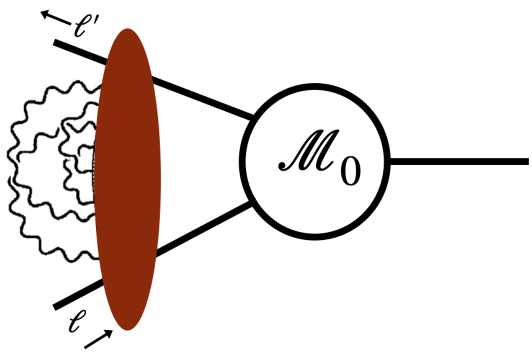

Figure 2.6: Virtual corrections due to n soft photons

The use of power counting techniques gives us an initial understanding of two crucial aspects of infrared enhancements, namely factorization, and exponentiation. To understand this, let us consider the emission of n photons with momenta $\{k_1, ..., k_n\}$ and polarization vectors $\{\epsilon_1, ..., \epsilon_n\}$. These photons are connected to both outgoing and incoming electron lines carrying momentum ℓ' and ℓ respectively, as shown in Fig.(2.5) (we have followed [31, 32]). We observe that each photon contributes an eikonal factor similar to Eq.(2.4). Consequently, the total amplitude for emisssion of n soft photons, connected in any possible order to the initial or final charged particle is obtained by summing up all such diagrams, and is given by:

$$\mathcal{M}_{\gamma}^{(n)} = Q_{\ell}^{n}\Pi_{i=1}^{n}\Big(\frac{\ell'.\epsilon_i}{\ell'.k_i} - \frac{\ell.\epsilon_i}{\ell.k_i}\Big)\mathcal{M}_0. \tag{2.17}$$

Based on the analysis above, we can infer that soft divergences occur in real photon emission processes. One can notice that in the leading of photon momentum, the eikonal current or soft factor is factored out from the rest of the matrix element. This factorization aligns with our understanding of soft divergences as manifestations of long-distance phenomena. Further, due to the indistinguishability of n identical bosons, it is necessary to include a factor of $1/n!$ in the phase-space integral. After summing over polarizations, the expression can be simplified.

$$\sigma_{real}^{(n)} = \sigma_0 \sum_n \frac{1}{n!}\Big[I_r\Big(\frac{m^2}{q^2}, \frac{\mu^2}{k_{max}^2}\Big)\Big]^n. \tag{2.18}$$

The series in Eq.(2.18) can be summed over the number of soft photons n, which leads to the exponentiation of the single-photon result, i.e.,

$$\sigma_{real}^{(n)} = \sigma_0 \exp\Big[I_r\Big(\frac{m^2}{q^2}, \frac{\mu^2}{E_k^2}\Big)\Big]. \tag{2.19}$$

It is to be noted that the steps similar to the one shown above, which lead to this expression, can be applied to the calculations of virtual corrections. Still, the combinatorial factors need to be considered carefully. Soft divergences are generated only by virtual photons that attach to external lines. For vertex corrections, i.e., where photons connect the two-electron lines, the eikonal identity in Eq.(2.13) can be utilized. This involves considering n such identity contributing to the n-photon vertex correction. In addition, it also considers the additional symmetry factor of $1/n!$ since interchanging the virtual photons with each other does not change the diagram. Lastly, the sum over n is performed. Self-energy corrections for every fermion line can be renormalized to vanish on-shell, and the eikonal factor present in the vertex corrections takes the form of Eq.(2.13) at $q^2 = 0$ with the appropriate symmetry factor of $1/2$. Therefore, in conclusion, one can say that the virtual corrections also exponentiate, i.e.,

$$\sigma_{vir}^{(n)} = \sigma_0 \exp\left[2I_v\left(\frac{m_\ell^2}{q^2}, \frac{\mu^2}{q^2}\right)\right] \tag{2.20}$$

By combining the real and virtual corrections, soft singularities have been canceled out. Further, one can note that this cancellation is replicated in all orders in perturbation theory. Hence, the resulting expression is:

$$\begin{aligned} \sigma_{tot} &= \sigma_0 \exp\left[I_r\left(\frac{m_\ell^2}{q^2}, \frac{\mu^2}{E_k^2}\right) + 2I_v\left(\frac{m_\ell^2}{q^2}, \frac{\mu^2}{q^2}\right)\right] && (2.21) \\ &\sim \sigma_0\left[1 - \frac{\alpha}{\pi}\ln\left(\frac{-q^2}{k_{max}^2}\right)\ln\left(\frac{-q^2}{m_\ell^2}\right) + \mathcal{O}(\alpha^2)\right]. && (2.22) \end{aligned}$$

Where the total cross-section, after combining real emissions and virtual corrections and summing these perturbative expansions, is found to be finite and well-behaved. Moreover, this cross-section exhibits the Sudakov behavior and vanishes exponentially at large momentum transfer, q^2, or for small threshold energy k_{max} and fermion mass m_ℓ.

2.1.4 Physical implications: second perspective

While the cancellation of soft divergences in perturbation theory is observed when summing transition rates over physically indistinguishable final states, the general applicability of this mechanism remains uncertain and may be considered fortuitous. The Bloch-Nordsieck theorem, which explains this cancellation in QED, is not applicable to non-abelian gauge theories [80–83], and therefore, a more comprehensive understanding of the cancellation and its underlying physical mechanism is essential.

The KLN theorem provides a framework for the cancellation of infrared singularities in theories with massless particles [60, 61, 84, 85]. It reveals that these singularities arise from degenerate quantum states with identical energy. However, the remarkable property is that these singularities cancel out when transition decay rates are summed over the sets of initial and final degenerate quantum states. The schematic form of KLN theorem is given by

$$\sum_{i,f\in[E_k-m_\gamma,E_k+m_\gamma]} |\langle f|S|i\rangle|^2 = finite \tag{2.23}$$

which relies on unitarity. Its proof involves the use of time-ordered perturbation theory (for general proof see [66]).

Further, this theorem provides a practical solution to the infrared problem by enabling the construction of observable quantities with finite predictions, order by order, in perturbation theory. In theories with massless particles, the presence of infrared singularities arises due to the slow decrease of emission and absorption probabilities at the distant past or the future. However, it does not coincide with the basic assumption in the construction of the S-matrix, which assumes that interactions become negligible at the very large distances and times. To address this, the identification of long-distance interactions and their reassignment to the free Hamiltonian, H_0 allows for an improved description of asymptotic states. In general, the asymptotic states are made up of the non-ineteracting particle states which is found to be inadequate to describe the state for massless particles at distant past or future.

This approach provides a more precise characterization of asymptotic states by considering them as eigenstates of the proper asymptotic Hamiltonian rather than the free Hamiltonian, H_0. These eigenstates, known as coherent states, defines the S-matrix in a consistent way in theories involving the massless particles. This concept was effectively explored in QED, with initial investigations found in Refs. [70, 77, 78], and a significant progress was made by Kulish and Faddeev [79]. In their seminal paper, the interaction Hamiltotian is defined, which is separable into the gauge invariant and the lorentz invariant Hilbert space of coherent states. Further in this coherent state basis, the finite-ness of the QED S matrix is shown to the all orders.

The interaction Hamiltonian for asymptotic time is given by

$$\mathcal{H}_I = \mathcal{H}_R + \mathcal{H}_A, \tag{2.24}$$

where $\mathcal{H}_R$ and $\mathcal{H}_A$ are regular and asymptotic Hamiltonian, respectively. They are both defined for the large times. Using $\mathcal{H}_A$, the asymptotic Moller operators are defined as (detailed construction of this can be seen in [86])

$$\Omega_{A,\pm} = \lim_{t\to\infty} T\exp\Big\{\int_{\mp t}^{0} dt\mathcal{H}_A(t)\Big\}. \tag{2.25}$$

This expression allows us to separate the log-distance contributions of the S-matrix by writing

$$S = \Omega^{\dagger}_{A,-}(E_k)\,\underbrace{\Omega^{\dagger}_{R,-}(E_k)\Omega_{R,+}(E_k)}_{S_R}\,\Omega_{A,+}(E_k), \tag{2.26}$$

where S_R is a regular S-matrix. It is important to note that the regular Hamiltonian $\mathcal{H}_R(t)$ does not generally commute with the asymptotic Hamiltonian. As a result, the computation of the regular Moller operator involves commutator terms and cannot be simply obtained by exponentiating $\mathcal{H}_R(t)$. The absence of infrared singularities in the regular S-matrix must therefore be verified using explicit definitions of the involved operators. With the above definition, the regular S-matrix elements computed within the conventional Fock space do not contain any IR divergences. More properly, the basis of the coherent states can be defined as

$$|\ell^-,\pm\rangle = \Omega^{\dagger}_{A,\pm}(E_k)|\ell^-\rangle. \tag{2.27}$$

Here, the coherent state is defined by applying the Moller operator on a general fock state $|\ell^-\rangle$.

In the context of Abelian gauge theories, the soft limit or the low energy limit provides a straightforward expression for the coherent state. The coherent state is useful in establishing the S-matrix finiteness in perturbation theory. Also, it can be used in the construction of the Hilbert space. This Hilbert space is found to be separable and gauge invariant. In addition, it further includes the gauge invariant subspace of the states having positive norms. In this way, the issue of the soft particle (problem due to the long-distance interactions) in the context of Abelian gauge theory can be solved. However, the situation becomes much more complicated for non-abelian theories because of inescapable collinear divergences arising from the interactions among massless gluons (for eg., triple and quartic gluon interactions).[87–91].

Other than the KLN approach, much effort has been dedicated to calculating the all-order structure of IR singularities using the principles of factorization and universality [92, 93]. These concepts apply to both amplitudes and cross-sections. IR singularities arise from phenomena that occur far away from the hard scattering center in terms of large times and distances. Consequently, the singularity structure is expected to exhibit a significant degree of independence from the specific characteristics of the short-distance process under examination. This permits the identification of universal factors that account for the singular behavior of the amplitude.

Hence, concretely via any method, in order to compute the corrections of order $\mathcal{O}(\alpha)$ for a decay process $i \to f$, it is necessary to consider its radiative counterpart $i \to f(\gamma E_k|m_\gamma)$. In practice, the IR problem in QED is often addressed by employing IR regularization techniques. One common approach is to introduce a regulator mass, denoted as m_γ, which allows for the control of infrared divergences. After performing calculations with this regulator, the final step involves taking the limit $m_\gamma \to 0$ to remove the regulator and obtain physical observables, such as decay rates, that are free from IR divergences.

2.1.5 IR problems beyond point-like

The study of QED corrections to hadronic decays, including non-point-like effects, is still in its early stages. The analogy with the hydrogen atom, where interactions between the electron, proton, and photons play a role, motivates the investigation of photon interactions with neutral B-mesons consisting of b- and d-valence quarks. The heavy-light nature of these mesons exhibits significant effects, but this may induce various challenges. Addressing cancellations of infrared divergences, which involve real radiation, goes beyond standard flavor physics and intersects with the confinement at long distances.

Some of the methods which can be utilized as continuum methods include Chiral perturbation theory, soft-collinear effective theory (SCET), and heavy quark symmetry. Chiral perturbation theory is well-established in QED [94, 95], however determining counterterms in this theory poses a challenge. SCET has been applied to study the leptonic FCNC decay $B_s \to \mu^+\mu^-$, where the primary uncertainty arises from the QCD B-meson distribution amplitude [96]. Hadronic decays like $B \to K\pi$ have also been investigated, but defining charged light-meson distribution amplitudes is problematic[97]. So far, SCET has only considered virtual contributions, with real radiation incorporated through the universal soft-photon part. Heavy quark symmetry has provided constraints in $B \to D^{(*)}\ell\nu_\ell(\gamma)$ decays [98].

2.2 Effective Field Theories (EFTs)

In this section, we will explore the concept of Effective Field Theories (EFTs) in detail as a powerful framework for understanding how physics at different energy scales can be decoupled from each other [21, 54] (see also [55, 56, 99, 100]). EFTs provide a systematic approach to incorporate the effects of higher energy scales into calculations at lower energy scales, allowing for accurate and reliable predictions.

An EFT organises the full theory description by lumping the effects of high scale ($\geq \mu$) physics in the effective couplings/strengths of operators (both renormalizable as well as higher dimensional, non-renormalizable operators) built from fields relevant at the scale μ. This thus provides a clear separation of physics at different scales. Long-distance physics resides in the matrix elements of the operators while the effective strengths of the operators (for higher dimensional operators called the Wilson Coefficients (WCs)) encode the short-distance physics [21, 54].

One of the key features of EFTs is the use of Renormalization Group Equations (RGEs) to run the coefficients of the operators, i.e., the WCs, from a high energy scale, say $\mu = M$ to the scale of the physical process of interest, i.e., $\mu = m$. This allows for the incorporation of large logarithms of the form

$\alpha_s^n \log^n(M/\mu)$, where α_s is the strong coupling constant. These large logarithms can arise in calculations involving high energy scales. By systematically accounting for these large logarithms, EFTs provide a reliable tool for describing physics at different energy scales [48, 101].

In order to calculate the WCs, the low energy theory is matched onto the full theory at the scale μ. This matching procedure ensures that the EFT accurately represents the full theory in calculations at the lower energy scale, taking into account the effects of the higher energy scales. This allows for a consistent treatment of the physics at different energy scales.

Following [54], we categorized EFTs into three kinds. This categorization mainly depends upon the DOF included. In the first kind, i.e., EFT-I, we will discuss the effective low-energy theory of weak interactions. On the other hand, in the second kind, i.e., EFT-II, we will discuss the EFT description of the physics of a meson containing a heavy quark. The third kind involves the description of objects having large momentum transfer but only in the fixed direction. In this thesis, we will focus on the first two kinds of EFTs to obtain SM predictions for exclusive and inclusive B decays. To appreciate the core features of EFTs, we start with an example where we consider four Fermion interactions as a limit of Yukawa interaction.

2.2.1 An example

The Lagrangian for the system having Yukawa interaction is given by:

$$\mathcal{L}_Y = \bar{\psi}(i\partial\!\!\!/ - m)\psi - \frac{1}{2}(\partial_\mu\phi)(\partial^\mu\phi) - \frac{1}{2}M_\phi^2\phi^2 - g_y\bar{\psi}\psi\phi \tag{2.28}$$

where ψ represents the fermion field, ϕ denotes the scalar field, m is the fermion mass, M_ϕ is the scalar mass, and g_y is the coupling between the scalar field and the fermions.

We consider the scenario where the experiment can probe the energy scale, which is much lower than the mass of the scalar, M_ϕ, i.e., $\mu \ll M_\phi$. This sets the scale for the system. Further, Green's function for the theory is computed from the generating functional, denoted as Z_Y, given by:

$$Z_Y = N\int[\mathcal{D}\psi][\mathcal{D}\phi]\exp\left\{i\int d^4x\mathcal{L}_Y\right\} \tag{2.29}$$

where N represents a normalization constant, and $[\mathcal{D}\psi]$ and $[\mathcal{D}\phi]$ denote the functional measures for the fermion and the scalar field, respectively.

In this energy regime, only initial and final states involving fermions, ψ can be considered, as the scalar field ϕ cannot be directly produced. Nevertheless, even though the scalar field may not directly participate in the fermion scattering processes, it can still contribute through off-shell propagation at the tree level and quantum loop effects. Hence, the relevant physical DOF of our theory is the fermion field, ψ. Now, one may ask the question: What happens if we integrate out the scalar field, ϕ, from the theory? To calculate this, we perform a functional integral with respect to ϕ in Eq.(2.29). To simplify the calculation, we introduce a notation $J(x) = -g\bar{\psi}\psi$ in Eq.(2.28) and obtain the Gaussian term for the scalar field, which adds an extra term to the action. The resulting expression for the partition function Z_Y becomes:

$$\begin{aligned} Z_Y &= N\int[\mathcal{D}\psi][\mathcal{D}\phi]\exp\left\{S_\psi - \frac{1}{2}\int d^4x(\phi(x)[-\partial^2 - M_\phi^2]\phi(x))\right. \\ &\quad \left. -i\int d^4x d^4y J(x)(-iD_F(x-y))J(y)\right\} \qquad (2.30) \\ &= N'\int[\mathcal{D}\psi]\exp\left\{S_\psi - i\int d^4x d^4y J(x)(-iD_F(x-y))J(y)\right\}. \qquad (2.31) \end{aligned}$$

Here, N' is a normalization constant given by $N' = N\mathrm{Det}(\partial^2 - M_\phi^2)^{\frac{-1}{2}}$, and $D_F(x-y)$ is the position space propagator for the ϕ field and given by:

$$D_F(x-y) = \int\frac{d^4p}{(2\pi)^4}\frac{i}{p^2 - M_\phi^2 + i\epsilon}e^{-ip.(x-y)}. \tag{2.32}$$

In the limit of $M_\phi \to \infty$, the non-local component of Eq.(2.31) can be expanded as a series in powers of $\frac{p^2}{M_\phi^2}$. The leading contribution is the delta function:

$$D_F(x-y) \sim \frac{-i}{M_\phi^2}\delta^4(x-y). \tag{2.33}$$

This contribution makes Eq.(2.31) local, and leads to an effective Lagrangian[2]:

$$\mathcal{L}_{eff} = \mathcal{L}_{\psi} + \frac{J^2}{M_{\phi}^2}. \tag{2.34}$$

where, $\mathcal{L}_{\psi} = \bar{\psi} i \partial\!\!\!/ \psi - m\bar{\psi}\psi$, and $J = -g\bar{\psi}\psi$.

This effective Lagrangian correctly describes low-energy physics, specifically the scattering of fermions with energies $E \ll M_{\phi}$. A crucial observation is that for each order in $1/M_{\phi}$, there exists a finite number of effective operators. This has implications in two different scenarios; (1) In cases where we do not know what lies beyond the energy scale, such as in the Standard Model. (2) In cases where the UV completion of the model is known, but the degrees of freedom in the IR modes are different, such as in Chiral Perturbation Theory.

It is important to emphasize that the effective Lagrangian, which respects all the symmetries of the complete theory, is expected to reproduce the same Green functions as the full theory. This suggests that by understanding the power-counting behavior of subleading operators, one can write down the most general set of operators respecting the symmetries of the full theory. Each operator is accompanied by an unknown coefficient, which can be determined by matching the results from the full theory to the effective theory. By employing this approach, we can exchange the effects of heavy degrees of freedom for an infinite number of local operators, where the contribution of each operator is suppressed by inverse powers of the masses of the heavy particles.

To ensure the consistency of Effective Field Theories (EFTs), it is important to guarantee that quantum corrections arising from loop diagrams are also suppressed by appropriate powers of the heavy scale. However, cutoff regularization is not suitable in this case as it disrupts power counting. In such cases, a preferable approach is to utilize mass-independent regularization methods, such as dimensional regularization. In dimensional regularization, quadratic divergences are absent, and the one-loop contributions are properly suppressed by the heavy scale, as needed for consistency. Hence, it can be inferred that at each order in $1/M$, the effective field theory exhibits the behavior of a renor-

[2] We followed [54] for this example.

malizable QFT. Next, we discuss both types of EFTs, EFT-I, and EFT-II, in detail.

2.2.2 EFT I: Fermi theory for weak decays of mesons

We derived the four fermion interactions in the previous section. Now, we apply EFT to weak decays of those mesons, which are described by four fermion (quarks) interactions, including QCD corrections. It is worth noting that in the context of effective electroweak operators, the QCD corrections can often have a significant impact, surpassing the contributions from power counting terms, especially in the low-energy processes. For example, one can see that the $\alpha_s(\mu) \gg \mu^2/m_W^2$ at, say, $\mu = m_b$. Hence, even two-loop perturbative QCD corrections may contribute more than the electroweak effects, i.e., $1/m_W^4$. Another importance of QCD corrections is that they generate a new operator and also employ the operator mixing when the scale is run down from $\mathcal{O}(m_W)$ to the hadronic scale $\mathcal{O}(1\ GeV)$. These EFTs are powerful frameworks that allow us to describe physics at both high and low energy scales. To set up the approach, we divide our scale of the theory into three pieces:

1. At $\mu = \mathcal{O}(m_W)$: Weak decays of hadrons are governed by the interaction of quarks. α_s at $\mu = m_W$ is small, and perturbation theory is applicable.

2. $1GeV < \mu < \mathcal{O}(m_W)$: $\alpha_s(\mu)$ increases and this variation should be taken into account. RGEs play an important role, and one encounters the summation of large logs.

3. $\mu \leq \mathcal{O}(1GeV)$: Perturbation theory fails. One has to rely on the non-perturbative theories as the confinement effects, which are responsible for the binding of the quarks and gluons, will get into action.

The running of the scale is governed by RGEs. Once a threshold is crossed, the particle with higher mass disappears from the theory, as we saw in Section-2.2.1.

The four fermion (quarks) interactions ($q_1 \rightarrow q_2 q_3 q_4$) in the full theory are mediated by electroweak W boson as shown in Fig.(2.7). At the leading order in α_s, dimension six operators are built from four quark fields, resulting in operators such as $Q_2 = (\bar{q}_1^\alpha \Gamma_\mu q_2^\alpha)(\bar{q}_3^\beta \Gamma_\mu q_4^\beta)$, with $\alpha, \beta = 1, 2, 3$ represent color indices. Due to the color quantum numbers carried by gluons, perturbative quantum chromodynamics (QCD) corrections give rise to additional operators in the effective theory, such as $Q_1 = (\bar{q}_1^\alpha \Gamma_\mu q_2^\beta)(\bar{q}_3^\beta \Gamma_\mu q_4^\alpha)$. The weak Hamiltonian for these transitions is given by:

$$\mathcal{H}_{eff} = \frac{4G_F}{\sqrt{2}} |V_{CKM}||V^*_{CKM}| \big(C_1(\mu)Q_1(\mu) + C_2(\mu)Q_2(\mu)\big), \tag{2.35}$$

where μ is the scale that separates the contributions of the short-distance physics (C_i) from the long-distance physics, i.e., matrix elements of Q_i. Eq.(2.35) takes the form of an operator product expansion (OPE). Switching off the QCD corrections in Equation (2.35), the Wilson coefficients (WCs) are calculated as $C_2 = 1$ and $C_1 = 0$. Including QCD corrections, the WCs C_1 and C_2 can be calculated using perturbation theory. The amplitude $q_1 \to q_2 q_3 q_4$ in the full theory is

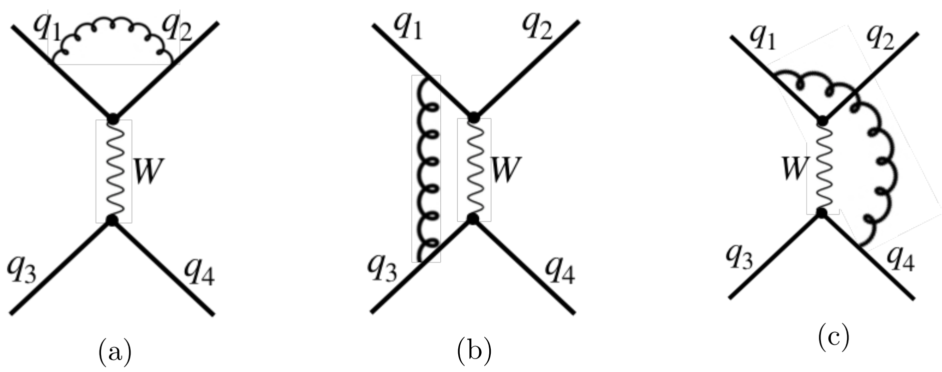

Figure 2.7: Feynman diagrams for $q_1 \to q_2 q_3 q_4$ with QCD corrections in full theory.

$$\begin{aligned}\mathcal{A}_{full} \;\; &= \;\; \left(1 + 2C_F \frac{\alpha_s}{4\pi}\left(\frac{1}{\epsilon} + \ln\left(\frac{\mu^2}{-p^2}\right)\right)\right) Q_2 + \frac{3}{N}\frac{\alpha_s}{4\pi} \ln\left(\frac{m_W^2}{-p^2}\right) Q_2 \\ &\quad -3\frac{\alpha_s}{4\pi} \ln\left(\frac{m_W^2}{-p^2}\right) Q_1. \end{aligned} \tag{2.36}$$

In calculating this amplitude, one can choose all external momenta p_i to be equal and set all quark masses to zero. We will verify at the end that this has no impact on the WCs, C_i. Further, the $1/\epsilon$ divergence in above expression can be removed by performing renormalization of the quark fields, but this is also not necessary in computing C_i. Hence, we used the amputed Green function, and therefore the gluonic self energy corrections to the external leg are not included.

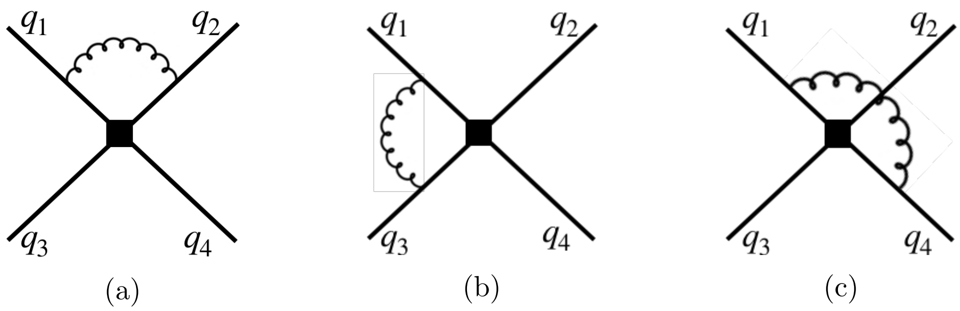

Figure 2.8: Feynman diagrams for effective theory of the process $q_1 \to q_2 q_3 q_4$.

Next, the four fermion (quarks) interactions ($q_1 \to q_2 q_3 q_4$) in the effective theory are shown in Fig.(2.8). The amplitude is given by

$$\mathcal{A}_{eff} = C_1 \mathcal{Q}_1 + C_2 \mathcal{Q}_2. \tag{2.37}$$

Where $\mathcal{Q}_1$ and $\mathcal{Q}_2$ are the renormalized operators. The Feynman diagrams shown in Fig.(2.8) provides the unrenormalized operators, which are given by,

$$\begin{aligned}
\mathcal{Q}_1^{(0)} &= \Big(1 + 2C_F \frac{\alpha_s}{4\pi}\Big(\frac{1}{\epsilon} + \ln\Big(\frac{\mu^2}{-p^2}\Big)\Big)\Big) Q_1 + \frac{3}{N}\frac{\alpha_s}{4\pi}\Big(\frac{1}{\epsilon} + \ln\Big(\frac{\mu^2}{-p^2}\Big)\Big) Q_1 \\
&\quad -3\frac{\alpha_s}{4\pi}\Big(\frac{1}{\epsilon} + \ln\Big(\frac{\mu^2}{-p^2}\Big)\Big) Q_2 \qquad (2.38) \\
\mathcal{Q}_2^{(0)} &= \Big(1 + 2C_F \frac{\alpha_s}{4\pi}\Big(\frac{1}{\epsilon} + \ln\Big(\frac{\mu^2}{-p^2}\Big)\Big)\Big) Q_2 + \frac{3}{N}\frac{\alpha_s}{4\pi}\Big(\frac{1}{\epsilon} + \ln\Big(\frac{\mu^2}{-p^2}\Big)\Big) Q_2 \\
&\quad -3\frac{\alpha_s}{4\pi}\Big(\frac{1}{\epsilon} + \ln\Big(\frac{\mu^2}{-p^2}\Big)\Big) Q_1. \qquad (2.39)
\end{aligned}$$

It is to be noted that the operators, Q_1 and Q_2, present in the above expression are unrenormalized. For the momenta and masses of the quarks we employ the same assumption which is used in calculating $\mathcal{A}_{full}$. In the above expressions, one can observe that carrying out the quark field renormalization to remove the divergence is not enough. It just removes divergences from the first terms of both $\mathcal{Q}_1$ and $\mathcal{Q}_2$. To remove the left-over UV divergences, one has to renormalize the composite object, known as operator renormalization. It is given by

$$Q_i^{(0)} = Z_{ij} Q_j, \tag{2.40}$$

where Z_{ij} is the 2×2 matrix. One can obtain the relation between the unrenormalized $\mathcal{Q}_i^{(0)}$ and the renormalized amputated amplitude, $\mathcal{Q}_i$, which is given by

$$\mathcal{Q}_i^{(0)} = Z_q^{-2} Z_{ij} \mathcal{Q}_j. \tag{2.41}$$

Where Z_q^{-2} removes the first terms of both $\mathcal{Q}_1$ and $\mathcal{Q}_2$, and Z_{ij} remove the remaining divergences. The explicit form of Z_{ij} is

$$\hat{Z} = 1 + \frac{\alpha_s}{4\pi}\frac{1}{\epsilon}\begin{pmatrix} 3/N & -3 \\ -3 & 3/N \end{pmatrix}. \tag{2.42}$$

After carrying out the renormalization, one can perform matching. The expression for matching is given by[3]

$$\mathcal{A}_{full} = \mathcal{A}_{eff} = C_1\mathcal{Q}_1 + C_2\mathcal{Q}_2. \tag{2.43}$$

It results into computation of C_1 and C_2:

$$C_1(\mu) = -\frac{3\alpha_s}{4\pi} ln\left(\frac{m_W^2}{\mu^2}\right), \text{ and} \tag{2.44}$$

$$C_2(\mu) = 1 + \frac{3}{N}\frac{\alpha_s}{4\pi} ln\left(\frac{m_W^2}{\mu^2}\right), \tag{2.45}$$

respectively. It is to be noted that the infrared regulator, $-p^2$, which was present in Eq.(2.37) and (2.36), is absent here. Moreover, these corrections are not solely proportional to Q_2 but also involve Q_1 and vice versa. It indicates that Q_1 and Q_2 mix under renormalization. This mixing is an example of how the basis of dimension six flavor-changing operators closes under renormalization, although it does not rule out the possibility of other operators appearing. The framework of EFTs encompasses all dimension six and dimension five operators to describe low-energy non-leptonic transitions of quarks. It is important to consider the possible

[3] The operators Q_1 and Q_2 in $\mathcal{A}_{full}$, do not require renormalization. Hence, $Q_1 = \mathcal{Q}_1$ and $Q_2 = \mathcal{Q}_2$

mixing of these new operators under QCD renormalization. While operators Q_1 and Q_2 may mix with other operators, vice-versa does not occur.

Weak decays consist of flavor change in the process, which is quantified by ΔF. For example, $\Delta F = 1$ is used to describe weak decays of $F = b,\ c$, and s quarks. For these types of weak decays, other operator structures beyond Q_1, and Q_2 arise in the SM. The penguin operator shown in Fig. (2.9) is one such example. These operators can be classified as gluonic or electroweak penguins. Further, we concentrate only on $\Delta b = 1$ transition; in particular, $b \to s$ decays.

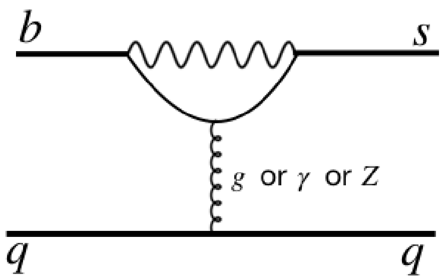

Figure 2.9: Feynman diagrams for penguin operators.

The general structure of effective Hamiltonian is

$$\begin{aligned}\mathcal{H}_{eff} &= \frac{4G_F}{\sqrt{2}} \sum_{q=u,c,t} \lambda_q \Big[C_1 Q_1 + C_2 Q_2 + \sum_{i=3,\ldots,10} C_i Q_i + C_{7\gamma} Q_{7\gamma} + C_{8g} Q_{8g} \\ &\quad + C_{9V} Q_{9V} + C_{10A} Q_{10A} \Big] + h.c. \end{aligned} \tag{2.46}$$

where $\lambda_q = V_{qb}^* V_{qs}$ denote the product of CKM matrix elements. For $\Delta b = 1$ transition, the charged current operators: Q_1 and Q_2 are

$$\begin{aligned} Q_1 &= (\bar{q}_\alpha b_\beta)_{V-A} (\bar{s}_\beta q_\alpha)_{V-A}, \text{ and} \\ Q_2 &= (\bar{q}_\alpha b_\alpha)_{V-A} (\bar{s}_\beta q_\beta)_{V-A}. \end{aligned} \tag{2.47}$$

Furthermore, $Q_{3,\ldots,6}$, which are the gluonic operators are:

$$
\begin{aligned}
Q_3 &= (\bar{s}b)_{V-A}\sum_q(\bar{q}q)_{V-A}, \\
Q_4 &= (\bar{s}_\alpha b_\beta)_{V-A}\sum_q(\bar{q}_\beta q_\alpha)_{V-A}, \\
Q_5 &= (\bar{s}b)_{V-A}\sum_q(\bar{q}q)_{V+A}, \text{ and} \\
Q_6 &= (\bar{s}_\alpha b_\beta)_{V-A}\sum_q(\bar{q}_\beta q_\alpha)_{V+A}.
\end{aligned} \tag{2.48}
$$

The electroweak penguin operators $Q_{7,\ldots,10}$ are given by

$$
\begin{aligned}
Q_7 &= \frac{3e_q}{2}(\bar{s}b)_{V-A}\sum_q(\bar{q}q)_{V+A}, \\
Q_8 &= \frac{3e_q}{2}(\bar{s}_\alpha b_\beta)_{V-A}\sum_q(\bar{q}_\beta q_\alpha)_{V+A}, \\
Q_9 &= \frac{3e_q}{2}(\bar{s}b)_{V-A}\sum_q(\bar{q}q)_{V-A}, \text{ and} \\
Q_{10} &= \frac{3e_q}{2}(\bar{s}_\alpha b_\beta)_{V-A}\sum_q(\bar{q}_\beta q_\alpha)_{V-A}.
\end{aligned} \tag{2.49}
$$

The two dipole operators are

$$
\begin{aligned}
Q_{7\gamma} &= -\frac{e}{8\pi^2}m_b(\bar{s}\sigma_{\mu\nu}(1-\gamma_5)b)F^{\mu\nu}, \text{ and} \\
Q_{8g} &= -\frac{e}{8\pi^2}m_b(\bar{s}\sigma_{\mu\nu}(1-\gamma_5)b)G^{\mu\nu}.
\end{aligned} \tag{2.50}
$$

The field strength tensor is defined in Eq.(1.3). Further, if the process is semi-leptonic like $b \to s\ell\ell$, the other two operators are

$$
\begin{aligned}
Q_{9V} &= \frac{e_q^2}{16\pi^2}(\bar{s}b)_{V-A}(\bar{\ell}\ell)_V, \text{ and} \\
Q_{10A} &= \frac{e_q^2}{16\pi^2}(\bar{s}b)_{V-A}(\bar{\ell}\ell)_A.
\end{aligned} \tag{2.51}
$$

With an example of four fermion interaction, we outlined the method to compute the WCs for the operator. In any theory, the procedure remains the same: First, these coefficients are typically calculated at leading order in

QCD, followed by the renormalization group improved perturbation theory. The only difference comes in the size of the basis of the operators. For details of calculations, refer to [48, 101]. However, it is important to note that even after resuming the logarithms, the WCs still exhibit scale dependence. Therefore, matching beyond one loop is advantageous. Furthermore, it is important to calculate the anomalous dimension beyond the leading order for consistency. The next-to-leading order (NLO) calculation introduces new features, like the final result is now dependent on the renormalization scheme, which is adopted during the calculation. Further details of the calculation can be found in [48, 101].

2.2.3 EFT II: Heavy Quark Effective Theory

As discussed in Section- 1.4, the underlying physics of the system is crucial to keep in mind when one derives an EFT. We are now interested in the bound states of heavy and light particles, specifically the heavy b quark and light antiquarks $\bar{u}$, $\bar{d}$, $\bar{s}$. The physics of these systems can be effectively studied in the rest frame of B mesons. In the context of QCD, There are two characteristic energy scales for the B meson. First, the heavy quark mass, i.e., $m_b \sim 5$ GeV, and second, the energy scale associated with the non-perturbative physics, i.e., $\Lambda_{QCD} \sim 300$ MeV. It is noteworthy that the light DOF in this system are relativistic, having energies and momenta at the order of Λ_{QCD}. Hence, irrelevant degrees of freedom can be integrated from the Lagrangian, resulting in an effective Lagrangian that describes the physics of the bound system. This effective theory is commonly known as Heavy Quark Effective Theory (HQET) and is particularly useful for describing heavy hadrons. Before delving into HQET, let us understand the QM of a heavy particle.

2.2.3.1 Quantum Mechanics of heavy particles

Let's start by examining the case of relativistic QM (see [54, 102, 103]). Consider a heavy spin-1/2 particle, denoted as Q, whose dynamics are governed by the

Dirac equation:

$$(i\partial\!\!\!/ - m_{\mathcal{Q}})\mathcal{Q}(x) = 0 \tag{2.52}$$

Here, $\mathcal{Q}(x)$ and $m_{\mathcal{Q}}$ represent the coordinate space wave function and the mass, respectively, of the Dirac particle $\mathcal{Q}$. In the rest frame of the heavy particle, the wave function of the particle will be proportional to $e^{-im_{\mathcal{Q}}t}$. As a result, we can redefine the wave function by separating the large mechanical part from it, which can be expressed as:

$$\mathcal{Q}(x) = e^{-im_{\mathcal{Q}}t}\tilde{\mathcal{Q}}(x). \tag{2.53}$$

Inserting this wave function back to the Eqn.(2.52), one get,

$$\begin{aligned}(i\partial\!\!\!/ - m_{\mathcal{Q}})Q(x) &= (i\gamma_0\partial^0 - m_{\mathcal{Q}})e^{-im_{\mathcal{Q}}t}\tilde{\mathcal{Q}}(x) \\ &= -m_{\mathcal{Q}}e^{-im_{\mathcal{Q}}t}(1-\gamma_0)\tilde{\mathcal{Q}}(x) = 0 \end{aligned} \tag{2.54}$$

The above equation is similar to the projection operator acting on the spinor $\tilde{Q}$

$$P^0_-\tilde{\mathcal{Q}} = 0 \tag{2.55}$$

The projection operator is defined by

$$P^0_\pm = \frac{I \pm \gamma^0}{2}, \tag{2.56}$$

where I is a 4×4 unit matrix. The explicit form of projection is useful to see the operation of it on the Dirac bi-spinor $\tilde{\mathcal{Q}}$

$$P^0_+\tilde{\mathcal{Q}} = \begin{pmatrix} \hat{I} & \hat{0} \\ \hat{0} & \hat{0} \end{pmatrix}\begin{pmatrix} \psi \\ \chi \end{pmatrix} = \begin{pmatrix} \psi \\ 0 \end{pmatrix} \tag{2.57}$$

And similarly for the P^0_-. The short-hand notations used for the two-component spinors are

$$\psi = \begin{pmatrix} \psi_1 \\ \\ \psi_2 \end{pmatrix}, \text{ and } \chi = \begin{pmatrix} \chi_1 \\ \\ \chi_2 \end{pmatrix}. \tag{2.58}$$

Since ψ describes positive energy degrees of freedom, the role of the projection operator P^0_+ is to project out negative energy (anti-particle solution from the theory).

Building upon the observation made in relativistic quantum mechanics, we can now apply it to non-relativistic EFT. To do so, we first introduce a four-velocity vector denoted as v^μ. In the rest frame of the particle, the four-vector v can be expressed as $v = (1, \overrightarrow{0})$, such that $v \cdot x = t$. By generalizing the Dirac equation, we can describe the dynamics of a particle moving in a non-relativistic frame of reference. In this scenario, the momentum of the particle, denoted as p_Q, can be expressed as:

$$p_Q = m_Q v + \Pi. \tag{2.59}$$

Here, Π represents the residual momentum, where $|\mathbf{\Pi}| \ll m_Q$, indicating that the particle is nearly at rest. The velocity of the particle is denoted as v, and we impose the constraint $v^2 = 1$ to ensure the particle is on-shell. Π accounts for small deviations from the particle being exactly on-shell.

The formalism described above is particularly useful when the mass scale of the particle under consideration is much larger than other scales involved in the problem. The projection operator will get generalized to:

$$P^v_\pm = \frac{1 \pm \not{v}}{2} \tag{2.60}$$

With this formalism, we can now make a transition from QM of heavy particles to QFT of heavy particles.

2.2.3.2 QFT of heavy particles

We now make a transition to the discussion of fields that describe heavy particles. Let us consider a field, $Q(x)$, which represents a heavy fermion, such as the heavy quark in the mesonic or the baryonic states. In this context, all the other quarks are assumed to be light, with masses of the order Λ_{QCD}. Such systems are often referred to as the "Hydrogen atoms of QCD" due to their similarity. In QCD bound states, the mass scale of the heavy quark is significantly larger than any other scale present in the system. It allows one to have an expansion in the ratio, Λ_{QCD}/m_Q, despite the problem being highly non-perturbative in the QCD coupling. The power counting in this system is dictated by its physics.

In the heavy quark limit, $Q(x)$ essentially acts to be a static source of chromomagnetic fields with its own dynamics considered to be negligible. The kinetic energy of the heavy quark, quantified by $K.E. = p_Q^2/2m_Q$, can be represented by an operator that is suppressed by inverse powers of the heavy quark mass. The power counting scheme involves counting the dimensions of operators, where higher dimensions correspond to stronger suppression by the heavy quark mass. The equations of motion for the heavy fermion field can be derived from the standard Dirac Lagrangian,

$$\mathcal{L} = \bar{Q}(x)\,(i\not{D} - m_Q)\,Q(x). \tag{2.61}$$

In order to take the non-relativistic limit, similar to the example in relativistic quantum mechanics discussed in the previous section, we can separate a large mechanical part of the field $Q(x)$ as follows:

$$\begin{aligned} Q(x) = e^{-im_Q v.x}\tilde{Q}(x) &= e^{-im_Q v.x}\Big(P_+^v\tilde{Q}(x) + P_-^v\tilde{Q}(x)\Big) \\ &= e^{-im_Q v.x}(h_v(x) + H_v(x)) \end{aligned} \tag{2.62}$$

where we have labeled the fields h_v and H_v according to their velocity, and used the fact that $P_+^v + P_-^v = 1$. By inserting the above equation into the Dirac

Lagrangian, one obtain:

$$\mathcal{L} = \bar{h}_v i\not{D} h_v + \bar{H}_v i\not{D} H_v + 2m_Q \bar{H}_v H_v + \bar{h}_v i\not{D} H_v + \bar{H}_v i\not{D} h_v. \tag{2.63}$$

By introducing two auxiliary fields, we can separate the fermion field into two components, each with known solutions to the equations of motion. The Lagrangian then contains terms that mix these fields. To simplify the Lagrangian and potentially diagonalize it, the gamma matrices in the initial terms can be eliminated by employing projection operators on both the fields. This yields a more streamlined Lagrangian, which can be expressed as follows:

$$\mathcal{L} \ = \bar{h}_v \ i(v.D) \ h_v - \bar{H}_v(iv.D - 2m_Q)H_v + \bar{h}_v i\not{D}_\perp \ H_v + \bar{H}_v i\not{D}_\perp h_v, \tag{2.64}$$

where we used the definition of a perpendicular component of any four-vector a^μ based on the condition $a_\perp.v = 0$, given by

$$a_\perp^\mu = a^\mu - (a.v)v^\mu. \tag{2.65}$$

One of the features of the Lagrangian in Eq.(2.64) is that it contains two fields: The massless field, h_v, and the heavy field, H_v. The mass of H_v turns out to be $2m_Q$, which in the limit $m_Q \to \infty$ can therefore be considered as a field that describes an infinitely heavy particle. Using a similar approach that is used in the previous section, we can integrate out this degree of freedom from our theory. The proper way to do so would involve writing an effective action in terms of the functional integral and performing the integration. For the problem at hand, we can simplify the process by using the equations of motion derived from Eq.(2.64) and Eq.2.62).

The equations of motion are given by

$$(i\not{D} - m_Q)Q(x) = 0 \implies i\not{D} h_v + (i\not{D} - 2m_Q)H_v = 0. \tag{2.66}$$

By applying the projection operator, one can simplify the expression as follows:

$$H_v = \frac{1}{2m_Q + iv.D} i\not{D}_\perp h_v \tag{2.67}$$

where the inverse of the operator can be expanded using a Taylor series:

$$\frac{1}{2m_Q + iv.D} = \frac{1}{2m_Q} \sum_{n=0}^{\infty} (-1)^n \left(\frac{iv.D}{2m_Q}\right)^n . \tag{2.68}$$

The expansion mentioned is convergent, allowing us to derive an effective Lagrangian with increasing operator dimension. Using Eqn.(2.67) in Eqn.(2.64) and utilizing the expression

$$i\not{D}_\perp i\not{D}_\perp = (i\not{D}_\perp)^2 + \frac{g_s}{2}\sigma_{\mu\nu}G^{\mu\nu}, \tag{2.69}$$

one can derive the HQET Lagrangian up to $1/m_Q$ as follows:

$$\begin{aligned} \mathcal{L}_{eff} &= \bar{h}_v i(v.D)h_v + \frac{1}{2m_Q}\bar{h}_v (i\not{D}_\perp)^2 h_v + C_g \frac{g_s}{4m_Q}\bar{h}_v \sigma_{\mu\nu}G^{\mu\nu}h_v \\ &\quad + \mathcal{O}\left(\frac{1}{m_Q^2}\right). \end{aligned} \tag{2.70}$$

The HQET Lagrangian to order $\mathcal{O}(1/m_Q)$ is given by Eq.(2.70). Remarkably, in the limit $m_Q \to \infty$, only the first term survives, as evident from the Lagrangian. It is noteworthy that this leading term does not contain any Dirac matrix, despite being used to describe fermions. As a result, it enlarges the spin symmetry group of the effective theory that results from HQET.

One observation is that field redefinitions are possible in HQET. We can now derive the equations of motion for the light fields, h_v and using Eq.(2.70), yielding:

$$i(v.D)h_v = -\frac{1}{2m_Q}\left((i\not{D}_\perp)^2 + C_g \frac{g_s}{2}\sigma_{\mu\nu}G^{\mu\nu}\right) h_v. \tag{2.71}$$

One can convince oneself that, in the above equation, the expression on the left remains $\mathcal{O}(1)$, while the expression on the right is of higher order in $1/m_Q$. This allows for a redefinition of the field h_v such that certain terms in the Lagrangian can be absorbed into h_v. The equations of motion are then modified by an operator which contributes at the order higher in $1/m_Q$.

The technique of field redefinition in HQET can be illustrated with an example where the terms of the form

$$\mathcal{L}' = \frac{1}{2m_Q}\bar{h}_v(iv.D)h_v. \tag{2.72}$$

are absent. Although such operators should be allowed, they have not been included in the Lagrangian because a field redefinition of the form

$$h_v \to \left(1 - \frac{(iv.D)^2}{4m_Q}\right) h_v \tag{2.73}$$

remove $\mathcal{L}'$ entirely from consideration through field redefinitions. One can apply similar redefinitions for the field at higher orders in $1/m_Q$ as well. As a result, operators that are proportional to the lowest-order equation of motion do not make practical contributions.

Another important observation is the manipulation of spin degrees of freedom. We perform an infinitesimal spin rotation of the h_v field, i.e.

$$h_v \to h'_v = (1 + i\alpha.\mathbf{S})h_v \tag{2.74}$$

where $\mathbf{S}$ is the fermion spin operators given by

$$S_i = \frac{1}{2}\begin{pmatrix} \sigma_i & 0 \\ 0 & \sigma_i \end{pmatrix}, \ [S_i, S_j] = i\epsilon_{ijk}S_k. \tag{2.75}$$

Since $\mathbf{S}$ commutes with γ^0 and $v.D$ contains no Dirac matrices, it follows that

$$\partial\mathcal{L}^{\infty}_{eff} \ = \ 0 \tag{2.76}$$

where $\mathcal{L}^{\infty}_{eff}$ is the effective Lagrangian at leading order in $1/m_Q$. The Lagrangian $\mathcal{L}^{\infty}_{eff}$ obtained through the field redefinition technique exhibits an additional spin symmetry given by a SU(2) group as the spin transformations belong to SU(2).

This symmetry is absent in the original lagrangian given in Eq.(2.61) as it appears as a consequence of spin transformations in $\mathcal{L}_{eff}^{\infty}$.

In QCD flavor-changing interactions are absent, which any EFT of QCD must respect. Till now, we have considered only one flavor of heavy quark. In nature, there are several flavors of heavy quarks (top, bottom, and charm), and thus, the total symmetry group of the HQET is enlarged. If N_f is the number of heavy quarks, the total symmetry becomes $SU(2N_f)$. Because of this property, HQET becomes a powerful tool for the computation of physical properties involving heavy quark transitions. Furthermore, when examining the symmetry-breaking (or $1/m_Q$ suppressed) terms in the Lagrangian of Eq.(2.70), it is illuminating to switch to a heavy quark rest frame. The first operator, i.e.,

$$\mathcal{O}_{kin} = \frac{1}{2m_Q}\bar{h}_v(iv.D)^2 h_v \implies \frac{1}{2m_Q}\bar{h}_v(\mathbf{D})^2 h_v, \tag{2.77}$$

can be reinterpreted as representing the kinetic energy carried by the heavy quark inside the hadron. Moreover, the second operator,

$$\mathcal{O}_{mag} = \frac{g_s}{4m_Q}\bar{h}_v\sigma_{\mu\nu}G^{\mu\nu}h_v \implies -\frac{1}{m_Q}\bar{h}_v(\mathbf{S}.\mathbf{B})h_v, \tag{2.78}$$

can be understood as the interaction of the heavy quark with the chromomagnetic field inside the heavy hadron. This provides physical insight into the meaning of these terms in the Lagrangian.

The spin symmetry of the heavy quark Lagrangian has direct implications for the spectroscopy of meson states such as B_q and B_q^*. These mesons are composed of a heavy $\bar{b}$ antiquark and a light u (or d or s) quark, with the only distinction being the spin configuration of these quarks. The B_q meson has a relative singlet spin state, while the B_q^* meson has a relative triplet spin state. A crucial observation is that, in the heavy quark limit, the spin interaction in HQET is subleading term in the expansion. As a result, the masses of these two states become degenerate. This is consistent with experimental observations, where the mass difference between B_q^* and B_q mesons is found to be small, with a value of 45.0 ± 0.4 MeV This phenomenon is a consequence of the spin symmetry in HQET and provides important insights into the spectroscopy of heavy mesons (for details, see [50, 53, 54, 104]).

With this brief description of IR divergences and EFTs of type I and II, we will now discuss their applications to exclusive and inclusive semi-leptonic B meson decays in the remaining of the thesis.

Chapter 3

Soft photon effects in $B \to K\ell\ell$

In this chapter, our main focus is on the decay modes $B \to K\ell^+\ell^-$, which are induced by the FCNC currents. We specifically calculate the impact of the soft photon QED corrections on its branching ratio and R_K (defined in Section- 3.1). These corrections involve both virtual corrections, and contributions from the emission of a single photon at $\mathcal{O}(\alpha_{em})$. We further establish that the combination of these two corrections leads to a finite result, which is a consequence of Bloch-Nordsieck theorem. Considering the significance of these decay modes (such as the construction of LFU observable, R_K), it is important to account for these effects to establish its theoretical cleanliness. This chapter is based on the findings of Ref. [26].

3.1 Introduction

As discussed in Chapter-1.1, the processes induced by FCNCs are considered rare in the SM. Fig.(3.1) shows the Feynaman diagrams of $B \to K\ell^+\ell^-$ decay mode for two different topologies (penguin and box). These decays, which are both loop and CKM suppressed, offer a perfect opportunity to search for physics beyond the SM. The quark level transition $b \to s\ell^+\ell^-$ has been significant in our search for new physics. It not only helps us uncover new phenomena but also enhances our understanding of the intricate interplay between the electroweak and strong interactions. This transition is particularly relevant in studying the purely leptonic decay channel $B_s \to \ell^+\ell^-$ as well as the exclusive semi-leptonic

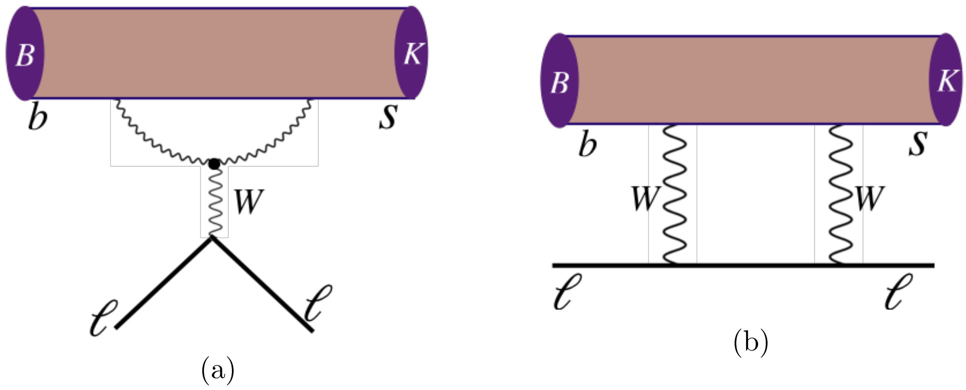

Figure 3.1: Feynaman diagrams of $B \to K\ell^+\ell^-$ for two different topologies: (a) penguin (b) box.

channels $B \to K^{(*)}\ell^+\ell^-$ (for examples, see [96, 105–110]).

Regarding the theory behind these decays, precise calculations have been carried out to improve our understanding of the involved form factors and related issues [67, 111], while at the experimental front, more refined data have indicated certain deviations from the expected results within the SM for the branching ratios of $B \to K\ell^+\ell^-$ decays. Although these deviations are not yet completely conclusive, they could be pointing towards the possibility of NP being just around the corner. Nevertheless, reaching a clear and definitive conclusion is somewhat obscured by uncertainties related to the behavior of particles within hadrons and potential interference from distant effects such as remnants of charmonium resonances [67, 111]. The search for precise tests of the SM using rare decays and the exploration of NP has prompted the consideration of theoretically clean observables, also known as optimized observables in certain specific contexts. The main idea is to consider or form observables, often in the form of ratios, that are mostly unaffected by uncertainties related to hadrons, at least within a chosen kinematic range.

The decay processes $B \to K\ell^+\ell^-$ provide a way to investigate LFU, which examines whether the decays into electrons ($\ell = e$) and muons ($\ell = \mu$) occur with the same probability. In the SM, the universal interaction of the Z-boson with leptons ensures this equality, accounting for the slight differences in lepton masses. When we choose a specific kinematical range in the decay process, such that the dilepton invariant mass is significantly larger than the mass of each individual lepton, we expect the ratio of the two measured branching ratios to be very close to one. This ratio is commonly used as a reliable test to examine LFU and, consequently, to assess the validity of the Standard Model [112, 113].

$$R_K^{\mu e} \equiv \frac{\int_{1GeV^2}^{6GeV^2} dq^2 \frac{d\Gamma(B^0 \to K^0 \mu^+ \mu^-)}{dq^2}}{\int_{1GeV^2}^{6GeV^2} dq^2 \frac{d\Gamma(B^0 \to K^0 e^+ e^-)}{dq^2}} \tag{3.1}$$

Within SM, this ratio is unity and the very recent experiment result [114] is in agreement with the SM within $\sim 1\sigma$:

$$R_K^{\mu e}|_{exp} = 0.949^{+0.042\ +0.041}_{+0.022\ -0.022} \tag{3.2}$$

Previously, the inconsistency between theoretical predictions and experimental results provided a strong incentive to conduct more precise theoretical calculations before drawing conclusions about NP. Though, the current experimental data aligns with the theoretical predictions, it is still important to thoroughly examine all potential sources of uncertainties and other effects that might impact theoretical predictions.

In terms of theory, the standard approach involves constructing an effective Hamiltonian by integrating out heavy degrees of freedom through the OPE. This Hamiltonian is then evolved down to the scale of the b quark using RGEs. Using the quark level operators $b \to s\ell\ell$, the calculations of physical hadronic matrix elements are performed. This step introduces the concept of form factors, which contribute to the uncertainties in the calculations, as mentioned earlier. To mitigate these uncertainties, observables that are minimally affected by form factors are considered. The effects of strong interactions, including both perturbative and non-perturbative aspects, are incorporated through the use of RGEs and form factors, respectively. Whether there are any additional effects that could be significant, particularly the corrections due to QED, have not been explicitly considered. Since charged particles are involved, the effects of soft photons may be non-negligible and should be accounted for systematically. Such corrections are found to be useful in the context of B-decays [22–25].

3.2 Non-radiative $B \to K\ell^+\ell^-$

The effective Hamiltonian (defined in Eq.(2.46)) relevant for describing the $b \to s\ell^+\ell^-$ transition reads [48, 49]

$$H_{eff} = 4\frac{G_F}{\sqrt{2}}V_{ts}^* V_{tb}\sum_{i=1}^{10} C_i(\mu)Q_i(\mu) \tag{3.3}$$

where all the operators are defined in Section-2.2. The operators Q_7, Q_9, and Q_{10} are particularly important for this semi-leptonic process. The matrix elements of these operators represent non-perturbative quantities, and they can be parametrized in terms of form factors incorporating both Dirac and Lorentz structures. The Wilson coefficients used in the calculation are: $C_7^{eff} = -0.319$, $C_9 = 4.228$ and $C_{10} = -4.410$. Further, C_9^{eff} is defined by [115]

$$\begin{aligned}
C_9^{eff} &= C_9 + Y^{pert}(q^2) \\
Y^{pert}(q^2) &= h(q^2, m_c)\left(\frac{4}{3}C_1 + C_2 + 6C_3 + 60C_5\right) - \frac{1}{2}h(q^2, m_b)\left(7C_3 + \frac{4}{3}C_4\right. \\
&+ \left. 76C_5 + \frac{64}{3}C_6\right) - \frac{1}{2}h(q^2, 0)\left(C_3 + \frac{4}{3}C_4 + 16C_5 + \frac{64}{3}C_6\right) \\
&+ \frac{4}{3}C_3 + \frac{64}{9}C_5 + \frac{64}{27}C_6
\end{aligned} \tag{3.4}$$

where

$$h(q^2, m_q) = \frac{4}{9}\ln\left(\frac{m_q^2}{\mu^2}\right) + \frac{8}{27} + \frac{4}{9}\left(\frac{4m_q^2}{q^2}\right) - \frac{4}{9}\left(2 + \frac{4m_q^2}{q^2}\right)\sqrt{\left|\frac{4m_q^2}{q^2} - 1\right|}
\begin{cases} -\frac{i\pi}{2} + \ln\left(\frac{1+\sqrt{1-\frac{4m_q^2}{q^2}}}{\sqrt{\frac{4m_q^2}{q^2}}}\right), & \text{if } \frac{4m_q^2}{q^2} \leq 1 \\ \arctan\left(\frac{1}{\sqrt{\frac{4m_q^2}{q^2}-1}}\right), & \text{if } \frac{4m_q^2}{q^2} < 1 \end{cases} \tag{3.5}$$

The probability amplitude for the decay mode $B(p_B) \to K(p_K)\ell^+(p_2)\ell^-(p_3)$ can be written in the following form [107]

$$\begin{aligned}
\mathcal{M}_0 &= \left(\frac{G_F \alpha_{em} |V_{ts}^* V_{tb}|}{2\sqrt{2}\pi}\right) \left[T_\mu^1 \, (\bar{l}\gamma^\mu l) + T_\mu^2 \, (\bar{l}\gamma^\mu \gamma^5 l)\right] \\
&= \left(\frac{G_F \alpha_{em} |V_{ts}^* V_{tb}|}{2\sqrt{2}\pi}\right) (\bar{l}\Gamma_A^\mu l) \, \otimes \, H_{A\mu}(p, p')
\end{aligned} \tag{3.6}$$

where

$$\Gamma^\mu_{A=1} = \gamma^\mu, \qquad T_{1\mu}(p_B, p_K) = A' \, p_\mu + B' \, q_\mu \tag{3.7}$$

and

$$\Gamma^\mu_{A=2} = \gamma^\mu \gamma^5, \qquad T_{2\mu}(p_B, p_K) = C' \, p_\mu + D' \, q_\mu \tag{3.8}$$

We have introduced the following momentum combinations: $p_\mu = (p_B + p_K)_\mu$ and $q_\mu = (p_B - p_K)_\mu = (p_2 + p_3)_\mu$. In the following analysis, two frequently used kinematical invariant variables are $s = p^2 = (p_B + p_K)^2$, and the dilepton invariant mass squared, $q^2 \equiv (p_B - p_K)^2 = (p_2 + p_3)^2$.

The remaining factors in the amplitude depend on the combinations of the Wilson coefficients (C_7^{eff}, C_9^{eff}, and C_{10}) and form factors (f_+, f_-, and f_T), and are expressed as follows:

$$\begin{aligned}
A' &= C_9^{eff} f_+(q^2) + \frac{2m_b}{m_K + m_B} C_7^{eff} f_T(q^2), \\
B' &= C_9^{eff} f_-(q^2) - \frac{2m_b(m_B - m_K)}{q^2} C_7^{eff} f_T(q^2), \\
C' &= C_{10} f_+(q^2), \qquad D' = C_{10} f_-(q^2)
\end{aligned} \tag{3.9}$$

Now, the non-radiative differential decay rate is calculated as:

$$\frac{d^2\Gamma_0(B \to K l^+ l^-)}{dq^2 ds} = \frac{1}{256\pi^3 m_B^3} |\mathcal{M}_0(B \to K l^+ l^-)|^2 \tag{3.10}$$

where the explicit structure of the matrix element, $\mathcal{M}_0$, is:

$$\begin{aligned}\mathcal{M}_0(B \to Kl^+l^-) &= \frac{G_F\alpha}{2\sqrt{2}\pi}V_{ts}^*V_{tb}\Bigg[\Bigg(\left\{C_9^{eff}f_+ + C_7^{eff}\frac{2f_Tm_b}{m_B+m_k}\right\}p^\mu \\ &+ \left\{C_9^{eff}f_- - C_7^{eff}\frac{2f_Tm_b}{q^2}(m_B-m_k)\right\}q^\mu\Bigg)\left(\bar{l}\gamma_\mu l\right) \\ &+ \left(C_{10}f_+p^\mu + C_{10}f_-q^\mu\right)\left(\bar{l}\gamma_\mu\gamma_5 l\right)\Bigg] \end{aligned} \tag{3.11}$$

The form factors $f_+(q^2)$, $f_-(q^2)$ and $f_T(q^2)$ are parametrized as [110, 116]

$$f_i(q^2) = \frac{f_i(0)}{1-\frac{q^2}{m^2_{res,i}}}\left[1+b_{1i}\left(z(q^2)-z(0)+\frac{1}{2}\left(z^2(q^2)-z^2(0)\right)\right)\right]$$

where, $i = +,\ 0,\ T$;

$$f_- = (f_0 - f_+)\,\frac{m_B^2-m_K^2}{q^2}$$

$z(q^2)$ is defined by

$$z(q^2) = \frac{\sqrt{\tau_+-q^2}-\sqrt{\tau_+-\tau_0}}{\sqrt{\tau_+-q^2}+\sqrt{\tau_+-\tau_0}} \tag{3.12}$$

where

$$\tau_0 = \sqrt{\tau_+}\left(\sqrt{\tau_+}-\sqrt{\tau_+-\tau_-}\right), \qquad \tau_\pm = (m_B \pm m_K)^2 \tag{3.13}$$

with $f_i(0) = \{0.34,\ 0.34,\ 0.39\}$, $b_{1i} = \{-2.1,\ -4.3,\ -2.2\}$ and $m_{res\ i} = \{5.83,\ 5.37,\ 5.41\}$ for $i = (+,\ 0,\ T)$, respectively.

3.3 QED Corrections to $B \to K\ell\ell$

Now, let us shift our focus to the consideration of QED corrections. Fig.(3.2) illustrates the diagrams involving photon emission where, $\times$ represents potential emission points, including those from the B and K meson legs when charged. These diagrams are computed assuming the mesons to be point-like and employing scalar QED. Fig.(3.2b) is commonly known as the "contact term" and arises when the gauge invariance of QED is demanded. Another way to compute the contact term is by assuming the mesonic level Lagrangian and following the minimal coupling prescription. This approach is discused in [117]. Fig.(3.3) shows

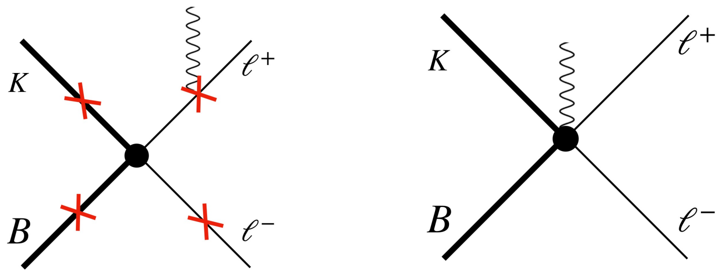

(a) X :photon emission (b) Contact term

Figure 3.2: Representative diagram for real photon emission

a set of representative diagrams that contribute to the virtual corrections. It is evident from the figure that the diagrams incorporating photons from the contact term are also accounted for to ensure the cancellation of infrared divergences and to obtain a gauge invariant result. The photon momentum is denoted by k in

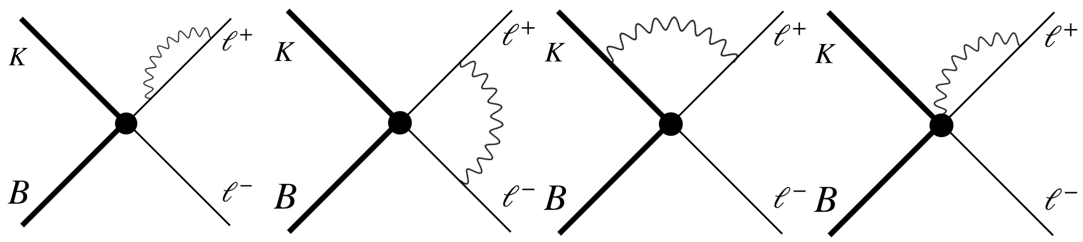

(a) (b) (c) (d)

Figure 3.3: Representative diagrams contributing to virtual corrections

the calculations below, and the polarization vector is denoted by $\epsilon_\alpha(k)$. Let us consider the general case where the charges of the B and K mesons are represented by Q_B and Q_K respectively. Since we are primarily concerned with lepton number conserving processes, we will eventually impose $Q_B = Q_K$. However, for the time being, we will keep them as general variables.

3.3.1 Contact Term

Before performing explicit calculations for the virtual corrections and real emission contributions, it is necessary to address the contact term. To do so, let us examine the emission of photons from different legs. The specific process under investigation is $B(p_B) \to K(p_K)\ell^+(p_2)\ell^-(p_3)\gamma(k)$. For the mesons, scalar QED is employed. Consequently, the matrix element for photon emission from the external legs, which is expressed in terms of quantities relevant to the non-radiative decay, can be written as follows:

$$\begin{aligned}
\tilde{M} &= -e\epsilon_\alpha(k)\bar{u}(p_2)\Gamma^\mu_A \frac{(\not{p}_3 + \not{k}) - m_l}{2p_3.k}\gamma^\alpha v(p_3) \otimes H_{A\mu}(p_B, p_K) \\
&+ e\epsilon_\alpha(k)\bar{u}(p_2)\gamma^\alpha \frac{(\not{p}_2 + \not{k}) + m_l}{2p_2.k}\Gamma^\mu_A v(p_3) \otimes H_{A\mu}(p_B, p_K) \\
&+ eQ_B\epsilon_\alpha(k)\frac{2p_B^\alpha}{2p_B.k}\bar{u}(p_2)\Gamma^\mu_A v(p_3) \otimes H_{A\mu}(p_B - k, p_K) \\
&- eQ_K\epsilon_\alpha(k)\frac{2p_K^\alpha}{2p_K.k}\bar{u}(p_2)\Gamma^\mu_A v(p_3) \otimes H_{A\mu}(p_B, p_K + k)
\end{aligned} \tag{3.14}$$

From the equation above, it is evident that when the photon is emitted from one of the leptons, the momentum dependence of the hadronic component $H_{A\mu}$ retains the same form as in the non-radiative decay. However, in the case of photon emission from the meson legs, the dependence is modified accordingly. By considering the specific structure of $H_{A\mu}$, we can express the above equation in a compact form:

$$\tilde{M} = \mathcal{M}_0 e\epsilon_\alpha \sum_i \frac{Q_i\eta_i p_i^\alpha}{p_i.k} + M'(k) \tag{3.15}$$

In the above equation, the momenta and charges of different particles are denoted by p_i and Q_i respectively, while η_i takes the values $+$ or $-$ depending on whether the particle is outgoing or incoming [118]. The term $\mathcal{M}_0$ represents the amplitude for the process without photon emission. The first term in the equation corresponds to the Low's soft photon amplitude: $M(a \to b\gamma(k))|_{k\to 0} = S \otimes M(a \to b)$, where S is the universal soft function that multiplies $\mathcal{M}_0$. It can be verified that the Low's term alone is gauge invariant. Computing this term is straightforward as the hadronic contribution is the same as in the case of the non-radiative amplitude. The remaining part is denoted as $M'(k)$ and represents the non-infrared contribution. Unlike the Low's term, which is of $\mathcal{O}(1/k)$, the terms in $M'(k)$ are of $\mathcal{O}(k)$ and higher. We will now focus on evaluating $M'(k)$.

We can express $M'(k)$ as the sum of two contributions: M'_{lept}, arising from photon emission from the leptons, and M'_{mes}, arising from photon emission from the mesons. These contributions are given by:

$$M'_{lept} = e\epsilon_\alpha(k)\left[\bar{u}(p_2)\gamma^\alpha \frac{\not{k}}{2p_2.k}\Gamma^\mu_A v(p_3) - \bar{u}(p_2)\Gamma^\mu_A \frac{\not{k}}{2p_3.k}\gamma^\alpha v(p_3)\right] \otimes H_{A\mu}(p_B, p_K) \tag{3.16}$$

and

$$M'_{mes} = -e\epsilon_\alpha(k)\left[Q_B\alpha_A \frac{2p_B^\alpha}{2p_B.k} + Q_K\beta_A \frac{2p_K^\alpha}{2p_K.k}\right] \bar{u}(p_2)\Gamma^\mu_A v(p_3)\, k_\mu \tag{3.17}$$

where $\alpha_A = A' + B'$ or $C' + D'$ and $\beta_A = A' - B'$ or $C' - D'$ for $A = 1, 2$. We have used the fact that the general structure of $H_{A\mu}$ can be written as

$$H_{A\mu}(p, q) = X_A\, p_\mu + Y_A\, q_\mu \tag{3.18}$$

which allows us to incorporate the appropriate momentum dependence when an additional photon is emitted.

Thus, the total contribution beyond Low's soft photon contribution is given by

$$M'(k) = M'_{lept} + M'_{mes} \tag{3.19}$$

The gauge invariance of $M'(k)$ can be verified by making the replacement $\epsilon_\alpha \to k_\alpha$. This replacement yields zero for M'_{lept}, indicating its gauge invariance. On the other hand, for M'_{mes}, the replacement yields

$$M'_{mes}|_{\epsilon_\alpha \to k_\alpha} = -e(Q_B + Q_K)\xi_A k_\mu \left[\bar{u}(p_2)\Gamma^\mu_A v(p_3)\right] \tag{3.20}$$

where $\xi_A = A'(q^2), (C'(q^2))$ for $A = 1(2)$.

This violation of gauge invariance indicates that a contribution should be added to ensure gauge invariance of the full amplitude. The contribution is a negative of the above quantity. This additional contribution takes the form of a contact term and can be incorporated into the effective Hamiltonian at the hadronic level as follows:

$$\mathcal{H}_{eff}^{CT} \ = ie\xi_A(Q_B + Q_K)\left[\bar{u}(p_2)\Gamma_A^{\alpha} v(p_3)\right] A_\alpha \tag{3.21}$$

This contact term, shown in Fig.(3.2b), contributes to both the real emission and virtual corrections and is of $\mathcal{O}(k)$. It should be noted that the contact term is proportional to the sum of the charges Q_B and Q_K, and thus has no effect when B and K are neutral.

Here, we would like to take a short detour and compare our method of calculating the contact term with the one adopted in Ref.[117]. Our method [26] of determining the contact terms differs from the approach adopted in [117]. In that work, a mesonic level Lagrangian with a specific operator structure is assumed, and the contact terms are obtained by applying the minimal coupling prescription $\partial_\mu \to \partial_\mu - ieA_\mu$. In contrast, the contact terms obtained here include effects from all operators contributing to this process. As a result, there may be slight differences in the numerical values of the corrections compared to those in [117]. However, there is generally good agreement between the two results.

After addressing the gauge invariance requirement by fixing the contact term, our next step is to compute the $\mathcal{O}(\alpha_{em})$ corrections. This involves evaluating the rate of real photon emission and the virtual corrections to the non-radiative amplitude at that order. We then square the amplitude, taking into account the interference terms between the lowest order and $\mathcal{O}(\alpha_{em})$ contributions. Finally, to compare with experimental observations, we add these two components incoherently. Our calculations closely follow the methodology described in [73]. To handle the infrared divergences, we introduce a small mass $m_\gamma = \lambda$ for the photon. This regularization takes care of IR divergences. While the loop integrals are regularized using Dimensional Regularization.

3.3.2 Real Photon Emission

The total contribution to the amplitude of real photon emission in the process $B(p_B) \to K(p_K)\ell^+(p_2)\ell^-(p_3)\gamma(k)$ is obtained by combining Low's infrared (IR) terms, $M'(k)$, with the contribution from the contact term. At the level of decay rate, we can express it as:

$$d\Gamma_{real} = d\Gamma_0(2\alpha_{em}\tilde{B}) + d\Gamma' \tag{3.22}$$

Here, $d\Gamma_0$ represents the decay rate without photon emission, and the quantity $\tilde{B}$ captures the IR contribution arising from Low's term. It is given by:

$$\tilde{B} = \frac{1}{8\pi^2}\int \frac{d^3k}{\sqrt{k^2+\lambda^2}}\left(\sum_i \frac{Q_i\eta_i p_i^\alpha}{p_i.k}\right)^2 \tag{3.23}$$

We can observe that in the present case, the universal soft factor S is given by the product of the photon polarization vector $\epsilon_\alpha(k)$ and $\tilde{T}^\alpha(k)$, which can be expressed as:

$$\tilde{T}^\alpha(k) = -\frac{2p_i^\alpha\eta_i}{2k.p_i\eta_i} + \frac{2p_j^\alpha\eta_j}{2k.p_j\eta_j}$$

By utilizing charge conservation ($\sum_i Q_i\eta_i = 0$), we can rewrite $\tilde{B}$ as:

$$\tilde{B} = \frac{1}{8\pi^2}\int_0^{k_{max}} \frac{d^3k}{\sqrt{k^2+\lambda^2}} \sum_{i\neq j, i<j} Q_iQ_j\eta_i\eta_j\left(\frac{p_i^\alpha}{p_i.k} - \frac{p_j^\alpha}{p_j.k}\right)^2 \tag{3.24}$$

Here, we have explicitly introduced $k_{\rm max}$, representing the maximum photon energy of the soft photon. The theoretical rate will therefore depend on the chosen value of $k_{\rm max}$. As evident from the above equation, the indices i and j take values of $i = 1, 2, 3$ and $j = 2, 3, 4$, corresponding to the particles B, K, ℓ^+, and ℓ^-, respectively.

The contribution of $\tilde{B}$ in the decay of the charged B meson consists of six terms, given by:

$$\tilde{B} = \tilde{B}_{BK} + \tilde{B}_{Bl^+} + \tilde{B}_{Bl^-} + \tilde{B}_{Kl^+} + \tilde{B}_{Kl^-} + \tilde{B}_{l^+l^-}$$

Upon integrating over k, $\tilde{B}$ can be expressed as (refer to Appendix-B for the encountered integrals during the calculation):

$$\tilde{B_{ij}} = \frac{Q_i Q_j \eta_i \eta_j}{2\pi} \left\{ \ln\left(\frac{k_{max}^2 m_i m_j}{\lambda^2 E_i E_j}\right) - \frac{p_i.p_j}{2}\left[\int_{-1}^{1} \frac{dx}{p_x^2} \ln\left(\frac{k_{max}^2}{E_x^2}\right) + \int_{-1}^{1} \frac{dx}{p_x^2} \ln\left(\frac{p_x^2}{\lambda^2}\right)\right]\right\} \tag{3.25}$$

To simplify the evaluation of the above integrals, we introduce the following combinations as convenient parameterizations:

$$\begin{aligned} 2p_x &= (1+x)p_i + (1-x)p_j \\ 2E_x &= (1+x)E_i + (1-x)E_j \\ 2p'_x &= (1+x)p_i\eta_i - (1-x)p_j\eta_j \end{aligned} \tag{3.26}$$

Here, $p_{i,j}$ represent the four-momenta, while $E_{i,j}$ denote the energies of the particles. These relations yield:

$$\begin{aligned} p_x^2 &= (1+x)^2 p_i^2 + (1-x)^2 p_j^2 + 2(1-x^2) p_i.p_j \\ p_x'^2 &= (1+x)^2 p_i^2 + (1-x)^2 p_j^2 - 2(1-x^2) p_i.p_j \eta_i \eta_j \end{aligned} \tag{3.27}$$

The contribution to the decay rate that does not involve IR effects consists of terms beyond the Low's term in the amplitude, starting from order $\mathcal{O}(k)$ and higher. These terms, along with the interference between the IR and non-IR terms, contribute to the remaining terms in the decay rate. Upon investigation, it is found that the squared non-IR terms have a negligible impact and are therefore not considered in the analysis. However, the interference terms play a significant role. These interference terms depend on the angle θ between the negatively charged lepton and the photon. It is observed (as demonstrated below) that the correction factor, denoted as Δ^i (with $i = e$ or μ), is highly sensitive to a lower angular cut θ_{cut} for $i = e$ due to the small mass of the electron. Conversely, for the chosen values of k_{max}, there is minimal effect when $i = \mu$.

3.3.3 Virtual Photon Corrections

There are three types of diagrams that contribute to virtual corrections: (a) diagrams with a photon starting and ending at the same charged particle leg (see Fig.(3.3a)); (b) diagrams with a photon line connecting two different charged particles (see Fig.(3.3b) and Fig.(3.3c)); (c) diagrams with a photon originating from the effective vertex (contact term) and ending on a charged particle leg (see Fig.(3.3d)).

Let us first examine the set of diagrams arising from the contact term, specifically focusing on the case where the photon from the contact vertex attaches to the lepton leg. This contribution is canceled out by an equally opposite diagram where the photon attaches to the anti-lepton leg. The other two diagrams, where the photon from the contact vertex ends at either the B or K leg, can be evaluated straightforwardly. These diagrams exhibit UV divergences as well as a finite part (M_{CT}). To eliminate or absorb these UV divergences systematically, additional higher-dimensional operators are required. It is important to note that the motivation behind introducing the contact term was to ensure gauge invariance of the real emission amplitude. Since this amplitude is of $\mathcal{O}(e)$, the resulting contact term is also of the same order, involving only one photon. It is possible, however, to have terms that vanish for on-shell photons but can contribute to virtual corrections. When evaluating the virtual corrections, an extra factor of e is introduced, making this correction of $\mathcal{O}(e^2)$. From the perspective of an effective theory, operators corresponding to terms involving leptons, B and K mesons, and two photons, such as the one depicted in Fig.(3.4), can exist. These operators would give rise to diagrams similar to those shown on the right side of Fig.(3.4). In dimensional regularization, scale-less integrals simply evaluate to zero. To ensure consistency, it becomes necessary to include other higher-dimensional operators at $\mathcal{O}(e)$, including derivative operators, up to the given order. One possible approach is to begin with the effective Hamiltonian, which includes the one-photon contact term, and then impose gauge invariance on the two-photon emission amplitude. This process would determine the two-photon contact term and potentially introduce additional terms corresponding to higher-dimensional operators. However, it should be noted that there is no guarantee that these terms will be completely determined, as their determination relies on the on-shellness of the two photons. Alternatively, following the suggested prescription in [117], one can consider higher-dimensional derivative

Figure 3.4: Two photon Contact Term. (Left) real emission (Right) Virtual correction

operators and use minimal coupling to generate the required terms. However, it is important to exercise caution, as the minimal coupling prescription may have ambiguities [119]. Careful consideration should be given to fixing the structure of such terms, while also acknowledging the possibility of multiple structures for these terms [1]. Perhaps a more suitable approach would involve starting with quark-level operators and computing the matrix element, for example, using the sum rule approach:

$$\begin{aligned}\langle K(p_K)\ell^+\ell^-\gamma(k)|(\bar{\ell}\Gamma_\mu\ell)\,(\bar{s}\Gamma'_\mu b)|B(p_B)\rangle \;\;\propto\;\; \epsilon^\alpha \int d^4x e^{ik.x}\langle K(p_K)\ell^+\ell^-|T\big[j^{em}_\alpha(x) \\ (\bar{\ell}\Gamma_\mu\ell)(\bar{s}\Gamma'_\mu b)(0)\big]|B(p_B)\rangle\end{aligned}$$

This matrix element generally consists of two types of terms: (i) photon emission from the leptons multiplied by the B to K matrix element, and (ii) photon emission from the hadronic system. By employing the QED Ward identity, the general structure of the hadronic tensor can be determined, and subsequently, the new form factors can be evaluated or at least estimated within the factorization approximation. This procedure can be repeated for the case of two-photon emission. It is evident that evaluating these new matrix elements can become quite challenging. Therefore, a separate analysis will be conducted, comparing the results obtained from different approaches. Considering the complexities involved, which are beyond the scope of this study, we opt to disregard the encountered UV divergences in the evaluation of diagrams involving the contact term and incorporate only the finite parts in our calculation. Explicit numerical tests confirm that these finite contributions are relatively insignificant and do

[1]The need to go beyond minimal coupling is also emphasized in [117].

not significantly impact the precision of the overall computation.

Upon evaluating the remaining diagrams, the following expression is obtained:

$$M_{\text{virtual}} = \mathcal{M}_0 \left[1 + \alpha_{em} B + \frac{\alpha_{em}}{2\pi}\right] + M_{CT} \tag{3.28}$$

In this equation, the last term in the parentheses represents the magnetic moment-like term, which is free from divergences. The quantity denoted as B encompasses contributions from the self-energy and vertex corrections, given by:

$$\begin{aligned} B \;\; = \;\; & \frac{i}{8\pi^3} \int d^4k \frac{1}{(k^2 - \lambda^2 + i\epsilon)} \Big[\sum_{i=1}^{4} \frac{Q_i^2 (2p_i - k)^2}{(k^2 - 2k.p_i)^2} \\ & -2 \sum_{i \neq j, i<j} \frac{Q_i Q_j \eta_i \eta_j (2p_i\eta_i - k).(2p_j\eta_j + k)}{(k^2 - 2k.p_i\eta_i)(k^2 + 2k.p_j\eta_j)} \Big] \end{aligned} \tag{3.29}$$

Using charge conservation $\sum_i Q_i \eta_i = 0$, B can be rewritten as:

$$B = \frac{-i}{8\pi^3} \int d^4k \frac{1}{(k^2 - \lambda^2 + i\epsilon)} \sum_{i \neq j, i<j} Q_i Q_j \eta_i \eta_j \left(\frac{2p_i^\alpha \eta_i - k^\alpha}{k^2 - 2k.p_i\eta_i} + \frac{2p_j^\alpha \eta_j + k^\alpha}{k^2 + 2k.p_j\eta_j} \right)^2 \tag{3.30}$$

Here, $i = 1, 2, 3$ and $j = 2, 3, 4$, where the numbers $1, 2, 3$, and 4 represent the particles B, K, ℓ^+, and ℓ^-, respectively.

Now, in the case of $B \to K\ell^+\ell^-$, where both the mesons and the leptons are charged, a total of six diagrams contribute to B. These contributions can be divided as follows:

$$B = B_{BK} + B_{Bl^+} + B_{Bl^-} + B_{Kl^+} + B_{Kl^-} + B_{l^+l^-}$$

After integrating over k and employing Dimensional Regularization, the general structure of B_{ij} is calculated to be:

$$B_{ij} = \frac{-1}{2\pi} Q_i Q_j \eta_i \eta_j \left[ln(\frac{m_i m_j}{\lambda^2}) + \frac{1}{4} \int_{-1}^{1} dx ln(\frac{p_x'^2}{m_i m_j}) + \frac{p_i.p_j \eta_i \eta_j}{2} \int_{-1}^{1} \frac{dx}{p_x'^2} ln(\frac{p_x'^2}{\lambda^2}) \right] \tag{3.31}$$

The relevant integrals encountered are collected in Appendix-B.

3.3.4 Sommerfeld factor

We have also taken into account the Sommerfeld enhancement factor, also known as the Coulomb factor, which arises from the difference in scattering between the presence and absence of a potential [71]. This correction is a multiplicative factor given by:

$$\Omega_c = \frac{-2\pi\alpha_{em}}{\beta_{ij}} \frac{1}{e^{\frac{-2\pi\alpha_{em}}{\beta_{ij}}} - 1} \tag{3.32}$$

Here, β_{ij} represents the relative velocity between the i^{th} and j^{th} particles and is defined as:

$$\beta_{ij} = \sqrt{1 - \frac{m_i^2 m_j^2}{(p_i.p_j)^2}}. \tag{3.33}$$

3.3.5 Total $\mathcal{O}(\alpha_{em})$ QED corrections

Now we can proceed to compute the decay rate up to $\mathcal{O}(\alpha_{em})$:

$$d\Gamma_{real} = d\Gamma_0 \left(1 + 2\alpha_{em}\tilde{B} + 2\alpha_{em}B + \frac{\alpha_{em}}{\pi}\right)\Omega_c \tag{3.34}$$

Both $\tilde{B}$ and B (or equivalently $\tilde{B}_{ij}$ and B_{ij}) depend on the fictitious photon mass λ, which was introduced to regulate the IR divergences. It is expected that the final result for the physical rate should be independent of λ. We define $\mathcal{H}_{ij} = B_{ij} + \tilde{B}_{ij}$ as follows:

$$\begin{aligned}
\mathcal{H}_{ij} \;=\; & \frac{-Q_iQ_j\eta_i\eta_j}{2\pi}\left[-\ln\left(\frac{k_{max}^2}{E_iE_j}\right) + \frac{1}{4}\int_{-1}^{1} dx \ln\left(\frac{p_x'^2}{m_im_j}\right)\right. \\
& + \frac{p_i.p_j\eta_i\eta_j}{2}\int_{-1}^{1}\frac{dx}{p_x'^2}\ln\left(\frac{p_x'^2}{\lambda^2}\right) + \frac{p_i.p_j}{2}\int_{-1}^{1}\frac{dx}{p_x^2}\ln\left(\frac{k_{max}^2}{E_x^2}\right) \\
& \left. + \frac{p_i.p_j}{2}\int_{-1}^{1}\frac{dx}{p_x^2}\ln\left(\frac{p_x^2}{\lambda^2}\right)\right]
\end{aligned} \tag{3.35}$$

where

$$\begin{aligned}
p_x'^2 &= (1+x)^2p_i^2 + (1-x)^2p_j^2 - 2(1-x^2)p_i.p_j\eta_i\eta_j \\
p_x^2 &= (1+x)^2p_i^2 + (1-x)^2p_j^2 + 2(1-x^2)p_i.p_j
\end{aligned}$$

We observe that for $\eta_i\eta_j = -1$ (i.e., one incoming and one outgoing particle), $p_x'^2 = p_x^2$, leading to the cancellation of the λ^2 term in $\mathcal{H}_{ij}$. In the other case when $\eta_i\eta_j = 1$ (both are either incoming or outgoing particles), changing $x \to 1/x$ leads to $p_x'^2 \to p_x^2/x^2$ and the final result is again independent of λ. (Note: Since $x \in (-1, 1)$, changing it to $\frac{1}{x}$ leads to trouble at $x = 0$. We have verified that the imaginary part of the quantity B corresponds to the Coulomb/Sommerfeld factor. As we have explicitly considered this term, we only consider the real part of B when evaluating the results.) This explicitly confirms that the physical rate is independent of the IR regulator λ introduced in the intermediate steps of the calculation, ensuring that it is free from IR divergences. This serves as a crucial validation of the performed calculation.

The double differential decay rate up to $\mathcal{O}(\alpha_{em})$, denoted by $i = 0$ or c for neutral and charged B decay modes respectively, can be expressed as follows:

$$\frac{d^2\Gamma^i}{dsdq^2} = \frac{d^2\Gamma_0}{dsdq^2}\left(1 + \Delta^i\right) \tag{3.36}$$

Here, the correction factor Δ^i is defined as

$$\Delta^i = \frac{\left(\frac{d^2\Gamma^i}{dsdq^2}\right)}{\left(\frac{d^2\Gamma_0}{dsdq^2}\right)} - 1 \tag{3.37}$$

The term Δ^i includes corrections arising from both IR factors and non-IR factors up to $\mathcal{O}(k)$ terms. We have explicitly verified that the contribution from $\mathcal{O}(k^2)$ terms is negligible and therefore disregarded in the analysis. Additionally, we consider the shift in $R_{K^{\mu e}}$ caused by the QED corrections, denoted as $\Delta^i_{R_{K^{\mu e}}}$, defined as follows:

$$\Delta^i_{R_{K^{\mu e}}} = R^0_{K^{\mu e}}\left(\frac{\Delta\Gamma^i_\mu}{\Gamma^i_\mu} - \frac{\Delta\Gamma^i_e}{\Gamma^i_e}\right) \tag{3.38}$$

In the following discussion, we will delve into the impact of these QED corrections.

3.4 Results

The QED corrections, including both real and virtual contributions up to $\mathcal{O}(\alpha_{em})$, are represented by the quantity Δ^i (refer to Eq. (4.34)). Here, i indicates the neutral ($i = 0$) or charged ($i = c$) B decay modes. The electron and muon channels are depicted in Fig.(3.5), illustrating the correction factors for different choices of the maximum photon energy k_{max} of these soft photons and the angular cut θ_{cut}. Notably, the correction factor for electrons is approximately three times larger than that for muons, with both factors being negative, indicating a decrease in the decay rate. This difference primarily arises from the significantly smaller electron mass compared to the muon mass, differing by approximately two orders of magnitude. Consequently, the QED corrections have a more substantial impact on lighter particles, whereas the influence on heavier charged particles is relatively diminished. A slight dependence on the chosen photon energy cut, k_{max}, can be observed. Another noteworthy aspect is the sensitivity to θ_{cut}, especially in the case of electrons. However, by selecting θ_{cut} to be around a few degrees, this sensitivity essentially vanishes.

An important group of terms to consider are the IR terms that exhibit a logarithmic dependence on the lepton mass, $\ln(m_l)$. Figure (3.6) illustrates the sensitivity to m_l. The lower two curves correspond to the expected behavior for electrons and muons, respectively, with a contribution of approximately 10% as seen in Δ^i. However, the blue curve represents the case where $m_l = 10^{-50}$ MeV, and it is evident that the contribution is significantly larger. This contribution will continue to increase as m_l approaches zero. To address this issue, employing a small θ_{cut} in the range of a few degrees is effective. These $\ln(m_l)$ terms correspond to hard collinear logarithms, which have been proven to cancel out rigorously. This agrees with [117]. It is worth noting that all other IR divergences, including the $\ln^2(m_l)$ terms, are explicitly observed to cancel out when the virtual corrections and real emission terms are combined.

Figure (3.7) illustrates the impact of QED effects on $\Delta^i_{R_K^{\mu e}}$, as defined in Eq. (3.38), for a θ_{cut} of 3° as a function of q^2. It is notable that the charged mode is more affected due to the additional contributions from the contact term, which

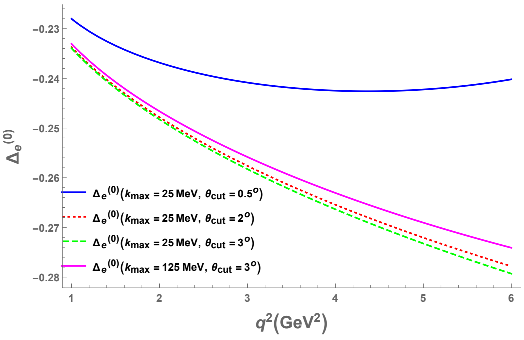

(a) $\Delta_e^{(0)}$ vs. q^2

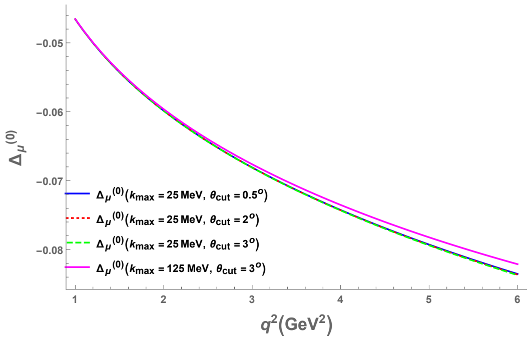

(b) $\Delta_\mu^{(0)}$ vs. q^2

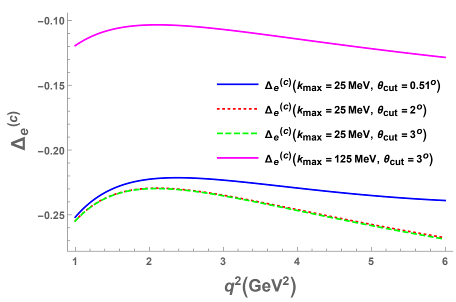

(c) $\Delta_e^{(c)}$ vs. q^2

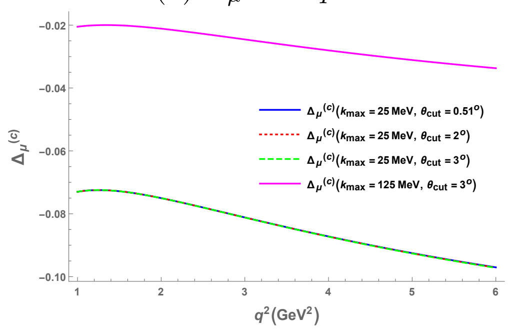

(d) $\Delta_\mu^{(c)}$ vs. q^2

Figure 3.5: $\mathcal{O}(\alpha_e m)$ corrections to neutral and charged $B \to K\ell\ell$ modes. Left: electrons, Right: muons

is absent in the neutral mode due to its proportional dependence on $(Q_B + Q_K)$. The QED effects are significant, reaching approximately 20% for electrons ($\sim 5\%$ for muons), resulting in an increase in $\Delta^i_{RK^{\mu e}}$ and subsequently in $R_K^{\mu e}$. However, it should be emphasized that all the quantities are sensitive to the choice of k_{max} and θ_{cut}. For $k_{max} = 25$ MeV, the shift in $R_K^{\mu e}$ over the q^2 range is approximately 20%. Nevertheless, as k_{max} is increased to 125 MeV, the shift decreases to about 10%. This outcome is expected, as with the increase in k_{max}, muons begin to behave similarly to electrons, where both their masses (m_e and m_μ) are much smaller than k_{max}. Consequently, we have verified that in such cases, $\Delta^i_{R_K^{\mu e}}$ approaches zero.

In particular, choosing $\theta_{cut} \sim$ few degrees and $k_{max} \sim 250$ MeV, leads to $\sim 5\%$, (positive) shift in $R_K^{\mu e}$:

$$\Delta^{(c)}_{R_K^{\mu e}} = 5.34\%, \qquad \Delta^{(0)}_{R_K^{\mu e}} = 7.43\% \tag{3.39}$$

The electron modes exhibit substantial QED corrections of approximately 20%,

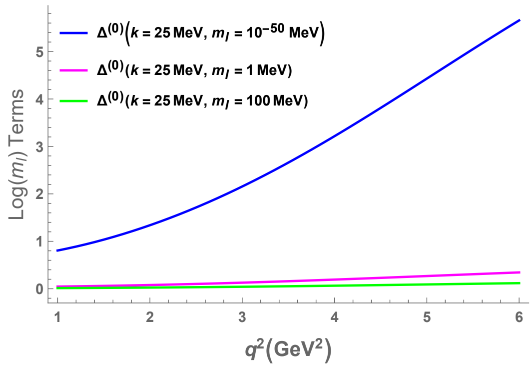

Figure 3.6: Behaviour of $\ln(m_l)$ terms

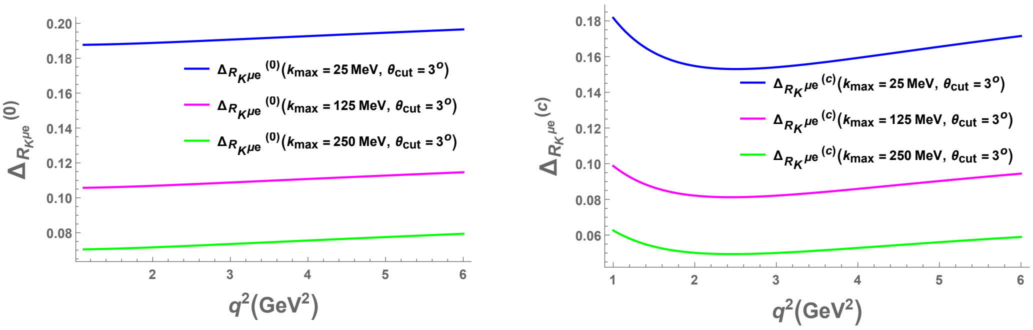

(a) $\Delta^0_{R_K^{\mu e}}$ vs. q^2

(b) $\Delta^{(c)}_{R_K^{\mu e}}$ vs. q^2

Figure 3.7: Shift in $R_K^{\mu e}$ due to $\mathcal{O}(\alpha_{em})$ QED effects

whereas the muon modes experience smaller corrections. We have also verified that selecting different k_{max} values for muons and electrons alters the shift in $R_K^{\mu e}$, resulting in a final value of $R_K^{\mu e}$, including the QED effects, deviating from unity by a few percent. This observation is broadly consistent with [117]. The two studies differ primarily in the treatment of the contact term(s), leading to some numerical discrepancies, as well as in handling the $\ln(m_l)$ terms and phase space. Despite these dissimilarities, it is encouraging to observe that similar conclusions are drawn regarding the physical quantities.

3.5 Discussion and Conclusions

We have performed the calculations of the $\mathcal{O}(\alpha_{em})$ QED effects in the decay process of $B \to K\ell^+\ell^-$. These corrections have a negative impact, resulting in a decrease in the decay rates. To ensure gauge invariance in the emission amplitude of a single photon, we treated the mesons as point particles and utilized scalar

QED. By doing so, we were able to determine the contact term. We proceeded to calculate both the real and virtual QED effects. During the computation of virtual corrections associated with the contact term, we encountered UV divergences, which are expected to cancel out when considering higher-dimensional terms like two-photon contact terms. However, for the present analysis, we took a phenomenological perspective and neglected these divergences, focusing solely on the finite terms. To regulate the IR divergences, we introduced a fictitious photon mass, denoted as λ, as an IR regulator. Importantly, we have shown that the physical differential decay rate remains independent of the chosen regulator λ, thereby confirming the cancellation of the soft divergences.

The choice of the maximum soft photon energy, k_{max}, and the photon angle relative to the charged lepton, θ_{cut}, has a notable impact on the physical decay rate and the ratio of rates between muons and electrons. We also discussed the significant influence of the $\ln(m_l)$ terms, which can be mitigated by setting θ_{cut} to a few degrees. In particular, the electron channels display corrections of approximately 10-20%, while the corrections for muons, under the same k_{max} and θ_{cut} conditions, are around 5%. With $k_{\text{max}} \sim 250$ MeV, the corrections to the lepton flavor universality ratio, $R_K^{\mu e}$, are roughly 5%. This correction appears significant, especially considering that the observable $R_K^{\mu e}$ is close to unity within the standard model, disregarding these QED effects. Consequently, this would further exacerbate the tension between theory and experimental observations. However, caution is necessary. The reported 5% positive shift in $R_K^{\mu e}$ is based on the assumption of using the same k_{max} and θ_{cut} values for both electrons and muons. Adjusting these parameters to match the actual experimental criteria would lead to different outcomes.

In conclusion, the study highlights the significance of including QED effects in $B \to K\ell^+\ell^-$ decays as a source of important corrections. While the individual decay rates, especially for electrons, undergo substantial corrections, it is crucial to consider appropriate experimental cuts that suit the specific observables. For instance, the lepton flavor universality ratio $R_K^{\mu e}$ may experience only minimal shifts of a few percent, contingent upon the chosen cuts. This emphasizes the need for meticulous attention when comparing experimental results with theoretical calculations. It should be noted that our study, along with the findings of [117], does not fully address the issue of remaining UV divergences and the computation of two-photon contact terms (as well as higher-dimensional operators relevant to the matter), warranting further investigation in this direction. This is particularly important to ensure an unambiguous comparison with experimental data, given that observables such as $R_K^{\mu e}$ are considered highly reliable probes of the SM and potential indicators of NP beyond it.

Chapter 4

A Novel observable: $\frac{|V_{ub}|}{|V_{cb}|}$

In Chapter-3, we observed that the decay rate for $B \to K\ell\ell\gamma$, γ being soft, and the LFU ratio R_K show sensitivity to k_{max} (maximum energy of the soft photon). On general grounds, similar corrections are expected for other modes as well; both charged current and neutral current. This motivates us to search for observables that exhibit minimal sensitivity to QED effect in addition to non-perturbative parameters such as form factors. This chapter involves the detailed study of one such observable, $R_V = \frac{|V_{ub}|}{|V_{cb}|}$, which is found to be least sensitive to the choice of form factors as well as QED corrections. Further, the CKM elements V_{ub} and V_{cb} individually show the tension between exclusive and inclusive measurements but the ratio, R_V, is found to be equal[1]. It then leads to phenomenological applications, which we discuss in this chapter. This chapter is based on the findings presented in [27].

4.1 Introduction

As discussed in Chapter 1, The Cabibbo-Kobayashi-Maskawa (CKM) matrix is a fundamental component of the SM that describes the mixing of quark flavors. It is a unitary matrix that relates the weak interaction eigenstates (flavor eigenstates) to the mass eigenstates of quarks. The CKM matrix is characterized by four independent parameters, which are fundamental in the SM. Consequently, a

[1] R_V is constructed using the PDG values of exclusive and inclusive measurements of V_{ub} and V_{cb}. See Secttion-4.1 for details

precise determination of the elements of the CKM matrix is of great significance, both for confirming the validity of the SM and for exploring physics beyond it. Exploring processes mediated by charged currents (CC) and neutral currents (NC) is essential for this goal. Within the framework of the SM, CC processes occur at the tree level, involving direct interactions between charged weak bosons (W bosons) and fermions. In contrast, FCNC processes exclusively occur at the loop level in the SM.

The decay of a B meson into a D or π meson at the quark level involves the exchange of a virtual W boson, which then decays into a ℓ-ν_ℓ pair. The amplitudes of these semileptonic decays of B mesons are governed by the CKM matrix elements $|V_{cb}|$ and $|V_{ub}|$ for D and π decays, respectively. These CKM elements represent the strengths of the flavor-changing weak interactions between different generations of quarks and are fundamental parameters in the Standard Model [120–122]. The amplitudes of these decays can be factorized into leptonic and hadronic parts, allowing us to separate the hadronic uncertainties arising from our limited understanding of strong interactions. These semileptonic decays present valuable opportunities to measure the CKM elements $|V_{cb}|$ and $|V_{ub}|$. An alternative approach to extract these CKM elements is through inclusive decays, such as $B \to X_{c,u}\ell\nu_\ell$ [111, 123–126]. While there are other exclusive modes that can be investigated, our discussion will primarily focus on the $B \to D\ell\nu$ and $B \to \pi\ell\nu$ decay modes.

Experimental measurements have revealed a notable difference of approximately 3σ for $|V_{cb}|$ and 3.5σ for $|V_{ub}|$ between the inclusive and exclusive measurements. These differences are commonly known as the $|V_{ub}|$ and $|V_{cb}|$ puzzles, or the "inclusive" versus "exclusive" puzzles [124, 127, 128]. Now, whether these discrepancies indicate hints of new physics or simply reflect the underestimation of theoretical and/or experimental uncertainties remains open[2] [130]. The main source of theoretical uncertainties arises from the computation of non-

[2] A recent article by Belle [129] highlights the simultaneous measurement of inclusive and exclusive $|V_{ub}|$, which reduces the discrepancy to approximately 1.6σ. Though, it reduced uncertainties but did not resolve the discrepancy completely. Also, the CKM element itself is not free from QED effects. Therefore, the current status is not fully conclusive. In light of this, the proposed observable R_V remains a promising alternative in this context.

perturbative quantities involved in the given decay modes and the application of appropriate kinematical cuts.

Although significant progress has been made in reducing theoretical uncertainties through the use of more precise form factors calculated using Light Cone Sum Rules (LCSRs) and lattice QCD, completely eliminating these uncertainties remains a formidable challenge with our current understanding of strong interactions. As a result, a quest for observables where the impact of hadronic uncertainties can be eliminated or significantly minimized is a natural step forward. In this context, Various lepton flavor universality (LFU) ratios have been proposed, such as $R_{K^{(*)}}$ and $R_{D^{(*)}}$ [131]. The ratio $R_{K^{(*)}}$ compares the branching ratio of $B \to K^{(*)}\mu\mu$ to that of $B \to K^{(*)}ee$, while $R_{D^{(*)}}$ compares the branching ratio of $B \to D^{(*)}\tau\nu$ to that of $B \to D^{(*)}\mu\nu$.

To ensure the reliability of LFU ratios, in probing new physics, it is essential to investigate the impact of soft photon corrections. While experimental analyses incorporate some effects of soft photons using tools like the PHOTOS Monte-Carlo generator [62, 63], certain contributions related to the hadron structure, interference between initial and final state emissions, and virtual corrections are not fully accounted for by PHOTOS. Consequently, understanding the complete dynamics, including these contributions, becomes crucial. Recent studies have demonstrated that incorporating these effects reveals sensitivity of LFU ratios to soft photon QED corrections [26], particularly when specific photon energy and angular cuts are applied. This highlights the need to identify observables that exhibit reduced sensitivity to both hadronic uncertainties and QED corrections arising from soft photons.

Experimentally the ratio of the CKM elements $\frac{|V_{ub}|}{|V_{cb}|}$ is determined using two different modes. Firstly, the baryonic modes $\Lambda_b^o \to p\mu^-\bar{\nu_\mu}$ and $\Lambda_b^o \to \Lambda_c^+\mu^-\bar{\nu_\mu}$ yield $|V_{ub}|/|V_{cb}| = 0.083 \pm 0.004$ [132, 133]. Secondly, the mesonic modes $B_s^o \to K^-\mu^+\nu_\mu$ and $B_s^o \to D_s^-\mu^+\nu_\mu$ give $|V_{ub}|/|V_{cb}| = 0.095 \pm 0.008$ (0.061 ± 0.004) for high q^2 (for low q^2) [134]. Interestingly, when considering the PDG values [45], the ratio $\frac{|V_{ub}|}{|V_{cb}|}$ obtained from exclusive determinations of $|V_{ub}|$ and $|V_{cb}|$ exhibits remarkable agreement with the ratio derived from their inclusive determinations.

More specifically,

$$\frac{|V_{ub}|}{|V_{cb}|}\Big|_{\text{excl}}^{\text{high } q^2} = 0.094 \pm 0.005 \qquad \frac{|V_{ub}|}{|V_{cb}|}\Big|_{\text{incl}}^{\text{high } q^2} = 0.101 \pm 0.007. \tag{4.1}$$

Intrigued and motivated by these findings, we consider the ratio $R_V = \frac{|V_{ub}|}{|V_{cb}|}$, in the present study. We demonstrate that the ratio R_V receives negligible corrections from soft photons and is also minimally influenced by choice of form factors used for $B \to D$ and $B \to \pi$ transitions. It should be noted that the experimental extractions mentioned earlier differ in the low- and high-q^2 regions due to variations in the employed form factors. This arises from the fact that different approaches yield form factors with different accuracies in different q^2 regions. Hence, it is crucial to carefully select the q^2 range to ensure that the observable is least affected by the choice of form factors. When we state that R_V is independent of form factor choice, we mean that it is less sensitive to the form factors.

Considering these advantages, we propose the use of R_V in phenomenological studies as it serves as a cleaner observable compared to conventional lepton flavor universality ratios. Furthermore, it has greater potential for probing new physics.

4.2 Non-radiative $B \to P\ell\nu_\ell$ $(P = D, \pi)$

Let us consider the decay process $B(p_B, m_B) \to P(p_P, m_P)\ell(p_l, m_l)\nu_\ell(p_n, 0)$, where P represents a pseudo-scalar meson such as D or π. The relevant Feynman diagram is shown in Fig.(4.1). The second-order differential decay rate for this process can be fully described by two independent Lorentz invariant variables:

$$y = \frac{2p_B.p_l}{m_B^2}, \text{ and } \quad z = \frac{2p_B.p_P}{m_B^2}. \tag{4.2}$$

Alternatively, we can use the Mandelstam variables $q^2 = (p_B - p_P)^2 \equiv m_B^2 + m_P^2 - 2p_B \cdot p_P$ and $s_{B\ell} = (p_B - p_l)^2 \equiv m_B^2 + m_l^2 - 2p_B \cdot p_l$ instead of y and z. The matrix element for $B \to P\ell\nu_\ell$ can be decomposed into the hadronic and leptonic

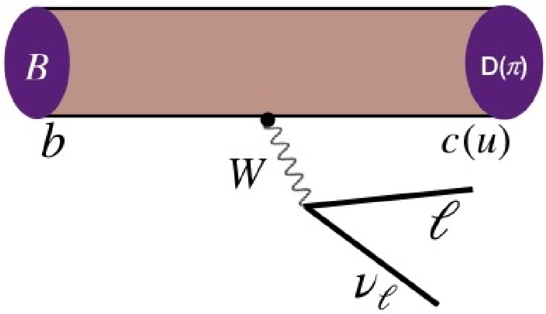

Figure 4.1: Feynman diagram for $B \to D(\pi)\ell\nu_\ell$.

part as:

$$\mathcal{M}_0(B \to P\ell\nu_\ell) = \frac{G_F}{\sqrt{2}} V_{qb} \mathcal{H}_\mu \mathcal{L}^\mu. \tag{4.3}$$

Here, $|V_{qb}|$ (where $q = c, u$) represents the CKM matrix element, and G_F is the Fermi constant. $\mathcal{L}^\mu (= \bar{\ell}\gamma^\mu(1-\gamma^5)\nu_\ell)$ and $\mathcal{H}_\mu$ are the leptonic and hadronic matrix elements, respectively. $\mathcal{H}_\mu$, can be expressed in terms of two form factors, $f+^P$ and f_0^P, which depend on the momentum transfer q^2:

$$\mathcal{H}_\mu = (p_B + p_P)_\mu \, f_+^P + (p_B - p_P)_\mu \, f_-^P \tag{4.4}$$

where $f_-^P = \frac{m_B^2 - m_P^2}{q^2}(f_0^P - f_+^P)$. The computation of these form factors involves various techniques like LCSRs and lattice QCD. However, as we shall see, the choice of form factors does not significantly affect the determination of $\frac{|V_{ub}|}{|V_{cb}|}$ (see Sec- 4.4).

For the present purpose, we adopt a model-independent parametrization for $B \to D\ell\nu_\ell$ and a z-expansion parametrization for $B \to \pi\ell\nu_\ell$.

Next, the total decay width of the non-radiative process $B \to P\ell\nu_\ell$ is given by:

$$\Gamma^0 \;=\; \frac{m_B}{256\pi^3} \int dz \int dy \, |\mathcal{M}_0|^2_{B \to P\ell\nu_\ell}\,, \tag{4.5}$$

$$\text{where} \qquad |\mathcal{M}_0|^2_{B \to P\ell\nu_\ell} = \frac{G_F^2}{2} |V_{qb}|^2 \left((f_0^P)^2 c_1 + (f_+^P)^2 c_2 + f_0^P f_+^P c_3\right), \tag{4.6}$$

and the coefficients c_i (where $i = 1, 2, 3$) are calculated as:

$$
\begin{aligned}
c_1 &= -\frac{4(m_B^2 - m_P^2)^2 m_l^2\Big((z-1)m_B^2 + m_l^2 - m_P^2\Big)}{(m_P^2 - (z-1)m_B^2)^2}, \\
c_2 &= -\frac{4m_B^2}{(m_P^2 - (z-1)m_B^2)^2}\Bigg[-(z-1)m_B^4\Big(m_l^2(4y(z-2) + 3z^2 - 8z + 8) \\
&\quad +4m_P^2(2y^2 + 2y(z-2) - 3z + 3)\Big) + m_B^2(m_P^2 m_l^2(4y(z-2) + 3z^2 - 4z + 4) \\
&\quad +(z-2)^2 m_l^4 + 4m_P^4(y^2 + y(z-2) - 3z + 3)) + 4(y-1)(z-1)^2 m_B^6 \\
&\quad (y + z - 1) - 4m_P^2 m_l^2 + 4m_P^2\Bigg], \text{ and} \\
c_3 &= \frac{8m_B^2(m_B^2 - m_P^2)m_l^2}{(m_P^2 - (z-1)m_B^2)^2}\Big[(z-1)m_B^2(2y + z - 2) - (z-2)m_l^2 \\
&\quad - m_P^2(2y + z - 2)\Big].
\end{aligned}
\tag{4.7}
$$

4.2.1 Form factors for $B \to P(= D, \pi)\ell\nu_\ell$

The form factors for the $B \to D\ell\nu_\ell$ decay in the model-independent parametrization can be expressed as: (based on [122])

$$
\begin{aligned}
f_+^D(q^2) &= \frac{1}{\sqrt{r}}\left[(1+r)h_+ - (1-r)h_-\right], \\
f_-^D(q^2) &= \frac{1}{\sqrt{r}}\left[(1+r)h_- - (1-r)h_+\right], \text{ and} \\
f_0^D(q^2) &= f_+^D(q^2) + \frac{1 + r^2 - 2rw}{1 - r^2} f_-^D(q^2).
\end{aligned}
$$

Here $r = \frac{m_D}{m_B}$, $w = \frac{p_B \cdot p_D}{m_B m_D}$,

$$
\begin{aligned}
h_+ &= \xi\left[1 + \frac{\alpha}{\pi}\left(C_{V_1} + \frac{1+w}{2}\left(C_{V_2} + C_{V_3}\right)\right) + \left(\epsilon_c - \epsilon_b\right)L_1\right], \text{ and} \\
h_- &= \xi\left[\frac{\alpha}{\pi}\frac{1+w}{2}\left(C_{V_2} - C_{V_3}\right) + \left(\epsilon_c - \epsilon_b\right)L_4\right]
\end{aligned}
$$

with $z = \frac{m_c}{m_b}$, $L_1 = 0.72(w-1)$, $L_4 = 0.24$, $\epsilon_c = 0.1807$, $\epsilon_b = 0.0522$, $\xi = \left(\frac{2}{1+w}\right)^2$,

$$\begin{aligned}
C_{V_1} &= \frac{1}{6z(w-w_z)}\Big[2(w+1)\left((3w-1)z - z^2 - 1\right) r_w + \Big(12z(w_z - w) - \\
&\quad (z^2-1)\log z\Big) + 4z(w-w_z)\Omega\Big], \\
C_{V_2} &= \frac{-1}{6z^2(w-w_z)^2}\Big[\left(4w^2+2w)z^2 - (2w^2+5w-1)z - (w+1)z^3 + 2\right) r_w \\
&\quad + z\left(2(z-1)(w_z - w) + \right)\Big], \\
C_{V_3} &= \frac{1}{6z(w-w_z)^2}\Bigg[\left((2w^2+5w-1)z^2 - (4w^2+2w)z - 2z^3 + w + 1\right) r_w \\
&\quad + \Big((3-2w)z^2 + (2-4w)z + 1\Big)\log z + 2z(z-1)(w_z - w)\Bigg].
\end{aligned}$$

with $r_w = \frac{\log(w_+)}{\sqrt{w^2-1}}$, $w_z = \frac{1}{2}\left(z + \frac{1}{2}\right)$ and

$$\begin{aligned}
\Omega &= \frac{w}{2\sqrt{w^2-1}}\left[2Li_2(1-w_-z) - 2Li_2(1-w_+z) + Li_2(1-w_+^2) - Li_2(1-w_-^2)\right] \\
&\quad - w r_w \log z + 1.
\end{aligned}$$

Here, $w_+ = w + \sqrt{w^2-1}$, $w_- = w - \sqrt{w^2-1}$.

For $B \to \pi\ell\nu_\ell$, the form factors in the z-expansion parametrization are expressed as,(based on [135]):

$$\begin{aligned}
f_+^\pi(q^2) &= \frac{f_+(0)^\pi}{1 - \frac{q^2}{m_{B*}^2}}\Bigg\{1 + \sum_{k=1}^{N-1} b_k\Big(z(q^2,t_0)^k - z(0,t_0)^k - (-1)^{N-K}\frac{k}{N}\big[z(q^2,t_0)^N \\
&\quad - z(0,t_0)^N\big]\Big)\Bigg\}, \text{ and} \\
f_0^\pi(q^2) &= f_0^\pi(0)\left\{1 + \sum_{k=1}^{N} b_k^0\left(z(q^2,t_0)^k - z(0,t_0)^k\right)\right\}.
\end{aligned}$$

Here, $z(q^2,t_0) = \frac{\sqrt{(m_B+m_\pi)^2 - q^2} - \sqrt{(m_B+m_\pi)^2 - t_0}}{\sqrt{(m_B+m_\pi)^2 - q^2} + \sqrt{(m_B+m_\pi)^2 - t_0}}$, $f_0^\pi(0) = f_+^\pi(0) = 0.281$, $b_1 = -1.62$, $b_1^0 = -3.98$ and $t_0 = (m_B + m_\pi)^2 - 2\sqrt{m_B m_\pi}\sqrt{(m_B+m_\pi)^2 - q^2}$. Importantly, these form factors are applicable across the entire range of q^2.

Now, let us discuss the impact of soft photon emission on this decay width.

4.3 Soft photon QED corrections to $B \to P\ell\nu_\ell$

We consider two scenarios for the charge assignment of the particles involved in the process: firstly, where the particle denoted as P is charged and the B meson is neutral, and secondly, where the B meson is charged and P is neutral. The computation of soft photon corrections in both cases follows a similar procedure, with minor variations in the selection of kinematic variables. In this discussion, our focus will be on the case of $B^- \to P^0\ell^-\bar{\nu}\ell$, and we will highlight any necessary distinctions for the case of $B^0 \to P^+\ell^-\bar{\nu}\ell$ when relevant.

4.3.1 Real photon emissions

The Feynman diagrams depicting the real emission of photon are illustrated in Figure (4.2). Assuming point-like mesons and utilizing scalar QED, the amplitude for $B \to P\ell\nu_\ell\gamma$ with a soft photon can be expressed as the sum of eikonal term (which is IR divergent) and an IR safe term.

$$\mathcal{M}_{B\to P\ell\nu_\ell\gamma} = \mathcal{M}_{\text{IR}} + \mathcal{M}_{\text{NIR}}. \tag{4.8}$$

Here,
$$\mathcal{M}_{\text{IR}} = e\epsilon_\alpha \mathcal{M}_0 \left(-\frac{p_B^\alpha}{p_B.k} + \frac{p_l^\alpha}{p_l.k}\right) \tag{4.9}$$

is the amplitude due to soft photon and the term in parenthesis is called the

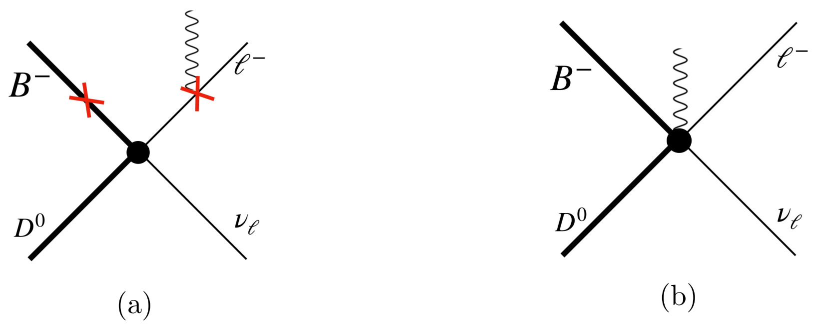

Figure 4.2: (a) Diagram illustrating real photon emission from one of the external charged particles (denoted by ×). (b) Diagram representing the Contact Term (CT) contribution.

universal soft factor. $\mathcal{M}_{\text{NIR}}$ includes the contributions from the contact term and the residual term. Explicitly, the $\mathcal{M}_{\rm NIR}$ is given by

$$\mathcal{M}_{\rm NIR} = \frac{G_F}{\sqrt{2}} V_{qb} (\mathcal{M}_{\rm res} + \mathcal{M}_{\rm CT}). \tag{4.10}$$

Here,

$$\begin{aligned}
\mathcal{M}_{\rm res} &= e\epsilon_\alpha(k)\Big[\Big(\bar{u}(p_l)\gamma^\alpha \frac{\not{k}}{2p_l.k}\Gamma^\mu v(p_n)\Big) \otimes H_\mu(p_B, p_P) \\
&\quad + (f_+^P + f_-^P)\frac{p_B^\alpha}{p_B.k}\bar{u}(p_l)\Gamma^\mu v(p_n)\, k_\mu\Big], \\
\mathcal{M}_{\rm CT} &= -e\epsilon_\mu(k)(f_+^P + f_-^P)\bar{u}(p_l)\Gamma^\mu v(p_n).
\end{aligned} \tag{4.11}$$

The inclusion of the contact term is crucial to fix the gauge invariance of the amplitude and is constructed following the procedure outlined in Chapter- 3. It is noteworthy that the contact term is proportional to the charge of the meson rather than the lepton. This implies that the leptonic contribution is gauge invariant on its own, while the contact term is required to ensure gauge invariance of the hadronic contribution. The contact term can be incorporated through an effective term in the Hamiltonian at the hadronic level, expressed as follows:

$$\mathcal{H}_{\rm CT} = -ie(f_+^P - f_-^P)\,[\bar{u}(p_l)\Gamma^\alpha v(p_n)]\, A_\alpha \phi_P^\dagger \phi_B. \tag{4.12}$$

It contributes to both real and virtual corrections. Taking into account the contribution from the CT, the complete gauge-invariant amplitude for real soft photon emission can be expressed as follows:

$$\begin{aligned}
\mathcal{M}_{B\to P\ell\nu_\ell\gamma} &= e\epsilon_\alpha(k)\Big[\mathcal{M}_0\left(-\frac{p_B^\alpha}{p_B.k} + \frac{p_l^\alpha}{p_l.k}\right) + \bar{u}(p_l)\frac{\gamma^\alpha \not{k}}{2p_l.k}\Gamma_\mu v(p_n)\mathcal{H}^\mu \\
&+ (f_+^P + f_-^P)\bar{u}(p_l)\left(\frac{p_B^\alpha}{p_B.k}\not{k} - \gamma^\alpha\right)(1-\gamma^5)v(p_n)\Big].
\end{aligned} \tag{4.13}$$

From Eqs. (4.9) and (4.10)

$$\begin{aligned}
|\mathcal{M}_{B\to P\ell\nu_\ell\gamma}|^2 &= |\mathcal{M}_{\rm IR}|^2 + |\mathcal{M}_{\rm res}|^2 + |\mathcal{M}_{\rm CT}|^2 + 2\mathcal{R}e(\mathcal{M}_{\rm IR}^*\mathcal{M}_{\rm res}) \\
&\quad + 2\mathcal{R}e(\mathcal{M}_{\rm IR}^*\mathcal{M}_{\rm CT}) + 2\mathcal{R}e(\mathcal{M}_{\rm res}^*\mathcal{M}_{\rm CT}).
\end{aligned} \tag{4.14}$$

Numerically contributions from $|\mathcal{M}_{\rm res}|^2$, $|\mathcal{M}_{\rm CT}|^2$, $2\mathcal{R}e(\mathcal{M}^*_{\rm IR}\mathcal{M}_{\rm CT})$ and $2\mathcal{R}e(\mathcal{M}^*_{\rm res}\mathcal{M}_{\rm CT})$ are found to be very small, typically less than 0.1%. Therefore, we neglect these terms and focus only on the remaining terms for numerical computations, as they provide significant contributions to the decay width.

Collinear divergences may arise during these computations. However, the decay rate is less sensitive to collinear divergences when the final state contains heavy leptons (ℓ being μ or τ),though it is still important to verify the cancellation of these divergences. To achieve this, we consider the photon to be inclusive and carefully choose the suitable set of kinematic variables.

4.3.1.1 Photon inclusive case

The total decay width for the process $B \to P\ell\nu_\ell\gamma$, photon being inclusive, is

$$\begin{aligned}\Gamma|_{B\to P\ell\nu_\ell\gamma} &= \frac{1}{2m_B}\int\frac{d^3p_P}{(2\pi)^3 2E_P}\int\frac{d^3p_l}{(2\pi)^3 2E_l}\int\frac{d^3p_n}{(2\pi)^3 2E_\nu}\int\frac{d^3k}{(2\pi)^3 2E_k}(2\pi)^4\\ &\quad \delta^4\left(Q-p_n-k\right)|\mathcal{M}|^2_{B\to P\ell\nu_\ell\gamma} \end{aligned} \tag{4.15}$$

where $Q = (p_B - p_D - p_l)$.

The process $B \to P\ell\nu_\ell\gamma$ is a four-body process that includes $B \to P\ell\nu_\ell$ as a

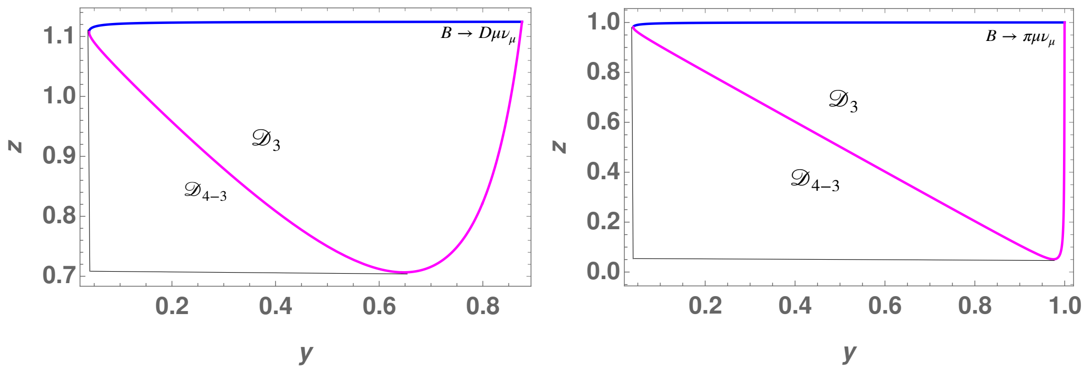

(a) (b)

Figure 4.3: (a) Dalitz plot displaying the phase space boundaries for the energies of the muon (magenta) and the D^0 meson (blue) in the decay $B^- \to D^0\mu^-\nu_\mu$. (b) Dalitz plot illustrating the phase space boundaries for the energies of the muon (magenta) and the π^0 meson (blue) in the decay $B^- \to \pi^0\mu^-\nu_\mu$.

subset. This can be visualized using the Dalitz plots, as depicted in Figure (4.3). The Dalitz plot exhibits a linear dependence on the decaying meson's energy and a quadratic dependence on the lepton energy.

It is important to note that the delta function in Equation (4.15) enforces $x \geq 0$, where x ($\equiv$ normalized total missing mass energy) is introduced as $x = Q^2/m_B^2$. This introduces the step function $\Theta(x)$, which divides the phase space into $\mathcal{D}_3$ (the three-body region) and $\mathcal{D}_{4-3}$ (the remaining region). This division enables us to express the decay width as follows:

$$\Gamma|_{B\to P\ell\nu_\ell\gamma} = \frac{m_B^3}{512\pi^4}\Big[\int_{\mathcal{D}_3} dydz \int_0^{x_+} dx + \int_{\mathcal{D}_{4-3}} dydz \int_{x_-}^{x_+} dx\Big] \int \frac{d^3k}{(2\pi)^3 2E_k} \int \frac{d^3p_n}{(2\pi)^3 2E_\nu} (2\pi)^4 \delta^4(Q - p_n - k)\, |\mathcal{M}|^2_{B\to P\ell\nu_\ell\gamma}\,. \tag{4.16}$$

Real photon emission contributes to both the three-body region ($\mathcal{D}_3$) and the four-body region ($\mathcal{D}_{4-3}$) of the phase space. Focusing on the first term of Equation (4.16), we obtain:

$$\Gamma_{\mathcal{D}_3}|_{B\to P\ell\nu_\ell\gamma} = \frac{m_B^3}{512\pi^4}\int_{\mathcal{D}_3} dydz \int_0^{x_+} dx \int \frac{d^3k}{(2\pi)^3 2E_k}(2\pi)^4 \delta(xm_B^2 - 2Q.k)\, |\mathcal{M}|^2_{B\to P\ell\nu_\ell\gamma} \tag{4.17}$$

$$\text{with} \qquad |\mathcal{M}|^2_{B\to P\ell\nu_\ell\gamma} = |\mathcal{M}_{\rm IR}|^2 + 2\mathcal{R}e(\mathcal{M}^*_{\rm IR}\mathcal{M}_{\rm res}). \tag{4.18}$$

The second-order differential decay rate, which is found to be independent of both IR and collinear divergences when contributions from the virtual corrections are properly considered, can be expressed as follows:

$$\frac{d^2\Gamma_{\mathcal{D}_3}}{dydz} = \frac{m_B^3}{256\pi^3}\frac{\alpha_{em}}{\pi}\Big[|\mathcal{M}_0|^2\,\mathcal{I}_0(y,z,m_\gamma^2) + \frac{G_F^2\,|V_{cb}|^2}{2}\int_0^{x_+} dx \sum_{m,n} C_{m,n}\mathcal{I}_{m,n}(x,y,z)\Big] \tag{4.19}$$

$$\text{with } \mathcal{I}_{m,n} = \frac{1}{8\pi}\int \frac{d^3p_n}{E_\nu}\int \frac{d^3k}{E_k}\delta^4(Q - p_n - k)\frac{1}{(p_B.k)^m (p_l.k)^n}, \text{ and} \tag{4.20}$$

$$\mathcal{I}_0 = \int_{m_\gamma^2/m_B^2}^{x_+} dx\Big[2p_B.p_l\mathcal{I}_{1,1}(x,y,z) - m_B^2\mathcal{I}_{2,0}(x,y,z) - m_l^2\mathcal{I}_{0,2}(x,y,z)\Big]. \tag{4.21}$$

The integrals ($\mathcal{I}_0$, $\mathcal{I}_{m,n}$) and the coefficients $C_{m,n}$ can be found in Appendix-B. However, for practical purposes, it is more convenient to focus on the photon-exclusive case, which will be discussed in the next subsection.

4.3.1.2 Photon exclusive case

Now, let us consider the photon-exclusive case, where the maximum energy carried by the soft photon is denoted as $k_{\max}$. Following the procedure outlined in chapter- 3, the second-order differential decay rate for $B \to P\ell\nu_\ell\gamma$ with a soft photon can be expressed as:

$$\frac{d^2\Gamma_{\text{real}}}{dydz} = \frac{d^2\Gamma^0}{dydz}(2\alpha_{em}\tilde{B}) + \frac{d^2\Gamma'}{dydz}, \tag{4.22}$$

$\frac{d^2\Gamma'}{dydz}$ is IR finite. $\tilde{B}$ contains the IR divergences, and can be expressed as

$$\tilde{B} = \frac{-1}{2\pi}\left\{\ln\left(\frac{k_{\max}^2 m_B m_l}{m_\gamma^2 E_B E_\ell}\right) - \frac{p_B{\cdot}p_l}{2}\left[\int_{-1}^{1}\frac{dt}{p_t^2}\ln\left(\frac{k_{\max}^2}{E_t^2}\right) + \int_{-1}^{1}\frac{dt}{p_t^2}\ln\left(\frac{p_t^2}{m_\gamma^2}\right)\right]\right\}. \tag{4.23}$$

The overall negative sign in the aforementioned expression arises from the conservation of charge. To simplify the integration process, we introduce convenient combinations of momenta denoted as E_t and p_t. These combinations are defined as follows: $2p_t = (1+t)p_B + (1-t)p_l$ and $2E_t = (1+t)E_B + (1-t)E_\ell$. All the integrals are listed in Appendix-B. Furthermore, we introduce a small fictitious mass m_γ for the photon, which serves as a regulator for IR effects.

The differential decay width in the photon exclusive case explicitly depends on $k_{\max}$. Experimental measurements are limited to photons with energies larger than $k_{\max}$, so the theoretical decay rate is expected to vary with $k_{\max}$. In a similar manner to the photon-inclusive case, the decay width for the photon-exclusive scenario includes a non-infrared (non-IR) contribution that encompasses terms beyond Low's term. However, the significance of terms other than the IR term and its interference with the residual term is negligible and thus not explicitly presented. The interference terms are dependent on the angle θ between the lepton and the photon. In the rest frame of the B meson, the angle between the lepton and the neutrino is assumed to be isotropic, resulting in $M_{\text{miss}}^2 \sim 2E_\nu E_\gamma$, where $E_\nu = m_B - E_D - E_\ell - E_\gamma$.

4.3.2 Virtual Photon Corrections

The virtual corrections include (1) the self-energy correction, where the photon originates and terminates at the same charged line (Fig.(4.4a)); (2) the vertex correction, where the photon connects two distinct charged lines (Fig.(4.4b)); and (3) the CT contribution, where the photon is emitted from the effective vertex and terminates on a charged particle (Fig.(4.4c)). These corrections are

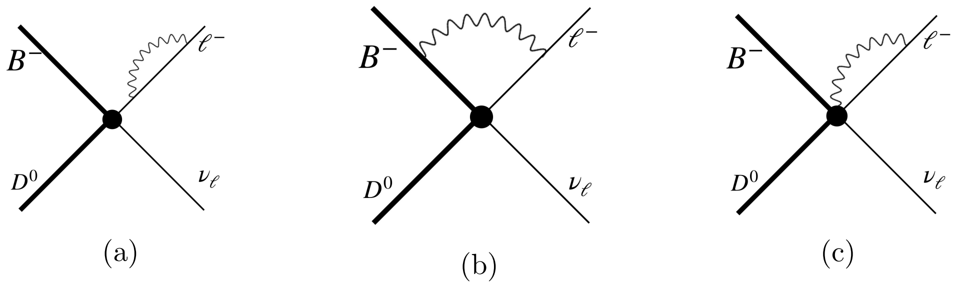

Figure 4.4: (a) self-energy correction to the lepton (a similar diagram for the self-energy correction to the B meson), (b) vertex correction, and (c) virtual correction due to the contact term (a similar diagram where the photon originates from the contact term and interacts with the B meson).

applicable to both the photon-inclusive and photon-exclusive cases. Now, let's discuss these three contributions individually. We begin with the contribution arising from the self-energy corrections for the charged lepton and the meson, respectively (as shown in Fig.(4.4a)), which can be expressed as follows:

$$\mathcal{M}_s = \frac{\mathcal{M}_0}{2}(\delta Z_\ell + \delta Z_B) \tag{4.24}$$

where δZ_ℓ and δZ_B represent the wave function renormalization for the charged lepton and meson, respectively, and are given by

$$\begin{aligned} \delta Z_\ell &= \frac{\alpha_{em}}{4\pi}\Big[2 - B_0(p_l^2, 0, m_l^2) + 4m_l^2 B_0'(p_l^2, m_\gamma^2, m_l^2)\Big], \text{ and} \\ \delta Z_B &= \frac{\alpha_{em}}{4\pi}\Big[2B_0(p_B^2, 0, m_l^2) + 4m_B^2 B_0'(p_B^2, m_\gamma^2, m_B^2)\Big]. \end{aligned} \tag{4.25}$$

In the expression above, $B_0(p_a^2, 0, m_a^2)$ and $B_0'(p_a^2, m_\gamma^2, m_a^2)$ (where $a = \ell(B)$) represent the Passarino-Veltman functions associated with scalar two-point integrals and their derivatives. The explicit forms of these functions can be found in Appendix-B. It is important to note that $B_0'(p_a^2, m_\gamma^2, m_a^2)$ contains IR divergences, which are regulated by introducing a fictitious mass, m_γ, for the photon. Further, the vertex correction contribution (as shown in Fig.(4.4c)) is given by

$$\begin{aligned}\mathcal{M}_{\text{vert}} &= \frac{\alpha_{em}}{4\pi}\bar{u}(p_l)\Big[\Big(-2m_l\not{p}_B - 2\not{p}_B\not{p}_\ell\Big)C_0(m_l^2, m_B^2, q^2, m_l^2, m_\gamma^2, m_B^2) - \Big(m_l\not{p}_B + \not{p}_B\not{p}_\ell \\ &\quad -2m_B^2\Big)C_1(m_B^2, q^2, m_l^2, 0, m_B^2, m_l^2) - \Big(m_l(\not{p}_\ell + m_l) + 2\not{p}_B\not{p}_\ell - 4p_B.p_l\Big) \\ &\quad C_2(m_B^2, q^2, m_l^2, 0, m_B^2, m_l^2) + B_0(q^2, m_B^2, m_l^2) - 2B_0(m_l^2, 0, m_l^2)\Big]\big((f_-^p + f_+^p)\not{p}_\ell \\ &\quad +2f_+^p\not{p}_P\big)(1-\gamma^5)v(p_n). \qquad (4.26)\end{aligned}$$

In the equation above, $C_r(m_l^2, m_B^2, q^2, m_l^2, m_\gamma^2, m_B^2)$ (where $r = 0, 1, 2$) represent the three-point Passarino-Veltman functions. Among these functions, C_0 contains the IR divergences, whereas the other two functions (C_1 and C_2) do not exhibit IR divergences. Consequently, we set $m_\gamma^2 = 0$ in C_1 and C_2.

The virtual correction originating from the contact term contributes through two diagrams: one where the photon terminates on the charged lepton and another where it terminates on the charged meson leg. This contribution introduces both ultraviolet (UV) divergences and a finite component. However, in numerical calculations, we neglect the UV divergences and only take into account the finite term. It has been observed that the finite term has a minimal impact on the process and does not significantly affect the precision of the calculation. Therefore, phenomenologically, the virtual corrections due to CT can be ignored.

At $\mathcal{O}(\alpha_{em})$, the squared matrix element for the process $B \to P\ell\nu_\ell$, incorporating contributions from $\mathcal{M}_s$ (self-energy correction) and $\mathcal{M}_{\text{vert}}$ (vertex correction), is expressed as follows:

$$\begin{aligned}|\mathcal{M}|^2 &= |\mathcal{M}_0|^2 + 2\mathcal{R}e(\mathcal{M}_0^* M_s) + 2\mathcal{R}e(\mathcal{M}_0^* M_{\text{vert}}) \qquad (4.27) \\ &\quad +\mathcal{O}(\alpha_{em}^2) \qquad (4.28) \\ \text{with } 2\mathcal{R}e(\mathcal{M}_0^* M_s) &= |\mathcal{M}_0|^2(\delta Z_\ell + \delta Z_B), \quad \text{and}\end{aligned}$$

$$2\mathcal{R}e(\mathcal{M}_0^* M_{\text{vert}}) = \frac{\alpha_{em}}{4\pi}\Big[|\mathcal{M}_0|^2 \Big(2B_0(q^2, m_B^2, m_l^2) - 4B_0(m_l^2, 0, m_l^2) - 4\big((p_B.p_l) + m_B^2\big)C_1(m_B^2, q^2, m_l^2, 0, m_B^2, m_l^2) - 8(p_B.p_l) C_0(m_l^2, m_B^2, q^2, m_l^2, m_\gamma^2, m_B^2) - 4m_l^2 C_2(m_B^2, q^2, m_l^2, 0, m_B^2, m_l^2)\Big) + \Big((-4f_+^p(f_-^p + f_+^p) - 2(f_-^p + f_+^p)^2)(p_B.p_l)(p_l.p_n) + 4(f_+^p)^2 m_P^2 (p_B.p_n) + (p_P.p_n)(-4(f_-^p + f_+^p)f_+^p - 4f_+^p(p_B.p_P)) + 4f_-^p f_+^p (p_B.p_n)(p_l.p_P) + (f_+^p + f_-^p)^2 m_l^2 (p_B.p_n) + 4(f_+^p)^2(p_B.p_n)(p_l.p_P)\Big) C_2(m_B^2, q^2, m_l^2, 0, m_B^2, m_l^2)\Big], \tag{4.29}$$

respectively. Hence, the differential decay width including the virtual QED corrections reads as

$$\frac{d^2\Gamma_{\text{vir}}}{dydz} = \frac{d^2\Gamma^0}{dydz}(1 + 2\alpha_{em}B) + \frac{d^2\Gamma'_{\text{vir}}}{dydz}. \tag{4.30}$$

In this case, analogous to the non-radiative decay, $\frac{d^2\Gamma'_{\text{vir}}}{dydz}$ is free from infrared (IR) divergences and includes the contributions arising from non-factorizable terms, which involve combinations of form factors and momenta as presented in Eq. (4.29). On the other hand, the factorizable correction factor, denoted as B, exhibits IR divergences and can be expressed as follows:

$$B = \frac{1}{8\pi}\Big[2B_0(q^2, m_B^2, m_l^2) - 4B_0(m_l^2, 0, m_l^2) - 4\left((p_B.p_l) + m_B^2\right) C_1(m_B^2, q^2, m_l^2, 0, m_B^2, m_l^2) - 8(p_B.p_l)C_0(m_l^2, m_B^2, q^2, m_l^2, m_\gamma^2, m_B^2) - 4m_l^2 C_2(m_B^2, q^2, m_l^2, 0, m_B^2, m_l^2) + 2 - B_0(p_l^2, 0, m_l^2) + 4m_l^2 B_0'(p_l^2, m_\gamma^2, m_l^2) + 2B_0(p_B^2, 0, m_l^2) + 4m_B^2 B_0'(p_B^2, m_\gamma^2, m_B^2)\Big]. \tag{4.31}$$

4.3.3 Total $\mathcal{O}(\alpha_{em})$ QED corrections

By combining $\frac{d^2\Gamma_{\text{real}}}{dydz}$ and $\frac{d^2\Gamma_{\text{vir}}}{dydz}$, we obtain the second order differential rate for the process $B \to P\ell\nu_\ell$ at $\mathcal{O}(\alpha)$, which includes both real and virtual soft photon corrections. It can be expressed as follows:

$$\frac{d^2\Gamma_\ell^{\text{QED}}}{dydz} = \frac{d^2\Gamma^0}{dydz}(1 + 2\alpha_{em}\mathcal{H}) + \frac{d^2\Gamma'}{dydz} + \frac{d^2\Gamma'_{\text{vir}}}{dydz}, \tag{4.32}$$

where $\mathcal{H} = \tilde{B} + B$. The individual quantities $\tilde{B}$ and B do depend on the IR regulator m_γ, but their sum, denoted as $\mathcal{H}$, is independent of m_γ. As a result, the infrared divergences cancel out in the total differential decay rate. The IR finite $\mathcal{H}$ is

$$\begin{aligned}\mathcal{H} &= \frac{1}{2\pi}\Bigg[-\ln\left(\frac{k_{max}^2}{E_B E_\ell}\right) + \frac{p_B.p_l}{2}\int_{-1}^{1}\frac{dt}{p_t^2}\frac{k_{max}^2}{E_t^2} + B_0(q^2, m_B^2, m_l^2) - 2B_0(m_l^2, 0, m_l^2) \\ &- 2\left((p_B.p_l) + m_B^2\right) C_1(m_B^2, q^2, m_l^2, 0, m_B^2, m_l^2) - 2m_l^2 C_2(m_B^2, q^2, m_l^2, 0, m_B^2, m_l^2) \\ &- 3 - \frac{1}{2}B_0(p_l^2, 0, m_l^2) + B_0(p_B^2, 0, m_B^2)\Bigg]. \qquad (4.33)\end{aligned}$$

The terms $\frac{d^2\Gamma'}{dydz}$ and $\frac{d^2\Gamma'_{\text{vir}}}{dydz}$ in Eq.(4.32) are free from IR divergences. Hence, the total differential rate, $\frac{d^2\Gamma_\ell^{\text{QED}}}{dydz}$, is IR safe. It can be simplified as

$$\frac{d^2\Gamma_\ell^{\text{QED}}}{dydz} = \frac{d^2\Gamma^0}{dydz}\left(1 + \Delta_\ell^{\text{QED}}\right). \qquad (4.34)$$

In the above expression, the lepton ℓ can take values of μ or τ, and Δ_ℓ^{QED} represents the correction factor to the differential decay rate. This correction factor includes terms up to $\mathcal{O}(k)$, where k denotes the photon energy. The contribution from the $\mathcal{O}(k^2)$ term is found to be small and has been neglected in the numerical analysis.

Expressing the CKM matrix element $|V_{qb}|$ without taking into account the QED corrections can be done by following Equation (4.5).

$$|V_{qb}^0| = \sqrt{\frac{\Gamma_{qb}^{\text{exp}}}{\mathcal{G}_{qb}^0}}. \qquad (4.35)$$

Here, Γ_{qb}^{exp} is the experimental decay width, and $\mathcal{G}_{qb}^0$ is further defined as

$$\mathcal{G}_{qb}^0 = \frac{m_B}{256\pi^3}\frac{G_F^2}{2}\int dy \int dz|\mathcal{M}_0|^2 \quad (q = u/c). \qquad (4.36)$$

Hence, the ratio of the CKM elements without taking into account the QED corrections, R_V^0, is

$$R_V^0 = \frac{|V_{ub}^0|}{|V_{cb}^0|} = \sqrt{\frac{\Gamma_{ub}^0 \mathcal{G}_{cb}^0}{\Gamma_{cb}^0 \mathcal{G}_{ub}^0}}. \tag{4.37}$$

Taus are more challenging to reconstruct, while electrons are highly sensitive to soft photon corrections. Hence, it is advisable to choose final states involving muons when extracting the CKM elements and their ratios. Focusing on muons in the final states ensures that the collinear logarithms, represented by $\sim \ln(m_\mu)$, are the same for both $B \to \pi$ and $B \to D$ transitions.

Now, the QED correction factors for the CKM matrix element, V_{qb}, and the ratio, R_V, are defined as follows:

$$\delta_{V_{qb}}^{\text{QED}} = \frac{|V_{qb}|}{|V_{qb}^0|} - 1, \quad \text{and} \tag{4.38}$$

$$\Delta_{R_V} = \delta_{V_{ub}}^{\text{QED}} - \delta_{V_{cb}}^{\text{QED}}, \tag{4.39}$$

respectively. Here, $|V_{qb}|$ represents the CKM element that is determined by incorporating the QED corrections up to $\mathcal{O}(\alpha_{em})$. To ensure completeness, we also consider the soft photon corrections to the ratio R_P, which corresponds to the ratio of the branching fractions between the τ and μ modes[3]. This correction factor is given by

$$\delta_{R_P} = R_P^0 \Big(\frac{\Delta_\tau^{\text{QED}}}{\Gamma_\tau^0} - \frac{\Delta_\mu^{\text{QED}}}{\Gamma_\mu^0} \Big) \tag{4.40}$$

where, Δ_τ^{QED} and Δ_μ^{QED} represent the correction factors for the τ and μ modes, respectively.

[3]Experimentally, R_P is defined by $R_p = \frac{\mathcal{BR}(B\to P\tau\nu_\tau)}{\mathcal{BR}(B\to P\ell\nu_\ell)}$, $\ell = \mu,\ e$ we do not consider electron here.

4.4 Results

We investigate the soft photon corrections to the $B \to P\ell\nu_\ell$ decay mode. Experimental analyses of this process employ two approaches:

1. The photon-inclusive approach, where the detection scheme focuses on the charged mesons and leptons, while the neutrino and photon are not directly detected.

2. The photon-exclusive approach, where the experiment is sensitive to the final state photons.

In the inclusive case, the decay width is determined by fitting the observed momenta of the charged mesons and leptons to the three-body kinematics. This fitting process takes into account the possibility of zero or non-zero missing mass. The total decay width is influenced by the range of maximum and minimum values of the missing mass considered in the fitting procedure. However, in this study, our focus is on the exclusive case, as we specifically aim to examine the explicit impact of soft photons. Theoretically, since the soft photon is a fourth particle, a portion of the four-body phase space (up to $k_{\max}$) also contributes to the decay width. Therefore, the total decay rate comprises contributions from both the three-body phase space region and regions beyond it.

The emission of a soft photon contributes to both the inside and outside regions of the Dalitz plot, as depicted in Figures 4.3(a) and 4.3(b). On the other hand, virtual corrections only affect the inside region of the Dalitz plot. The correction factor exhibits reduced sensitivity to phase space points outside the Dalitz region primarily because of the involvement of heavy leptons (muon) in the decay process. Nevertheless, this region remains important for studying long-distance effects as the photon momentum approaches zero ($k \to 0$), and it plays a crucial role in enhancing precision. Additionally, exploring the dependence of the decay width on the angle θ between the photon and the lepton enables the examination of collinear divergences and their implications.

In our analysis, we have observed that the correction factor Δ_ℓ^{QED} (where ℓ can be either μ or τ) is not significantly affected by the cut on θ (denoted as θ_{cut}) for both muons and taus, due to their heaviness. However, if we were considering electrons in the final state, this dependence would be more pronounced. Generally, the correction factor Δ_ℓ^{QED} is larger for the muon channel (approximately 3-5%) compared to the tau channel (almost negligible) in both the $B \to D$ and $B \to \pi$ decay modes. To illustrate, at $k_{max} = 100$ MeV, the $B^- \to D^0$ ($B^0 \to D^+$) mode experiences a QED shift of around 0.1% (approximately -1%) for the tau mode while it is approximately -1.6% (approximately -3.4%) for the muon mode. Figures 4.5(a) and 4.5(b) show the soft photon cor-

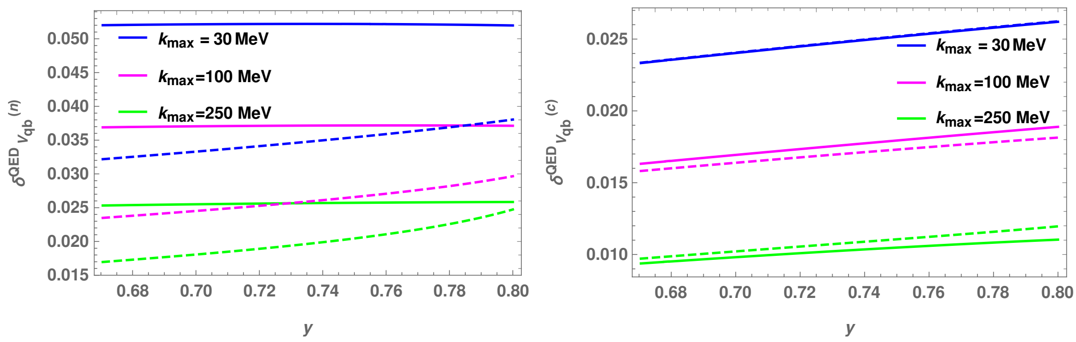

(a) (b)

Figure 4.5: Radiative corrections to the CKM elements $|V_{cb}|$ and $|V_{ub}|$, represented by the dashed line ($\delta^{\text{QED}}V_{cb}$) and solid line ($\delta^{\text{QED}}V_{ub}$) respectively. These corrections are plotted for different thresholds on the photon energy, k_{max}, in the context of the decays (a) $B^0 \to P^+$ (where P^+ can be D^+ or π^+) and (b) $B^- \to P^0$ (where P^0 can be D^0 or π^0) involving a muon (μ^-) and a neutrino (ν_μ).

rections to the CKM elements $|V_{cb}|$ and $|V_{ub}|$ for the neutral and charged modes, respectively. In the case of the charged mode, the corrections to both CKM elements are nearly identical since the photon is emitted from the B-meson and the lepton in both $B \to \pi\ell\nu_\ell$ and $B \to D\ell\nu_\ell$ processes. However, for the neutral mode, we observe some difference between the two curves due to the emission of photons from π and D instead of the B-meson. Consequently, the mass difference between π and D becomes a crucial factor in determining these differences.

We now turn our attention to studying the effects of soft photons on the ratio of CKM elements, specifically denoted as $R_V = \frac{|V_{ub}|}{|V_{cb}|}$. The correction factor to this ratio, denoted as Δ_{R_V}, is illustrated in Fig.(4.7) for both the neutral and charged modes. It is noteworthy that the charged modes exhibit a negligible correction, whereas the neutral modes experience a very small correction on the order of $\mathcal{O}(10^{-3})$. This distinction arises from the photon emission originating from π as opposed to D in the neutral mode, as discussed earlier. Furthermore, we investigate the dependence of the correction factor on the chosen maximum photon energy, $k_{\max}$. It is observed that the correction factor diminishes as $k_{\max}$ increases, leading to the suppression of collinear and infrared effects (as illustrated in Fig.(4.7)). Similar trends have been reported in Ref.[23]. We have

	$\Delta_\tau^{(n)}$ (with (w/o) Coulomb)	$\Delta_\mu^{(n)}$ (with (w/o) Coulomb)
Ref. [23]	1.7(−1.2)	−1.2(−3.5)
Our results	1.7(−1.0)	−1.1(−3.4)

Table 4.1: Comparison of the QED shifts (%) in the decay rate (for both tau and muon modes) at $k_{\max} = 100$ MeV with Ref. [23], considering the inclusion (exclusion) of the extra Coulomb factor arising from the final-state charged particles (as considered in Ref. [23]).

found our results to be in full agreement with the findings of Ref. [23] (see Table (4.1) for a comparative study). Fig.(4.6) displays the QED-corrected CKM

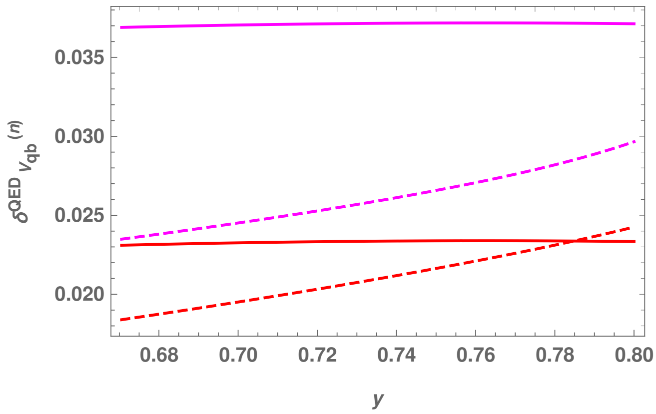

Figure 4.6: Radiative corrections to the CKM elements $|V_{cb}|$ and $|V_{ub}|$ (i.e., $\delta^{\rm QED}Vcb$ (dashed) and $\delta^{\rm QED}Vub$ (solid)) for $k_{\max} = 100$ MeV in the decay process $B^0 \to P^+(= D^+, \pi^+)\mu^-\nu_\mu$, considering the inclusion of the extra Coulomb factor from the final-state charged particles (red) and not considering it (magenta).

elements $|V_{cb}|$ and $|V_{ub}|$ for the neutral B mode, both with and without the additional Coulomb factor. The inclusion of this factor results in a reduction of QED effects from approximately $\sim 3\%$ to around $\sim 2\%$. It is worth emphasizing that while this factor does influence QED corrections to the individual CKM elements, it has a negligible impact on the proposed observable R_V, thus showcasing the robustness of R_V against various types of QED corrections.

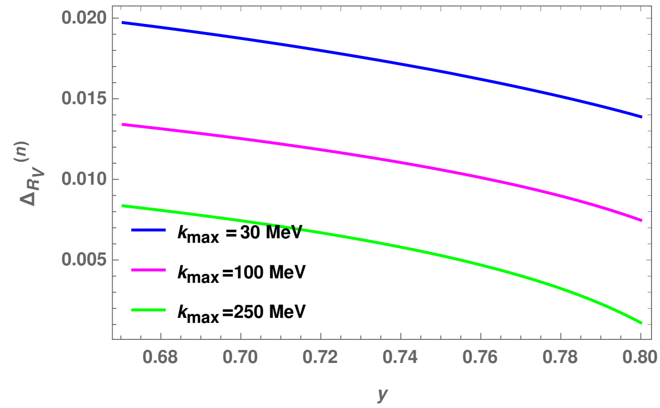

(a)

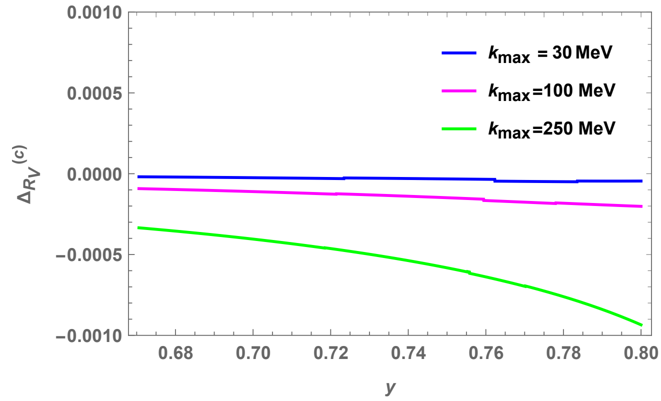

(b)

Figure 4.7: Radiative corrections to V_{ub}/V_{cb} (i.e. ΔR_V) as a function of lepton energy for the different tsoft photon maximum energy, k_{max} for (a) $B^0 \to P^+(= D^+, \pi^+)\mu^-\nu_\mu$ and (b) $B^- \to P^0(= D^0, \pi^0)\mu^-\nu_\mu$.

	$(f^{(I)}_{B\to\pi}; f^{(I)}_{B\to D})$	$(f^{(II)}_{B\to\pi}; f^{(I)}_{B\to D})$	$(f^{(I)}_{B\to\pi}; f^{(II)}_{B\to D})$	$(f^{(II)}_{B\to\pi}; f^{(II)}_{B\to D})$
R_V	0.091	0.093	0.091	0.093

Table 4.2: The ratio, R_V obtained with the different choice of $f^{(A)}_{B\to\pi}$ and $f^{(A)}_{B\to D}$ for the corresponding form factors.

We investigate the impact of different form factors used in the $B \to \pi$ and $B \to D$ transitions on the sensitivity of R_V. To investigate this, we consider two sets of form factors: (I) the form factors utilized in the present analysis (refer to Section-4.2.1 for details), and (II) the form factors derived from lattice analysis [127]. The impact of the form factor choice on R_V is summarized in Table (4.2). Our focus remains on the large q^2 region, ensuring the reliability of selected form factors and facilitating meaningful comparisons. The table clearly reveals minimal influence resulting from the choice of form factors. Given the resilience of R_V against soft photon corrections and form factor variations, it emerges as a promising observable.

Furthermore, we extend our investigation to encompass the effect of soft photons on the LFU ratios, $R_{P(=D,\pi)}$ (illustrated in Fig.(4.8)). We observed that the soft photons induce the corrections approximately 2% for $k_{max} = 250$ MeV in both ratios.

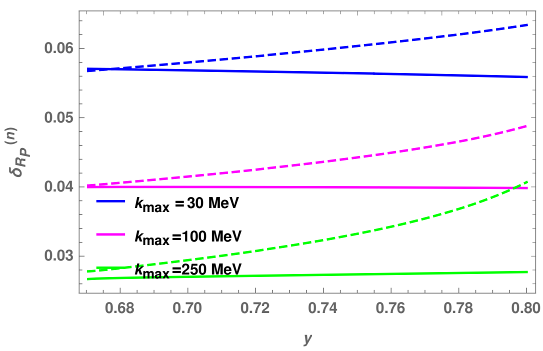

(a)

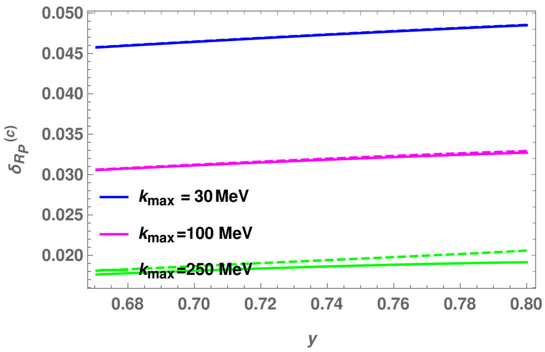

(b)

Figure 4.8: Effects of radiative corrections on the ratio R_P (with $P = D$ represented by the dashed line and $P = \pi$ represented by the solid line) are shown for various thresholds on the photon energy, k_{max}, in the decays (a) $B^0 \to P^+(= D^+, \pi^+)\ell^-\nu_\ell$ and (b) $B^- \to P^0(= D^0, \pi^0)\ell^-\nu_\ell$.

4.4.1 Phenomenological application of R_V

We have established the robustness of the ratio, R_V, against the soft photon corrections and the choice of form factors. To explore the possibility of probing physics beyond the SM using R_V, we focus on the potential impact of right-handed currents in the quark sector as a form of NP. This NP scenario can be described by an effective Hamiltonian given by:

$$H_{\rm NP} = \frac{4G_F}{\sqrt{2}} V_{qb} c_R^q (\bar{\ell}\gamma_\mu P_L \nu)\,(\bar{q}\gamma_\mu P_R b)\,, \tag{4.41}$$

where $q = u, c$, and c_R^q are the Wilson coefficients. The differential decay rate for the exclusive process $B \to P\ell\bar{\nu}_\ell$ can be expressed as

$$\frac{d^2\Gamma_{B\to P\ell\bar{\nu}_\ell}}{dy} = \frac{d^2\Gamma_{B\to P\ell\bar{\nu}_\ell}}{dy}\Big|_{\text{SM}} |1 + c_R^q|^2. \tag{4.42}$$

For the inclusive case with $m_u/m_b \to 0$, the differential decay rate is calculated as

$$\frac{d^2\Gamma_{B\to X_q\ell\bar{\nu}_\ell}}{dy} = |1 + c_R^q|^2 \frac{d^2\Gamma_{B\to X_q\ell\bar{\nu}_\ell}}{dy}\Big|_{\text{SM}} + c_R^q \frac{d^2\Gamma_{B\to X_q\ell\bar{\nu}_\ell}}{dy}\Big|_{\text{LR}}. \tag{4.43}$$

The explicit expressions of $\frac{d^2\Gamma_{B\to X_q\ell\bar{\nu}_\ell}}{dy}\Big|_{\text{SM,LR}}$ is given by [136, 137]

$$\begin{aligned}
\frac{\mathrm{d}\Gamma_{B\to X_q\ell\nu_\ell}}{\mathrm{d}y}\Big|_{SM} &= \left(\frac{2(y-3)y^2\rho^3}{(y-1)^3} - \frac{6y^2\rho^2}{(y-1)^2} - 6y^2\rho + 2(3-2y)y^2\right) \\
&+ \left(\frac{4\left(y^2-5y+10\right)\rho^3y^3}{3(y-1)^5} + \frac{2(5-2y)\rho^2y^3}{(y-1)^4} + \frac{10y^3}{3}\right)\frac{\lambda_1^2}{m_b^2} \\
&+ \Bigg(\frac{10y^2\left(y^2-4y+6\right)\rho^3}{(y-1)^4} - \frac{18(y-2)y^2\rho^2}{(y-1)^3} + \frac{12y^2(2y-3)\rho}{(y-1)^2} \\
&+ 2y^2(5y+6)\Bigg)\frac{3\lambda_2^2}{m_b^2}
\end{aligned} \tag{4.44}$$

$$\begin{aligned}
\frac{\mathrm{d}\Gamma_{B\to X_q\ell\nu_\ell}}{\mathrm{d}y}\Big|_{LR} &= \sqrt{\rho}\left(-\frac{12\rho^2y^2}{(y-1)^2} - \frac{24\rho y^2}{y-1} - 12y^2\right) + \sqrt{\rho}\Bigg(\frac{4(5-2y)\rho^2y^3}{(y-1)^4} \\
&+ \frac{4(5-3y)\rho y^3}{(y-1)^3}\Bigg)\frac{\lambda_1^2}{m_b^2} + \sqrt{\rho}\Bigg(\frac{12\rho y^3}{(y-1)^2} - \frac{36(y-2)\rho^2y^2}{(y-1)^3} \\
&+ \frac{24(2y-3)y^2}{y-1}\Bigg)\frac{3\lambda_2^2}{m_b^2}.
\end{aligned} \tag{4.45}$$

where $\rho = m_q/m_b$

Considering this NP, we can determine the CKM elements V_{ub} and V_{cb} by analyzing different decay modes of $b \to u$ and $b \to c$ transitions, including both inclusive and exclusive decays. The values of these CKM elements, along with their corresponding values in the absence of NP (V_{qb}^{SM}), are presented in Table (4.3). The presence of NP effects also affects the observable R_V. The ratio of R_V^{NP} to R_V^{SM} is calculated for different combinations of channels and summarized in Table 4.4. Equating the ratio R_V obtained from inclusive and exclusive determinations, as explained in Section 4.1, it is possible to derive

	Modes	V_{qb}^{NP}
Exclusive Decays	$B \to D\ell\nu_\ell$	$V_{cb}^{NP} = \frac{V_{cb}^{(\mathrm{SM})}}{1+c_R^c}$
	$B \to D^*\ell\nu_\ell$	$V_{cb}^{NP} = \frac{V_{cb}^{(\mathrm{SM})}}{1-c_R^c}$
	$B \to \pi\ell\nu_\ell$	$V_{ub}^{NP} = \frac{V_{ub}^{(\mathrm{SM})}}{1+c_R^u}$
	$B \to \rho\ell\nu_\ell$	$V_{ub}^{NP} = \frac{V_{ub}^{(\mathrm{SM})}}{1-c_R^u}$
Inclusive Decay	$B \to X_c\ell\nu_\ell$	$V_{cb} = \frac{V_{cb}(\mathrm{SM})}{1-0.34c_R^c}$
	$B \to X_u\ell\nu_\ell$	$V_{ub} = V_{ub}^{(\mathrm{SM})}$ (for $m_u \sim 0$)

Table 4.3: V_{qb}^{NP} for various exclusive and inclusive B decay modes

	$\frac{B\to X_u}{B\to X_c}$	$\frac{B\to\pi}{B\to D}$	$\frac{B\to\pi}{B\to D^*}$	$\frac{B\to\rho}{B\to D}$	$\frac{B\to\rho}{B\to D^*}$
$\left(\frac{\lvert V_{ub}\rvert}{\lvert V_{cb}\rvert}\right)^{NP} / \left(\frac{\lvert V_{ub}\rvert}{\lvert V_{cb}\rvert}\right)_{\mathrm{SM}}$	$1-0.34c_R^c$	$1+c_R^c-c_R^u$	$1-c_R^c-c_R^u$	$1+c_R^c+c_R^u$	$1-c_R^c+c_R^u$

Table 4.4: Ratio of R_V in the NP to R_V in the SM for inclusive $B \to X_u/X_c$ modes and four different combination of exclusive $B \to \pi/D/\rho/D^*$ modes

constraints on new physics. By equating the ratio calculated from the inclusive modes (first column) to the ratio obtained from the exclusive modes, we derive constraints on the parameter c_R^u as $c_R^u \in [-1.34, 1.34]c_R^c$. This demonstrates the significant probing capability of R_V in tightly correlating the strength of right-handed up-quark interactions with the NP coupling of the charm quark. Although this was a simple example, it is evident that the ratio, R_V, possesses similar probing power in the case of other NP modifications as well.

In the context of addressing the puzzles associated with V_{cb} and V_{ub} in a model-independent manner, it is common to treat the new physics couplings in the two modes independently. However, it is important to note that in specific models, this assumption may not hold true. Interestingly, the equality between $R_V|_{\mathrm{incl}}$ and $R_V|_{\mathrm{excl}}$ allows for the establishment of simple relations between the two couplings, even within a model-independent framework. This provides valuable insights and constraints on the interplay between new physics effects in $b \to u$ and $b \to c$ transitions.

As an additional phenomenological application, we aim to derive constraints on $\mathcal{BR}(B_c \to \tau\nu_\tau)$ using $\mathcal{BR}(B \to \tau\nu_\tau)$. The branching ratio of $B(B_c) \to \tau\nu_\tau$ in the considered NP model can be expressed as follows:

$$\mathcal{BR}(B(B_c) \to \tau\nu_\tau) = (1 - 2c_R^{u(c)})\mathcal{BR}(B(B_c) \to \tau\nu_\tau)|_{\rm SM} \tag{4.46}$$

where,

$$\mathcal{BR}(B(B_c) \to \tau\nu_\tau)|_{\rm SM} = \tau_{B(B_c)} \frac{G_F^2 m_{B(B_c)} m_\tau^2}{8\pi} \left(1 - \frac{m_\tau^2}{m_{B(B_c)}^2}\right) f_{B(B_c)}^2 |V_{u(c)b}|^2 \tag{4.47}$$

with the decay constant for the B and B_c mesons as $f_B = 185$ MeV and $f_{B_c} = 434$ MeV respectively. We can then use the experimentally measured branching ratio $\mathcal{BR}(B \to \tau\nu_\tau)|_{\rm exp} = 1.09 \times 10^{-4}$ (reference) to determine the value of c_R^u. Using this obtained value of c_R^u, the estimated branching ratio for $B_c \to \tau\nu\tau$ falls within the range of $[1.9 - 2.4]\%$. This value is well below the upper bound of $\mathcal{BR}(B_c \to \tau\nu_\tau) \leq 30\%$ as provided in [138]. If the branching ratio $\mathcal{BR}(B_c \to \tau\nu_\tau)$ had exceeded this bound, it would have contradicted the new physics couplings. This would have complicated not only the resolution of the V_{cb} puzzle but also the V_{ub} puzzle since the new physics effects in the up-type quarks are closely related to those in the charm sector.

4.5 Discussion and Conclusions

The determinations of $|V_{cb}|$ and $|V_{ub}|$ from exclusive and inclusive processes have consistently exhibited discrepancies. However, it is challenging to attribute these discrepancies confidently to BSM physics due to the involved hadronic uncertainties and possible experimental issues/systematics. To explore potential sources of uncertainty, we investigate the corrections due to soft photon in the determination of the CKM matrix elements $|V_{cb}|$ and $|V_{ub}|$ in the decay processes $B \to P\ell\nu_\ell$, where P represents D or π. Our findings reveal that these CKM elements undergo a significant shift of approximately 3-4% due to the inclusion of QED corrections. To provide more specific information, when considering a value of $k_{\max} = 100$ MeV, we observed a correction of about 2.2% (3.5%) for the charged $B \to D$ (π) mode, while the neutral B decay modes involving both D and π experienced a correction of approximately 1.7%.

In our calculation of the decay width, we carefully incorporate radiative corrections originating from both within and outside the Dalitz region, considering both the neutral and charged decay modes. The impact of these corrections is primarily influenced by the chosen maximum photon energy, $k_{\max}$, while exhibiting minimal sensitivity to the lepton-photon angle. This characteristic renders them largely free from collinear divergences. In the case of the neutral B mode, we observe total QED corrections of approximately -3.4% and -1% for the muon and tau channels, respectively, with $k_{\max} = 100$ MeV. Although these corrections are on the order of a few percent, they become significant when aiming for sub-percent precision and necessitate careful consideration and inclusion in the analysis.

To address the challenges posed by QED and hadronic uncertainties, we propose utilizing the ratio of CKM elements, specifically $R_V = \frac{|V_{ub}|}{|V_{cb}|}$, as an observable with reduced sensitivity to these effects, making it a promising probe of the SM. Notably, we observe that this ratio experiences minimal corrections originating from soft photon QED effects. Moreover, we explicitly examine the influence of form factor choices by exploring various parametrizations and options. Our investigation reveals that, when evaluated within a carefully selected q^2 range, this ratio remains largely unaffected by the choice of form factors. Another noteworthy finding is the remarkable agreement between the values of R_V obtained from exclusive and inclusive determinations. Consequently, while the individual CKM elements exhibit complex behavior and are susceptible to QED and hadronic effects, the ratio R_V emerges as a resilient observable, exhibiting practical insensitivity to such influences. The collective findings highlight the remarkable usefulness of R_V as an invaluable observable in our endeavors to test the SM and search for physics beyond the SM. Not only does R_V serve as a clean observable, but the close agreement between inclusive and exclusive determinations of R_V enables us to equate the theoretically computed expressions for both cases. This equivalence establishes simple relationships between new physics contributions in the $b \to u$ and $b \to c$ semileptonic modes. In conventional approaches addressing the puzzles related to $|V_{cb}|$ and $|V_{ub}|$, the new physics couplings in these two modes are typically treated independently. However, in certain models, there may exist a connection between them. By establishing the equality of $R_V|_{\text{incl}}$ and $R_V|_{\text{excl}}$, we establish a direct link between these coupling types, even in a model-independent framework. Such relationships can then be carefully examined within specific models to identify frameworks that can successfully address these puzzles.

Based on these findings, we are motivated to put forward the utilization of R_V as a valuable observable in our study of the SM and the quest for NP. This includes its application in experimental investigations as well as in the phenomenology.

Chapter 5

Radiative Inclusive B decays

In Chapter-3 and Chapter-4, we explored the impact of soft photon corrections on B meson semi-leptonic decays and introduced a new observable that exhibits robustness against theoretical uncertainties. In this chapter, we investigate how the experimental determination of the total decay width for $B \to X_u \ell \nu_\ell \gamma$ decay, combined with the data on the total decay width for $B \to X_u \ell \nu_\ell$, can aid in determining the non-perturbative parameters λ_1 and λ_2. It is important to note that the emitted photon in this context is a hard photon and should not be considered as a soft photon correction to $B \to X_u \ell \nu_\ell$. The content of this chapter is based on the findings presented in Ref. [139].

5.1 Introduction

Chapter-1 and Chapter-2 discussed the intricate nature of B meson decays. Despite their complexity, these decays provide an ideal stage for precision studies of the SM. This is primarily attributed to the involvement of multiple physical scales. When considering theoretical cleanliness, inclusive decay modes are favored over exclusive ones, as highlighted in Chapter-4. This preference stems from the difficulties involved in calculating transition form factors for exclusive decays. In the case of B meson decays, an additional advantage arises from the presence of a significant hard scale, m_b, which greatly surpasses the characteristic scale of QCD, Λ_{QCD}. The significant separation of scales facilitates perturbative calculations, which are made possible by the Heavy Quark Effective Theory (HQET) [50, 104]. The HQET systematically eliminates all the heavy degrees of freedom except the b quarks since they are in the initial and the final states.As a result, a systematic theoretical treatment can be employed to accurately calculate the decay rates.

As noted in Ref.[54, 103, 140], for a single heavy particle (here, quark), the non-relativistic Quantum Mechanical treatment, instead of QFT, can be used. It is due to the following reasons: (i) The number of heavy quarks and antiquarks are separately conserved. (ii) In the non-relativistic kinematics, the process of $Q\bar{Q}$ pair creation is power suppressed since the virtuality of the intermediate state is of the order of $2m_Q$. (iii) Appearance of heavy quarks in the loop is also suppressed since this effect is $\sim \mathbf{k}^2/m_Q^2$ when the momentum of gluon: $\mathbf{k} \ll m_Q$. As a result, a full QFT treatment is not necessary for the description of heavy quark, and a QM treatment is sufficient. This simplification is a key aspect of the non-relativistic expansion. However, our interest lies in the bound states such as B meson rather than a single heavy particle. Hence, QFT treatment is necessary in this case since the light cloud represents a complicated strongly-interacting system. Symmetry properties of heavy quarks are discussed in Section-2.2.3.

Further, the OPE proves to be a powerful tool in the systematic treatment of non-perturbative QCD effects. OPE enables the separation of effects originating at short and long-distance scales. Specifically, in the context of a heavy quark system, the OPE takes the form of a series expansion in powers of $\frac{\Lambda_{\rm QCD}}{m_b}$ [141–143] when combined with the theory of non-relativistic expansion.

The corrections to the leading term ($m_b \to \infty$) in the HQET are expected to be small in the high-energy region of the phase space. This region allows for contributions from various hadronic states that satisfy the condition $m_X^2 \to m_q^2 + \#\Lambda_{\rm QCD} m_b$. Consequently, observables such as decay rates, which average over these hadronic states, can be reliably predicted.

5.2 Non-perturbative parameters: λ_1 and λ_2

In the HQET up to $\mathcal{O}(1/m_b^2)$, the primary source of uncertainty in the predictions of decay rates arises from the non-perturbative parameters λ_1 and λ_2. Throughout this Chapter, we consistently work at $\mathcal{O}(\frac{1}{m_b^2})$ in HQET. These parameters are defined as [53, 144]

$$\lambda_1 = \frac{1}{2m_{H_Q}}\langle H_Q|\bar{Q}\mathbf{\Pi}^2 Q|H_Q\rangle,\ (\mathbf{\Pi} = i\mathbf{D}),\ \text{and} \tag{5.1}$$

$$3\lambda_2 = \frac{1}{2m_{H_Q}}\langle H_Q|\bar{Q}\frac{i}{2}\sigma_{\mu\nu}G^{\mu\nu}Q|H_Q\rangle \tag{5.2}$$

where, D is covariant derivative, and $|H_Q\rangle$ represent the heavy meson states. Physically, λ_1 provides information about the average squared spatial momentum of the heavy quark, while λ_2 quantifies the strength of the color magnetic field generated by the light cloud around the heavy quark's position [51, 140].

Historically, the determination of the parameters λ_1 and λ_2 has relied on QCD models [52, 145–147] and fitting them to experimental data [148–151]. In Ref.[152], the values of μ_π^2 and μ_G^2 in quenched lattice QCD are determined using the NRQCD action, incorporating $\mathcal{O}(\frac{1}{m_Q})$ corrections for the heavy quark. While they explicitly compute λ_2, they do not calculate λ_1 directly but instead evaluate the difference of matrix elements using two distinct methods. It is worth noting that these two methods yield different central values. Therefore, obtaining unambiguous predictions for these parameters holds significant importance.

It should be noted that both $B \to X_c\ell\nu_\ell$ and $B \to X_u\ell\nu_\ell$ exhibit similar decay signatures characterized by a high-momentum lepton, a hadronic system, and undetected neutrino energy. Thus, distinguishing between these two processes is challenging. Further, close to the lepton energy end point regions, non-perturbative shape functions enter the description of the decay kinematics, making predictions for the decay rates dependent on the precise modeling of these shape functions. For the present, it is not necessary to distinguish between these two modes at this level. Instead, we are exploring the possibility of determining the non-perturbative parameters in an efficient manner. Considering modes with similar cuts such as $B \to X_{u(c)}\ell\nu_\ell$ together with $B \to X_{u(c)}\ell\nu_\ell\gamma$ may provide complementary information allowing to extract the non-perturbative parameters. Further, the inclusion of a hard photon in the decay process introduces additional degrees of freedom, such as the angle between the lepton and the photon. As an example, the forward backward symmetry has been calculated (for details, see section- 5.5). The complete angular analysis is left for future work.

In this chapter, we explore how the experimental determination of the decay rate for the $B \to X_u \ell \nu_\ell \gamma$ mode, in conjunction with the $B \to X_{u/c} \ell \nu_\ell$ mode. It is worth reiterating that the emitted photon is a hard photon and the process should not be thought of as soft photon correction to $B \to X_u \ell \nu_\ell$. To this order in $1/m_b^2$, both the decay widths of $B \to X_u \ell \nu_\ell$ and $B \to X_u \ell \nu_\ell \gamma$ exhibit a linear dependence on the parameters λ_1 and λ_2.

$$\text{decay width} \sim A + B\lambda_1 + C\lambda_2. \tag{5.3}$$

By considering the two modes, a simultaneous set of linear equations can be formed. Thus, knowing or experimentally measuring one side of these equations enables the unambiguous determination of λ_1 and λ_2. While we include terms $\mathcal{O}((\Lambda_{QCD}/m_b)^2)$ in the HQET, it is tedious but straightforward to incorporate higher-order terms as well. To mitigate uncertainties arising from the presence of the CKM element (V_{ub}), we propose to examine the ratio of the decay width in different ranges of leptonic energy rather than directly working with the decay width itself (refer to Section-5.5 for further details). Such ratios can be defined as

$$R_1 = \frac{\int_0^{0.2} dy \frac{d\Gamma_\gamma}{dy}}{\int_0^{0.5} dy \frac{d\Gamma_\gamma}{dy}} \qquad \text{and} \qquad R_2 = \frac{\int_0^{0.5} dy \frac{d\Gamma}{dy}}{\int_0^{1} dy \frac{d\Gamma}{dy}} \tag{5.4}$$

where y is the lepton energy expressed in dimensionless units. Here Γ_γ corresponds to $B \to X_u \ell \nu \gamma$ mode. We choose to calculate the decay rate using a direct application of Cutkosky method applied to individual diagrams.

5.3 An example: $B \to X_u \ell \nu_\ell$

The weak Hamiltonian density for the inclusive semi-leptonic B meson decays to final state containing a u quark ($B \to X_u \ell \nu_\ell$) is given by

$$\mathcal{H}_{weak} = \frac{4G_F}{\sqrt{2}} V_{ub} (\bar{u}\gamma_\mu P_L b)(\bar{\ell}\gamma^\mu P_L \nu_\ell) \tag{5.5}$$

where, G_F and V_{ub} are Fermi constant and CKM element, respectively. The

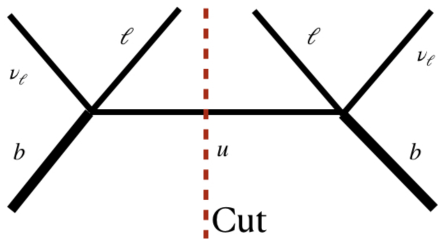

Figure 5.1: Representative Diagram of forward scattering for $b \to u \ell \nu_\ell$

process $B \to X_u \ell \nu_\ell$ involves the transition $b \to u$ and the sum over final state mesons containing the u quark. To calculate the decay width for this inclusive process, the forward scattering matrix element plays a crucial role. In Fig.(5.1), the Feynman diagram illustrates the forward scattering matrix element of the inclusive semi-leptonic decay $B \to X_u \ell \nu_\ell$. The imaginary part of the forward scattering matrix element, also known as the transition matrix element $\langle B|\hat{T}|B\rangle$, is connected to the decay into an inclusive final state through the optical theorem. It can be expressed as

$$\Gamma \propto \frac{1}{2m_B} Im\big\{\langle B|\hat{T}(b \to u \to b)|B\rangle\big\} \tag{5.6}$$

where the operator sandwiched in between the hadronic states is defined as a forward scattering operator or transition operator. The explicit form of the transition operator reads

$$\hat{T}^{\mu\nu}(b \to u \to b) = i \int d^4x e^{-iq.x} \frac{1}{2m_B} T\{J_w^{\mu\dagger}(x) J_w^\nu(0)\} \tag{5.7}$$

where T denotes the time ordered product and J_w^μ ($= \bar{u}\gamma^\mu P_L b$) is the weak current. Further, the differential decay rate for $B \to X_u \ell \nu_\ell$ process is given by

$$\begin{aligned}
\frac{d^3\Gamma}{dq^2 dE_\ell dE_\nu} &= \frac{1}{4}\sum_{X_u}\sum_{\text{spins}} \frac{1}{2m_B} |\langle X_u \ell \nu | \mathcal{H}_{weak} | B \rangle|^2 \delta^4(p_B - p_X - p_l - p_n) \\
&= 2G_F^2 |V_{ub}|^2 \mathcal{M}_{\mu\nu}\mathcal{L}^{\mu\nu} \qquad (5.8)
\end{aligned}$$

where $q^2 = (p_l + p_n)^2$, E_ℓ denotes energy of the lepton, and E_ν represents the neutrino energy. Moreover, the leptonic tensor, $\mathcal{L}_{\mu\nu}$, is directly defined from the electroweak Lagrangian. It is given by

$$\mathcal{L}_{\mu\nu} = (\bar{\nu}_\ell \gamma_\mu (1-\gamma_5)\ell)(\bar{\ell}\gamma_\nu(1-\gamma_5)\nu) \qquad (5.9)$$

whereas the hadronic tensor, $\mathcal{M}_{\mu\nu}$, is expressed in terms of matrix elements of electroweak currents and given by

$$\mathcal{M}_{\mu\nu} = \frac{1}{2m_B}\sum_{X_u} \langle B|J^\mu|X_u\rangle\langle|X_u|J^\nu|B\rangle \delta^4(p_B - p_X - p_l - p_n). \qquad (5.10)$$

The hadronic tensor ($\mathcal{M}_{\mu\nu}$) is defined as the absorptive part of the matrix element of the transition operator (i.e., Eq.(5.7)). Explicitly,

$$\mathcal{M}_{\mu\nu} = -i \; Disc.(\langle B|\hat{T}_{\mu\nu}|B\rangle) \qquad (5.11)$$

Instead of using the general parametrization of the hadronic tensor and relying on analytical properties, we directly compute the transition operator ($\hat{T}_{\mu\nu}$) in conjunction with the leptonic tensor ($\mathcal{L}_{\mu\nu}$) to determine the matrix element involved in the inclusive semi-leptonic decay $B \to X_u \ell \nu_\ell$. In the perturbative expansion at the lowest order (i.e., in terms of α_s), the amplitude at the quark level ($\mathcal{M}_{NR}$) for the diagram shown in Fig.(5.1) can be expressed as

$$\mathcal{M}_{NR} = \frac{i}{(p_b + \Pi - q)^2 - m_u^2 + i\epsilon} \bar{b}\gamma_\nu P_L(\not{p}_b + \not{\Pi} - \not{q} + m_b)\gamma_\mu P_L b \mathcal{L}^{\mu\nu} \qquad (5.12)$$

The subscript 'NR' denotes the non-radiative process, indicating that there is no photon in the final state. Additionally, $p_b + \Pi$ represents the effective momentum of the b quark, where $p_b = m_b v$ corresponds to the momentum of the heavy quark, and Π accounts for the residual momentum of the heavy quark. Moreover, q (given by $q = p_l + p_n$) is of the order of m_b, while Π is of the order of $\Lambda_{\rm QCD}$. Consequently, expanding $\mathcal{M}_{NR}$ in powers of Π results in an expansion in terms of $\frac{\Lambda \rm QCD}{m_b}$. By expanding the denominator up to $(\frac{\Lambda_{\rm QCD}}{m_b})^2$, we obtain:

$$\begin{aligned}\frac{1}{(p_b+\Pi-q)^2-m_u^2} &= \frac{1}{((p_b-q)^2-m_u^2)}\Big[1-\frac{2(p_b-q).\Pi+\Pi^2}{((p_b-q)^2-m_u^2)} \\ &\quad +\frac{2((p_b-\Pi).\Pi)^2}{((p_b-q)^2-m_u^2))^2}\Big] \end{aligned} \tag{5.13}$$

The hadronic part of $\mathcal{M}_{NR}$ is then sandwiched between the B meson states. The obtained matrix elements are simplified as [53]

$$\begin{aligned}\langle B(v)|\bar{b}\gamma^\mu b|B(v)\rangle &= 2p_B^\mu \\ \langle B(v)|\bar{b}\gamma_\mu\Pi_\tau b|B(v)\rangle &= \frac{\lambda_1+3\lambda_2}{3m_b}(2g_{\mu\tau}-5v_\mu v_\tau) \\ \langle B(v)|\bar{b}\gamma_\mu\Pi_{(\alpha}\Pi_{\beta)}b|B(v)\rangle &= \frac{2\lambda_1}{3m_b}(g_{\alpha\beta}-v_\alpha v_\beta)v_\mu \\ \langle B(v)|\bar{b}\gamma_\mu\Pi^2 b|B(v)\rangle &= \frac{2\lambda_1}{m_b}v_\mu \end{aligned} \tag{5.14}$$

Next, we calculate the imaginary part of the denominator,

$$\frac{1}{((p_b-q)^2-m_u^2+i\epsilon)} \to (-2\pi i)\delta((p_b-q)^2-m_u^2)\Theta((p_b^0-q^0)). \tag{5.15}$$

Integrating over the neutrino energy, the double differential decay rate for $B \to X_u \ell \nu_\ell$ mode is calculated as

$$\begin{aligned}\frac{d^2\Gamma}{dyd\hat{q}^2} &= \frac{G_F^2|V_{ub}|^2 m_b^5}{96\pi^3}y\Big[6(1-\frac{\hat{q}^2}{y})(1-\rho-y+\hat{q}^2)+\lambda_1\Big(-3+3\rho+4\frac{\hat{q}^2}{y}-4\rho\frac{\hat{q}^2}{y}-6\hat{q}^2 \\ &+4\frac{(\hat{q}^2)^2}{y}-\delta(z)\Big(1-2\rho+\rho^2-3y(1-\rho)-3\frac{\hat{q}^2}{y}+2\rho\frac{\hat{q}^2}{y}+\rho^2\frac{\hat{q}^2}{y}+11\hat{q}^2-3\rho\hat{q}^2 \\ &-3x\hat{q}^2-6\frac{(\hat{q}^2)^2}{y}-2\rho\frac{(\hat{q}^2)^2}{y}+2(\hat{q}^2)^2+\frac{(\hat{q}^2)^3}{y}\Big)+\delta'(z)(1-\frac{\hat{q}^2}{y})(1-\rho-y+\hat{q}^2) \\ &(1-2\rho+\rho^2-2\hat{q}^2-2\rho\hat{q}^2+(\hat{q}^2)^2)\Big)+3\lambda_2\Big(1-5\rho+2\frac{\hat{q}^2}{y}+10\rho\frac{\hat{q}^2}{y}+10\hat{q}^2 \\ &(1-\frac{\hat{q}^2}{y})-\delta(z)\Big(-1+6\rho-5\rho^2+y(1-5\rho)+\frac{\hat{q}^2}{y}(1-2\rho)+5\rho^2\frac{\hat{q}^2}{y}+\hat{q}^2 \\ &(1+15\rho)+5y\hat{q}^2-2\frac{(\hat{q}^2)^2}{y}-10(1+y)\frac{(\hat{q}^2)^2}{y}+\frac{(\hat{q}^2)^3}{y}\Big)\Big)\Big] \end{aligned} \tag{5.16}$$

where $y = \dfrac{2E_\ell}{m_b}$, $q^2 = (p_l + p_n)^2$, $\hat{q}^2 = \dfrac{q^2}{m_b^2}$, $\rho = \dfrac{m_u^2}{m_b^2}$ and $z = 1 - y - \frac{\hat{q}^2}{y} + \hat{q}^2 - \rho$. Eq. (5.16) is in perfect agreement with [52]. The lepton spectrum for $B \to X_u \ell \nu_\ell$ in the limit $\rho \to 0$ is

$$\frac{d\Gamma}{dy} = 2\Gamma_0\Big[y^2(3-2y) - \frac{\lambda_1}{m_b^2}\Big(-\frac{5}{3}y^3 + \frac{1}{6}\delta(1-y) + \frac{1}{6}\delta'(1-y)\Big) - \frac{\lambda_2}{m_b^2}\Big(-(6+5y)y^2 + \frac{11}{2}\delta(1-y)\Big)\Big] \tag{5.17}$$

Here, we have $\Gamma_0 = \frac{G_F^2|V_{ub}|^2 m_b^5}{192\pi^3}$. It is worth noting that the contribution from the parton model, given by $2y^2(3-2y)$, does not vanish at the endpoint. As a result, delta functions and their derivatives appear in the lepton spectrum. Upon integrating over the lepton energy, we obtain the total decay rate as follows:

$$\Gamma = \Gamma_0\Big(1 + \frac{\lambda_1}{2m_b^2} - 9\frac{\lambda_2}{2m_b^2}\Big) \tag{5.18}$$

which has the same form as shown in Eq.(5.3).

5.4 Differential rate of $B \to X_u \ell \nu_\ell \gamma$

Now we calculate the differential rate for the $B \to X_u \ell \nu_\ell \gamma$ mode. Fig.(5.2) illustrates all the Feynman diagrams[1] contributing to the decay width of $B \to X_u \ell \nu_\ell \gamma$ at the leading order in perturbation theory. In the leading order ($m_b \to \infty$), the decay width for the process $B \to X_u \ell \nu_\ell \gamma$ is obtained from the partonic result, while the preasymptotic effects, i.e., the sub-leading contributions in the HQET, are expressed in powers of $\frac{\Lambda_{\rm QCD}}{m_b}$. Similar to Section-5.3, our focus lies on the $B \to B$ forward scattering matrix element rather than the amplitude for $B \to X_u \ell \nu_\ell \gamma$ itself. The imaginary part of the amplitude depicted in Fig.(5.3) is associated with the inclusive rate for the $B \to X_u \ell \nu_\ell \gamma$ transition, as dictated by the optical theorem. However, the $B \to X_u \ell \nu_\ell \gamma$ process is significantly more intricate compared to the $B \to X_u \ell \nu_\ell$ mode due to the presence of a photon line between the charged quarks and leptons, as shown in Fig.(5.2). This implies that certain diagrams, such as Figs.5.2b and 5.2c, do not readily separate

[1] We consider only those diagrams that, upon cutting the photon and u-quark lines, lead to $B \to X_u \ell \nu_\ell \gamma$.

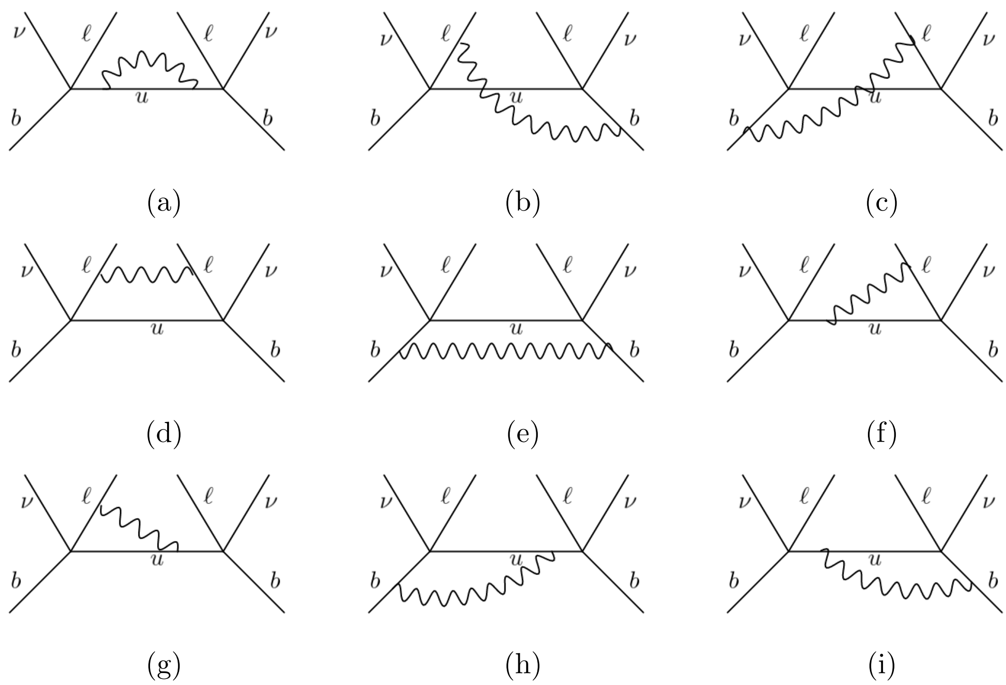

Figure 5.2: Feynman diagrams for $B \to X_u \ell \nu_\ell \gamma$.

into leptonic and hadronic components like in the $B \to X_u \ell \nu_\ell$ mode. Since the hadronic part in some of the diagrams interacts with the leptonic part through the photon, the calculation of the matrix element becomes more complex when expressed in terms of invariant tensors and utilizing analytic properties of the transition operator. Furthermore, in the present case, the transition tensor will be a four-index object, with two indices for the weak currents and two for the electromagnetic currents representing photon emission. Therefore, employing the Cutkosky method directly to compute the matrix element is more straightforward. As we verified in the previous section, this method yields correct results for the decay rate of the $B \to X_u \ell \nu_\ell$ mode.

The decay rate for the semi-leptonic inclusive process $B \to X_u \ell \nu_\ell \gamma$ is given by

$$\Gamma_\gamma = \Big(\frac{4G_F}{\sqrt{2}}\Big)^2 |V_{ub}|^2 \frac{1}{2m_B} \int \frac{d^3p_l}{(2\pi)^3 2E_l} \int \frac{d^3p_n}{(2\pi)^3 2E_\nu} \int \frac{d^4k}{(2\pi)^4} Im\Big[\langle B| I\mathcal{M}_{\mu\nu}\mathcal{L}^{\mu\nu}|B\rangle\Big] \tag{5.19}$$

$$\text{with} \quad I\mathcal{M}_{\mu\nu}\mathcal{L}^{\mu\nu} = \sum_{m=1}^{9} I_m \mathcal{M}^{(m)}_{\mu\nu}\mathcal{L}^{\mu\nu(m)} \tag{5.20}$$

Here, $\mathcal{M}^{(m)}_{\mu\nu}$ and $\mathcal{L}^{(m)}_{\mu\nu}$ represent the Dirac structures for the quark and leptonic parts, respectively, while I_m includes the denominator part of the propagator. further, $m = 1, ..., 9$ corresponds to Fig.(5.2a,...5.2i). In these expressions, k denotes the photon four-momentum, and $p_{\ell(\nu)}$ represents the four-momentum of the lepton (neutrino). We now present the explicit calculation of the forward scattering operator for Fig.(5.2a), and the calculations for the other diagrams follow a similar procedure which is provided below. The evaluation of the hadronic and leptonic tensors requires computing $\mathcal{M}^{(m)}_{\mu\nu}$, $\mathcal{L}^{(m)}_{\mu\nu}$, and I_m.

In the leading order of α_s, the explicit forms of $\mathcal{M}^{(1)}_{\mu\nu}$, $\mathcal{L}^{(1)}_{\mu\nu}$, and I_1 are:

$$\begin{aligned}
\mathcal{M}^{(1)}_{\mu\nu} &= 2(-ig^{\alpha\beta})\bar{b}\gamma^{\nu}\left(1-\gamma^5\right) i\left(\not{p}_b + \not{\Pi} - \not{q}\right)(-ieQ_u)\gamma^{\alpha} i\left(\not{p}_b + \not{\Pi} - \not{k} - \not{q} + m_u\right) \\
&\quad (-ieQ_u)\gamma^{\beta} i\left(\not{p}_b + \not{\Pi} - \not{q}\right)\gamma^{\mu}\left(1-\gamma^5\right) b, \\
\mathcal{L}^{(1)}_{\mu\nu} &= \left(\bar{\ell}\gamma^{\mu}(1-\gamma^5)\nu_\ell\right)\left(\bar{\nu}_\ell\gamma^{\nu}(1-\gamma^5)\ell\right),
\end{aligned} \tag{5.21}$$

and

$$\begin{aligned}
I_1 &= (k^2 + i\epsilon)^{-1}((p_b + \Pi - q)^2 - m_u^2 + i\epsilon)^{-1}((p_b + \Pi - q - k)^2 - m_u^2 + i\epsilon)^{-1} \\
&\quad ((p_b + \Pi - q)^2 - m_u^2 + i\epsilon)^{-1}
\end{aligned} \tag{5.22}$$

respectively. Similarly, we express the effective momentum of the b quark as $p_b + \Pi$. Expanding I_1 in powers of Π allows us to obtain an expansion in terms of $\frac{\Lambda_{\text{QCD}}}{m_b}$, which is analogous to the $B \to X_u \ell \nu_\ell$ mode. The explicit expression for I_1 up to $\mathcal{O}(\Pi^2)$ is derived from Eq.(5.22) and is given as follows:

$$\begin{aligned}
I_1 &= \frac{1}{k^2((p_b - q - k)^2 - m_u^2)}\left[\frac{1}{(p_u \cdot k)^2} - \frac{2(p_b - q).\Pi}{(p_u \cdot k)^3} - \frac{\Pi^2}{(p_u \cdot k)^3} + \frac{2((p_b - q).\Pi)^2}{(p_u \cdot k)^4}\right] \\
&- \frac{1}{k^2((p_b - q - k)^2 - m_u^2)^2}\left[\frac{2p_u \cdot \Pi}{(p_u \cdot k)^2} - \frac{4(p_u \cdot \Pi)(p_b - q).\Pi}{(p_u \cdot k)^3} - \frac{\Pi^2}{(p_u \cdot k)^2}\right] \\
&+ \frac{1}{k^2((p_b - q - k)^2 - m_u^2)^3}\left[\frac{2(p_u \cdot \Pi)^2}{(p_u \cdot k)^2}\right]
\end{aligned} \tag{5.23}$$

Similar to Section-5.3, the Cutkosky method is exploited (see Fig.(5.3)) to calculate the imaginary part of the matrix element. Mathematically, this essentially

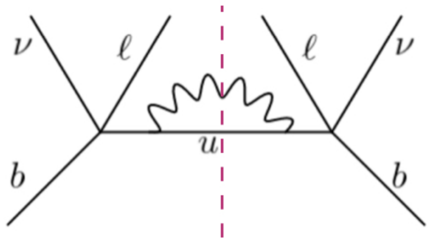

Figure 5.3: Representative diagram with explicit cut

replaces the cut propagator by a product of delta function and theta function enforcing the positive energy condition. For example

$$\frac{1}{((p_b - q - k)^2 - m_u^2 + i\epsilon)} \;\to\; (-2\pi i)\delta((p_b - q - k)^2 - m_u^2)\Theta((p_b^0 - q^0 - k^0)). \tag{5.24}$$

More generally one has the identity

$$-\frac{1}{\pi} Im\Big(\frac{1}{(p_b - q - k)^2 - m_u^2}\Big)^n = \frac{(-1)^{(n-1)}}{(n-1)!}\delta^{(n-1)}((p_b - q - k)^2 - m_u^2), \tag{5.25}$$

The superscript of the delta function indicates the $(n-1)$th derivative with respect to its argument. Handling terms involving derivatives of the delta function requires caution. The initial step involves applying integration by parts to eliminate the derivatives from the delta function and transfer them to other functions that multiply it. However, it is essential to handle the theta function carefully during this process, as it determines the minimum value of the neutrino energy, represented by E_ν. Additional information regarding the kinematics can be found in Appendix C.

Next, we proceed by combining the terms $\mathcal{M}\mu\nu^{(1)}$, $\mathcal{L}\mu\nu^{(1)}$, and I_1 to evaluate the imaginary part of the amplitude. Interestingly, our analysis reveals that no new operators are generated beyond those already present in the decay rate of the $B \to X_u \ell \nu_\ell$ process. All the relevant operators, up to dimension five, are listed in Eq.(5.14).

It is evident that only I_1 contributes to the imaginary part of the matrix element. Thus, we provide an explicit expression for the matrix element based on the representation outlined in Eq.(5.23). Each square bracket contains terms with expansions in Π up to the second order. The imaginary parts of the coefficients in these square brackets contribute to the delta function and its derivatives. We denote the forward scattering matrix element as

$$\mathcal{J}_1(n;\alpha) = \langle B(v)|Im\{I_1\mathcal{M}^{(1)}_{\mu\nu}\mathcal{L}^{(1)}_{\mu\nu}\}|B(v)\rangle(n;\alpha). \tag{5.26}$$

Here, $n = 0,1,2$ represents the expansion powers of Π, and $\alpha = a,c,d$ corresponds to the square brackets in Eq.(5.23) in sequence. For instance, in $\mathcal{J}(0;a)$, '0' signifies the expansion in Π up to $\mathcal{O}(\Pi^0)$, and 'a' indicates the selection of elements from the first square bracket of Eq.(5.23). We now provide explicit expressions for each of the terms in I_1, excluding the delta function or its derivatives.

$$\begin{aligned}
&\mathcal{O}(\Pi^0):\\
&\mathcal{J}_1(0;a) = \frac{-1}{m_b(p_u\cdot k)^2}16(p_b\cdot p_l)\Big((q^2+m_b^2-2(p_b\cdot q))(p_n.(p_b+k-q))\\
&\qquad -2((p_b-q)\cdot k)(q-p_b)\cdot p_n\Big)
\end{aligned} \tag{5.27}$$

$$\begin{aligned}
&\mathcal{O}(\Pi):\\
&\mathcal{J}_1(1;a) = \frac{-1}{3m_b^3(p_u\cdot k)^3}64(\lambda_1+3\lambda_2)\Big(2m_b^2(p_l\cdot q)+(p_b\cdot p_l)(3m_b^2-5(p_b\cdot q))\Big)\Big((q^2+m_b^2\\
&\qquad -2(p_b\cdot q))(p_n.(p_b+k-q))-2((p_b-q)\cdot k)(p_n.q-p_b\cdot p_n)\Big)
\end{aligned} \tag{5.28}$$

$$\begin{aligned}
&\mathcal{O}(\Pi^2):\\
&\mathcal{J}_1(2;a) = \frac{1}{3m_b^3(p_u\cdot k)^4}32\lambda_1(p_b\cdot p_l)\Big(-2(p_u\cdot k)^2\big(m_b^2(p_n\cdot k-5(p_n.q))+(p_b\cdot p_n)\\
&\qquad (2(p_b\cdot(q+k))+3m_b^2)\big)+\big((q^2+m_b^2-2(p_b\cdot q))(p_n.(p_b+k-q))-2(p_b-q)\cdot k\\
&\qquad ((p_b-q)\cdot p_n)\big)((p_b\cdot q)^2+m_b^2(3(p_u\cdot k)-q^2))+4(p_u\cdot k)\Big(m_b^2((p_l\cdot p_n)\big(2p_b\cdot(q+k)\\
&\qquad -4(q\cdot k)-3q^2\big)+(p_b\cdot p_n)(p_b\cdot q+2(q\cdot k+q^2))+2q^2(p_n\cdot k))+(p_b\cdot q)\big(2(p_n.q)\\
&\qquad (p_b\cdot(q+k))-2(p_b\cdot q)(p_n\cdot k)+(p_b\cdot p_n)(q^2+2(q\cdot k)-4p_b\cdot(q+k))\big)-m_b^4(p_n.q)\Big)\Big)
\end{aligned} \tag{5.29}$$

The combination $\mathcal{J}_1(0;a)+\mathcal{J}_1(1;a)+\mathcal{J}_1(2;a)$ is multiplied by $\delta(k^2)\theta(k^0)\delta(((p_b-q-k)^2-m_u^2))\theta((p_b-q-k)^0)$. Similarly, the terms arising from the second square brackets of Eq.(5.23) involving the hadronic and leptonic tensors (Eq.(5.21)) are expanded in powers of Π. As this set of terms is multiplied by $\frac{1}{((p_b-q-k)^2-m_u^2)^2}$, which represents the square of the propagator, the sum of these terms carries an overall factor of $\delta(k^2)\theta(k^0)\delta'(((p_b-q-k)^2-m_u^2))\theta((p_b-q-k)^0)$.

$\mathcal{O}(\Pi)$:

$$\begin{aligned}\mathcal{J}_1(1;c) \;=\;& \frac{-1}{3m_b^3(p_u\cdot k)^2}128(\lambda_1+3\lambda_2)\Big((m_b^2+q^2-2p_b\cdot q)((p_b-q+k)\cdot p_n)-2((p_b-q)\cdot k)\\ & ((p_b-q)\cdot p_n)\Big)\Big((p_b\cdot p_l)(5p_b\cdot(q+k)-3m_b^2)-2m_b^2(p_l\cdot(q+k))\Big) \qquad (5.30)\end{aligned}$$

$\mathcal{O}(\Pi^2)$:

$$\begin{aligned}\mathcal{J}_1(2;c) \;=\;& \frac{-1}{3m_b^3(p_u\cdot k)^3}128\Big(\lambda_1(p_b\cdot p_l)\Big(8((p_u\cdot k+p_b\cdot q)(p_n.q)--(2(p_u\cdot k)+p_b\cdot q)(p_b\cdot p_n))\\ & (p_b\cdot k)^2+2\Big(\big(4(p_n\cdot k)(p_u\cdot k)+(7p_u\cdot k-4k\cdot q-4q^2)(p_n.q)+\big(4(q\cdot k)-3(p_u\cdot k)\\ & +4q^2\big)(p_b\cdot p_n)\big)m_b^2-2(p_b\cdot q)\big((p_n\cdot k)(2(p_u\cdot k)-q^2+2(p_b\cdot q)-m_b^2)+(p_n.q)\\ & (2k\cdot q-4(p_u\cdot k)+q^2-4(p_b\cdot q)+m_b^2)\big)+2\big(2(q\cdot k)(p_u\cdot k+p_b\cdot q)+(p_u\cdot k)\big(q^2\\ & -8(p_b\cdot q)+m_b^2\big)+(p_b\cdot q)(q^2-4(p_b\cdot q)+m_b^2)\big)(p_b\cdot p_n)\big)(p_b\cdot k)+\Big(8(p_b-p_n).q\\ & (k\cdot q)^2+2(2(3q^2-2(q\cdot p_b)+m_b^2)(p_n.q-p_b\cdot p_n)+p_u\cdot k(11(p_b\cdot p_n)-15(q\cdot p_n)))\\ & (k\cdot q)+4q^2(q^2-2(p_b\cdot q)-m_b^2)(p_b-q)\cdot p_n+p_u\cdot k((2(p_b\cdot q)-m_b^2)(7q-3p_b)\cdot p_n\\ & +q^2(11p_b-15q)\cdot p_n)\Big)m_b^2+4(p_b\cdot q)\Big(p_b\cdot qp_n.q(2(p_u-q)\cdot k-q^2+2p_b\cdot q-m_b^2)\\ & +(2(q\cdot k)(p_u\cdot k+p_b\cdot q)+p_u\cdot k(q^2-4p_b\cdot q+m_b^2)+p_b\cdot q(q^2-2p_b\cdot q+m_b^2))(p_b\cdot p_n)\Big)\\ & +(p_n\cdot k)\Big(4(q^2-2p_b\cdot q+m_b^2)((p_b\cdot q)^2-(q^2+k\cdot q)m_b^2)+(p_u\cdot k)\big((7q^2+2p_b\cdot q\\ & -m_b^2)m_b^2-8(p_b\cdot q)^2\big)\Big)\Big)\Big) \qquad (5.31)\end{aligned}$$

In a similar way, we then consider the imaginary part of the third square bracket of Eq. (5.23) and combine it with Eq.(5.21). Explicitly the amplitude expanded in powers of Π is

$\mathcal{O}(\Pi^2)$:

$$\begin{aligned}\mathcal{J}_1(2;d) \;=\;& \frac{1}{3m_b^3(p_u\cdot k)^2}256\lambda_1(p_b\cdot p_l)\Big((-2p_b\cdot q+m_b^2+q^2)(p_b+k-q)\cdot p_n-2(p_b-q)\cdot k\\ & (q-p_b)\cdot p_n\Big)\Big(((q+k).p_b)^2-m_b^2(2q\cdot k+q^2)\Big). \qquad (5.32)\end{aligned}$$

Here, 'd' refers to the elements of the third square bracket of Eq. (5.23). Moreover, the $\mathcal{J}_1(2;d)$ has a multiplicative factor of $\delta(k^2)\theta(k^0)\delta''(((p_b-q-k)^2-m_u^2))\theta((p_b-q-k)^0)$.

Next, combining all the amplitudes, the total forward matrix element for Fig.5.2a is given by

$$\langle B|Im\{I_1\mathcal{M}^{(1)}_{\mu\nu}\mathcal{L}^{(1)}_{\mu\nu}|B\}\rangle = \delta(k^2)\theta(k^0)\Big[(\mathcal{J}_1(0;a)+\mathcal{J}_1(1;a)+\mathcal{J}_1(2;a))\delta\big((p_b-q-k)^2 -m_u^2\big)+(\mathcal{J}_1(1b)+\mathcal{J}_1(2b))\delta'((p_b-q-k)^2-m_u^2)+ (\mathcal{J}_1(2;c))\delta''((p_b-q-k)^2-m_u^2)\Big]\theta((p_b-q-k)^0) \tag{5.33}$$

Integration by parts is then used to simplify such expressions:

$$\delta'(x)\theta(x)f(x) = -\delta(x)\delta(x)f(x)-\delta(x)\theta(x)f'(x), \text{ and} \tag{5.34}$$

$$\delta''(x)\theta(x)f(x) = \delta(x)\delta'(x)f(x)+2\delta(x)\delta(x)f'(x)+\delta(x)+\theta(x)f''(x). \tag{5.35}$$

These relations will be utilized for performing integrals over phase space. Likewise, the forward matrix elements for the remaining eight Feynman diagrams depicted in Fig.(5.2) are computed. The relevant explicit expressions for $\mathcal{M}^{(m)}_{\mu\nu}$, $\mathcal{L}^{(m)}_{\mu\nu}$, and I_m with $m=2,...9$ for all the Feynman diagrams are given by

1. Fig.(2(b)):

$$\begin{aligned}
\mathcal{M}^{(2)}_{\mu\nu} &= 2(-ig^{\alpha\beta})\bar{b}(-ieQ_b)\gamma_\alpha i\left(\not{p}_b+\not{\Pi}-\not{k}+m_b\right)\gamma^\nu(1-\gamma^5)i\left(\not{p}_b+\not{\Pi}-\not{k}-\not{q}+m_u\right)\\
&\quad\gamma^\mu\left(1-\gamma^5\right)b\\
\mathcal{L}^{(2)}_{\mu\nu} &= \left(\bar{\ell}(-ieQ_\ell)\gamma_\beta i\left(\not{p}_l+\not{k}+m_l\right)\gamma^\mu(1-\gamma^5)\nu_\ell\right)\left(\bar{\nu}_\ell\gamma^\nu(1-\gamma^5)\ell\right)
\end{aligned} \tag{5.36}$$

$$\begin{aligned}
I_2 &= \frac{1}{k^2((p_b-q-k)^2-m_u^2)}\Big[\frac{-1}{(p_b\cdot k)(p_l\cdot k)}-\frac{(p_b-k).\Pi}{(p_l\cdot k)(p_b\cdot k)^2}-\frac{\Pi^2}{2(p_l\cdot k)(p_b\cdot k)^2}-\\
&\quad\frac{((p_b-k).\Pi)^2}{2(p_l\cdot k)(p_b\cdot k)^3}\Big]-\frac{1}{k^2((p_b-q-k)^2-m_u^2)^2}\Big[\frac{2p_u\cdot\Pi}{(p_l\cdot k)(p_b\cdot k)}+\frac{2(p_u\cdot\Pi)(p_b-k).\Pi}{(p_l\cdot k)(p_b\cdot k)^2}\\
&\quad+\frac{\Pi^2}{(p_l\cdot k)(p_b\cdot k)}\Big]-\frac{1}{k^2((p_b-q-k)^2-m_u^2)^3}\Big[\frac{2(p_u\cdot\Pi)^2}{(p_l\cdot k)(p_b\cdot k)}\Big]
\end{aligned} \tag{5.37}$$

$\mathcal{O}(\Pi^0)$:

$$\begin{aligned}
\mathcal{J}_2(0;a) &= \frac{-1}{m_b(p_b\cdot k)(p_l\cdot k)}16\Big(-2(p_b\cdot p_n)\Big(2(p_b\cdot p_l)^2+(p_l\cdot k)^2+p_l\cdot k(p_b\cdot q+p_l\cdot q-\\
&\quad 3p_b\cdot p_l)-(p_b\cdot k)(p_l\cdot k)-p_b\cdot p_l(q\cdot k-2p_b\cdot k+2p_l\cdot q)\Big)+m_b^2\Big(p_l\cdot k((p_b+q)\cdot p_n)\\
&\quad +p_l\cdot p_n(p_b\cdot k-q\cdot k-2p_l\cdot k)-((q-p_b).p_l)(p_n\cdot k+2p_l\cdot p_n)\Big)-2((p_b\cdot p_l)(p_n\cdot k)\\
&\quad -(p_b\cdot k)(p_l\cdot p_n))((q+k-p_b).p_l)\Big)
\end{aligned} \tag{5.38}$$

$\mathcal{O}(\Pi)$:

$$\begin{aligned}
\mathcal{J}_2(1;a) \;=\;& \frac{-1}{3m_b^3(p_b\cdot k)^2(p_l\cdot k)} 32(\lambda_1+3\lambda_2)\Big(2m_b^2\Big(p_n\cdot k\big(p_b\cdot p_l(p_l\cdot q-2q\cdot k-3p_l\cdot k)\\
&-(p_b\cdot p_l)^2+2p_l\cdot k(p_b\cdot q+2p_l\cdot k+2p_l\cdot q)\big)+p_b\cdot p_n\big(6(p_b\cdot p_l)^2-p_b\cdot p_l\\
&(7p_l\cdot k+3q\cdot k+6p_l\cdot q)+p_l\cdot k(3p_b\cdot q+p_l\cdot(q+k))\big)\Big)+(p_b\cdot k)^2\big(10(p_l\cdot p_n\\
&(q+k-p_b).p_l)+p_b\cdot p_n(p_l\cdot q-2p_b\cdot p_l)+m_b^2p_l\cdot p_n\big)+p_b\cdot k\Big(-10p_b\cdot p_n\\
&\big(2(p_b\cdot p_l)^2-p_b\cdot p_l(3p_l\cdot k+q\cdot k+2p_l\cdot q)+p_l\cdot k(p_b\cdot q+(q+k).p_l)\big)+m_b^2\\
&\big(p_n\cdot k(9p_b-5q).p_l+p_l\cdot k(9p_b-12p_l+q)-p_l\cdot p_n(12(q-p_b).p_l+q\cdot k)\\
&-6p_b\cdot p_n(q-2p_b).p_l\big)-10(p_b\cdot p_l)(p_n\cdot k)\big((q+k-p_b).p_l\big)-3m_b^4(p_l\cdot p_n)\Big)\\
&+m_b^4\big(3(p_b-q).p_l((k+2p_l)\cdot p_n)+3(q\cdot k)(p_l\cdot p_n)-3(p_l\cdot k)(p_n.(p_b-2p_l+q))\\
&+4p_n\cdot k\big)\Big) \qquad (5.39)
\end{aligned}$$

$$\begin{aligned}
\mathcal{J}_2(1;c) \;=\;& \frac{1}{3m_b^3(p_b\cdot k)(p_l\cdot k)} 128(\lambda_1+3\lambda_2)\Big(m_b^4\big(p_n\cdot k((q-3p_b).p_l)-p_l\cdot k\big(\big(4k+5q+\\
&3p_b-6p_l\big)\cdot p_n\big)+p_l\cdot p_n(5k\cdot q+6p_l\cdot q-6p_b\cdot p_l)\big)+\big(2((4k+2q+p_b)\cdot p_n)(p_l\cdot k)^2\\
&+\big(2p_n\cdot k(2q\cdot p_b+6q\cdot p_l-3p_b\cdot p_l)+4p_n.q((q-2p_b).p_l)+2q^2(p_b\cdot p_n)-2\big(\big(q+\\
&7p_b\big).p_l\big)p_b\cdot p_n+p_b\cdot q((5q+11p_b-6p_l)\cdot p_n)-4(q\cdot k)(p_l\cdot p_n)\big)p_l\cdot k+4(p_n.q)\\
&(p_b\cdot p_l)((p_b-q).p_l)+p_n\cdot k\big(4(q\cdot p_l)^2-2(p_b\cdot p_l)^2-p_b\cdot q((q-5p_b).p_l)-2p_b\cdot p_l\\
&(2k\cdot q+q^2+p_l\cdot q)\big)-2p_b\cdot p_n\big(2q\cdot p_l((k+p_l).q)+p_b\cdot p_l((3k+4p_l).q)-\\
&6(p_b\cdot p_l)^2\big)+p_l\cdot p_n\big(6p_b\cdot q((p_b-q).p_l)+k\cdot q(4p_b\cdot p_l-4q\cdot p_l-5q\cdot p_b)\big)\big)m_b^2+10\\
&q\cdot p_b\big(-(p_n\cdot k)(p_b\cdot p_l)((k+q-p_b).p_l)-p_b\cdot p_n\big(2(p_b\cdot p_l)^2-p_b\cdot p_l(k\cdot q+3k\cdot p_l\\
&+2q\cdot p_l)+p_l\cdot k(k\cdot p_l+q\cdot p_b+q\cdot p_l)\big)\big)\big)+(p_b\cdot k)^2\big(m_b^2p_l\cdot p_n+10((q-2p_b).p_l)\\
&(p_b\cdot p_n)+((k+q-p_b).p_l)(p_l\cdot p_n)\big)+p_b\cdot k\big(-3(p_l\cdot p_n)m_b^4+\big(p_n\cdot k((9p_b-q).p_l)\\
&+p_l\cdot k((q+p_b)\cdot p_n)+p_l\cdot p_n(2q^2+q\cdot p_b-12k\cdot p_l-k\cdot q)-2((2q+p_b+6p_l)\cdot p_n)\\
&(q\cdot p_l)+4p_b\cdot p_l((q+3p_b+3p_l)\cdot p_n)\big)m_b^2+10\big(-(p_n\cdot k)(p_b\cdot p_l)((k+q-p_b).p_l)\\
&-p_b\cdot p_n\big((p_l\cdot k)^2+p_l\cdot k(q\cdot p_b+q\cdot p_l-3p_b\cdot p_l)+2(p_b\cdot p_l)^2-(q\cdot p_b)(q\cdot p_l)-\big(\big(k-\\
&2p_b+2p_l\big).q\big)\big)+((k+q-p_b).p_l)(p_b\cdot q)(p_l\cdot p_n)\big)\big)\big)\Big) \qquad (5.40)
\end{aligned}$$

$\mathcal{O}(\Pi^2)$:

$$\begin{aligned}
\mathcal{J}_2(2;a) \;=\;& \frac{1}{3m_b^3(p_b\cdot k)^2(p_l\cdot k)} 16\lambda_1\Big(\big(3(p_l\cdot k)((q+p_b)\cdot p_n)-3p_l\cdot p_n((3q+10p_l)\cdot k)-\\
&3p_l\cdot(q-p_b)((k+2p_l)\cdot p_n)\big)m_b^4-2\big(p_n\cdot k((7k+5q-5p_b).p_l)(p_b\cdot p_l)+p_b\cdot p_n\\
&\big(6(p_b\cdot p\ell)^2-3p_b\cdot p_l(k\cdot q+5k\cdot p_l+2q\cdot p_l)+p_l\cdot k(7p_l\cdot k+3p_b\cdot q+5p_l\cdot q)\big)\big)m_b^2\\
&+(p_b\cdot k)^2\big(2p_l\cdot q((p_b-p_l)\cdot p_n)-2p_b\cdot p_l((2p_b+p_l)\cdot p_n)-p_l\cdot p_n(3m_b^2+2p_l\cdot k)\big)\\
&+p_b\cdot k\big(3(p_l\cdot p_n)m_b^4-4(p_b\cdot p_n)m_\ell^2m_b^2+6((q-2p_b).p_l)(p_b\cdot p_n)m_b^2-\big(k\cdot q-\\
&8q\cdot p_l+8p_b\cdot p_l\big)(p_l\cdot p_n)m_b^2+p_b\cdot p_n\big(2(p_l\cdot k)^2-4(p_b\cdot p_l)^2+2(q\cdot k)(p_b\cdot p_l)+4\\
&(p_l\cdot q)(p_b\cdot p_l)\big)+p_n\cdot k\big(2(pb.p_l)((q+p_b).p_l)-((q-5p_b).p_l)m_b^2\big)+p_l\cdot k\big(\big(\big(q\\
&+5p_b+12p_l\big)\cdot p_n\big)m_b^2+2(p_n\cdot k)(p_b\cdot p_l)+2(p_l\cdot q-p_b\cdot q+3p_b\cdot p_l)(p_b\cdot p_n)\big)\big)\Big) \qquad (5.41)
\end{aligned}$$

$$
\begin{aligned}
\mathcal{J}_2(2;c) \quad = \quad & \frac{-1}{3m_b^3(p_b\cdot k)^2(p_l\cdot k)}128\lambda_1\big(m_b^4\big(-k.(2q+3p_b)\big(k\cdot p_n((q-p_b).p_l)-k\cdot p_l\big((q+\\
& p_b)\cdot p_n\big)\big)-p_l\cdot p_n\big(2(k\cdot q)^2+q\cdot k(5p_b\cdot k+4(k+q-p_b).p_l)+p_b\cdot k\big(\big(10k+10q\\
& -6p_b\big).p_l-3p_b\cdot k\big)\big)\big)+2\big((p_l\cdot p_n)(p_b\cdot k)^3+(p_b\cdot k)^2\big((p_b\cdot p\nu)(p_l\cdot(k+5q))+p_l\cdot p_n\\
& (7k\cdot p_l-q^2+q\cdot p_b+7q\cdot p_l)+p_b\cdot p_l((k+2q-6p_b-3p_l)\cdot p_n)\big)+\big(-7(p_b\cdot p_n)\\
& (p_l\cdot k)^2+\big((p_b\cdot p_n)(q^2-4q\cdot p_b-9q\cdot p_l)+p_b\cdot p_l((15p_b-2q-7k)\cdot p_n)+2(p_l\cdot p_n)\\
& ((k+p_b).q)\big)p_l\cdot k+2(q\cdot p_n)(p_b\cdot p_l)(p_b\cdot p_l-k\cdot q-q\cdot p_l)+(p_n\cdot k)(p_b\cdot p_l)(q^2-q\cdot p_b\\
& -7q\cdot p_l+5p_b\cdot p_l)-2(q\cdot p_l)^2(p_b\cdot p_n)-(p_b\cdot p_l)(p_b\cdot p_n)(6p_b\cdot p_l-3k\cdot q-12q\cdot p_l)+\\
& 2(p_l\cdot p_n)((q\cdot p_b)(q\cdot p_l)+k\cdot q\big(q\cdot p_b+q\cdot p_l-p_b\cdot p_l\big))\big)p_b\cdot k+2k\cdot q\big(-(p_n\cdot k)\big(\big(k+q\\
& -p_b\big).p_l\big)(p_b\cdot p_l)-p_b\cdot p_n\big(2(p_b\cdot p_l)^2-p_b\cdot p_l(k\cdot q+3p_l\cdot k+2q\cdot p_l)+p_l\cdot k\big(k\cdot p_l+\\
& q.(p_b+p_l)\big)\big)\big)\big)m_b^2-4k\cdot p_b((k+q).p_b)\big(-p_b\cdot p_n(p_l\cdot k)^2-p_l\cdot k\big((p_n\cdot k)(p_b\cdot p_l)+\\
& (q\cdot p_l)(p_b\cdot p_n)-(p_b\cdot k)(p_l\cdot p_n)\big)+p_b\cdot p_l\big(2p_b\cdot p_n((k+p_l).p_b)-(k\cdot p_n)(q\cdot p_l)\big)+\\
& (k\cdot p_b)(q\cdot p_l)(p_l\cdot p_n)\big)\big) \qquad (5.42)\\
\mathcal{J}_2(2;d) \quad = \quad & \frac{-1}{3m_b^3(p_b\cdot k)(p_l\cdot k)}256\lambda_1\big(((q+k).p_b)^2-m_b^2(2k\cdot q+q^2)\big)\Big(-2p_b\cdot p_n\big(2(p_b\cdot p_l)^2+\\
& (p_l\cdot k)^2+p_l\cdot k(q.(p_l+p_b)-3p_b\cdot p_l)-(p_b\cdot k)(q\cdot p_l)-p_b\cdot p_l(k\cdot q+2q\cdot p_l-2k\cdot p_b)\big)\\
& +m_b^2\big(k\cdot p_l((p_b+q)\cdot p_n)+(p_l\cdot p_n)((p_b-2p_l-q)\cdot k)-((q-p_b).p_l)((k+2p_l)\cdot p_n)\big)\\
& -2(p_b\cdot p_l)(k\cdot p_n)(-p_b+k+q).p_l+2(k\cdot p_b)(p_l\cdot p_n)((k+q-p_b).p_l)\Big) \qquad (5.43)
\end{aligned}
$$

2. Fig.(2(c)):

$$
\begin{aligned}
\mathcal{M}^{(3)}_{\mu\nu} \quad = \quad & 2(-ig^{\alpha\beta})\bar{b}\gamma^\nu(1-\gamma^5)i\left(\not{p}_b+\not{l}-\not{q}-\not{k}+m_u\right)\gamma^\mu\left(1-\gamma^5\right)i\left(\not{p}_b+\not{l}-\not{k}+m_b\right)\\
& (-ieQ_b)\gamma_\alpha b\\
\mathcal{L}^{(3)}_{\mu\nu} \quad = \quad & \left(\bar{\ell}\gamma^\mu(1-\gamma^5)\nu_\ell\right)\left(\bar{\nu}_\ell\gamma^\nu(1-\gamma^5)(-ieQ_l)\gamma_\alpha i\left(\not{p}_l+\not{k}+m_l\right)\ell\right) \qquad (5.44)\\
I_3 \quad = \quad & I_2 \qquad (5.45)
\end{aligned}
$$

$\mathcal{O}(\Pi^0)$:

$$
\begin{aligned}
\mathcal{J}_3(0;a) \quad = \quad & \frac{1}{m_b(p_b\cdot k)(p_l\cdot k)}16\Big(-(p_b\cdot p_n)(p_l\cdot k)^2+p_l\cdot k\big(m_b^2((p_b-2p_l+q)\cdot p_n)-2p_b\cdot p_n\\
& (-2p_b\cdot p_l+q.(p_b+p_l))\big)-m_b^2\big((q\cdot p_l-p_b\cdot p_l)(k\cdot p_n+2p_l\cdot p_n)+(k\cdot q)(p_l\cdot p_n)\big)\\
& +k\cdot p_b\big(p_l\cdot p_n(2q\cdot p_l+m_b^2)+2p_b\cdot p_n((q-2p_b).p_l)+m_\ell^2k\cdot p_n+k\cdot p_l\big((p_l-\\
& 2k)\cdot p_n\big)\big)+2p_b\cdot p_l\big(p_b\cdot p_n(k\cdot q+2q\cdot p_l-2p_b\cdot p_l)-(k\cdot p_n)(q\cdot p_l)\big)\Big) \qquad (5.46)
\end{aligned}
$$

$\mathcal{O}(\Pi)$:

$$\begin{aligned}
\mathcal{J}_3(1;a) \quad = \quad & \frac{-1}{3m_b^3(p_b\cdot k)^2(p_l\cdot k)}32(\lambda_1+3\lambda_2)\Big((p_b\cdot k)^2\big(5p_l\cdot k(2k\cdot p_n-p_l\cdot p_n)-5m_\ell^2(k\cdot p_n)\\
& -10p_b\cdot p_n((q-2p_b).p_l)-p_l\cdot p_n(10q\cdot p_l+m_b^2)\big)+p_b\cdot k\big(5(p_b\cdot p_n)(p_l\cdot k)^2+m_b^2\\
& \big(p_l\cdot p_n(k\cdot q+12q\cdot p_l-6p_b\cdot p_l)+6p_b\cdot p_n\big(q\cdot p_l-2p_b\cdot p_l\big)\big)+k\cdot p_l\big(m_b^2\big(\big(q-9p_l\\
& +6k-9p_b\big)\cdot p_n\big)+15(p_b\cdot p_l)(k\cdot p_n)+10p_b\cdot p_n(q.(p_b+p_l)-2p_b\cdot p_l)\big)+k\cdot p_n\\
& \big(5q\cdot p_l(2p_b\cdot p_l+m_b^2)+3m_b^2(m_\ell^2-3p_b\cdot p_l)\big)-10(p_b\cdot p_l)(p_b\cdot p_n)(-2p_b\cdot p_l+k\cdot q\\
& +2q\cdot p_l)+3m_b^4(p_l\cdot p_n)\big)+m_b^2\big(-p_n\cdot k\big(4(p_b\cdot p_l)^2+p_b\cdot p_l(5k\cdot p_l-4k\cdot q+2q\cdot p_l)\\
& +4k\cdot p_l(q\cdot p_b+2k\cdot p_l+2q\cdot p_l)\big)+p_b\cdot p_n\big((k\cdot p_l)^2-2k\cdot p_l(3q\cdot p_b+q\cdot p_l-4p_b\cdot p_l)\\
& +6p_b\cdot p_l(k\cdot q+2q\cdot p_l-2p_b\cdot p_l)\big)+m_b^2\big(k\cdot p_l((3p_b-2p_l+q)\cdot p_n+4k\cdot p_n)-3\\
& (q\cdot p_l-p_b\cdot p_l)(k\cdot p_n+2p_l\cdot p_n)-3(k\cdot q)(p_l\cdot p_n)\big)\big)\big)\Big) \qquad (5.47)
\end{aligned}$$

$$\begin{aligned}
\mathcal{J}_3(1;c) \quad = \quad & \frac{1}{3m_b^3(p_b\cdot k)(p_l\cdot k)}128(\lambda_1+3\lambda_2)\Big(5(p_b\cdot k)^2\big(k\cdot p_l((2k+4q-4p_b-p_l)\cdot p_n)-m_\ell^2\\
& ((k+2q-2p_b)\cdot p_n)+2p_b\cdot p_l((p_l-2(k+q-p_b))\cdot p_n)\big)+\big(5(p_b\cdot p_n)(p_l\cdot k)^2+\\
& \big(3m_b^2((p_l+4p_b-4q)\cdot p_n)+10p_b\cdot p_l((2q-3p_b)\cdot p_n)+5q\cdot p_b((4q-4p_b-p_l)\cdot p_n)\\
& +k\cdot p_n(-6m_b^2+10q\cdot p_b+15p_b\cdot p_l)\big)p_l\cdot k+\big(2(q-p_b)\cdot p_n(6m_b^2-5q\cdot p_b)+p_n\cdot k\\
& (9m_b^2-5q\cdot p_b)\big)m_\ell^2+2p_b\cdot p_l\big(3m_b^2((2q-2p_b-p_l)\cdot p_n)-10(q\cdot p_b+p_b\cdot p_l)\big(q\cdot p_n\\
& -p_b\cdot p_n\big)+5(q\cdot p_b)(p_l\cdot p_n)+k\cdot p_n\big(6m_b^2-10q\cdot p_b-15p_b\cdot p_l\big)\big)\big)p_b\cdot k+2m_b^2\big(k\cdot q\\
& ((k+2q-2p_b)\cdot p_n)+3((k+q-p_b)\cdot p_n)(q\cdot p_b-m_b^2)\big)m_\ell^2+2p_b\cdot p_l\big(\big((2q\cdot p_l+\\
& 3p_b\cdot p_l\big)(3k\cdot p_n+2q\cdot p_n-2p_b\cdot p_n)+k\cdot q((4(k+q-p_b)-2p_l)\cdot p_n)\big)m_b^2-5(q\cdot p_b)\\
& (p_b\cdot p_l)(3k\cdot p_n+2q\cdot p_n-2p_b\cdot p_n)\big)+p_l\cdot k\big(\big(k\cdot p_n(7p_b\cdot p_l-6q\cdot p_l)-8(q\cdot p_l)(q\cdot p_n)\\
& +2(4q\cdot p_l+5p_b\cdot p_l)p_b\cdot p_n+2k\cdot q\big(4p_b\cdot p_n+p_l\cdot p_n-4q\cdot p_l-2k\cdot p_n\big)\big)m_b^2+5(q\cdot p_b)\\
& (p_b\cdot p_l)((3k+4q-6p_b)\cdot p_n)\big)+(p_l\cdot k)^2\big(5p_b\cdot p_n(m_b^2+q\cdot p_b)-2\big(4k\cdot p_n+\\
& 5q\cdot p_n\big)m_b^2\big)\Big) \qquad (5.48)
\end{aligned}$$

$\mathcal{O}(\Pi^2)$:

$$
\begin{aligned}
\mathcal{J}_3(2;a) &= \frac{1}{3m_b^3(p_b\cdot k)^2(p_l\cdot k)}16\lambda_1\Big((p_b\cdot k)^2\big(-m_\ell^2(p_n\cdot k)+2((q-2p_b).p_l)(p_b\cdot p_n)+\\
&\quad k\cdot p_l((2k-p_l)\cdot p_n)-p_l\cdot p_n(9m_b^2+2q\cdot p_l+4p_b\cdot p_l)\big)+\big(3(p_l\cdot p_n)m_b^4+(p_b\cdot p_n)\\
&\quad m_b^2(2m_\ell^2+6q\cdot p_l-12p_b\cdot p_l)-\big(k\cdot q-8q\cdot p_l+2p_b\cdot p_l\big)(p_l\cdot p_n)m_b^2+\big((k\cdot p_l)^2\\
&\quad -4(p_b\cdot p_l)^2+2(k\cdot q)(p_b\cdot p_l)+4(q\cdot p_l)(p_b\cdot p_l)\big)(p_b\cdot p_n)+p_l\cdot k\big(\big((q+2p_b+\\
&\quad 9p_l)\cdot p_n\big)m_b^2+2(q\cdot p_l+4p_b\cdot p_l-q\cdot p_b)p_b\cdot p_n+3(p_n\cdot k)(p_b\cdot p_l-2m_b^2)\big)+p_n\cdot k\\
&\quad \big(3m_b^2m_\ell^2+q\cdot p_l(2p_b\cdot p_l-m_b^2)+4p_b\cdot p_l(2m_b^2+p_b\cdot p_l)\big)\big)p_b\cdot k+m_b^2\big(-11\\
&\quad (p_b\cdot p_n)(p_l\cdot k)^2+\big(m_b^2((3q+3p_b-10p_l)\cdot p_n)-17(k\cdot p_n)(p_b\cdot p_l)-2p_b\cdot p_n\big(3q\cdot p_b\\
&\quad +5q\cdot p_l-12p_b\cdot p_l\big)\big)p_l\cdot k+3(k\cdot q+2q\cdot p_l-2p_b\cdot p_l)\big(2(p_b\cdot p_l)(p_b\cdot p_n)-(p_l\cdot p_n)\\
&\quad m_b^2\big)+k\cdot p_n\big(p_b\cdot p_l(3m_b^2+4p_b\cdot p_l)-q\cdot p_l(3m_b^2+10p_b\cdot p_l)\big)\big)\Big) \qquad (5.49)\\
\mathcal{J}_3(2;c) &= \frac{-1}{3m_b^3(p_b\cdot k)^2(p_l\cdot k)}128\Big(2\big(\left(2q\cdot p_n+k\cdot p_n\right)m_l^2+k\cdot p_l\left(-2k\cdot p_n+p_l\cdot p_n-4q\cdot p_n\right)\\
&\quad +p_b\cdot p_l\left(4p_b\cdot p_n-2p_l\cdot p_n\right)\big)(k\cdot p_b)^3+\big(-2\left(p_b\cdot p_n\right)\left(k\cdot p_l\right)^2+k\cdot p_l\big(\big(28q\cdot p_n-\\
&\quad 20\left(p_b\cdot p_n\right)-3\left(p_l\cdot p_n\right)\big)m_b^2+\big(22m_b^2-4q\cdot p_b-6p_b\cdot p_l\big)\,k\cdot p_n+4p_b\cdot p_l\big(p_b\cdot p_n-\\
&\quad 2q\cdot p_n\big)+2q\cdot p_b\left(p_l\cdot p_n-4q\cdot p_n\right)\big)+m_l^2\big(\big(-11k\cdot p_n+6p_b\cdot p_n-14q\cdot p_n\big)m_b^2+\\
&\quad 2q\cdot p_b\left(2q\cdot p_n+k\cdot p_n\right)\big)+4p_b\cdot p_l\left(\left(p_b\cdot p_l\right)\left(2p_b\cdot p_n+k\cdot p_n\right)+q\cdot p_b\left(2p_b\cdot p_n-p_l\cdot p_n\right)\right)\\
&\quad +2m_b^2\big(2\left(2q\cdot p_l-5p_b\cdot p_l\right)k\cdot p_n+4q\cdot p_l\left(q\cdot p_n-p_b\cdot p_n\right)+p_b\cdot p_l\big(-10q\cdot p_n+6p_b\cdot p_n\\
&\quad +3p_l\cdot p_n\big)\big)\big)(k\cdot p_b)^2+2\left(k\cdot q\right)m_b^2\big(p_b\cdot p_n(k\cdot p_l)^2+2m_b^2m_l^2\left(-p_b\cdot p_n+k\cdot p_n+q\cdot p_n\right)\\
&\quad -2(p_b\cdot p_l)^2\big(3k\cdot p_n+2q\cdot p_n-2p_b\cdot p_n\big)+\left(k\cdot p_l\right)\left(p_b\cdot p_l\right)\left(3k\cdot p_n+4q\cdot p_n-6p_b\cdot p_n\right)\big)\\
&\quad +k\cdot p_b\big(\big(3m_b^2-2q\cdot p_b\big)\left(p_b\cdot p_n\right)\left(k\cdot p_l\right)^2-2m_b^2\big(\left(3p_b\cdot p_n-5\left(k\cdot p_n+q\cdot p_n\right)\right)m_b^2+\\
&\quad 2q\cdot p_b\left(k\cdot p_n+q\cdot p_n\right)+k\cdot q\left(2q\cdot p_n+k\cdot p_n-2p_b\cdot p_n\right)\big)m_l^2+2p_b\cdot p_l\big(\big(2p_b\cdot p_n\big(3p_b\cdot p_l\\
&\quad -2q\cdot p_l\big)+\left(4q\cdot p_l-13p_b\cdot p_l\right)k\cdot p_n+2\left(2q\cdot p_l-5p_b\cdot p_l\right)q\cdot p_n+2\left(k\cdot q\right)\big(p_l\cdot p_n-2\\
&\quad \left(-p_b\cdot p_n+k\cdot p_n+q\cdot p_n\right)\big)\big)m_b^2+2\left(q\cdot p_b\right)\left(p_b\cdot p_l\right)\left(2p_b\cdot p_n+k\cdot p_n\right)\big)+\left(k\cdot p_l\right)\\
&\quad \big(\big(p_b\cdot p_l\left(25k\cdot p_n+28q\cdot p_n-26p_b\cdot p_n\right)+\left(k\cdot q\right)\big(4k\cdot p_n+8q\cdot p_n-8\left(p_b\cdot p_n\right)-2\\
&\quad \left(p_l\cdot p_n\right)\big)\big)m_b^2-2\left(q\cdot p_b\right)\left(p_b\cdot p_l\right)\left(3k\cdot p_n+4q\cdot p_n-2p_b\cdot p_n\right)\big)\big)\Big) \qquad (5.50)\\
\mathcal{J}_3(2;d) &= \frac{1}{3m_b^3(p_b\cdot k)(p_l\cdot k)}256\lambda_1\big(\left(k\cdot p_b+q\cdot p_b\right)^2-m_b^2\left(2k\cdot q+q^2\right)\big)\Big(-2\left(p_b\cdot p_l\right)^2\big(-2\\
&\quad p_b\cdot p_n+3k\cdot p_n+2q\cdot p_n\big)+\left(p_b\cdot p_n\right)\left(k\cdot p_l\right)^2+2m_b^2m_l^2\left(-p_b\cdot p_n+k\cdot p_n+q\cdot p_n\right)+\\
&\quad k\cdot p_b\big(m_l^2\left(2p_b\cdot p_n-k\cdot p_n-2q\cdot p_n\right)+\left(k\cdot p_l\right)\left(-4p_b\cdot p_n+2k\cdot p_n-p_l\cdot p_n+4q\cdot p_n\right)\\
&\quad +2\left(p_b\cdot p_l\right)\left(p_l\cdot p_n-2\left(-p_b\cdot p_n+k\cdot p_n+q\cdot p_n\right)\right)\big)+\left(p_b\cdot p_l\right)\left(k\cdot p_l\right)\big(-6p_b\cdot p_n+\\
&\quad 3k\cdot p_n+4q\cdot p_n\big)\Big) \qquad (5.51)
\end{aligned}
$$

3. Fig.(2(d)):

$$\begin{aligned}
\mathcal{M}^{(4)}_{\mu\nu} &= \bar{b}\gamma^\nu(1-\gamma^5)i\left(\not{p}_b + \not{\Pi} - \not{q} - \not{k} + m_b\right)\gamma^\mu\left(1-\gamma^5\right)b \\
\mathcal{L}^{(4)}_{\mu\nu} &= (-ig^{\alpha\beta})\left(\bar{\ell}(-ieQ_l)\gamma_\alpha i\left(\not{p}_l + \not{k} + m_l\right)\gamma^\mu(1-\gamma^5)\nu_\ell\right)\Big(\bar{\nu}_\ell\gamma^\nu(1-\gamma^5)i\left(\not{p}_l + \not{k} + m_l\right) \\
&\quad (-ieQ_l)\gamma_\beta\ell\Big) \qquad (5.52) \\
I_4 &= \frac{1}{k^2((p_b-q-k)^2-m_u^2)}\left[\frac{1}{(p_l\cdot k)^2}\right] - \frac{1}{k^2((p_b-q-k)^2-m_u^2)^2}\left[\frac{2p_u\cdot\Pi}{(p_l\cdot k)^2} + \frac{\Pi^2}{(p_l\cdot k)^2}\right] \\
&+ \frac{1}{k^2((p_b-q-k)^2-m_u^2)^3}\left[\frac{2(p_u\cdot\Pi)^2}{(p_l\cdot k)^2}\right] \qquad (5.53)
\end{aligned}$$

$\mathcal{O}(\Pi^0)$:

$$\mathcal{J}_4(0;a) = \frac{1}{m_b(p_l\cdot k)^2}64 p_b\cdot p_n\Big(k\cdot p_l(k\cdot q - k\cdot p_b) - m_\ell^2(k\cdot p_l + k\cdot q + q\cdot p_l - k\cdot p_b - p_b\cdot p_l)\Big) \qquad (5.54)$$

$\mathcal{O}(\Pi)$:

$$\begin{aligned}
\mathcal{J}_4(1;a) &= \frac{-1}{3m_b^3(p_l\cdot k)^2}64(\lambda_1+3\lambda_2)\Big(m_\ell^2(2m_b^2(k\cdot p_n + p_l\cdot p_n) - 5p_b\cdot p_n(k\cdot p_b + p_b\cdot p_l)) \\
&\quad + k\cdot p_l\big(5(k\cdot p_b)(p_b\cdot p_n) - 2m_b^2 k\cdot p_n\big)\Big) \qquad (5.55) \\
\mathcal{J}_4(1;c) &= \frac{1}{3m_b^3(p_l\cdot k)^2}512(\lambda_1+3\lambda_2)\big(m_\ell^2(k\cdot p_l + k\cdot q + q\cdot p_l - k\cdot p_b - p_b\cdot p_l) \\
&\quad + k\cdot p_l(k\cdot p_b - k\cdot q)\big)\big(2m_b^2(k\cdot p_n + q\cdot p_n) + p_b\cdot p_n(3m_b^2 - 5(k\cdot p_b + q\cdot p_b))\big) \qquad (5.56)
\end{aligned}$$

$\mathcal{O}(\Pi^2)$:

$$\begin{aligned}
\mathcal{J}_4(2;a) &= 0 \qquad (5.57) \\
\mathcal{J}_4(2;c) &= \frac{-1}{3m_b^3(p_l\cdot k)^2}256\lambda_1\Big(4p_b\cdot p_n\left(m_\ell^2 - k\cdot p_l\right)(k\cdot p_b)^2 + 2k\cdot p_b\big(m_\ell^2\big(m_b^2\left(k\cdot p_n + q\cdot p_n\right) \\
&\quad + p_b\cdot p_n\big(2\left(p_b\cdot p_l + q\cdot p_b\right) + 3m_b^2\big)\big) - \left(p_b\cdot p_n\right)\left(k\cdot p_l\right)\left(2q\cdot p_b + 3m_b^2\right) - m_b^2 m_\ell^2\big(k\cdot p_n \\
&\quad + q\cdot p_n\big)\big) + m_\ell^2\big(m_b^2\big(p_b\cdot p_l\left(6p_b\cdot p_n + k\cdot p_n + q\cdot p_n\right) - p_b\cdot p_n\big(11\left(k\cdot p_l + q\cdot p_l\right) \\
&\quad + 12k\cdot q\big)\big) + 4\left(p_b\cdot p_l\right)\left(p_b\cdot p_n\right)\left(q.p_b\right)\big) + m_b^2\big(10\left(k\cdot q\right)\left(p_b\cdot p_n\right)\left(k\cdot p_l\right) + m_\ell^2\big(\left(p_b\cdot p_n\right) \\
&\quad \left(k\cdot p_l + 2k\cdot q + q\cdot p_l\right) - \left(p_b\cdot p_l\right)\left(k\cdot p_n + q\cdot p_n\right)\big)\big)\Big) \qquad (5.58) \\
\mathcal{J}_4(2;d) &= \frac{1}{3m_b^3(p_l\cdot k)^2}1024\lambda_1 p_b\cdot p_n\big((k\cdot p_b + q\cdot p_b)^2 - m_b^2(2k\cdot q + q^2)\big)\Big(m_\ell^2\big(-k\cdot p_b - p_b\cdot p_l \\
&\quad + k\cdot p_l + k\cdot q + q\cdot p_l\big) + k\cdot p_l(k\cdot p_b - k\cdot q)\Big) \qquad (5.59)
\end{aligned}$$

4. Fig.(2(e)):

$$\begin{aligned}
\mathcal{M}^{(5)}_{\mu\nu} &= (-ig^{\alpha\beta})\bar{b}(-ieQ_b)\gamma^\alpha i\left(\not{p}_b+\not{\Pi}-\not{k}+m_b\right)\gamma^\nu(1-\gamma^5)i\left(\not{p}_b+\not{\Pi}-\not{q}-\not{k}+m_u\right)\\
&\quad \gamma^\mu\left(1-\gamma^5\right)i\Big(\not{p}_b+\not{\Pi}-\not{k}+m_b\Big)(-ieQ_b)\gamma^\beta b\\
\mathcal{L}^{(5)}_{\mu\nu} &= \left(\bar{\ell}\gamma^\mu(1-\gamma^5)\nu_\ell\right)\left(\bar{\nu}_\ell\gamma^\nu(1-\gamma^5)\gamma_\alpha\ell\right) \qquad (5.60)\\
I_5 &= \frac{1}{k^2((p_b-q-k)^2-m_u^2)}\Big[\frac{1}{(p_b\cdot k)^2}+\frac{2(p_b-k).\Pi}{(p_b\cdot k)^3}+\frac{\Pi^2}{(p_b\cdot k)^3}+\frac{((p_b-k).\Pi)^2}{(p_b\cdot k)^4}\Big]\\
&+ \frac{1}{k^2((p_b-q-k)^2-m_u^2)^2}\Big[\frac{-2p_u\cdot\Pi}{(p_b\cdot k)^2}-\frac{4(p_u\cdot\Pi)(p_b-k).\Pi}{(p_b\cdot k)^3}-\frac{\Pi^2}{(p_b\cdot k)^2}\Big]\\
&+ \frac{1}{k^2((p_b-q-k)^2-m_u^2)^3}\frac{2(p_u\cdot\Pi)^2}{(p_b\cdot k)^2} \qquad (5.61)
\end{aligned}$$

$\mathcal{O}(\Pi^0)$:

$$\begin{aligned}
\mathcal{J}_5(0;a) &= \frac{1}{m_b(p_b\cdot k)^2}32\Big(m_b^2\big(k\cdot p_n(p_b\cdot p_l-2q\cdot p_l)+k\cdot p_l(p_b\cdot p_n-2k\cdot p_n)-p_b\cdot p_l(q\cdot p_n)\\
&\quad +p_b\cdot p_n(q\cdot p_l)\big)+2k\cdot p_b(k\cdot p_n)((k+q-p_b).p_l)\Big) \qquad (5.62)
\end{aligned}$$

$\mathcal{O}(\Pi)$:

$$\begin{aligned}
\mathcal{J}_5(1;a) &= \frac{1}{3m_b^3(p_b\cdot k)^3}128(\lambda_1+3\lambda_2)\Big(10k\cdot p_n(k\cdot p_b)^2((k+q-p_b).p_l)+m_b^4\big(k\cdot p_n\big(8q\cdot p_l\\
&\quad -5p_b\cdot p_l\big)+k\cdot p_l((2q+10k-5p_b)\cdot p_n)+3p_b\cdot p_l(q\cdot p_n)-3p_b\cdot p_n(q\cdot p_l)\big)+m_b^2\\
&\quad p_b\cdot k\big(k\cdot p_n(11p_b\cdot p_l-16q\cdot p_l)+k\cdot p_l(p_b\cdot p_n-16k\cdot p_n)-5p_b\cdot p_l(q\cdot p_n)+p_b\cdot p_n\\
&\quad (4p_b\cdot p_l+q\cdot p_l)\big)\Big) \qquad (5.63)\\
\mathcal{J}_5(1;c) &= \frac{1}{3m_b^3(p_b\cdot k)^2}256(\lambda_1+3\lambda_2)\Big(m_b^2\big(4p_l\cdot p_n(k\cdot p_b)^2+k\cdot p_b\big(k\cdot p_n(11p_b\cdot p_l-16q\cdot p_l)\\
&\quad +k\cdot p_l\big(p_b\cdot p_n-4(4k\cdot p_n+q\cdot p_n)\big)-q\cdot p_n(p_b\cdot p_l+4q\cdot p_l)+p_b\cdot p_n(4p_b\cdot p_l+q\cdot p_l)\big)\\
&\quad -4k\cdot q(k\cdot p_n-p_b\cdot p_n)((k+q-p_b).p_l)+q\cdot p_b\big(k\cdot p_n(p_b\cdot p_l-6q\cdot p_l)+k\cdot p_l\big(p_b\cdot p_n\\
&\quad -6k\cdot p_n\big)-5p_b\cdot p_l(q\cdot p_n)+p_b\cdot p_n(4p_b\cdot p_l+q\cdot p_l)\big)\big)+m_b^4\big(5k\cdot p_n(2q\cdot p_l-p_b\cdot p_l)\\
&\quad +k\cdot p_l((10k+44q-5p_b)\cdot p_n)+q\cdot p_n(p_b\cdot p_l+4q\cdot p_l)-5p_b\cdot p\nu(q\cdot p_l)\big)+10k\cdot p_b\\
&\quad (k\cdot p_n)(k\cdot p_b+q\cdot p_b)(k\cdot p_l+q\cdot p_l-p_b\cdot p_l)\Big) \qquad (5.64)
\end{aligned}$$

$\mathcal{O}(\Pi^2)$:

$$\begin{aligned}
\mathcal{J}_5(2;a) &= \frac{1}{3m_b^3(p_b\cdot k)^3}64\lambda_1\Big(2k\cdot p_n(k\cdot p_b)^2((p_b+k+q).p_l)+m_b^4\big(k\cdot p_n(10q\cdot p_l-7p_b\cdot p_l)\\
&\quad +7k\cdot p_l(2k\cdot p_n-p_b\cdot p_n)-2k\cdot p_b(p_l\cdot p_n)+3p_b\cdot p_l(q\cdot p_n)-3(p_b\cdot p_n)(q\cdot p_l)\big)+m_b^2\\
&\quad k\cdot p_b\big(k\cdot p_n(7p_b\cdot p_l-12q\cdot p_l)-8k\cdot p_l(p_b\cdot p_n+2k\cdot p_n)+2k\cdot p_b(p_l\cdot p_n)-p_b\cdot p_l\big(q\cdot p_n\\
&\quad -13p_b\cdot p_n\big)-6p_b\cdot p_n(q\cdot p_l)\big)\Big) \qquad (5.65)\\
\mathcal{J}_5(2;c) &= \frac{-1}{3m_b^3(p_b\cdot k)^3}256\lambda_1\Big(4(k\cdot p_b+q\cdot p_b)(k\cdot p_b)^2\big(2k\cdot p_n(k\cdot p_l+q\cdot p_l-p_b\cdot p_l)-p_b\cdot p_n\\
&\quad (k\cdot p_l)\big)+m_b^4\big(4k\cdot q\big(p_b\cdot p_l(q\cdot p_n)-p_b\cdot p_n(k\cdot p_l+q\cdot p_l)-p_b\cdot p_l(k\cdot p_n)+2q\cdot p_l\\
&\quad (k\cdot p_n)\big)+k\cdot p_b\big(k\cdot p_n(p_b\cdot p_l+2q\cdot p_l)+k\cdot p_l(p_b\cdot p_n-2k\cdot p_n-8q\cdot p_n)+q\cdot p_n\\
&\quad (7p_b\cdot p_l-4q\cdot p_l)+p_b\cdot p_n(q\cdot p_l)\big)\big)+2m_b^2p_b\cdot k\big(2q\cdot p_b\big(p_b\cdot p_n\big((q+2k-2p_b).p_l\big)\\
&\quad -2k\cdot p_n((q+k-p_b).p_l)\big)+2k\cdot q\big(k\cdot p_n(p_b\cdot p_l-2q\cdot p_l)+p_b\cdot p_l(p_b\cdot p_n-q\cdot p_n)\\
&\quad -2k\cdot p_l(k\cdot p_n)\big)+k\cdot p_b\big(k\cdot p_n(7p_b\cdot p_l-5q\cdot p_l)+k\cdot p_l(2p_b\cdot p_n-3k\cdot p_n+4q\cdot p_n)\\
&\quad -4p_b\cdot p_l(p_b\cdot p_n)+2q\cdot p_l(q\cdot p_n)\big)\big)\big)\Big) \qquad (5.66)\\
\mathcal{J}_5(2;d) &= \frac{-1}{3m_b^3(p_l\cdot k)^2}512\lambda_1\big((pb\cdot k+p_b\cdot q)^2-m_b^2(2k\cdot q+q^2)\big)\big(m_b^2\big(p_n\cdot k(p_b\cdot p_l-2q\cdot p_l)\\
&\quad +k\cdot p_l(p_b\cdot p_n-2k\cdot p_n)-p_b\cdot p_l(q\cdot p_n)+(p_b\cdot p_n)(q.p\ell)\big)+2k\cdot p_b(k\cdot p_n)\big(k\cdot p_l\\
&\quad +q\cdot p_l-p_b\cdot p_l\big)\big). \qquad (5.67)
\end{aligned}$$

5. Fig.(2(f)):

$$\begin{aligned}
\mathcal{M}^{(6)}_{\mu\nu} &= (-ig^{\alpha\beta})\bar{b}\gamma^\nu(1-\gamma^5)i\left(\not{p}_b+\not{\Pi}-\not{q}-\not{k}+m_u\right)(-ieQ_u)\gamma^\alpha i\left(\not{p}_b+\not{\Pi}-\not{q}+m_u\right)\\
&\quad \gamma^\mu\left(1-\gamma^5\right)b\\
\mathcal{L}^{(6)}_{\mu\nu} &= \left(\bar{\ell}\gamma^\mu(1-\gamma^5)\nu_\ell\right)\left(\bar{\nu}_\ell\gamma^\nu(1-\gamma^5)i\left(\not{p}_l+\not{k}+m_l\right)(-ieQ_l)\gamma_\beta\ell\right) \qquad (5.68)\\
I_6 &= I_7=\frac{1}{k^2((p_b-q-k)^2-m_u^2)}\Big[\frac{1}{(p_u\cdot k)(p_l\cdot k)}-\frac{(p_b-q).\Pi}{(p_l\cdot k)(p_u\cdot k)^2}-\frac{\Pi^2}{2(p_l\cdot k)(p_u\cdot k)^2}\\
&\quad +\frac{((p_b-q).\Pi)^2}{2(p_l\cdot k)(p_u\cdot k)^3}\Big]+\frac{1}{k^2((p_b-q-k)^2-m_u^2)^2}\Big[\frac{-2p_u\cdot\Pi}{(p_l\cdot k)(p_u\cdot k)}+\frac{2(p_u\cdot\Pi)(p_b-q).\Pi}{(p_l\cdot k)(p_u\cdot k)^2}\\
&\quad -\frac{\Pi^2}{(p_l\cdot k)(p_u\cdot k)}\Big]+\frac{1}{k^2((p_b-q-k)^2-m_u^2)^3}\frac{2(p_u\cdot\Pi)^2}{(p_l\cdot k)(p_u\cdot k)} \qquad (5.69)
\end{aligned}$$

$\mathcal{O}(\Pi^0)$:

$$\mathcal{J}_6(0;a) = \frac{1}{m_b(p_l\cdot k)(p_u\cdot k)}32p_b\cdot p_n\Big(2(q\cdot p_l-p_b\cdot p_l)\big(k\cdot p_l+k\cdot q+q\cdot p_l-k\cdot p_b-p_b\cdot p_l\big) -m_\ell^2\big(k\cdot q+m_b^2+q^2-k\cdot p_b-2q\cdot p_b\big)\Big) \tag{5.70}$$

$\mathcal{O}(\Pi)$:

$$\mathcal{J}_6(1;a) = \frac{1}{3m_b^3(p_l\cdot k)(k\cdot p_u)^2}64(\lambda_1+3\lambda_2)\big(2m_b^2q\cdot p_n+p_b\cdot p_n(3m_b^2-5q\cdot p_b)\big)\Big(2\big(q\cdot p_l- p_b\cdot p_l\big)\big(k\cdot p_l+k\cdot q+q\cdot p_l-p_b\cdot p_l-k\cdot p_b\big)-m_\ell^2(k\cdot q+q^2+m_b^2-k\cdot p_b-2q\cdot p_b)\Big) \tag{5.71}$$

$$\mathcal{J}_6(1;c) = \frac{1}{3m_b(p_l\cdot k)(p_u\cdot k)}256(\lambda_1+3\lambda_2)\Big(m_\ell^2(k\cdot q+q^2+m_b^2-k\cdot p_b-2q\cdot p_b)-2(q\cdot p_l -p_b\cdot p_l)\big(k\cdot p_l+k\cdot q+q\cdot p_l-k\cdot p_b-p_b\cdot p_l\big)\Big)\big(p_b\cdot p_n(5(k\cdot q+q\cdot p_b)-3m_b^2)-2m_b^2 (k\cdot p_n+q\cdot p_n)\big) \tag{5.72}$$

$\mathcal{O}(\Pi^2)$:

$$\mathcal{J}_6(2;a) = \frac{1}{3m_b^3(p_l\cdot k)(p_u\cdot k)^3}32\lambda_1p_b\cdot p_n\Big(2k\cdot p_u\big(m_\ell^2(m_b^2(k\cdot q+2q^2)-2(q\cdot p_b)^2)+2(k\cdot p_l +2q\cdot p_l-2p_b\cdot p_l)\big((p_b\cdot p_l)(q\cdot p_b)-m_b^2(q\cdot p_l)\big)+2k\cdot q\big(p_b\cdot p_l(q\cdot p_b+m_b^2)-2m_b^2 q\cdot p_l\big)+k\cdot p_b\big(2m_b^2q\cdot p_l+q\cdot p_b(2q\cdot p_l-4p_b\cdot p_l-m_\ell^2)\big)\big)-\big(2(q\cdot p_l-p_b\cdot p_l)\big(k\cdot p_l +k\cdot q+q\cdot p_l-k\cdot p_b-p_b\cdot p_l\big)-m_\ell^2\big(k\cdot q+q^2+m_b^2-k\cdot p_b-2q\cdot p_b\big)\big)\big((q\cdot p_b)^2+ m_b^2(3k\cdot p_u-q^2)\big)-2(k\cdot p_u)^2\big(m_b^2(m_\ell^2-2k\cdot p_l)+2p_b\cdot p_l(k\cdot p_b+p_b\cdot p_l)\big)\Big) \tag{5.73}$$

$$\mathcal{J}_6(2;c) = \frac{-1}{3m_b^3(p_l\cdot k)(p_u\cdot k)^2}128\lambda_1\Big(m_b^2(k\cdot p_u)(q\cdot p_n)(2(p_b\cdot p_l)^2-m_b^2p_l\cdot k+k\cdot p_l(q\cdot p_b)- 2(k\cdot q)(p_b\cdot p_l)-3(k\cdot p_l)(p_b\cdot p_l)-4(q\cdot p_l)(p_b\cdot p_l))+m_b^2(q\cdot p_l)^2(p_b\cdot p_n)\big(8k\cdot q- 24k\cdot p_u+8q^2\big)+m_b^2(p_b\cdot p_l)^2(p_b\cdot p_n)\big(8k\cdot q-12k\cdot p_u+8q^2\big)+m_b^2p_b\cdot p_n\big((p_u\cdot k) (p_l\cdot k)(q\cdot p_b-6p_l\cdot k-8k\cdot q-q^2)+\big)\Big) \tag{5.74}$$

$$\mathcal{J}_6(2;d) = -\frac{1}{3\,(k\cdot p_l)\,(k\cdot p_u)^2}128\lambda_1\Big(\,(q\cdot p_n)\,(k\cdot p_u)\,\big(-(k\cdot p_l)\,m_b^4-4\,(q\cdot p_l)\,(p_b\cdot p_l)\,m_b^2 -2\,(k\cdot q)\,(p_b\cdot p_l)\,m_b^2-3\,(k\cdot p_l)\,(p_b\cdot p_l)\,m_b^2\big)+(k\cdot p_u)\,(p_b\cdot p_n)\,\big(-24\,(q\cdot p_l)^2\,m_b^2 -12\,(p_b\cdot p_l)^2\,m_b^2\big)+q^2\,(p_b\cdot p_n)\,m_b^2\big(8\,(q\cdot p_l)^2+8\,(p_b\cdot p_l)^2-(k\cdot p_l)\,(k\cdot p_u)\,\big)+ 8\,(k\cdot q)\,(p_b\cdot p_n)\,m_b^2\big(\,(q\cdot p_l)^2+(p_b\cdot p_l)^2+(k\cdot q+q^2)q\cdot p_l\big)+(q\cdot p_l)\,(p_b\cdot p_n)\,m_b^2 \big(8(q^2+k\cdot q)\,(k\cdot p_l)-6(4k\cdot q+5k\cdot p_l)k\cdot p_u\big)-8\,(p_b\cdot p_n)\,m_b^2\big(p_b\cdot p_l\big(k\cdot q+k\cdot p_l +2q\cdot p_l\big)(q^2+k\cdot q)-(6k\cdot p_l+8k\cdot q)\,(k\cdot p_l)\,(k\cdot p_u)\,\big)+(k\cdot p_u)\,m_b^2\big(q\cdot p_n\big(2\,(p_b\cdot p_l)^2 +(q\cdot p_b)\,(k\cdot p_l)\,\big)+(q\cdot p_b)\,(k\cdot p_l)\,(p_b\cdot p_n)+\big(19k\cdot q+26k\cdot p_l+38q\cdot p_l+2q^2 +3k\cdot q)\,(p_b\cdot p_l)\,(p_l\cdot p_n)\,\big)+\big(4(\big(\,\big(q^2+k\cdot q+p_b\cdot q\big)\,m_b^2+q\cdot p_b\big(q^2+k\cdot q-3q\cdot p_b\big)\big)$$

$$
\begin{aligned}
& m_l^2 - 2\,(q\cdot p_l - p_b\cdot p_l)\,\big(\,(q^2 + k\cdot q)\,m_b^2 + q\cdot p_b\big(k\cdot q - p_b\cdot q + p_l\cdot q - p_b\cdot p_l + k\cdot p_l\big)\big)\big) \\
& (p_b\cdot p_n) + \big(-(p_l\cdot p_n)\,(q\cdot p_b)^2 - m_b^2\big((k\cdot p_l + 2q\cdot p_l)\,(q\cdot p_n) + 6(2\,(p_b\cdot p_l) + m_l^2) \\
& (p_b\cdot p_n)\,\big) + \big(\,(p_b\cdot p_l)^2 - (2q\cdot p_l + k\cdot p_l - 2p_b\cdot p_l)\,m_b^2\big)\,(k\cdot p_n) + 2(p_b\cdot p_l + m_b^2) \\
& (p_b\cdot p_l)\,(q\cdot p_n) + (p_b\cdot p_n)\,\big(-16\,(p_b\cdot p_l)^2 + 8m_b^2\,(k\cdot p_l) + 19m_b^2\,(q\cdot p_l) + 7\,(p_b\cdot p_l) \\
& \big(k\cdot q + k\cdot p_l + 2q\cdot p_l\big)\big) + (q^2 + 2k\cdot q)m_b^2\,(p_l\cdot p_n) + (q\cdot p_b)\,\big(-9\,(p_b\cdot p_n)\,m_l^2 + \big(7q\cdot p_l \\
& + k\cdot p_l\big)\,(p_b\cdot p_n) + (p_b\cdot p_l)\,(2q\cdot p_n - 16\,(p_b\cdot p_n) - 3\,(p_l\cdot p_n))\,\big)\big)\,(k\cdot p_u)\,\big)\,(k\cdot p_b) - 8 \\
& ((q\cdot p_b)^2\,(q\cdot p_l)^2 + (q\cdot p_b + 2k\cdot p_u)\,(q\cdot p_b)\,(p_b\cdot p_l)^2)\,(p_b\cdot p_n) + \big(-4\,(k\cdot q)^2\,m_b^2 - 4 \\
& \big(q^2 + m_b^2 - 2\,(q\cdot p_b)\big)\,\big(q^2 m_b^2 - (q\cdot p_b)^2\big) + \big(-4m_b^4 + \big(-8q^2 + 8\cdot p_b q + 15k\cdot p_u\big) \\
& m_b^2 + 4\,(q\cdot p_b)^2\,)\,(k\cdot q) + 6\left(m_b^4 + 2\left(q^2 - q\cdot p_b\right)m_b^2 - (q\cdot p_b)^2\right)(k\cdot p_u)\,\big)m_l^2\,(p_b\cdot p_n) \\
& -8\,(q\cdot p_b)^2\,(q\cdot p_l)\,(p_b\cdot p_n)\,\big(k\cdot q + k\cdot p_l\big) + 8\,(q\cdot p_b)^2\,(p_b\cdot p_l)\,(p_b\cdot p_n)\,\big(k\cdot q + k\cdot p_l + \\
& 2q\cdot p_l\big) - (k\cdot p_u)\,(p_l\cdot p_n)\,(2\,(q\cdot p_b)^2\,(p_b\cdot p_l) + (k\cdot p_b)^3) + (k\cdot p_b)^2\big(4\,(q\cdot p_b)\,\big(-m_l^2 + \\
& 2q\cdot p_l - 2\,(p_b\cdot p_l)\,\big)\,(p_b\cdot p_n) + (p_b\cdot p_l)\,(k\cdot p_n)\,(k\cdot p_u) + \big(-3\,(p_b\cdot p_n)\,m_l^2 + \big(7q\cdot p_l + \\
& k\cdot p_l\big)\,(p_b\cdot p_n) - 2\,(q\cdot p_b)\,(p_l\cdot p_n) + (p_b\cdot p_l)\,(2q\cdot p_n - p_l\cdot p_n - 16p_b\cdot p_n)\,\big)k\cdot p_u\big) + \big(- \\
& (k\cdot p_l)\,m_b^4 + p_b\cdot p_l\,\big(q^2 - 2k\cdot p_l + 2p_b\cdot p_l - 3q\cdot p_l\big)\,m_b^2 + \big((p_b\cdot p_l)^2 + m_b^2 k\cdot p_l\big)\,q\cdot p_b \\
& -(q\cdot p_b)^2\,(p_b\cdot p_l)\,\big)\,(k\cdot p_n)\,(k\cdot p_u) + (2\,(p_b\cdot p_l)\,(q\cdot p_n) + 7\big(k\cdot q + k\cdot p_l + 2q\cdot p_l)p_b\cdot p_n\big) \\
& (q\cdot p_b)\,(p_b\cdot p_l)\,(k\cdot p_u)\,\Big) \qquad (5.75)
\end{aligned}
$$

6. Fig.(2(g)):

$$
\begin{aligned}
\mathcal{M}^{(7)}_{\mu\nu} &= (-ig^{\alpha\beta})\bar{b}\gamma^\nu(1-\gamma^5)i\left(\not{p}_b + \not{l} - \not{q} + m_u\right)(-ieQ_u)\gamma^\alpha i\left(\not{p}_b + \not{l} - \not{q} - \not{k} + m_u\right) \\
&\quad \gamma^\mu\left(1-\gamma^5\right)b \\
\mathcal{L}^{(7)}_{\mu\nu} &= \left(\bar{\ell}(-ieQ_l)\gamma_\beta i\left(\not{p}_l + \not{k} + m_l\right)\gamma^\mu(1-\gamma^5)\nu_\ell\right)\left(\bar{\nu}_\ell\gamma^\nu(1-\gamma^5)\ell\right) && (5.76) \\
I_7 &= I_6 && (5.77)
\end{aligned}
$$

$$
\begin{aligned}
\mathcal{O}(\Pi^0):\ \mathcal{J}_7(0;a) &= \mathcal{J}_6(0;a) && (5.78) \\
\mathcal{O}(\Pi):\ \mathcal{J}_7(1;a) &= \mathcal{J}_6(1;a), \mathcal{J}_7(1;c) = \mathcal{J}_6(1;c) && (5.79) \\
\mathcal{O}(\Pi^2):\ \mathcal{J}_7(2;a) &= \mathcal{J}_6(2;a),\ \mathcal{J}_7(2;c) = \mathcal{J}_6(2;c),\ \mathcal{J}_7(2;d) = \mathcal{J}_6(2;d) && (5.80)
\end{aligned}
$$

7. Fig.(2(h)):

$$
\begin{aligned}
\mathcal{M}^{(8)}_{\mu\nu} &= (-ig^{\alpha\beta})\bar{b}\gamma^{\nu}(1-\gamma^5)i\left(\not{p}_b+\not{\Pi}-\not{q}+m_u\right)(-ieQ_u)\gamma^{\alpha}i\big(\not{p}_b+\not{\Pi}-\not{q}-\not{k}\\
&\quad +m_u\big)\gamma^{\mu}\left(1-\gamma^5\right)i\Big(\not{p}_b+\not{\Pi}-\not{k}+m_b\Big)(-ieQ_b)\gamma^{\alpha}b\\
\mathcal{L}^{(8)}_{\mu\nu} &= \left(\bar{\ell}\gamma^{\mu}(1-\gamma^5)\nu_\ell\right)\left(\bar{\nu}_\ell\gamma^{\nu}(1-\gamma^5)\ell\right) \qquad (5.81)\\
I_8 &= \frac{1}{k^2((p_b-q-k)^2-m_u^2)}\Big[\frac{-1}{(p_u\cdot k)(p_b\cdot k)}+\frac{(p_b-q).\Pi}{(p_b\cdot k)(p_u\cdot k)^2}-\frac{(p_b-k).\Pi}{(p_b\cdot k)^2(p_u\cdot k)}+\\
&\quad \frac{\Pi^2}{2(p_b\cdot k)(p_u\cdot k)^2}-\frac{\Pi^2}{2(p_b\cdot k)^2(p_u\cdot k)}-\frac{((p_b-q).\Pi)^2}{2(p_b\cdot k)(p_u\cdot k)^3}-\frac{((p_b-k).\Pi)^2}{2(p_b\cdot k)^3(p_u\cdot k)}+\\
&\quad \frac{((p_b-q).\Pi)((p_b-k).\Pi)}{(p_u\cdot k)^2(p_b\cdot k)^2}\Big]+\frac{1}{k^2((p_b-q-k)^2-m_u^2)^2}\Big[\frac{2p_u\cdot\Pi}{(p_b\cdot k)(p_u\cdot k)}-\\
&\quad \frac{2(p_u\cdot\Pi)(p_b-q).\Pi}{(p_b\cdot k)(p_u\cdot k)^2}+\frac{2(p_u\cdot\Pi)(p_b-k).\Pi}{(p_b\cdot k)^2(p_u\cdot k)}+\frac{\Pi^2}{(p_b\cdot k)(p_u\cdot k)}\Big]+\\
&\quad \frac{1}{k^2((p_b-q-k)^2-m_u^2)^3}\frac{-2(p_u\cdot\Pi)^2}{(p_b\cdot k)(p_u\cdot k)} \qquad (5.82)
\end{aligned}
$$

$\mathcal{O}(\Pi^0)$:

$$
\begin{aligned}
\mathcal{J}_8(0;a) &= \frac{1}{m_b\,(k.p_b)\,(k.p_u)}16\Big(-2\,(p_l\cdot p_n)\,(k.p_b)^2+m_b^2\big(-(p_l\cdot p_n)\,\big(-2\,(k\cdot p_b)-2\\
&\quad (q\cdot p_b)+k\cdot q+q^2\big)-2\,(p_b\cdot p_l)\,(q\cdot p_n)+2\,(q\cdot p_l)\,(p_b\cdot p_n+q\cdot p_n)\big)+(k\cdot p_n)\\
&\quad \big((q\cdot p_l)\,\big(2\,(q\cdot p_b)-m_b^2\big)-(p_b\cdot p_l)\,\big(-2k\cdot p_b+2k\cdot q+q^2\big)\big)+(k\cdot p_l)\,\big(2\,(k\cdot p_n)\\
&\quad \big(q\cdot p_b-m_b^2\big)-2\,(k.p_b)\,(q\cdot p_n)+(p_b\cdot p_n)\,\big(2\,(k\cdot p_b)-q^2\big)+m_b^2\,(q\cdot p_n)\big)-2\\
&\quad (k\cdot p_b)\,(p_b\cdot p_n)\,(q\cdot p_l)-2\,(k\cdot p_b)\,(q\cdot p_l)\,(q\cdot p_n)+2\,(k.p_b)\,(p_b\cdot p_l)\,(q\cdot p_n)+2\,(k\cdot q)\\
&\quad (p_b\cdot p_n)\,(q\cdot p_l)+q^2\,(k.p_b)\,(p_l\cdot p_n)+2\,(k\cdot q)\,(k.p_b)\,(p_l\cdot p_n)-2\,(k.p_b)\,(q.p_b)\,(p_l\cdot p_n)\\
&\quad +m_b^4\,(-(p_l\cdot p_n))-4\,(p_b\cdot p_n)\,(q.p_b)\,(q\cdot p_l)+2q^2\,(p_b\cdot p_l)\,(p_b\cdot p_n)\Big) \qquad (5.83)
\end{aligned}
$$

$\mathcal{O}(\Pi)$:

$$
\begin{aligned}
\mathcal{J}_8(1;a) &= \frac{1}{3m_b^3\,(k.p_b)^2\,(k.p_u)^2}16(\lambda_1+3\lambda_2)\big(2p_l\cdot p_n(k\cdot p_b)^3(5q\cdot p_b-3m_b^2)+(p_b\cdot k)^2\big(6m_b^4\\
&\quad (p_l\cdot p_n)+m_b^2\big(-2q\cdot p_n(3k\cdot p_l+7q\cdot p_l-5p_b\cdot p_l)+k\cdot p_n(4q\cdot p_l+6p_b\cdot p_l)+6p_b\cdot p_n\\
&\quad (k\cdot p_l-q\cdot p_l)+(2k\cdot q+8k\cdot p_u+5q^2-16q\cdot p_b)p_l\cdot p_n\big)+10\big(-(k\cdot p_u-q\cdot p_b)\big(k\cdot p_l\\
&\quad +q\cdot p_l\big)q\cdot p_n-q\cdot p_b(q\cdot p_l-k\cdot p_l)(p_b\cdot p_n)\big)+5\big(2(q\cdot p_b)^2-(2k\cdot q+q^2)q\cdot p_b+k\cdot p_u\\
&\quad (2k\cdot q+q^2)\big)p_l\cdot p_n\big)+p_b\cdot k\big(-3(p_l\cdot p_n)m_b^6+m_b^4\big(-8(q\cdot p_n)(p_b\cdot p_l)+2q\cdot p_l\big(5q\cdot p_n\\
&\quad +4p_b\cdot p_n\big)+p_l\cdot p_n\big(k\cdot q-6k\cdot p_u-3q^2+9q\cdot p_b\big)\big)+m_b^2\big(2q\cdot p_n\big(5(k\cdot p_u-q\cdot p_b)q\cdot p_l\\
&\quad +p_b\cdot p_l(2k\cdot q-4k\cdot p_u+q^2+3q\cdot p_b)\big)+2p_b\cdot p_n\big(q\cdot p_l(5k\cdot q+2k\cdot p_u-q^2-13q\cdot p_b)\\
&\quad +(5q^2-2k\cdot q)p_b\cdot p_l\big)+p_l\cdot p_n\big(4(k\cdot q)^2+k\cdot q\big(2q^2-15k\cdot p_u-3q\cdot p_b\big)+3q\cdot p_b\big(q^2-\\
&\quad 2q\cdot p_b\big)+k\cdot p_u(8q\cdot p_b-5q^2)\big)\big)\big)+10p_b\cdot p_n\big(q\cdot p_l(2(q\cdot p_b)^2+k\cdot q(k\cdot p_u-q\cdot p_b))-q^2\\
&\quad (q\cdot p_b)(p_b\cdot p_l)\big)+k\cdot p_n\big(-7(q\cdot p_l)m_b^4-m_b^2\big(q\cdot p_l(4k\cdot q+k\cdot p_u-2q^2-15q\cdot p_b)+
\end{aligned}
$$

$$
p_b \cdot p_l\big(6k \cdot q + 2k \cdot p_u + 9q^2 - 4q \cdot p_b)\big) + 5(k \cdot p_u - q \cdot p_b)\big(2(q \cdot p_b)(q \cdot p_l) - (2k \cdot q + q^2)
p_b \cdot p_l)\big) + k \cdot p_l\big(3m_b^4(q \cdot p_n - 2k \cdot p_n) - \big(4k \cdot p_n(2k \cdot p_u - q^2 - 3q \cdot p_b) + q \cdot p_n\big(4k \cdot q -
15k \cdot p_u + 2q^2 + q \cdot p_b\big) + p_b \cdot p_n(5(2k \cdot p_u + q^2) - 4k \cdot q)\big)m_b^2 + 5\big(k \cdot p_u - q \cdot p_b\big)\big(2k \cdot p_n
(q \cdot p_b) - q^2(p_b \cdot p_n)\big)\big)\big) + (k \cdot p_u)m_b^2\big(3(p_b \cdot p_l)m_b^4 - m_b^2\big(k \cdot p_n(q \cdot p_l - 2p_b \cdot p_l) - 6
(q \cdot p_n)(p_b \cdot p_l) + 6q \cdot p_l(q \cdot p_n + p_b \cdot p_n) - 3(q^2 - 2q \cdot p_b)p_l \cdot p_n\big) - \big(2(q \cdot p_b)(q \cdot p_l) - q^2
(p_b \cdot p_l)\big)(k \cdot p_n - 6p_b \cdot p_n) + k \cdot q\big(3m_b^2(p_l \cdot p_n) + k \cdot p_n(14p_b \cdot p_l - 8q \cdot p_l) - 2p_b \cdot p_n\big(q \cdot p_l
+2p_b \cdot p_l)\big) + k \cdot p_l\big(- 3m_b^2(q \cdot p_n) + p_b \cdot p_n\big(- 2m_b^2 + q^2 + 4q \cdot p_b\big) + 2k \cdot p_n\big(5m_b^2 + 2q^2
-7q \cdot p_b)\big)\big)\big)\Big) \tag{5.84}
$$

$$
\begin{aligned}
\mathcal{J}_8(1;c) \quad = \quad & \frac{1}{3\big(k \cdot p_b\big)\big(k \cdot p_u\big)m_b}128\big(- 3\big(p_l \cdot p_n\big)m_b^6 + \big(\big(p_l \cdot p_n\big)\big(- 3q^2 + k \cdot q + 9p_b \cdot q\big) + \big(3q \cdot p_l \\
& +2p_b \cdot p_l\big)\big(k \cdot p_n\big) + 2\big(5q \cdot p_l + 4p_b \cdot p_l\big)\big(q \cdot p_n\big) - 8\big(q \cdot p_l\big)\big(p_b \cdot p_n\big) - \big(k \cdot p_l\big)\big(10k \cdot p_n + \\
& 3q \cdot p_n + 2p_b \cdot p_n\big)\big)m_b^4 + \big(- 2\big(k \cdot p_n\big)\big(q \cdot p_l\big)q^2 - 3\big(k \cdot p_n\big)\big(p_b \cdot p_l\big)q^2 - 2\big(q \cdot p_n\big)\big(p_b \cdot p_l\big) \\
& q^2 + 2\big(q \cdot p_l\big)\big(p_b \cdot p_n\big)q^2 + 10\big(p_b \cdot p_l\big)\big(p_b \cdot p_n\big)q^2 - \big(k \cdot p_n\big)\big(q \cdot p_b\big)\big(q \cdot p_l\big) - 10\big(q \cdot p_b\big) \\
& \big(q \cdot p_n\big)\big(q \cdot p_l\big) - 4\big(k \cdot p_n\big)\big(q \cdot p_b\big)\big(p_b \cdot p_l\big) - 26\big(q \cdot p_b\big)\big(q \cdot p_n\big)\big(p_b \cdot p_l\big) - 4\big(k \cdot q\big)\big(q \cdot p_l\big) \\
& \big(k \cdot p_n\big) + 4\big(k \cdot q\big)\big(p_b \cdot p_l\big)\big(k \cdot p_n\big) + 6\big(k \cdot q\big)\big(p_b \cdot p_l\big)\big(q \cdot p_n\big) + 4\big(k \cdot q\big)\big(q \cdot p_l\big)\big(p_b \cdot p_n\big) + 6 \\
& \big(q \cdot p_b\big)\big(q \cdot p_l\big)\big(p_b \cdot p_n\big) + \big(- 6\big(q \cdot p_b\big)^2 + 2\big(k \cdot q\big)\big(q^2 + 2k \cdot q\big) + 3\big(q^2 - k \cdot q\big)\big(q \cdot p_b\big)\big) \\
& \big(p_l \cdot p_n\big) + \big(k \cdot p_l\big)\big(\big(q \cdot p_b\big)\big(20k \cdot p_n + 11q \cdot p_n + 4p_b \cdot p_n\big) + \big(q^2 + 2k \cdot q\big)\big(2\big(q \cdot p_n\big) - 7 \\
& \big(p_b \cdot p_n\big)\big)\big)\big)m_b^2 + \big(9\big(p_l \cdot p_n\big)m_b^4 + \big(\big(p_l \cdot p_n\big)\big(8q^2 + 7k \cdot q - 22\big(q \cdot p_b\big)\big) - 4\big(5q \cdot p_l + \\
& 4p_b \cdot p_l\big)\big(q \cdot p_n\big) + 16\big(q \cdot p_l\big)\big(p_b \cdot p_n\big)\big)m_b^2 + \big(- 11\big(q \cdot p_l\big)m_b^2 + \big(5q^2 + 6m_b^2\big)\big(p_b \cdot p_l\big) \\
& +10\big(q \cdot p_b\big)\big(q \cdot p_l - p_b \cdot p_l\big)\big)\big(k \cdot p_n\big) + 10\big(\big(q \cdot p_b\big)\big(q \cdot p_l\big) - \big(k \cdot q - 3\big(q \cdot p_b\big)\big)\big(p_b \cdot p_l\big)\big) \\
& \big(q \cdot p_n\big) - 10\big(\big(p_b \cdot p_l\big)q^2 + \big(q \cdot p_b\big)\big(q \cdot p_l\big)\big)\big(p_b \cdot p_n\big) - 5\big(q^2 + 2k \cdot q - 2\big(q \cdot p_b\big)\big)\big(q \cdot p_b\big) \\
& \big(p_l \cdot p_n\big) + \big(k \cdot p_l\big)\big(\big(10k \cdot p_n + 14p_b \cdot p_n + q \cdot p_n\big)m_b^2 + 5\big(q^2 + 2k \cdot q\big)\big(p_b \cdot p_n\big) - 10 \\
& \big(q \cdot p_b\big)\big(k \cdot p_n + q \cdot p_n + p_b \cdot p_n\big)\big)\big)\big(k \cdot p_b\big) + 10\big(k \cdot p_b\big)^3\big(p_l \cdot p_n\big) + \big(k \cdot p_b\big)^2\big(- 16\big(p_l \cdot p_n\big) \\
& m_b^2 - 5\big(q^2 + 2k \cdot q - 4\big(q \cdot p_b\big)\big)\big(p_l \cdot p_n\big) + 10\big(- \big(p_b \cdot p_n\big)\big(k \cdot p_l + q \cdot p_l\big) + \big(q \cdot p_l - \\
& p_b \cdot p_l\big)\big(k \cdot p_n\big) + \big(q \cdot p_l + p_b \cdot p_l\big)\big(q \cdot p_n\big)\big)\big) + 5\big(q \cdot p_b\big)\big(\big(p_b \cdot p_l\big)\big(q^2\big(k \cdot p_n - 2\big(p_b \cdot p_n\big)\big) \\
& -2\big(k \cdot q - 2\big(q \cdot p_b\big)\big)\big(q \cdot p_n\big)\big) + \big(k \cdot p_l\big)\big(\big(q^2 + 2k \cdot q\big)\big(p_b \cdot p_n\big) - 2\big(q \cdot p_b\big)\big(k \cdot p_n + \\
& q \cdot p_n\big)\big)\big)\big)\big(\lambda_1 + 3\lambda_2\big)
\end{aligned} \tag{5.85}
$$

$\mathcal{O}(\Pi^2)$:

$$
\begin{aligned}
\mathcal{J}_8(2;a) &= \frac{1}{3(k\cdot p_b)^2(k\cdot p_u)^3 m_b^3}16\Big(2(k\cdot p_u)^2(k\cdot p_b)(2(3q\cdot p_l+k\cdot p_l)(p_b\cdot p_n)+(-3m_b^2\\
&+4k\cdot p_b+2q\cdot p_b)(p_l\cdot p_n)-2(p_b\cdot p_l)(3k\cdot p_n+q\cdot p_n))m_b^2+((k\cdot p_u)(2(k\cdot q)\\
&-3(k\cdot p_u))m_b^2+((3(k\cdot p_u)-q^2)m_b^2+(k\cdot p_u-q\cdot p_b)^2)(k\cdot p_b))((p_l\cdot p_n)m_b^4\\
&+((p_l\cdot p_n)(q^2+k\cdot q-2(k\cdot p_b)-2(q\cdot p_b))+2(p_b\cdot p_l)(q\cdot p_n)-2(q\cdot p_l)(q\cdot p_n\\
&+p_b\cdot p_n))m_b^2+(-(q\cdot p_n)m_b^2+2(m_b^2-q\cdot p_b)(k\cdot p_n)+2(k\cdot p_b)(q\cdot p_n)+(q^2\\
&-2(k\cdot p_b))(p_b\cdot p_n))(k\cdot p_l)-2(k\cdot p_b)(q\cdot p_n)(p_b\cdot p_l)+((p_b\cdot p_l)(q^2+2k\cdot q-\\
&2(k\cdot p_b))+(m_b^2-2(q\cdot p_b))(q\cdot p_l))(k\cdot p_n)+2(k\cdot p_b)(q\cdot p_l)(q\cdot p_n)-2(k\cdot q)\\
&(q\cdot p_l)(p_b\cdot p_n)+2(k\cdot p_b)(q\cdot p_l)(p_b\cdot p_n)+4(q\cdot p_b)(q\cdot p_l)(p_b\cdot p_n)-2q^2(p_b\cdot p_l)\\
&(p_b\cdot p_n)+2(((k\cdot p_b)))^2(p_l\cdot p_n)-(k\cdot p_b)q^2(p_l\cdot p_n)-2(k\cdot q)(k\cdot p_b)(p_l\cdot p_n)+\\
&2(k\cdot p_b)(q\cdot p_b)(p_l\cdot p_n))-2(k\cdot p_u)(((k\cdot p_l)(k\cdot p_u)(2k\cdot p_n-p_b\cdot p_n-2q\cdot p_n)+\\
&(k\cdot p_b)(-2(p_l\cdot p_n)q^2-(q\cdot p_n)(p_b\cdot p_l)-2(q\cdot p_l)(k\cdot p_n)+(q\cdot p_l)(2q\cdot p_n+\\
&p_b\cdot p_n))+((p_b\cdot p_l)(k\cdot p_n)+2(k\cdot q)(p_l\cdot p_n))(k\cdot p_u))m_b^4+(2((q^2+k\cdot q)(p_l\cdot p_n)\\
&-(q\cdot p_n)(-p_b\cdot p_l+k\cdot p_l+q\cdot p_l))(k\cdot p_b)^2+(k\cdot p_b)(-(p_b\cdot p_l)(q\cdot p_n)q^2+\\
&(q\cdot p_l)(p_b\cdot p_n)q^2+2(p_b\cdot p_l)(p_b\cdot p_n)q^2+2((q\cdot p_b)(q\cdot p_l+p_b\cdot p_l)-(q^2+k\cdot q+\\
&2k\cdot p_u)(p_b\cdot p_l))(k\cdot p_n)+2(q\cdot p_b)(q\cdot p_l)(q\cdot p_n)-2(q\cdot p_b)(p_b\cdot p_l)(q\cdot p_n)+2(k\cdot q)\\
&(q\cdot p_l)(p_b\cdot p_n)-2(q\cdot p_b)(q\cdot p_l)(p_b\cdot p_n)-2(k\cdot q)(p_b\cdot p_l)(p_b\cdot p_n)-2((q\cdot p_b)(k\cdot p_u\\
&-q\cdot p_b)+(k\cdot q)(k\cdot p_u))(p_l\cdot p_n)+2(p_b\cdot p_l)(q\cdot p_n)(k\cdot p_u)+2(k\cdot p_l)(k\cdot p_n+q\cdot p_n)\\
&(k\cdot p_u))+((p_b\cdot p_n)((k\cdot p_l)(q^2+2p_b\cdot q)-2(k\cdot q)(q\cdot p_l+p_b\cdot p_l))+((q^2+\\
&2k\cdot q)(p_b\cdot p_l)-2(q\cdot p_b)(k\cdot p_l+q\cdot p_l))(k\cdot p_n))(k\cdot p_u))m_b^2+2(k\cdot p_b)(k\cdot p_u-\\
&q\cdot p_b)((p_l\cdot p_n)(((k\cdot p_b)))^2-((k\cdot p_l-q\cdot p_l)(p_b\cdot p_n)-(q\cdot p_b)(p_l\cdot p_n)+(p_b\cdot p_l)\\
&(k\cdot p_n+q\cdot p_n))(k\cdot p_b)+(2(q\cdot p_b)(q\cdot p_l)-q^2(p_b\cdot p_l))(p_b\cdot p_n))))\Big)\lambda_1 \qquad (5.86)\\
\mathcal{J}_8(2;c) &= -\frac{1}{3(k\cdot p_b)^2(k\cdot p_u)^2}128\Big(4(q\cdot p_b)(p_l\cdot p_n)(k\cdot p_b)^4+2(-2(q^2+k\cdot q+p_b\cdot q)\\
&(p_l\cdot p_n)m_b^2-2(k\cdot p_n)((q\cdot p_b)(p_b\cdot p_l-q\cdot p_l)+(q\cdot p_l)(k\cdot p_u))+(q\cdot p_b)(-\\
&(p_l\cdot p_n)(q^2+2k\cdot q-4(q\cdot p_b))+2(q\cdot p_l+p_b\cdot p_l)(q\cdot p_n)-2(k\cdot p_l+q\cdot p_l)(p_b\cdot p_n))\\
&+((p_l\cdot p_n)(q^2+2k\cdot q+5m_b^2)-2(q\cdot p_l)(q\cdot p_n))(k\cdot p_u))(k\cdot p_b)^3+(2(2(q^2+\\
&k\cdot q-2(k\cdot p_u))+q\cdot p_b)(p_l\cdot p_n)m_b^4+((p_l\cdot p_n)(4(k\cdot q)^2-8(q\cdot p_b)^2-2(-3q^2\\
&+p_b\cdot q+6k\cdot p_u)(k\cdot q)-2(q^2-5(k\cdot p_u))(q\cdot p_b)+q^2(2q^2-9(k\cdot p_u)))+2
\end{aligned}
$$

$$
\begin{aligned}
&\big((q\cdot p_l)(p_b\cdot p_n)(2k\cdot q+2(q^2+p_b\cdot q)-5(k\cdot p_u))+(p_b\cdot p_l)((k\cdot p_n)(2q^2+\\
&2k\cdot q-3(k\cdot p_u))-(2k\cdot q+2(q^2+p_b\cdot q)-5(k\cdot p_u))(q\cdot p_n))+(q\cdot p_l)(-\\
&(q\cdot p_n)(2k\cdot q+2(q^2+p_b\cdot q)-7(k\cdot p_u))+(2(q^2+k\cdot q-4(k\cdot p_u))+q.p_b)\\
&(-k\cdot p_n))))m_b^2+2((2(p_b\cdot p_n)(q^2+k\cdot q)+(q\cdot p_b)(q\cdot p_n))m_b^2+2(q\cdot p_b)(m_b^2\\
&-q\cdot p_b+k.p_u)(k\cdot p_n)+(q\cdot p_b)((q^2+2k\cdot q)(p_b\cdot p_n)-2(q\cdot p_b)(q\cdot p_n+p_b\cdot p_n))+\\
&(-(q\cdot p_n)m_b^2-(p_b\cdot p_n)(q^2+2k\cdot q+7m_b^2)+2(q\cdot p_b)(q\cdot p_n))(k\cdot p_u))(k\cdot p_l)+2\\
&(((p_b\cdot p_l)((q^2-2(q\cdot p_b))(q\cdot p_b)-(k\cdot p_u)q^2)+2(q\cdot p_b)(q\cdot p_l)(q\cdot p_b-k\cdot p_u))\\
&(k\cdot p_n)+2((p_b\cdot p_l)(3(q\cdot p_b)^2+(k\cdot q)(k\cdot p_u-q\cdot p_b))+(q\cdot p_b)(q\cdot p_l)(q\cdot p_b-\\
&k\cdot p_u))(q\cdot p_n)-2(q\cdot p_b)((p_b\cdot p_l)q^2+(q\cdot p_b)(q\cdot p_l))(p_b\cdot p_n)+(2(q\cdot p_b)^2-(q^2\\
&+2k\cdot q)(q\cdot p_b)+(q^2+2k\cdot q)(k\cdot p_u))(q\cdot p_b)(p_l\cdot p_n)))(k\cdot p_b)^2+((-2q^2-2k\cdot q\\
&+3k\cdot p_u)(p_l\cdot p_n)m_b^6+(-2(p_l\cdot p_n)(k\cdot q)^2+((2q^2-7(k\cdot p_u))(q\cdot p_l)-2(k\cdot p_u)\\
&(p_b\cdot p_l))(k\cdot p_n)+2(2(p_b\cdot p_l)(q^2-2(k\cdot p_u))+(q\cdot p_l)(2q^2-5(k\cdot p_u)))(q\cdot p_n)+\\
&4(2(k\cdot p_u)-q^2)(q\cdot p_l)(p_b\cdot p_n)+(2(q\cdot p_b)^2+q^2(7k\cdot p_u-2q^2)+4(q\cdot p_b)(q^2-\\
&2k\cdot p_u))(p_l\cdot p_n)+(k\cdot q)((p_l\cdot p_n)(-4q^2+4p_b\cdot q+3k\cdot p_u)-4(p_b\cdot p_n)(q\cdot p_l)+2\\
&(q\cdot p_l)(k\cdot p_n)+4(q\cdot p_l+p_b\cdot p_l)(q\cdot p_n)))m_b^4+(4((q\cdot p_n)(p_b\cdot p_l)-(k\cdot p_u)(p_l\cdot p_n))\\
&(k\cdot q)^2+2(-2(p_l\cdot p_n)(q\cdot p_b)^3+((p_l\cdot p_n)q^2-2(q\cdot p_l+p_b\cdot p_l)(q\cdot p_n)+2(q\cdot p_l)\\
&(p_b\cdot p_n))(q\cdot p_b)^2+q^2(((q\cdot p_l)(k\cdot p_u)+(p_b\cdot p_l)(2q^2-5(k\cdot p_u)))(p_b\cdot p_n)-(k\cdot p_u)\\
&(q\cdot p_n)(p_b\cdot p_l))+(q\cdot p_b)(2(5(k\cdot p_u)-2q^2)(q\cdot p_n)(p_b\cdot p_l)-(k\cdot p_u)q^2(p_l\cdot p_n)))+\\
&((p_b\cdot p_l)((k\cdot p_u)(5q^2+4\cdot p_b q)-2q^4)+2(q\cdot p_b)(k\cdot p_u-q\cdot p_b)(q\cdot p_l))(k\cdot p_n)+2\\
&(k\cdot q)((p_l\cdot p_n)(((q\cdot p_b)))^2+(2(k\cdot p_u)(q\cdot p_l)-(q^2+2k\cdot p_u)(p_b\cdot p_l))(k\cdot p_n)+2\\
&(p_b\cdot p_l)((p_b\cdot p_n)q^2+(q^2-2(q\cdot p_b))(q\cdot p_n))+((p_l\cdot p_n)(q\cdot p_b-q^2)-5(p_b\cdot p_l)\\
&(q\cdot p_n)+2(q\cdot p_l)(q\cdot p_n-p_b\cdot p_n))(k\cdot p_u)))m_b^2+(2(q\cdot p_b-m_b^2)(-2(q\cdot p_b)^2+2\\
&(q^2+k\cdot q)m_b^2+(2(q\cdot p_b)-5m_b^2)(k\cdot p_u))(k\cdot p_n)-2((q\cdot p_b)^2-(q^2+k\cdot q)m_b^2)\\
&((q\cdot p_n)(2(q\cdot p_b)-m_b^2)-(q^2+2k\cdot q)(p_b\cdot p_n))+((7q\cdot p_n+2p_b\cdot p_n)m_b^4+(9q^2+\\
&10k\cdot q)(p_b\cdot p_n)m_b^2+2(-8(q\cdot p_n)m_b^2-(p_b\cdot p_n)(q^2+2k\cdot q+2m_b^2))(q\cdot p_b)+4\\
&(q\cdot p_b)^2(q\cdot p_n))(k\cdot p_u))(k\cdot p_l)+2(q\cdot p_b)(p_b\cdot p_l)(-2(q\cdot p_b)(p_b\cdot p_n)q^2+(k\cdot p_n)(q\cdot p_b\\
&-k\cdot p_u)q^2+2(2(q\cdot p_b)^2+(k\cdot q)(k\cdot p_u-q\cdot p_b))(q\cdot p_n)))(k\cdot p_b)+2(k\cdot q)m_b^2((p_l\cdot p_n)\\
&m_b^4+((p_l\cdot p_n)(q^2+k\cdot q-2(q\cdot p_b))-2(q\cdot p_n)(q\cdot p_l+p_b\cdot p_l)+2(q\cdot p_l)(p_b\cdot p_n)+\\
&(q\cdot p_l)(-k\cdot p_n))m_b^2+(k\cdot p_l)((2k\cdot p_n+q\cdot p_n)m_b^2+(q^2+2k\cdot q)(p_b\cdot p_n)-2(q\cdot p_b)\\
&(k\cdot p_n+q\cdot p_n))+(p_b\cdot p_l)(q^2(k\cdot p_n-2(p_b\cdot p_n))-2(k\cdot q-2(q\cdot p_b))(q\cdot p_n)))(k\cdot p_u)\big)\lambda_1
\end{aligned}
\tag{5.87}
$$

$$\begin{aligned}
\mathcal{J}_8(2;d) \quad = \quad & \frac{1}{3m_b^3\big(k.p_b\big)\big(k.p_u\big)}256\lambda_1\big(\big(k\cdot p_b+q.p_b\big)^2-m_b^2\big(2k\cdot q+q^2\big)\big)\big(2\big(p_l\cdot p_n\big)\big(k.p_b\big)^2 \\
& +m_b^2\big(\big(p_l\cdot p_n\big)\big(-2\big(q.p_b\big)+k\cdot q+q^2\big)-2\big(q\cdot p_n\big)\big(p_b\cdot p_l+q\cdot p_l\big)+2\big(p_b\cdot p_n\big) \\
& \big(q\cdot p_l\big)-\big(k\cdot p_n\big)\big(q\cdot p_l\big)\big)+\big(k\cdot p_l\big)\big(m_b^2\big(2k\cdot p_n+q\cdot p_n\big)+\big(p_b\cdot p_n\big)\big(-2\big(k.p_b\big) \\
& +2k\cdot q+q^2\big)-2\big(q.p_b\big)\big(k\cdot p_n+q\cdot p_n\big)\big)+\big(k.p_b\big)\big(-\big(p_l\cdot p_n\big)\big(-2\big(q\cdot p_b\big)+ \\
& 2k\cdot q+q^2+2m_b^2\big)+2\big(k\cdot p_n\big)\big(q\cdot p_l-p_b\cdot p_l\big)-2\big(p_b\cdot p_n\big)\big(q\cdot p_l\big)+2\big(q\cdot p_n\big)\big(p_b\cdot p_l \\
& +q\cdot p_l\big)\big)+\big(p_b\cdot p_l\big)\big(q^2\big(k\cdot p_n-2\big(p_b\cdot p_n\big)\big)-2\big(q\cdot p_n\big)\big(k\cdot q-2\big(q.p_b\big)\big)\big)+m_b^4 \\
& \big(p_l\cdot p_n\big)\big) \qquad (5.88)
\end{aligned}$$

8. Fig.(2(i)):

$$\begin{aligned}
\mathcal{M}_{\mu\nu}^{(9)} \quad = \quad & (-ig^{\alpha\beta})\bar{b}(-ieQ_b)\gamma^\alpha i\left(\not{p}_b+\not{l}-\not{k}+m_b\right)\gamma^\nu(1-\gamma^5)i\left(\not{p}_b+\not{l}-\not{q}-\not{k}+m_u\right) \\
& (-ieQ_u)\gamma^\beta i\Big(\not{p}_b+\not{l}-\not{q}+m_u\Big)\gamma^\mu\left(1-\gamma^5\right)b \\
\mathcal{L}_{\mu\nu}^{(9)} \quad = \quad & \left(\bar{\ell}\gamma^\mu(1-\gamma^5)\nu_\ell\right)\left(\bar{\nu}_\ell\gamma^\nu(1-\gamma^5)\ell\right) \qquad (5.89)
\end{aligned}$$

$$I_9 = I_8 \qquad (5.90)$$

$\mathcal{O}(\Pi^0)$:

$$\begin{aligned}
\mathcal{J}_9(0;a) \quad = \quad & \frac{1}{m_b\big(k.p_b\big)\big(k.p_u\big)}16\big(-2\big(p_l\cdot p_n\big)\big(k.p_b\big)^2+m_b^2\big(\big(p_l\cdot p_n\big)\big(2k.p_b+2q.p_b-k\cdot q \\
& -q^2\big)-2\big(p_b\cdot p_l\big)\big(q\cdot p_n\big)+2\big(q\cdot p_l\big)\big(p_b\cdot p_n+q\cdot p_n\big)\big)+\big(k\cdot p_n\big)\big(\big(q\cdot p_l\big)\big(2\big(q.p_b\big) \\
& -m_b^2\big)-\big(p_b\cdot p_l\big)\big(-2k.p_b+2k\cdot q+q^2\big)\big)+\big(k\cdot p_l\big)\big(2\big(k\cdot p_n\big)\big(q.p_b-m_b^2\big)- \\
& 2\big(k.p_b\big)\big(q\cdot p_n\big)+\big(p_b\cdot p_n\big)\big(2\big(k.p_b\big)-q^2\big)+m_b^2\big(q\cdot p_n\big)\big)-2\big(k.p_b\big)\big(p._bp_n\big) \\
& \big(q\cdot p_l\big)-2\big(k.p_b\big)\big(q\cdot p_l\big)\big(q\cdot p_n\big)+2\big(k.p_b\big)\big(p_b\cdot p_l\big)\big(q\cdot p_n\big)+2\big(k\cdot q\big)\big(p_b\cdot p_n\big)\big(q\cdot p_l\big) \\
& +q^2\big(k.p_b\big)\big(p_l\cdot p_n\big)+2\big(k\cdot q\big)\big(k.p_b\big)\big(p_l\cdot p_n\big)-2\big(k.p_b\big)\big(q.p_b\big)\big(p_l\cdot p_n\big)-m_b^4p_l\cdot p_n \\
& -4\big(p_b\cdot p_n\big)\big(q.p_b\big)\big(q\cdot p_l\big)+2q^2\big(p_b\cdot p_l\big)\big(p_b\cdot p_n\big)\big) \qquad (5.91)
\end{aligned}$$

$\mathcal{O}(\Pi)$:

$$\begin{aligned}
\mathcal{J}_9(1;a) \quad = \quad & \frac{1}{3(k\cdot p_b)^2\big(k\cdot p_u\big)^2m_b^3}16\big(2\big(5\big(q\cdot p_b\big)-3m_b^2\big)\big(p_l\cdot p_n\big)\big(k\cdot p_b\big)^3+\big(6\big(p_l\cdot p_n\big)m_b^4+ \\
& \big(\big(p_l\cdot p_n\big)\big(5q^2+2k\cdot q-16\big(q\cdot p_b\big)+8k\cdot p_u\big)+\big(4q\cdot p_l+6p_b\cdot p_l\big)\big(k\cdot p_n\big)- \\
& 2\big(3k\cdot p_l+7q\cdot p_l-5\big(p_b\cdot p_l\big)\big)\big(q\cdot p_n\big)+6\big(k\cdot p_l-q\cdot p_l\big)\big(p_b\cdot p_n\big)\big)m_b^2+5 \\
& \big(2\big(q\cdot p_b\big)^2-\big(q^2+2k\cdot q\big)\big(q\cdot p_b\big)+\big(q^2+2k\cdot q\big)\big(k\cdot p_u\big)\big)\big(p_l\cdot p_n\big)+10\big(- \\
& \big(q\cdot p_b\big)\big(k\cdot p_n+q\cdot p_n\big)\big(p_b\cdot p_l\big)-\big(k\cdot p_u-q\cdot p_b\big)\big(k\cdot p_l+q\cdot p_l\big)\big(q\cdot p_n\big) \\
& +\big(q\cdot p_b\big)\big(q\cdot p_l-k\cdot p_l\big)\big(p_b\cdot p_n\big)\big)\big)\big(k\cdot p_b\big)^2+\big(k\cdot p_b\big)\big(-3\big(p_l\cdot p_n\big)m_b^6+\big(\big(p_l\cdot p_n\big)
\end{aligned}$$

$$
\begin{aligned}
& \big(-3q^2+.kq+9\cdot p_b q-6(k\cdot p_u)\big)-8(p_b\cdot p_l)(q\cdot p_n)+2(q\cdot p_l)(5q\cdot p_n+4p_b\cdot p_n)\big)m_b^4+ \\
& \big((p_l\cdot p_n)\big(4(k\cdot q)^2+3(q\cdot p_b)(q^2-2(q\cdot p_b))+(k\cdot q)(2q^2-3(q\cdot p_b)-18k\cdot p_u)+(8(q\cdot p_b) \\
& -5q^2)(k\cdot p_u)\big)+2\big(5(q\cdot p_l)(k\cdot p_u-q\cdot p_b)+(q^2+2k\cdot q+3\cdot p_b q-4(k\cdot p_u))(p_b\cdot p_l)\big)(q\cdot p_n) \\
& +2\big((p_b\cdot p_l)(5q^2-2(k\cdot q))+(-q^2+5k\cdot q-13(q\cdot p_b)+2k\cdot p_u)(q\cdot p_l)\big)(p_b\cdot p_n)\big)m_b^2+ \\
& \big(-7(q\cdot p_l)m_b^4-\big((p_b\cdot p_l)(9q^2+6k\cdot q-4(q\cdot p_b)+2k\cdot p_u)+(-2q^2+4k\cdot q-15(q\cdot p_b) \\
& +4k\cdot p_u)(q\cdot p_l)\big)m_b^2+5(k\cdot p_u-q\cdot p_b)\big(2(q\cdot p_b)(q\cdot p_l)-(q^2+2k\cdot q)(p_b\cdot p_l)\big)\big)(k\cdot p_n)+ \\
& 10\big(\big(2(q\cdot p_b)^2+(k\cdot q)(k\cdot p_u-q\cdot p_b)\big)(q\cdot p_l)-q^2(q\cdot p_b)(p_b\cdot p_l)\big)(p_b\cdot p_n)+(k\cdot p_l)\big(3(q\cdot p_n \\
& -2(k\cdot p_n))m_b^4-\big((p_b\cdot p_n)(5(q^2+2k\cdot p_u)-4(k\cdot q))+4(-q^2-3(q\cdot p_b)+2k\cdot p_u)(k\cdot p_n) \\
& +(2q^2+4k\cdot q+.p_b q-18(k\cdot p_u))(q\cdot p_n)\big)m_b^2+5(k\cdot p_u-q\cdot p_b)\big(2(k\cdot p_n)(q\cdot p_b)-q^2 \\
& (p_b\cdot p_n)\big)\big)\big)+m_b^2\big(3(p_l\cdot p_n)m_b^4-\big(-3(p_l\cdot p_n)(q^2-2(q\cdot p_b))-6(q\cdot p_n)(p_b\cdot p_l)+(q\cdot p_l \\
& -2(p_b\cdot p_l))(k\cdot p_n)+6(q\cdot p_l)(.qp_n+.p_b p_n)\big)m_b^2+\big(-3(q\cdot p_n)m_b^2+2(2q^2+5m_b^2-7 \\
& (q\cdot p_b))(k\cdot p_n)+(q^2+4\cdot p_b q-2m_b^2)(p_b\cdot p_n)\big)(k\cdot p_l)-\big(2(q\cdot p_b)(q\cdot p_l)-q^2(p_b\cdot p_l)\big) \\
& (k\cdot p_n-6(p_b\cdot p_n))+(k\cdot q)\big(3(p_l\cdot p_n)m_b^2+(14(p_b\cdot p_l)-8(q\cdot p_l))(k\cdot p_n)-2(2p_b\cdot p_l+ \\
& q\cdot p_l)(p_b\cdot p_n)\big)\big)\big)(k\cdot p_u)\big)(\lambda_1+3\lambda_2)
\end{aligned}
\tag{5.92}
$$

$$
\begin{aligned}
\mathcal{J}_9(1;c) \;=\; & -\frac{1}{3(k\cdot p_b)(k\cdot p_u)m_b^3}128\big(-3(p_l\cdot p_n)m_b^6+\big((p_l\cdot p_n)(-3q^2+k\cdot q+9p_b\cdot q)-(k\cdot p_n) \\
& (3q\cdot p_l+2p_b\cdot p_l)+2(5(q\cdot p_l)-4(p_b\cdot p_l))(q\cdot p_n)+8(q\cdot p_l)(p_b\cdot p_n)+(k\cdot p_l)(-10k\cdot p_n \\
& +3q\cdot p_n+2p_b\cdot p_n)\big)m_b^4+\big(-2(p_b\cdot p_n)(q\cdot p_l)q^2-7(k\cdot p_n)(p_b\cdot p_l)q^2+2(q\cdot p_l)(k\cdot p_n)q^2 \\
& +2(p_b\cdot p_l)(q\cdot p_n)q^2+10(p_b\cdot p_l)(p_b\cdot p_n)q^2-10(q\cdot p_b)(q\cdot p_n)(q\cdot p_l)-26(q\cdot p_b)(p_b\cdot p_n) \\
& (q\cdot p_l)-14(k\cdot q)(k\cdot p_n)(p_b\cdot p_l)+4(k\cdot q)(q\cdot p_l)(k\cdot p_n)+11(q\cdot p_b)(q\cdot p_l)(k\cdot p_n)+4 \\
& (q\cdot p_b)(p_b\cdot p_l)(k\cdot p_n)+4(k\cdot q)(p_b\cdot p_l)(q\cdot p_n)+6(q\cdot p_b)(p_b\cdot p_l)(q\cdot p_n)+6(k\cdot q)(q\cdot p_l) \\
& (p_b\cdot p_n)+\big(-6(q\cdot p_b)^2+2(k\cdot q)(q^2+2k\cdot q)+3(q^2-k\cdot q)(q\cdot p_b)\big)(p_l\cdot p_n)+(k\cdot p_l) \\
& \big(20(q\cdot p_b)(k\cdot p_n)-(2q^2+4k\cdot q+.p_b q)(q\cdot p_n)+(-3q^2+4k\cdot q-4(q\cdot p_b))(p_b\cdot p_n)\big)\big) \\
& m_b^2+\big(9(p_l\cdot p_n)m_b^4+\big((p_l\cdot p_n)(8q^2+7k\cdot q-22(q\cdot p_b))+16(p_b\cdot p_l)(q\cdot p_n)-4(q\cdot p_l) \\
& (5q\cdot p_n+4p_b\cdot p_n)\big)m_b^2+\big((q\cdot p_l)m_b^2+(5q^2+10k\cdot q+14m_b^2)(p_b\cdot p_l)-10(q\cdot p_b)(q\cdot p_l \\
& +p_b\cdot p_l)\big)(k\cdot p_n)+10(q\cdot p_b)(q\cdot p_l-p_b\cdot p_l)(q\cdot p_n)-10\big((p_b\cdot p_l)q^2+(k\cdot q-3(q\cdot p_b)) \\
& (q\cdot p_l)\big)(p_b\cdot p_n)-5(q^2+2k\cdot q-2(q\cdot p_b))(q\cdot p_b)(p_l\cdot p_n)+(k\cdot p_l)\big(5(p_b\cdot p_n)q^2-10 \\
& (q\cdot p_b)(-q\cdot p_n+k\cdot p_n+p_b\cdot p_n)+m_b^2(10k\cdot p_n+6p_b\cdot p_n-11q\cdot p_n)\big)\big)(k\cdot p_b)+(k\cdot p_b)^2 \\
& \big(-(p_l\cdot p_n)(16m_b^2+5(q^2+2k\cdot q-4(q\cdot p_b)))-10(p_b\cdot p_l)(k\cdot p_n+q\cdot p_n)+10(q\cdot p_l) \\
& (q\cdot p_n+p_b\cdot p_n)+10(k\cdot p_l)(q\cdot p_n-p_b\cdot p_n)\big)+10(k\cdot p_b)^3(p_l\cdot p_n)+5(q\cdot p_b)\big((p_b\cdot p_n) \\
& (q^2(k\cdot p_l-2p_b\cdot p_l)-2(k\cdot q-2(q\cdot p_b))(q\cdot p_l))+((q^2+2k\cdot q)(p_b\cdot p_l)-2(q\cdot p_b) \\
& (k\cdot p_l+q\cdot p_l))(k\cdot p_n)\big)\big)(\lambda_1+3\lambda_2)
\end{aligned}
\tag{5.93}
$$

$\mathcal{O}(\Pi^2)$:

$$\begin{aligned}
\mathcal{J}_9(2;a) \quad = \quad & -\frac{1}{3(k\cdot p_b)^2(k\cdot p_u)^3 m_b^3} 16\big(2\big(-(q\cdot p_b)^2+(k\cdot p_u)^2+q^2m_b^2-3m_b^2(k\cdot p_u)\big)(p_l\cdot p_n) \\
& (k\cdot p_b)^3+\big(2\big(3k\cdot p_u-q^2\big)(p_l\cdot p_n)m_b^4+\big((p_l\cdot p_n)\big(2(q\cdot p_b)^2+q^2\big(9k\cdot p_u-q^2\big)+(k\cdot q) \\
& \big(6k\cdot p_u-2q^2\big)+2(q\cdot p_b)\big(q^2-5k\cdot p_u\big)\big)+2\big((p_b\cdot p_l)\big(5(k\cdot p_u)-q^2\big)+(q\cdot p_l)\big(q^2- \\
& 7k\cdot p_u\big)\big)(q\cdot p_n)+2(q\cdot p_l)(p_b\cdot p_n)\big(q^2-3(k\cdot p_u)\big)\big)m_b^2+\big(-(2p_b\cdot p_n+q\cdot p_n)\big(((k\cdot p_u))\big)^2 \\
& -2(q\cdot p_n-p_b\cdot p_n)\big(\big(((q\cdot p_b))\big)^2-q^2m_b^2\big)+2\big(\big(3(p_b\cdot p_n)-5(q\cdot p_n)\big)m_b^2+2(q\cdot p_b) \\
& (q\cdot p_n)\big)(k\cdot p_u)\big)(k\cdot p_l)-2(k\cdot p_u)^2(q\cdot p_n)(p_b\cdot p_l)+\big(-(2p_b\cdot p_l+q\cdot p_l)(k\cdot p_u)^2+ \\
& 2\big((q\cdot p_b)^2-q^2m_b^2\big)(p_b\cdot p_l)+6m_b^2(p_b\cdot p_l)(k\cdot p_u)\big)(k\cdot p_n)-2(q\cdot p_b)^2(q\cdot p_l)(q\cdot p_n)- \\
& 2(k\cdot p_u)^2(q\cdot p_l)(q\cdot p_n)+2(q\cdot p_b)^2(p_b\cdot p_l)(q\cdot p_n)-2(q\cdot p_b)^2(q\cdot p_l)(p_b\cdot p_n)+2(k\cdot p_u)^2 \\
& (q\cdot p_l)(p_b\cdot p_n)-2(q\cdot p_b)^3(p_l\cdot p_n)+(q\cdot p_b)^2q^2(p_l\cdot p_n)+(k\cdot p_u)^2q^2(p_l\cdot p_n)+2(q\cdot p_b)^2 \\
& (k\cdot q)(p_l\cdot p_n)+(k\cdot p_u)^2(k\cdot q)(p_l\cdot p_n)+2(k\cdot p_u)^2(q\cdot p_b)(p_l\cdot p_n)-2(k\cdot p_u)q^2(q\cdot p_b)(p_l\cdot p_n) \\
& -4(k\cdot q)(k\cdot p_u)(q\cdot p_b)(p_l\cdot p_n)+4(q\cdot p_b)(q\cdot p_l)(q\cdot p_n)(k\cdot p_u)\big)(k\cdot p_b)^2+(k\cdot p_b)\big((p_l\cdot p_n) \\
& \big(q^2-3(k\cdot p_u)\big)m_b^6+\big(2(q\cdot p_l)(p_b\cdot p_n)\big(4(k\cdot p_u)-q^2\big)+2\big((q\cdot p_l)\big(5(k\cdot p_u)-q^2\big)+ \\
& (p_b\cdot p_l)\big(q^2-4k\cdot p_u\big)\big)(q\cdot p_n)+\big(q^4-2(q\cdot p_b)q^2-(q\cdot p_b)^2-(k\cdot p_u)^2+(k\cdot q)\big(q^2+ \\
& k.p_u\big)+\big(8(q\cdot p_b)-7q^2\big)(k\cdot p_u)\big)(p_l\cdot p_n)\big)m_b^4+\big((p_l\cdot p_n)\big(2(q\cdot p_b)^3-\big(q^2+k\cdot q\big)(q\cdot p_b)^2 \\
& +\big(2\big(k\cdot q-2(k\cdot p_u)\big)q^2+(k\cdot q)\big(4(k\cdot q)-13(k\cdot p_u)\big)\big)(k\cdot p_u)+2\big(q^2-2(k\cdot q)\big)(q\cdot p_b) \\
& (k\cdot p_u)\big)+2\big((p_b\cdot p_l)\big((k\cdot p_u)\big(2(k\cdot q)-q^2\big)-(q\cdot p_b)^2\big)+\big((q\cdot p_b)^2+4(k\cdot p_u)^2-2(k\cdot q) \\
& (k\cdot p_u)\big)(q\cdot p_l)\big)(q\cdot p_n)+2\big(\big((q\cdot p_b)^2+(k\cdot q)\big(5(k\cdot p_u)-q^2\big)+(k\cdot p_u)\big(q^2-2(k\cdot p_u)\big)+ \\
& 2(q\cdot p_b)\big(q^2-5(k\cdot p_u)\big)\big)(q\cdot p_l)-\big(\big(q^2-5k\cdot p_u\big)q^2+2(k\cdot q)(k\cdot p_u)\big)(p_b\cdot p_l)\big)(p_b\cdot p_n)\big)m_b^2 \\
& +\big(-\big(-13(q\cdot p_n)m_b^2+(q\cdot p_b)(q\cdot p_n)+\big(q^2+10m_b^2\big)(p_b\cdot p_n)\big)(k\cdot p_u)^2+\big(q^2m_b^2 \\
& -(q\cdot p_b)^2\big)\big(q^2(p_b\cdot p_n)-(q\cdot p_n)m_b^2\big)+2\big(\big(q^2-3k\cdot p_u\big)m_b^4+\big(-(q\cdot p_b)^2+(k\cdot p_u)^2+ \\
& \big(5k\cdot p_u-q^2\big)(q\cdot p_b)\big)m_b^2+(q\cdot p_b)\big(k\cdot p_u-q\cdot p_b\big)^2\big)(k\cdot p_n)+\big(3(q\cdot p_n)m_b^4+4(k\cdot q)\big(p_b\cdot p_n- \\
& q\cdot p_n\big)m_b^2+q^2\big(2(q\cdot p_b)-5m_b^2\big)(p_b\cdot p_n)\big)(k\cdot p_u)\big)(k\cdot p_l)+\big(\big((q\cdot p_l)m_b^2-(p_b\cdot p_l)\big(q^2+2k\cdot q \\
& +2m_b^2\big)+3(q\cdot p_b)(q\cdot p_l)\big)(k\cdot p_u)^2+\big((q\cdot p_b)^2-q^2m_b^2\big)\big((q\cdot p_l)\big(2(q\cdot p_b)-m_b^2\big)-\big(q^2+ \\
& 2k\cdot q\big)(p_b\cdot p_l)\big)+\big(-7(q\cdot p_l)m_b^4-3\big(3q^2+2k\cdot q\big)(p_b\cdot p_l)m_b^2+2\big(7(q\cdot p_l)m_b^2+\big(q^2+2k\cdot q \\
& +2m_b^2\big)(p_b\cdot p_l)\big)(q\cdot p_b)-4(q\cdot p_b)^2(q\cdot p_l)\big)(k\cdot p_u)\big)(k\cdot p_n)-4(q\cdot p_b)^3(q\cdot p_l)(p_b\cdot p_n)+2 \\
& (q\cdot p_b)^2(k\cdot q)(q\cdot p_l)(p_b\cdot p_n)+2(k\cdot p_u)^2(k\cdot q)(q\cdot p_l)(p_b\cdot p_n)+4(k\cdot p_u)^2(q\cdot p_b)(q\cdot p_l)(p_b\cdot p_n) \\
& -4(k\cdot q)(k\cdot p_u)(q\cdot p_b)(q\cdot p_l)(p_b\cdot p_n)+2(q\cdot p_b)^2q^2(p_b\cdot p_l)(p_b\cdot p_n)-2\big(k\cdot p_u\big)^2q^2(p_b\cdot p_l) \\
& (p_b\cdot p_n)+(k\cdot p_u)^2(k\cdot q)(q\cdot p_b)(p_l\cdot p_n)\big)+m_b^2\big(-2\big((p_l\cdot p_n)m_b^2+2(p_b\cdot p_l)(k\cdot p_n)-2 \\
& (q\cdot p_l)(p_b\cdot p_n)\big)\big(k\cdot q\big)^2+(k\cdot q)\big(-2(p_l\cdot p_n)m_b^4+\big((p_l\cdot p_n)\big(-2q^2+4\cdot p_bq+7k\cdot p_u\big)-2 \\
& (q\cdot p_l)(k\cdot p_n)+4(q\cdot p_l-p_b\cdot p_l)(q\cdot p_n)+4(q\cdot p_l)(p_b\cdot p_n)+2(k\cdot p_l)\big(q\cdot p_n-2(k\cdot p_n)\big)\big)m_b^2
\end{aligned}$$

$$
\begin{aligned}
& +2\big((p_b\cdot p_l)(7(k\cdot p_u)-q^2)+2(q\cdot p_b)(k.p_l+q.p_l)\big)(k\cdot p_n)-2\big((k\cdot p_l)q^2+(4q\cdot p_b+5k\cdot p_u) \\
& (q\cdot p_l)+2(k\cdot p_u-q^2)(p_b\cdot p_l)\big)(p_b\cdot p_n)\big)+\big(3(p_l\cdot p_n)m_b^4+\big(3(p_l\cdot p_n)(q^2-2(q\cdot p_b))+ \\
& (3q\cdot p_l+2p_b\cdot p_l)(k\cdot p_n)+6(p_b\cdot p_l)(q\cdot p_n)-6(q\cdot p_l)(q\cdot p_n+p_b\cdot p_n)\big)m_b^2+\big(-7(q\cdot p_n)m_b^2 \\
& +2(5m_b^2-7(q\cdot p_b))(k\cdot p_n)+(5q^2+4p_b\cdot q-2m_b^2)(p_b\cdot p_n)\big)(k\cdot p_l)-\big(2(q\cdot p_b)(q\cdot p_l)-q^2 \\
& (p_b\cdot p_l)\big)(5(k\cdot p_n)-6(p_b\cdot p_n))\big)(k\cdot p_u)\big)(k\cdot p_u)\big)\lambda_1 \qquad (5.94)
\end{aligned}
$$

$$
\begin{aligned}
\mathcal{J}_9(2;c) \;=\; & -\frac{1}{3(k\cdot p_b)^2(k\cdot p_u)^2}128\big(4(q\cdot p_b)(p_l\cdot p_n)(k\cdot p_b)^4+2\big(-2(q^2+k\cdot q+p_b\cdot q)(p_l\cdot p_n)m_b^2 \\
& +(q\cdot p_b)\big(-(p_l\cdot p_n)(q^2+2k\cdot q-4(q\cdot p_b))-2(p_b\cdot p_l)(k\cdot p_n+q\cdot p_n)+2(q\cdot p_l)(q\cdot p_n \\
& +p_b\cdot p_n)\big)-2(k\cdot p_l)\big((q\cdot p_b)(p_b\cdot p_n-q\cdot p_n)+(q\cdot p_n)(k\cdot p_u)\big)+\big((p_l\cdot p_n)(q^2+2k\cdot q+ \\
& 3m_b^2)-2(q\cdot p_l)(q\cdot p_n)\big)(k\cdot p_u)\big)(k\cdot p_b)^3+\big(2(2(q^2+k\cdot q-2(k\cdot p_u))+q.p_b)(p_l\cdot p_n)m_b^4 \\
& +\big((p_l\cdot p_n)\big(4(k\cdot q)^2-8(q\cdot p_b)^2-2(-3q^2+p_b\cdot q+7k\cdot p_u)(k\cdot q)-2(q^2-3(k\cdot p_u)) \\
& (q\cdot p_b)+q^2(2q^2-11k\cdot p_u)\big)+2\big((p_b\cdot p_l)(2q^2+2k\cdot q-9(k\cdot p_u))+(q\cdot p_b)(q\cdot p_l)\big)(k\cdot p_n) \\
& +2\big((2k\cdot q+2(q^2+.p_bq)-3(k\cdot p_u))(p_b\cdot p_l)-(2k\cdot q+2(q^2+p_b\cdot q)-9(k\cdot p_u))(q\cdot p_l)\big) \\
& (q\cdot p_n)-2(2k\cdot q+2(q^2+.p_bq)-3(k\cdot p_u))(q\cdot p_l)(p_b\cdot p_n)\big)m_b^2+2\big(-\big((2(q^2+k\cdot q)+ \\
& q\cdot p_b)(q\cdot p_n)-2(q^2+k\cdot q)(p_b\cdot p_n)\big)m_b^2-(k\cdot p_u)\big(-9(q\cdot p_n)m_b^2+2(q\cdot p_b)(q\cdot p_n)+(q^2+ \\
& m_b^2)(p_b\cdot p_n)\big)+2(q\cdot p_b)(m_b^2-q\cdot p_b+.kp_u)(k\cdot p_n)+(q\cdot p_b)\big(2(q\cdot p_b)(q\cdot p_n)+(q^2-2(q\cdot p_b)) \\
& (p_b\cdot p_n)\big)\big)(k\cdot p_l)+2\big(-2(q\cdot p_b)(q\cdot p_n)\big((q\cdot p_b)(p_b\cdot p_l-q\cdot p_l)+(q\cdot p_l)(k\cdot p_u)\big)+\big((p_b\cdot p_l) \\
& (-2(q\cdot p_b)^2-(k\cdot p_u)(q^2+2k\cdot q)+(q^2+2k\cdot q)(q\cdot p_b))+2(q\cdot p_b)(k\cdot p_u-q\cdot p_b)(q\cdot p_l)\big) \\
& (k\cdot p_n)+2\big((3(q\cdot p_b)^2+(k\cdot q)(k\cdot p_u-q\cdot p_b))(q\cdot p_l)-q^2(q\cdot p_b)(p_b\cdot p_l)\big)(p_b\cdot p_n)+\big(2(q\cdot p_b)^2 \\
& -(q^2+2k\cdot q)(q\cdot p_b)+(q^2+2k\cdot q)(k\cdot p_u)\big)(q\cdot p_b)(p_l\cdot p_n)\big)\big)(k\cdot p_b)^2+\big((-2q^2-2k\cdot q \\
& +3k\cdot p_u)(p_l\cdot p_n)m_b^6+\big(-2(p_l\cdot p_n)(k\cdot q)^2+\big((k\cdot p_u)(7q\cdot p_l+2p_b\cdot p_l)-2q^2(q\cdot p_l)\big)(k\cdot p_n) \\
& +2\big(2(p_b\cdot p_l)(2(k\cdot p_u)-q^2)+(q\cdot p_l)(2q^2-5k\cdot p_u)\big)(q\cdot p_n)+\big(2(q\cdot p_b)^2+q^2(7(k\cdot p_u)-2q^2) \\
& +4(q\cdot p_b)(q^2-2(k\cdot p_u))\big)(p_l\cdot p_n)+(k\cdot q)\big((p_l\cdot p_n)(-4q^2+4\cdot p_bq+3k\cdot p_u)-4(q\cdot p_n)(p_b\cdot p_l) \\
& -2(q\cdot p_l)(k\cdot p_n)+4(q\cdot p_l)(.qp_n+.p_bp_n)\big)+4(q\cdot p_l)(p_b\cdot p_n)(q^2-2(k\cdot p_u))\big)m_b^4+\big(-4\big((p_b\cdot p_l) \\
& (k\cdot p_n)-(q\cdot p_l)(p_b\cdot p_n)+(p_l\cdot p_n)(k\cdot p_u)\big)(k\cdot q)^2+\big((p_b\cdot p_l)\big((k\cdot p_u)(11q^2-4(q\cdot p_b))-2q^4\big)+ \\
& 2(q\cdot p_b)(2q^2+p_b\cdot q-9k\cdot p_u)(q\cdot p_l)\big)(k\cdot p_n)+2\big(-2(p_l\cdot p_n)(q\cdot p_b)^3+\big((p_l\cdot p_n)q^2+2(p_b\cdot p_l) \\
& (q\cdot p_n)-2(q\cdot p_l)(q\cdot p_n+p_b\cdot p_n)\big)(q\cdot p_b)^2+q^2\big((k\cdot p_u)(q\cdot p_n)(p_b\cdot p_l)-\big((p_b\cdot p_l)(5(k\cdot p_u)-2q^2) \\
& +(q\cdot p_l)(k\cdot p_u)\big)(p_b\cdot p_n)\big)+(q\cdot p_b)\big(2(5(k\cdot p_u)-2q^2)(q\cdot p_l)(p_b\cdot p_n)-(k\cdot p_u)q^2(p_l\cdot p_n)\big)\big)+2 \\
& (k\cdot q)\big((p_l\cdot p_n)(q\cdot p_b)^2+\big((p_b\cdot p_l)(7(k\cdot p_u)-3q^2)+2(q\cdot p_b)(q\cdot p_l)\big)(k\cdot p_n)+2\big((p_b\cdot p_l)q^2+(q^2 \\
& -2(q\cdot p_b))(q\cdot p_l)\big)(p_b\cdot p_n)+\big(-(p_l\cdot p_n)(q^2-2(q\cdot p_b))+2(q\cdot p_l-p_b\cdot p_l)(q\cdot p_n)-7(q\cdot p_l) \\
& (p_b\cdot p_n)\big)(k\cdot p_u)\big)\big)m_b^2+\big(-2\big((q^2+.kq)m_b^2-(q\cdot p_b)^2\big)\big(q^2(p_b\cdot p_n)-(q\cdot p_n)m_b^2\big)+2\big((k\cdot p_u) \\
& (5m_b^4-9(q\cdot p_b)m_b^2+2(q\cdot p_b)^2)-2(q\cdot p_b-m_b^2)\big((q\cdot p_b)^2-(q^2+k\cdot q)m_b^2\big)\big)(k\cdot p_n)+\big(-(7q\cdot p_n \\
& +2p_b\cdot p_n)m_b^4+\big(4(k\cdot q)(q\cdot p_n)+(7q^2-4k\cdot q+4\cdot p_bq)(p_b\cdot p_n)\big)m_b^2-2q^2(q\cdot p_b)(p_b\cdot p_n)\big)(k\cdot p_u)\big) \\
& (k\cdot p_l)+2(q\cdot p_b)\big(2(p_b\cdot p_n)\big((2(q\cdot p_b)^2+(k\cdot q)(k\cdot p_u-q\cdot p_b))(q\cdot p_l)-q^2(q\cdot p_b)(p_b\cdot p_l)\big)+(k\cdot p_u
\end{aligned}
$$

$$-q\cdot p_b)(2(q\cdot p_b)(q\cdot p_l)-(q^2+2k\cdot q)(p_b\cdot p_l))(k\cdot p_n)))(k\cdot p_b)+2(k\cdot q)m_b^2((p_l\cdot p_n)m_b^4+((p_l\cdot p_n)$$
$$(q^2+k\cdot q-2(q\cdot p_b))+2(p_b\cdot p_l)(q\cdot p_n)-2(q\cdot p_l)(q\cdot p_n+p_b\cdot p_n))m_b^2+((p_b\cdot p_n)q^2+2(m_b^2-$$
$$q\cdot p_b)(k\cdot p_n)+m_b^2(-(q\cdot p_n)))(k\cdot p_l)+((p_b\cdot p_l)(q^2+2k\cdot q)+(m_b^2-2(q\cdot p_b))(q\cdot p_l))(k\cdot p_n)-$$
$$2((p_b\cdot p_l)q^2+(k\cdot q-2(q\cdot p_b))(q\cdot p_l))(p_b\cdot p_n))(k\cdot p_u))\lambda_1 \tag{5.95}$$

$$\begin{aligned}\mathcal{J}_9(2;d) \quad = \quad & \frac{1}{3m_b^3(k.p_b)(k.p_u)}256\lambda_1((k.p_b+q.p_b)^2-m_b^2(2k\cdot q+q^2))(2(p_l\cdot p_n)(k\cdot p_b)^2\\
&+m_b^2((p_l\cdot p_n)(-2(k.p_b)-2(q.p_b)+k\cdot q+q^2)+2(p_b\cdot p_l)(q\cdot p_n)-2(q\cdot p_l)\\
&(p_b\cdot p_n+q\cdot p_n))+(k\cdot p_n)((p_b\cdot p_l)(-2(k\cdot p_b)+2k\cdot q+q^2)+(q\cdot p_l)(m_b^2-\\
&2q\cdot p_b))+(k\cdot p_l)(2(k\cdot p_n)(m_b^2-q.p_b)+2(k\cdot p_b)(q\cdot p_n)+(p_b\cdot p_n)(q^2-2(k.p_b))\\
&+m_b^2(-q\cdot p_n))-2(k\cdot q)(p_b\cdot p_n)(q\cdot p_l)+2(k.p_b)(q\cdot p_l)(q\cdot p_n)-2(k.p_b)(p_b\cdot p_l)\\
&(q\cdot p_n)+2(k.p_b)(p_b\cdot p_n)(q\cdot p_l)-q^2(k.p_b)(p_l\cdot p_n)-2(k\cdot q)(k.p_b)(p_l\cdot p_n)+2\\
&(k\cdot p_b)(q.p_b)(p_l\cdot p_n)+m_b^4(p_l\cdot p_n)+4(p_b\cdot p_n)(q.p_b)(q\cdot p_l)-2q^2(p_b\cdot p_l)(p_b\cdot p_n))\end{aligned} \tag{5.96}$$

5.5 Results

The kinematics of inclusive decays involve five distinct variables in the four-body phase space. In addition to these variables, inclusive decays introduce an extra variable, which is the invariant mass squared of the final state meson (p_X^2). This variable is exchanged with q'^2 ($=(p_l+p_n+k)^2$), where p_l, p_n, and k represent the momenta of the lepton, neutrino, and photon, respectively. The remaining independent variables are the lepton energy y ($=\frac{2p_b\cdot p_l}{m_B^2}$), the energy of the hard photon x ($=\frac{2p_b\cdot k}{m_B^2}$), the neutrino energy, and three angles. All these variables are defined in the rest frame of the B meson. A comprehensive description of the kinematics can be found in Appendix-C.2.

In order to study the charged lepton spectrum for different x values, we perform integration over all variables except y. This integration enables us to obtain the differential decay rate as a function of the lepton energy (y) for various photon energy values (x). The resulting differential decay rate, shown in Fig. (5.4a), illustrates that as the photon energy decreases, the lepton energy end point also shifts accordingly, in accordance with the kinematics of the process.

To provide a complete picture of the differential decay rate distribution, we present the distribution for $x_{\min}=0.3$, corresponding to a minimum photon

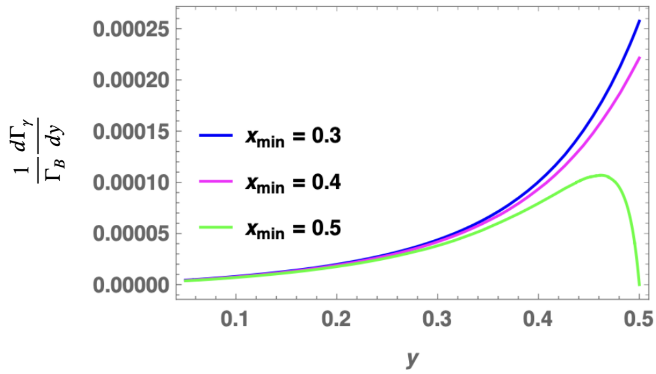

(a)

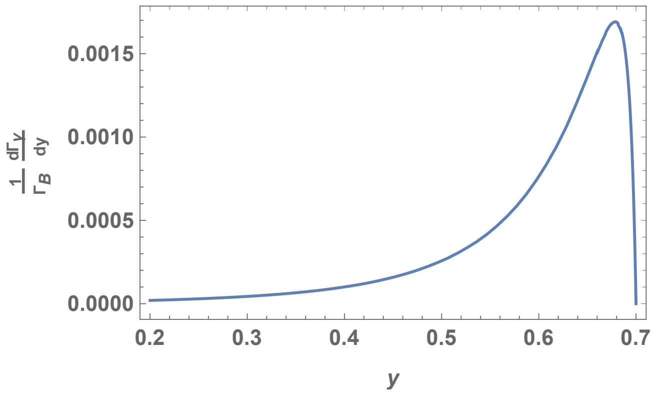

(b)

Figure 5.4: (a) Differential decay width of $B \to X_u \mu \nu_\mu \gamma$ as a function of normalized lepton energy, y, for various values of normalized photon energy, x. (b) Differential decay width of $B \to X_u \mu \nu_\mu \gamma$ as a function of normalized lepton energy (y) for a specific normalized photon energy ($x_{\min} = 0.3$).

energy of $k_{\min} \sim 0.8$ GeV, as depicted in Fig.(5.4b). The plot illustrates that the distribution reaches its endpoint at a kinematic boundary, which is expected to be larger than that for $x_{\min} = 0.5$, and is more inclined towards the non-radiative case of $B \to X_u \ell \nu_\ell$.

Furthermore, as an example of a potential additional observable, we define the forward-backward asymmetry of the photon (differential), denoted as $A_{\mathrm{FB}}(y)$, with respect to the recoiling final state hadron.

$$A_{FB}(y) = \frac{\int_0^1 dt \frac{d^2\Gamma_\gamma}{dydt} - \int_{-1}^0 dt \frac{d^2\Gamma_\gamma}{dydt}}{\int_{-1}^1 dt \frac{d^2\Gamma_\gamma}{dydt}} \tag{5.97}$$

where $t = cos\theta_{X\gamma}$ is the angle between the outgoing photon and recoiling hadron (X) in the rest frame of B meson. The forward-backward asymmetry is shown in Fig.(5.5) for $\lambda_1 = -0.2$ and $\lambda_2 = 0.12$.

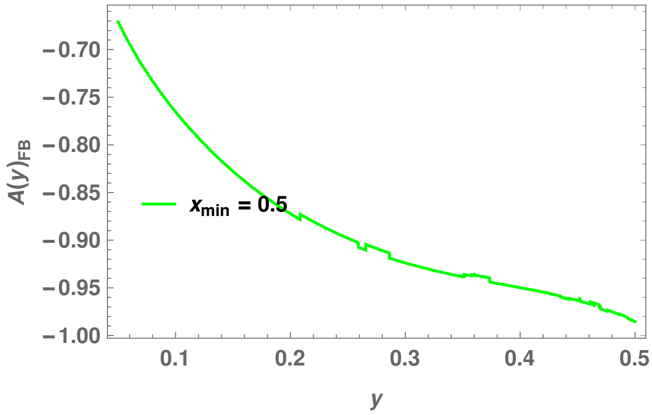

Figure 5.5: Forward-backward asymmetry (A_{FB}) as a function of lepton energy, y.

Finally, Fig.(5.6) illustrates the differential decay rate as a function of the normalized photon energy (x), revealing that as the photon energy decreases, the decay rate exhibits behavior similar to that of the non-radiative mode.

It is important to highlight that the presence of infrared divergences can be effectively removed by assigning a sufficiently large mass to the photon, ensuring its hardness. To avoid contributions from mass singularities, we specifically consider muons in the final state. Additionally, by implementing a lower cutoff for the polar angle, we can eliminate any potential collinear singularities that may arise.

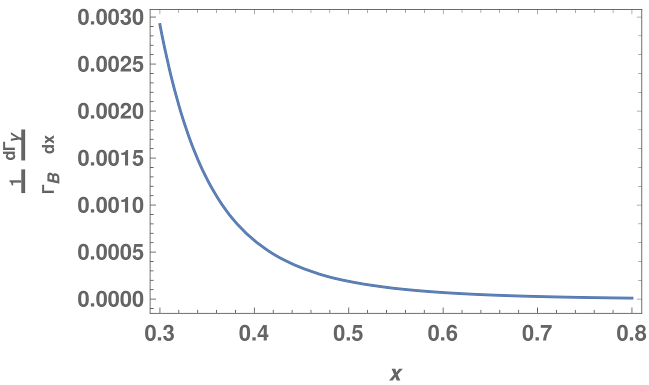

Figure 5.6: Differential decay rate of the $B \to X_u \mu \nu_\mu \gamma$ decay mode as a function of the photon energy (x).

In the case of $B \to X_u \mu \nu_\mu \gamma$, where the photon is hard, the total decay width (Γ_γ) for the radiative mode is expected to be suppressed by $\mathcal{O}(\alpha_{em})$ compared to the total decay width for $B \to X_u \mu \nu_\mu$. To verify this expectation, we calculate the ratio of the radiative decay width (Γ_γ) to the non-radiative decay width (Γ). Our calculations reveal that this ratio is approximately 0.01 for photons with high energy around 1 GeV ($x_{min} = 0.5$), thus confirming the expected suppression.

5.5.1 Determination of non-perturbative parameters

Having determined the decay width, we now present a simple and efficient method for calculating the non-perturbative parameters λ_1 and λ_2. We find that using ratios of decay widths, rather than the widths themselves, is more suitable as it helps mitigate uncertainties arising from the CKM element V_{ub}. Additionally, these ratios yield simple expressions involving λ_1 and λ_2. By knowing the experimentally measured values of R_1 and R_2, we can solve these two linear equations simultaneously to determine λ_1 and λ_2. The proposed ratios are given by Eq.(5.4). Both the numerator and denominator of each ratio can be expressed in form $A + B\lambda_1 + C\lambda_2$, allowing for a straightforward determination of the non-perturbative parameters.

$$\frac{A + B\lambda_1 + C\lambda_2}{A' + B'\lambda_1 + C'\lambda_2} = R_1 \text{ (say)} \tag{5.98}$$

and similarly for R_2. These equations form a system of two linear equations in terms of λ_1 and λ_2. To demonstrate the case of obtaining λ_1 and λ_2 once the suggested ratios are experimentally available, we obtain a value for R_2 using the known values of λ_1 and λ_2, and for R_1 we use the decay rate for $B \to X_u \mu \nu_\mu \gamma$ is α_{em} times the decay rate for $B \to X_u \ell \nu_\ell$. With these values, we can then numerically calculate the non-perturbative parameters λ_1 and λ_2. Our results yield $\lambda_1 = -0.24\ GeV^2$ and $\lambda_2 = 0.15\ GeV^2$, which are consistent with previously values reported in the literature [151, 153]: $\lambda_1 = -0.19 \pm 0.10\ GeV^2$ and $\lambda_2 = 0.12 \pm 0.01\ GeV^2$. This motivates the need for a measurement of experimental measurement of the decay width of $B \to X_u \ell \nu_\ell \gamma$. As mentioned earlier, our focus has been on $\mathcal{O}(1/m_b^2)$ terms in the HQET. Thus we are primarily sensitive to λ_1 and λ_2 (or μ_π^2 and μ_G^2). At higher orders, the expressions become dependent on additional non-perturbative parameters. Therefore, measurements of the $B \to X_u \ell \nu_\ell \gamma$ rate and the ratio R_1 will be invaluable in simultaneously and easily determining these parameters when combined with $B \to X_u \ell \nu_\ell$ data and the ratio R_2.

5.6 Discussion and Conclusion

To summarize, we have presented a methodology for determining the non-perturbative parameters λ_1 and λ_2 in the inclusive decays of B mesons. Our approach involves directly calculating the decay widths for the inclusive modes $B \to X_u \ell \nu_\ell$ and $B \to X_u \ell \nu_\ell \gamma$ using the Cutkosky method in conjunction with the Heavy Quark Effective Theory (HQET), considering terms up to order $((\Lambda_{QCD} m_b)^2)$. Due to the involvement of a hard photon in the radiative mode $B \to X_u \ell \nu_\ell \gamma$, the tensorial structure of the amplitude becomes more complex, with four indices compared to two for $B \to X_u \ell \nu_\ell$. To properly account for the analytic properties and evaluate the decay rate, we opted to directly compute the relevant amplitude using the Cutkosky method, despite the associated complications. We obtained the differential rate and forward-backward asymmetry of the decay by integrating over the phase space variables for the four-body final state. By varying the parameter x_{min}, which determines the photon hardness, we investigated the behavior of the differential rate and asymmetry as functions of lepton energy. Notably, we observed that the decay rate for the radiative mode ($B \to X_u \ell \nu_\ell \gamma$) is approximately proportional to $\mathcal{O}(\alpha_{em})$ times that of the non-radiative mode ($B \to X_u \ell \nu_\ell$) when the photon possesses sufficient hardness.

In the subsequent analysis, we constructed two ratios, namely R_1 and R_2, by comparing the differential decay rates of the radiative and non-radiative modes for different lepton energy ranges, specifically considering a photon energy above a few times Λ_{QCD} (approximately 500 MeV). Importantly, these ratios are independent of the CKM element and provide a system of two linear equations in λ_1 and λ_2. This enables a precise determination of these non-perturbative parameters without any ambiguity.

To illustrate the applicability of our method, we have provided a simple example in Section-5.5.1 where we calculate the values of λ_1 and λ_2. Significantly, our findings align with the previously reported values found in the literature, thus providing consistency and validation. It is important to emphasize that, at present, the radiative mode lacks experimental measurements. However, the results of our study advocate for the necessity of precise measurements of the radiative mode to further enhance our understanding of the process.

In the process of $B \to X_u \ell \nu_\ell$, the differential rate for the free quark decay exhibits a proportionality to $2y^2(2y-3)$, where y represents the lepton energy in dimensionless unit in the rest frame of the B meson. This characteristic highlights a distinction between the partonic and hadronic end points, occurring at $\frac{m_b}{2}$ and $\frac{m_B}{2}$, respectively. As a result, an end point region of approximately $\bar{\Lambda} = m_B - m_b$ emerges. To accurately account for this region, it is essential to include an infinite number of terms in the heavy quark expansion. However, this expansion, expressed in terms of $\frac{\bar{\Lambda}}{m_b}$, introduces higher-order derivatives of the delta function at each successive order, leading to the breakdown of the Operator Product Expansion (OPE) and QCD perturbation theory in this region. Consequently, to properly incorporate the end-point behavior, the decay rates of $B \to X_u \ell \nu_\ell$ and $B \to X_s \gamma$ modes necessitate the introduction of the shape function, which describes the distribution of the heavy quark.

In the radiative decay mode $(B \to X_u \ell \nu_\ell \gamma)$, the presence of a hard photon in the final state leads to a shift in the endpoint compared to the non-radiative decay. Specifically, the partonic and hadronic endpoints are located at $\frac{m_b}{2} - x_{\min}$ and $\frac{m_B}{2} - x_{\min}$, respectively. However, similar to the $B \to X_u \ell \nu_\ell$ mode, the challenge posed by the disparity between partonic and hadronic endpoints necessitates the inclusion of a shape function for an accurate treatment of this process as well.

One potential approach is to consider a simplified form of the shape function, such as $(1-y-x)^a e^{(1+a)(x+y)}$, which has been proposed for the non-radiative decay mode in previous works [154, 155]. However, it is crucial to investigate the validity of this form by explicitly calculating the shape function specific to the radiative decay process and verifying its universality before drawing conclusive statements. While the specific form of the shape function remains an open question that requires further investigation, the fundamental concept that the radiative inclusive decay rate can facilitate a rapid determination of λ_1 and λ_2 remains unaffected.

To summarize, our proposed method provides a complementary approach for computing the non-perturbative parameters λ_1 and λ_2 in inclusive B decays, with the condition that the experimental measurement of the decay rate for the radiative mode $B \to X_u \ell \nu_\ell \gamma$ is available.

Chapter 6

Summary and Future Work

In this chapter, we summarize the key findings and contributions of the thesis, while also highlighting some important observations. Additionally, we outline our future plans.

6.1 Summary

The B meson system consists of a heavy quark, denoted as b, and light degrees of freedom. The mass of the b quark serves as a scale that incorporates the interplay between perturbative and non-perturbative physics. The substantial mass of the b quark has two fold advantage. The first advantage is that the B meson exhibits a wide range of decay modes, including both charged and neutral current induced processes. At low energy, it contains the observables such as the decay rates and the CKM elements like V_{ub} and V_{cb} often have higher theoretical uncertainties due to the involvement of non-perturbative parameters such as form factors. Computing these parameters with accuracy is challenging. On the other hand, the observables, such as LFU ratios like $R_{K^{(*)}}$, $R_{D^{(*)}}$ and the angular variables like P_5', are constructed in a way that minimizes theoretical uncertainties. These observables are designed to be less sensitive to the non-perturbative effects and can provide cleaner tests of the SM. The main goal of constructing and studying these observables is to check the consistency of the SM and explore the potential presence of new physics phenomena.

The second advantage of the heaviness of the b quark's mass is that it allows us to consider the inverse of its mass, $1/m_b$, as a perturbative expansion parameter. In the limit of $m_b \to \infty$, the dynamics of the B meson decay gets simplified and described solely in terms of the decay of the b quark itself. However, in reality, the mass of the b quark is finite, necessitating the inclusion of $1/m_b$ corrections that play a crucial role. The framework that incorporates these $1/m_b$ corrections and treats the b quark as a heavy quark is known as the Heavy Quark Expansion (HQE). In this expansion, the matrix elements contain non-perturbative parameters that need to be computed (Chapter-5 provides detailed discussions on the HQE and the computation of these non-perturbative parameters).

Further, B meson decays either into exclusive or inclusive channels, involve a combination of perturbative and non-perturbative contributions. While the computation of the perturbative part is a time-consuming and challenging task, we have a fair degree of control over it. However, the computation of non-perturbative contributions presents a greater challenge. In exclusive decays, these contributions manifest as decay constants and form factors, while in inclusive decays, they appear as hadronic matrix elements of kinetic and chromomagnetic operators up to $\mathcal{O}(1/m_Q)$ in HQE, as well as shape functions. Unfortunately, there is currently no rigorous first-principle method available to calculate these non-perturbative quantities directly. One approach is to employ lattice QCD, which comes with its own challenges, including heavy numerical computations and limitations in controlling systematic uncertainties.

In light of these, the observables such as the LFU ratios, including $R_{K^{(*)}}$ and $R_{D^{(*)}}$, as well as angular optimized variables such as P_5' have gained significance. These observables, except for the $R_{K^{(*)}}$[114], have shown deviations from the predictions of the SM, indicating the potential presence of NP phenomena. Before concluding anything, it is important to check if any theoretical contributions have been overlooked, particularly soft photon effects.

It motivated us to study the effects of soft photon corrections to $B \to K\ell\ell$. In our calculations, we treated the mesons as point-like particles and employed scalar QED. To ensure gauge invariance of the matrix element, we fixed the contact term. Further, we demonstrated that the differential decay rate remains independent of the IR regulator and collinear divergences by choosing a cut in the photon angle with respect to the charged lepton, denoted as $\theta_{\rm cut}$. An important finding of this investigation is the dependence of the decay rate and the ratio R_K on the maximum energy of the soft photon, represented as $k_{\rm max}$ (which corresponds to the experimental detector threshold). For instance, when $k_{\rm max}$ is set to 250MeV, exclusive emission of soft photons leads to positive corrections of approximately 4% in R_K (details in Chapter-3).

The dependence of the rate and the ratio R_K on $k_{\rm max}$ leads us to ask whether we can construct any observable that are theoretically clean and independent of $k_{\rm max}$. In this regard, we proposed an observable denoted as $R_V = \frac{|V_{ub}|}{|V_{cb}|}$, which exhibits a high degree of insensitivity to hadronic parameters and QED effects. We demonstrated that the equality of R_V calculated using inclusive and exclusive measurements of CKM matrix elements establishes a correlation between the coefficients of two distinct sectors: $b \to u$ and $b \to c$. Using this correlation, we make a prediction for the branching ratio $\mathcal{B}(B_c \to \tau\nu_\tau)$, which aligns with the constraint provided by [156] (details are in Chapter-4).

Furthermore, we explored the possibility of computing the non-perturbative parameters in a simple yet efficient manner. Specifically, we focused on the inclusive decays of the B meson due to theoretical cleanliness. In this regard, we calculated the decay width of $B \to X_u \ell \nu_\ell \gamma$ using the framework of HQET. We employed the Cutkosky cut method, including terms up to order $(\frac{\Lambda_{QCD}}{m_b})$. During this computation, we made an interesting observation: no new operators are generated in comparison to the non-radiative process $B \to X_u \ell \nu_\ell$. Hence, the total decay rate for the radiative mode resulted into the linear combination of non-perturbative parameters λ_1 and λ_2 similar to the non-radiative one. Consequently, the radiative case becomes particularly interesting, as it allows for the simultaneous determination of both non-perturbative parameters λ_1 and λ_2 in a definitive manner (explicit definitions of λ_1 and λ_2 are provided in Chapter-5). This approach offers a complementary avenue for computing the non-perturbative parameters in inclusive decays.

6.2 Future Work

For the future, our plan is to delve into the calculation of QED-corrected form factors for semileptonic decays of B mesons. In a previous study [26], we treated the mesons as point-like particles and computed the QED corrections based on this assumption. However, it is crucial to acknowledge that mesons possess a composite structure rather than being point-like particles like leptons. Moreover, the transition between different mesons is effectively described by form factors, which are functions of the momentum transfer squared. In the case of QED radiative decays, this momentum transfer is not solely represented by q^2, but also involves $(q+k)^2$, where k represents the momentum of the emitted photon. This additional momentum carried by the photon is expected to play a significant role in providing valuable insights into the decay of mesons, surpassing the limitations of their point-like approximation. Therefore, our intention is to calculate the QED-corrected form factors, specifically utilizing the Light Cone Sum Rules (LCSR) method.

Additionally, we aim to explore the implications of considering the charged meson as a dressed particle [157, 158] in the context of its semileptonic decays. This approach goes beyond the point-like approximation and takes into account the composite nature of the meson. By considering the meson as a dressed particle, we expect to gain valuable insights into optimized observables and non-perturbative parameters associated with these decays. Further, we are interested in investigating the impact of the dressed meson approach on the computation of form factors. Incorporating the dressed nature of the meson in the calculation of form factors could potentially yield new and improved results, providing a more accurate description of the decay processes. Moreover, we anticipate that this dressed approach may offer insights into resolving the Contact Term, which arises on demanding gauge invariance of the total amplitude in semileptonic decays. The Contact Term is a challenging aspect to be handled theoretically, and exploring the effects of the dressed meson on this term could potentially shed light on its nature and behavior.

Apart from these, we are also interested in investigating the geometric viewpoint of the Standard Model Effective Field Theory (SMEFT). Ref.[159–161] have focused on the scattering of bosons and fermions using geometric invariants, such as field space curvature, and solving the renormalization group equations for scalars at one loop, which simplifies calculations. It would be important to generalize this approach to the case of fermions and investigate its potential connections to phenomenology.

Appendix A

Essential definitions and Identities

A.1 Essential definitions

1. The metric tensor and Levi-Civita pseudotensor:

$$g^{\mu} = g_{\mu} = diag(1, -1, -1, -1), \quad \epsilon_{0123} = -\epsilon^{0123} = 1 \tag{A.1}$$

2. Dirac matrices:

$$\gamma^{\mu} = (\gamma^0, \boldsymbol{\gamma}), \quad \{\gamma^{\mu}, \gamma^{\nu}\} = 2g^{\mu\nu}, \quad \gamma^5 = i\gamma^0\gamma^1\gamma^2\gamma^3 \tag{A.2}$$

$$\gamma^0 = \begin{pmatrix} I & 0 \\ 0 & -I \end{pmatrix}, \quad \boldsymbol{\gamma} = \begin{pmatrix} 0 & \boldsymbol{\sigma} \\ -\boldsymbol{\sigma} & 0 \end{pmatrix}, \quad \gamma^5 = \begin{pmatrix} 0 & I \\ I & 0 \end{pmatrix} \tag{A.3}$$

$$(\gamma^0)^2 = 1, \quad (\gamma^i)^2 = -1, \quad (\gamma^5)^2 = 1 \tag{A.4}$$

Where I and $\boldsymbol{\sigma}$ are 2×2 identity and Pauli matrices.

3. Pauli matrices:

$$\sigma_1 = \begin{pmatrix} 0 & 1 \\ 1 & 0 \end{pmatrix}, \quad \sigma_2 = \begin{pmatrix} 0 & -i \\ i & 0 \end{pmatrix}, \quad \sigma_3 = \begin{pmatrix} 1 & 0 \\ 0 & -1 \end{pmatrix}.$$

4. Gell-Mann matrices λ_a $(a = 1, ..., 8)$ are:

$$\lambda_1 = \begin{pmatrix} 0 & 1 & 0 \\ 1 & 0 & 0 \\ 0 & 0 & 0 \end{pmatrix}, \quad \lambda_2 = \begin{pmatrix} 0 & -i & 0 \\ i & 0 & 0 \\ 0 & 0 & 0 \end{pmatrix}, \quad \lambda_3 = \begin{pmatrix} 1 & 0 & 0 \\ 0 & -1 & 0 \\ 0 & 0 & 0 \end{pmatrix},$$

$$\lambda_4 = \begin{pmatrix} 0 & 0 & 1 \\ 0 & 0 & 0 \\ 1 & 0 & 0 \end{pmatrix}, \quad \lambda_5 = \begin{pmatrix} 0 & 0 & -i \\ 0 & 0 & 0 \\ i & 0 & 0 \end{pmatrix}, \quad \lambda_6 = \begin{pmatrix} 0 & 0 & 0 \\ 0 & 0 & 1 \\ 0 & 1 & 0 \end{pmatrix},$$

$$\lambda_7 = \begin{pmatrix} 0 & 0 & 0 \\ 0 & 0 & -i \\ 0 & i & 0 \end{pmatrix}, \quad \lambda_8 = \frac{1}{\sqrt{3}} \begin{pmatrix} 1 & 0 & 0 \\ 0 & 1 & 0 \\ 0 & 0 & -2 \end{pmatrix}.$$

A.2 Essential Identities

1. Dirac Identities

$$\gamma_\mu \gamma^\mu = D, \quad \gamma_\mu \gamma_\alpha \gamma^\mu = (2 - D)\gamma_\alpha, \tag{A.5}$$

$$\gamma_\mu \gamma_\alpha \gamma_\beta \gamma^\mu = 4 g_{\alpha\beta} + (D - 4)\gamma_\alpha \gamma_\beta, \tag{A.6}$$

$$\gamma_\mu \gamma_\alpha \gamma_\beta \gamma_\rho \gamma^\mu = -2\gamma_\rho \gamma_\beta \gamma_\alpha - (D - 4)\gamma_\alpha \gamma_\beta \gamma_\rho, \tag{A.7}$$

$$\gamma_\mu \gamma_\nu = g_{\mu\nu} - i\sigma_{\mu\nu} \tag{A.8}$$

$$\gamma_\mu \gamma_\alpha \gamma_\nu = (g_{\mu\alpha} g_{\nu\beta} + g_{\mu\beta} g_{\alpha\nu} - g_{\mu\nu} g_{\alpha\beta})\gamma^\beta - i\gamma^5 \epsilon_{\mu\alpha\nu\beta} \gamma^\beta \tag{A.9}$$

2. Dirac traces

$$Tr(\gamma_\mu \gamma_\nu) = 4g_{\mu\nu}, \tag{A.10}$$

$$Tr(\gamma_\mu \gamma_\nu \gamma_\rho \gamma_\sigma) = 4(g_{\mu\nu} g_{\rho\sigma} - g_{\mu\rho} g_{\nu\sigma} + g_{\mu\sigma} g_{\nu\rho}), \tag{A.11}$$

$$Tr(\gamma^\mu \gamma^\nu \gamma^\alpha \gamma^\beta \gamma^5) = 4i\epsilon^{\mu\nu\alpha\beta}. \tag{A.12}$$

Appendix B

Useful Integrals

B.1 Real photon emission

1. Photon inclusive case

$$\begin{aligned}
\int_0^{x_+} dx \mathcal{I}_{1,1} &= \frac{1}{4m_B^2}\int_{-1}^{1} dt \frac{1}{p_t^2}\log\left(\frac{x_+^2 p_t^2}{m_\gamma^2 E_t^2}\right) + non-IR, \\
\int_0^{x_+} dx \mathcal{I}_{2,0} &= \frac{1}{2m_B^4}\log\left(\frac{x_+^2}{m_\gamma^2}\right) + non-IR, \quad \text{and} \\
\int_0^{x_+} dx \mathcal{I}_{0,2} &= \frac{1}{2m_B^2 m_l^2}\log\left(\frac{x_+^2}{m_\gamma^2}\right) + non-IR,
\end{aligned}$$

These integrals contribute to $\mathcal{I}_0$. Further, we list the coefficients , $C_{m,n}$ and the integrals, $\mathcal{I}_{m,n}$ for $\{m,n\} \in \{-2,2\}$, encountered in determination of the differential decay width

$$\begin{aligned}
C_{1,1} &= 2xym_B^4((-3f_-^2 + 2f_-f_+ + f_+^2)m_l^2 - 4f_+m_B^2(f_-y + f_+)), \\
C_{1,-1} &= 16f_+m_B^2(f_- - f_+)(y+z), \qquad C_{-2,2} = 64f_+^2 m_l^2, \\
C_{-1,1} &= -32f_+\left(f_+m_B^2(x+2y+z-1) - m_P^2 f_+ - (f_- - 2f_+)m_l^2\right), \\
C_{2,-1} &= -16f_+m_B^4(f_- + f_+)\left(2x+y+z-2\right), \\
C_{2,0} &= 8xm_B^4(f_- + f_+)\left(f_+ym_B^2 + (f_- - f_+)m_l^2\right) \\
C_{-1,2} &= -16f_+m_l^2\big(m_B^2(f_-(x+z-1) + f_+(-x+2y+z-3)) - (f_- - f_+) \\
&\quad (m_P^2 - m_l^2)\big),
\end{aligned}$$

$$\begin{aligned}
C_{1,0} &= -4m_B^2\Big[-2f_+m_B^2\big(f_-(3xy+4x+4z-4)+f_+x(y+4)+2f_+(y+1)\\
&\quad (y+z-2)\big)+8f_-f_+m_P^2+m_l^2\big(f_-^2(y+z-2)-2f_-f_+(y+z+2)\\
&\quad +f_+^2(y+z-2)\big)\Big],\\
C_{0,1} &= 4\Big[m_B^2\left(m_l^2(f_-^2(x+z-1)-2f_-f_+(3x+2y+z-1)+f_+^2(5x+z+3)\right)\\
&- 4f_+m_B^4(f_-y(x+z-1)+f_+(x(y-1)+2y(z-2)-z+1))+(f_-+f_+)^2\\
&\quad m_l^2(m_l^2-m_P^2)\Big],\\
C_{0,2} &= 4xm_B^2m_l^2\Big[2f_+m_B^2(f_-y-f_+(y-2))+(f_--f_+)^2m_l^2\Big],\\
C_{0,0} &= -16f_+\Big[m_B^2(f_-(x+2y+z-1)-f_+(x+4y+3z-1))-(f_--f_+)\\
&\quad (-m_P^2-m_l^2)\Big],
\end{aligned}$$

$$\begin{aligned}
\mathcal{I}_{0,0} &= \frac{1}{4}, \qquad\qquad \mathcal{I}_{1,1}=\frac{1}{4}\frac{2}{Q^2(p_B.p_l)\beta_{B\ell}}\log\left(\frac{1+\beta_{B\ell}}{1-\beta_{B\ell}}\right),\\
\mathcal{I}_{2,0} &= \frac{1}{m_B^2Q^2}, \qquad \mathcal{I}_{1,0}=\frac{1}{4(p_B.Q)\beta_{BQ}}\log\left(\frac{1+\beta_{BQ}}{1-\beta_{BQ}}\right),\\
\mathcal{I}_{1,-1} &= \frac{1}{4}\left(\frac{p_Bp_l:Q}{(p_B.Q)^2\beta_{BQ}^2}+\frac{Q^2(p_lQ:p_B)}{2(p_B.Q)^3\beta_{BQ}^2}\log\left(\frac{1+\beta_{BQ}}{1-\beta_{BQ}}\right)\right),\\
\mathcal{I}_{2,-1} &= \frac{1}{4}\Big(\frac{2(p_lQ:p_B)}{m_B^2(p_B.Q)^2\beta_{BQ}^2}+\frac{(p_Bp_l:Q)}{(p_B.Q)^3\beta_{BQ}^3}\log\left(\frac{1+\beta_{BQ}}{1-\beta_{BQ}}\right)\Big),\ \text{and}\\
\mathcal{I}_{-2,2} &= \frac{1}{4}\Big[\frac{Q^2(p_BQ:p_l)^2}{m_l^2(p_l.Q)^4\beta_{\ell Q}^4}+\frac{Q^2(p_BQ:p_l)(p_Bp_l:Q)}{(p_l.Q)^5\beta_{\ell Q}^5}\log\left(\frac{1+\beta_{\ell Q}}{1-\beta_{\ell Q}}\right)+\frac{(p_Bp_l:Q)^2}{(p_l.Q)^4\beta_{\ell Q}^4}\\
&- \frac{(p_B.Q)^2(p_l.Q)^2\beta_{BQ}^2\beta_{\ell Q}^2-(p_Bp_l:Q)^2}{2(p_l.Q)^4\beta_{\ell Q}^4}\left(2-\frac{1}{\beta_{\ell Q}}\log\left(\frac{1+\beta_{\ell Q}}{1-\beta_{\ell Q}}\right)\right)\Big].
\end{aligned}$$

Here, $\beta_{ij}=\sqrt{1-\frac{m_i^2m_j^2}{(p_i.p_j)^2}}$, $p_ip_j:p_k=(p_i.p_k)(p_j.p_k)-p_k^2(p_i.p_j)$ and $\mathcal{I}_{m,n}(p_i,p_j)=\mathcal{I}_{n,m}(p_j,p_i)$. The integrals $\mathcal{I}_{m,n}$ are found to be consistent with [162].

2. Photon exclusive case

$$\int_0^{k_{max}}\frac{d^3k}{(k^2+\lambda^2)^{1/2}}\frac{1}{(k.p_i)^2} = 2\pi\frac{1}{m_i^2}\ln\left(\frac{k_{max}^2m_i^2}{E_i^2\lambda^2}\right) \tag{B.1}$$

$$\int_0^{k_{max}}\frac{d^3k}{(k^2+\lambda^2)^{1/2}}\frac{1}{(k.p_j)^2} = 2\pi\frac{1}{m_j^2}\ln\left(\frac{k_{max}^2m_j^2}{E_i^2\lambda^2}\right) \tag{B.2}$$

$$\int_0^{k_{max}}\frac{d^3k}{(\overrightarrow{k}^2+\lambda^2)^{1/2}}\frac{1}{(k.p_i)(k.p_j)} = 2\pi\frac{1}{2}\int_{-1}^{1}\frac{dx}{p_x^2}\ln\left(\frac{k_{max}^2p_x^2}{E_x^2\lambda^2}\right) \tag{B.3}$$

B.2 Virtual Corrections

1. Integrals involved in the calculations

$$\int \frac{d^4k}{(k^2-\lambda^2)}\frac{1}{(k^2-2k.p_j\eta_j)^2} = \frac{-i\pi^2}{2m_j^2}\ln\left(\frac{m_j^2}{\lambda^2}\right) \tag{B.4}$$

$$\int \frac{d^4k}{(k^2-\lambda^2)}\frac{1}{(k^2-2k.p_i\eta_i)^2} = \frac{-i\pi^2}{2m_i^2}\ln\left(\frac{m_i^2}{\lambda^2}\right) \tag{B.5}$$

$$\lim_{\lambda\to 0}\int \frac{d^4k}{(k^2-\lambda^2)}\frac{1}{(k^2-2k.p_i\eta_i)(k^2-2k.p_j\eta_j)} = \frac{-i\pi^2}{4}\int_{-1}^{1}\frac{dx}{p_x'^2}\ln\left(\frac{p_x'^2}{\lambda^2}\right) \tag{B.6}$$

$$\int d^4k\frac{1}{(k^2-2k.p_j\eta_j)^2} = -i\pi^2\ln\left(m_j^2\right) \tag{B.7}$$

$$\int d^4k\frac{1}{(k^2-2k.p_i\eta_i)(k^2-2k.p_j\eta_j)} = \frac{-i\pi^2}{2}\int_{-1}^{1}dx\ln\left(p_x'^2\right) \tag{B.8}$$

2. Useful functions involved in the calculations

   The scalar two-point and three-point Passarino-Veltman functions and their derivatives, regulated by m_γ and Λ for IR and UV regularization, respectively, are given by:

$$B_0(m_a^2,0,m_a^2) = 2-\ln\left(\frac{m_a^2}{\Lambda^2}\right), \quad \text{and} \tag{B.9}$$

$$B_0(q^2,m_a^2,m_b^2) = -\int_0^1 du\ln\frac{-u(1-u)q^2+um_b^2+(1-u)m_a^2}{\Lambda^2} \tag{B.10}$$

$$B_0'(m_i^2,m_\gamma^2,m_i^2) = \frac{-1}{2m_i^2}\left(2+\ln\left(\frac{m_\gamma^2}{m_i^2}\right)\right) \tag{B.11}$$

$$C_0(m_B^2,m_l^2,q^2,m_B^2,m_\gamma^2,m_l^2) = \frac{-1}{4}\int_{-1}^{1}dt\frac{1}{p_t^2}\ln\left(\frac{m_\gamma^2}{p_t^2}\right), \tag{B.12}$$

$$\begin{aligned} C_1(m_B^2,m_l^2,q^2,m_B^2,0,m_l^2) &= \frac{1}{2m_l^2\beta^2}\Big[m_l^2\Big(B_0[m_l^2,0,m_l^2]-B_0[q^2,m_l^2,m_B^2]\Big) \\ &- p_B.p_l\Big(B_0[m_B^2,0,m_B^2]-B_0[q^2,m_l^2,m_B^2]\Big)\Big], \end{aligned} \tag{B.13}$$

$$\begin{aligned} C_2(m_B^2,m_l^2,q^2,m_B^2,0,m_l^2) &= \frac{-1}{2m_B^2\beta^2}\Big[p_B.p_l\Big(B_0[m_l^2,0,m_l^2]-B_0[q^2,m_l^2,m_B^2]\Big) \\ &+ p_B^2\Big(B_0[m_B^2,0,m_B^2]-B_0[q^2,m_l^2,m_B^2]\Big)\Big], \end{aligned} \tag{B.14}$$

respectively. Here, $\beta = \frac{|\mathbf{p_l}|}{E_\ell}$ represents the velocity of the charged lepton in the rest frame B meson.

Appendix C

Kinematics of decay rate

C.1 Three body kinematics

It includes the kinematics for three body decays for both exclusive and inclusive decay modes.

C.1.1 Exclusive decay modes

The kinematics for the three-body decay $B \to P\ell\nu_\ell$ can be expressed in terms of three Lorentz invariant kinematic variables: x, y, and z. These variables are

$$x = \frac{Q^2}{m_B^2}, \quad y = \frac{2p_B.p_l}{m_B^2}, \quad z = \frac{2p_B.p_P}{m_B^2} \tag{C.1}$$

where $Q^2 = p_n^2 = (p_B - p_D - p_l)^2$. It is worth noting that in the process $B \to P\ell\nu_\ell$, the squared momentum transfer Q^2 is zero due to the mass of the neutrino. However, when considering the case of real emission of a photon (soft), Q^2 assumes a non-zero value and is defined as the missing mass ($Q^2 = (p_n + k)^2$).

The total decay rate for $B \to P\ell\nu_\ell$ is

$$\Gamma_0 \;\; = \;\; \frac{m_B}{256\pi^3} \int dz \int dy \, |\mathcal{M}|^2_{B\to P\ell\nu_\ell} \, . \tag{C.2}$$

It is observed that the final result is independent of the variable x, thereby requiring only two independent Lorentz invariant kinematic variables, namely y and z. The kinematic boundaries for these variables are given by: $z_- \leq z \leq$

z_+, and $y_- \leq y \leq y_+$

$$\text{where,} \quad z_{\pm} = \frac{(2-y)(1+\frac{m_P^2}{m_B^2}+\frac{m_l^2}{m_B^2}-y) \pm \sqrt{y^2 - 4\frac{m_l^2}{m_B^2}}(1-\frac{m_P^2}{m_B^2}+\frac{m_l^2}{m_B^2}-y)}{2(1+\frac{m_l^2}{m_B^2}-y)},$$

$$y_- = 2\sqrt{r_\ell}, \text{ and} \qquad y_+ = 1 - \frac{m_P^2}{m_B^2} + \frac{m_l^2}{m_B^2}.$$

C.1.2 Inclusive decay modes

Now, we consider the kinematics for the three-body inclusive decay mode $B \to X_{u/c}\ell\nu_\ell$. It consist of three independent variable where one extra variable compared to exclusive decay mode is due to invariant mass squared for decayed hadron (p_X^2). Here, we have traded p_X^2 with $q'^2 (= (p_l + p_n)^2)$. The three kinematical variables are E_ℓ, E_ν, and $q^2 = (p_l + p_n)^2$. The general form of triple differential decay rate is given by

$$\begin{aligned} \frac{d^3\Gamma}{dq^2 dE_\ell dE_\nu} &= \int \frac{d^4 p_l}{(2\pi)^4} 2\pi\delta(p_l^2 - m_l^2)\theta(p_l^0) \int \frac{d^4 p_n}{(2\pi)^4} 2\pi\delta(p_n^2)\theta(p_n^0)\delta(E_\ell - p_l^0)\delta(E_\nu - p_n^0) \\ & \delta(q^2 - (p_l + p_n)^2) \frac{1}{2m_B} \sum_X |\langle X_{u/c}\ell\nu_\ell|\mathcal{M}|B\rangle|^2 (2\pi)^4 \delta^4(p_B - q - p_x), \end{aligned} \tag{C.3}$$

where

$$\delta(q^2 - (p_l + p_n)^2) = \delta(q^2 - 2E_\ell E_\nu(1 - \cos\theta_{\ell\nu})). \tag{C.4}$$

Performing the delta functions and integrating over $\cos\theta_{\ell\nu}$, the differential decay width is

$$\frac{d^3\Gamma}{dq^2 dE_\ell dE_\nu} = \frac{1}{4}\frac{1}{2m_B} \sum_X |\langle X_{u/c}\ell\nu_\ell|\mathcal{M}|B\rangle|^2 \delta^4(p_B - q - p_X - k), \tag{C.5}$$

where $\theta_{\ell\nu}$ is the angle between the lepton and neutrino. Further the delta function with Π can be expanded in the power of Π. Explicitly, it is given by

$$\begin{aligned} \delta\big(p_b + \Pi - q\big)^2 &= \delta\big(p_b - q\big)^2 + 2\Pi.(p_b - q)\delta'\big(p_b - q\big)^2 + \Pi^2\Big(\delta'\big(p_b - q\big)^2 \\ & +2(p_b - q)^2\delta''\big(p_b - q\big)^2\Big) + \ldots \end{aligned} \tag{C.6}$$

Another important point to note is that the integration domain in E_ν has a boundary from below:

$$E_\nu \geq \frac{q^2 - m_l^2}{4E_\ell}. \tag{C.7}$$

Therefore, it should be ensured that E_ν does not cross the boundary. This is enforced by introducing appropriate theta function in the integral. This plays an important role in the integration of delta functions and their derivative present in the differential rate $\frac{d^2\Gamma}{dq^2 dE_\ell}$.

C.2 Four body kinematics

C.2.1 Exclusive decay modes:

The decay width for the process $B \to P\ell\nu_\ell\gamma$ is given in terms of ten Lorentz invariant kinematic variables out of which five variables are independent and they are choosen as x, y, z, p_n and k. The four body decay region is divided into two regions: $\mathcal{D}_3$ and $\mathcal{D}_{4-3}$. The decay width in these two regions is given by

$$\begin{aligned}
\Gamma_{\mathcal{D}_3}|_{B\to P\ell\nu_\ell\gamma} &= \frac{m_B^3}{512\pi^4}\int_{\mathcal{D}_3} dydz \int_{\frac{m_\gamma^2}{m_B^2}}^{x_+} dx \int \frac{d^3p_n}{(2\pi)^3 2E_\nu}\int \frac{d^3k}{(2\pi)^3 2E_k}(2\pi)^4\delta^4\left(Q - p_n\right. \\
&- \left. k\right)|\mathcal{M}|^2_{B\to P\ell\nu_\ell\gamma}, \text{ and} \qquad \text{(C.8)} \\
\Gamma_{\mathcal{D}_{4-3}}|_{B\to P\ell\nu_\ell\gamma} &= \frac{m_B^3}{512\pi^4}\int_{\mathcal{D}_{4-3}} dydz \int_{x_-}^{x_+} dx \int \frac{d^3p_n}{(2\pi)^3 2E_\nu}\int \frac{d^3k}{(2\pi)^3 2E_k}(2\pi)^4\delta^4\left(Q - p_n\right. \\
&- \left. k\right)|\mathcal{M}|^2_{B\to P\ell\nu_\ell\gamma}, \qquad \text{(C.9)}
\end{aligned}$$

respectively. Here the kinematic boundaries for y and z in the region $\mathcal{D}_{4-3}$ are

$$\begin{aligned}
z_- &= 2\sqrt{\frac{m_P^2}{m_B^2}}, \qquad z_+ = \frac{(2-y)(1+\frac{m_P^2}{m_B^2}+\frac{m_l^2}{m_B^2}-y)}{2(1+\frac{m_l^2}{m_B^2}-y)} - \frac{\sqrt{y^2 - 4\frac{m_l^2}{m_B^2}}(1-\frac{m_P^2}{m_B^2}+\frac{m_l^2}{m_B^2}-y)}{2(1+\frac{m_l^2}{m_B^2}-y)}, \\
y_- &= 2\sqrt{\frac{m_l^2}{m_B^2}}, \text{ and} \qquad y_+ = 1 - \frac{m_P^2}{m_B^2} + \frac{\frac{m_l^2}{m_B^2}}{1-\sqrt{\frac{m_P^2}{m_B^2}}}.
\end{aligned}$$

C.2.2 Inclusive decay modes:

Lastly, we describe the kinematics involved in the inclusive decay for $B \to X_{u/c}\ell\nu_\ell\gamma$. Typically, a four-body decay involves five independent kinematic variables. However, in the inclusive four-body decay, we have six independent variables, as we introduce an extra variable related to the squared invariant mass of the decayed hadron, denoted as p_X^2. To simplify the analysis, we can instead use q'^2, which is defined as $(p_l + p_n + k)^2$, where p_l, p_n, and k represent the momenta of the lepton, neutrino, and photon, respectively. The two Lorentz invariant variables are defined as

$$y = \frac{2p_B.p_l}{m_B^2} \text{ and } x = \frac{2p_B.k}{m_B^2} \tag{C.10}$$

The remaining three variables in the inclusive four-body decay are the neutrino energy (E_ν) and two angles: (a) $\theta_{X\gamma}$, which represents the angle between the recoiling hadron (X) and the hard photon, (b) $\theta_{X\ell}$, which represents the angle between the final state recoiling hadron (X) and the charged lepton. The triple differential decay is given by

$$\begin{aligned} \frac{d^3\Gamma}{dq'^2 dE_\ell dE_\nu} &= \int \frac{d^4p_l}{(2\pi)^4}(2\pi)\delta(p_l^2 - m_l^2)\theta(p_l^0) \int \frac{d^4p_n}{(2\pi)^4}(2\pi)\delta(p_n^2)\theta(p_n^0)\delta(E_\ell - p_l^0) \\ & \delta(E_\nu - p_n^0)\delta(q'^2 - (q+k)^2) \int \frac{d^4k}{(2\pi)^4} \frac{1}{k^2((p_b + \Pi - q - k)^2 - m_u^2)} \\ & \sum_X |\langle X_{u/c}\ell\nu_\ell\gamma|\mathcal{M}|B\rangle|^2 (2\pi)^4\delta^4(p_b - q' - p_X). \end{aligned} \tag{C.11}$$

Cutcosky method implies that

$$\int \frac{d^4k}{(2\pi)^4} \to \int \frac{d^4k}{(2\pi)^4} \int \frac{d^4p_X}{(2\pi)^4}(2\pi)^4\delta^4(p_b - q - p_X - k), \tag{C.12}$$

and the propagator is replaced with delta functions. For example, in the Fig.(5.3), propagators are

$$\frac{1}{k^2} \to -2\pi i\delta(k^2)\theta(k^0) \tag{C.13}$$

$$\frac{1}{((p_b + \Pi - q - k)^2 - m_u^2)} \to -2\pi i\delta(((p_b + \Pi - q - k)^2 - m_u^2))\theta((p_b + \Pi - q - k)^0). \tag{C.14}$$

Incorporating the Cutkosky method, the differential decay width is

$$\begin{aligned}
\frac{d^3\Gamma}{dq'^2 dE_\ell dE_\nu} &= \int \frac{d^3p_l}{(2\pi)^3}\delta(p_l^2)\theta(p_l^0)\int \frac{d^3p_n}{(2\pi)^3}\delta(p_n^2)\theta(p_n^0)\delta(q'^2-(q+k)^2) \\
&\quad \int \frac{d^4k}{(2\pi)^4}\frac{d^4p_X}{(2\pi)^4}(-2\pi i)\delta(k^2)\theta(k^0)(-2\pi i)\delta((p_b+\Pi-q-k)^2-m_u^2) \\
&\quad (2\pi)^4\delta^4(p_b-q'-p_X)(2\pi)^4\sum_X |\langle X_{u/c}\ell\nu_\ell\gamma|\mathcal{M}|B\rangle|^2 \\
&\quad \delta^4(p_B-q-p_X-k) \\
&= -\frac{1}{8\pi^2}E_\ell E_\nu\int d(cos\theta_{\ell\nu})\delta(q'^2-(q+k)^2)\int\frac{d^3k}{2E_\gamma}\delta\big((p_B+\Pi-q-k)^2 \\
&\quad -m_u^2\big)\sum_X|\langle X_{u/c}\ell\nu_\ell\gamma|\mathcal{M}|B\rangle|^2\delta^4(p_B-q-p_X-k) \\
&= -\frac{1}{8\pi^2}\int\frac{d^3k}{2E_\gamma}\delta((p_B+\Pi-q-k)^2-m_u^2)\sum_X|\langle X_{u/c}\ell\nu_\ell\gamma|\mathcal{M}|B\rangle|^2 \\
&\quad \delta^4(p_B-q-p_X-k).
\end{aligned} \tag{C.15}$$

Similar to three-body decay, the expansion of the delta function in the power of Π is given by

$$\begin{aligned}
\delta\big(p_b+\Pi-q-k\big)^2 &= \delta\big(p_b-q-k\big)^2+2\Pi.(p_b-q-k)\delta'\big(p_b-q-k\big)^2+\Pi^2\Big(\delta'\big(p_b \\
&\quad -q-k\big)^2+2(p_b-q-k)^2\delta''\big(p_b-q-k\big)^2\Big)+...
\end{aligned} \tag{C.16}$$

Another important point to note is that the integration domain in E_ν has a boundary from below:

$$E_\nu \geq \frac{q'^2-2q.k-m_l^2}{4E_\ell}. \tag{C.17}$$

Therefore, it must be ensured that the neutrino energy (E_ν) does not exceed a certain boundary and that an appropriate theta function is introduced in the integral. This theta function plays a crucial role in integrating the delta functions and their derivatives present in the differential rate $\frac{d^2\Gamma}{dq'^2 dE_\ell}$.

Bibliography

1. Glashow, S. L. Partial Symmetries of Weak Interactions. *Nucl. Phys.* **22,** 579–588 (1961).

2. Salam, A. Weak and Electromagnetic Interactions. *Conf. Proc. C* **680519,** 367–377 (1968).

3. Weinberg, S. A Model of Leptons. *Phys. Rev. Lett.* **19,** 1264–1266 (1967).

4. Schwartz, M. D. *Quantum Field Theory and the Standard Model* ISBN: 978-1-107-03473-0, 978-1-107-03473-0 (Cambridge University Press, Mar. 2014).

5. Cheng, T.-P. & Li, L.-F. *Gauge Theory of Elementary Particle Physics* ISBN: 978-0-19-851961-4, 978-0-19-851961-4 (Oxford University Press, Oxford, UK, 1984).

6. Cottingham, W. N. & Greenwood, D. A. *An introduction to the standard model of particle physics* ISBN: 978-0-511-27136-6, 978-0-521-85249-4 (Cambridge University Press, Apr. 2007).

7. Bertone, G. & Hooper, D. History of dark matter. *Rev. Mod. Phys.* **90,** 045002. arXiv: 1605.04909 [astro-ph.CO] (2018).

8. Oks, E. Brief review of recent advances in understanding dark matter and dark energy. *New Astron. Rev.* **93,** 101632. arXiv: 2111.00363 [astro-ph.CO] (2021).

9. Cline, J. M. *Baryogenesis* in *Les Houches Summer School - Session 86: Particle Physics and Cosmology: The Fabric of Spacetime* (Sept. 2006). arXiv: hep-ph/0609145.

10. Davidson, S., Nardi, E. & Nir, Y. Leptogenesis. *Phys. Rept.* **466,** 105–177. arXiv: 0802.2962 [hep-ph] (2008).

11. Langacker, P. Grand Unified Theories and Proton Decay. *Phys. Rept.* **72,** 185 (1981).

12. Buras, A. J., Ellis, J. R., Gaillard, M. K. & Nanopoulos, D. V. Aspects of the Grand Unification of Strong, Weak and Electromagnetic Interactions. *Nucl. Phys. B* **135,** 66–92 (1978).

13. Mohapatra, R. N. & Smirnov, A. Y. Neutrino Mass and New Physics. *Ann. Rev. Nucl. Part. Sci.* **56** (eds Anagnostopoulos, K. *et al.*) 569–628. arXiv: hep-ph/0603118 (2006).

14. Bilenky, S. M. & Petcov, S. T. Massive Neutrinos and Neutrino Oscillations. *Rev. Mod. Phys.* **59.** [Erratum: Rev.Mod.Phys. 61, 169 (1989), Erratum: Rev.Mod.Phys. 60, 575–575 (1988)], 671 (1987).

15. Arnold, P. B. Can the Electroweak Vacuum Be Unstable? *Phys. Rev. D* **40,** 613 (1989).

16. Kobakhidze, A. & Spencer-Smith, A. Electroweak Vacuum (In)Stability in an Inflationary Universe. *Phys. Lett. B* **722,** 130–134. arXiv: 1301.2846 [hep-ph] (2013).

17. Coleman, S. R. The Fate of the False Vacuum. 1. Semiclassical Theory. *Phys. Rev. D* **15.** [Erratum: Phys.Rev.D 16, 1248 (1977)], 2929–2936 (1977).

18. Aad, G. *et al.* Observation of a new particle in the search for the Standard Model Higgs boson with the ATLAS detector at the LHC. *Phys. Lett. B* **716,** 1–29. arXiv: 1207.7214 [hep-ex] (2012).

19. Chatrchyan, S. *et al.* Observation of a New Boson at a Mass of 125 GeV with the CMS Experiment at the LHC. *Phys. Lett. B* **716,** 30–61. arXiv: 1207.7235 [hep-ex] (2012).

20. Albrecht, H. *et al.* Observation of B0 - anti-B0 Mixing. *Phys. Lett. B* **192** (ed Tran Thanh Van, J.) 245–252 (1987).

21. Manohar, A. V. Introduction to Effective Field Theories (eds Davidson, S., Gambino, P., Laine, M., Neubert, M. & Salomon, C.) arXiv: 1804.05863 [hep-ph] (Apr. 2018).

22. Atwood, D. & Marciano, W. J. Radiative Corrections and Semileptonic B Decays. *Phys. Rev. D* **41,** 1736 (1990).

23. De Boer, S., Kitahara, T. & Nisandzic, I. Soft-Photon Corrections to $\bar{B} \to D\tau^-\bar{\nu}_\tau$ Relative to $\bar{B} \to D\mu^-\bar{\nu}_\mu$. *Phys. Rev. Lett.* **120,** 261804. arXiv: 1803.05881 [hep-ph] (2018).

24. Becirevic, D., Haas, B. & Kou, E. Soft Photon Problem in Leptonic B-decays. *Phys. Lett. B* **681,** 257–263. arXiv: 0907.1845 [hep-ph] (2009).

25. Isidori, G. Soft-photon corrections in multi-body meson decays. *Eur. Phys. J. C* **53,** 567–571. arXiv: 0709.2439 [hep-ph] (2008).

26. Mishra, D. & Mahajan, N. Impact of soft photons on $B \to K\ell^+\ell^-$. *Phys. Rev. D* **103,** 056022. arXiv: 2010.10853 [hep-ph] (2021).

27. Bansal, A., Mahajan, N. & Mishra, D. $\frac{|V_{ub}|}{|V_{cb}|}$ and quest for new physics. *JHEP* **02,** 130. arXiv: 2112.00363 [hep-ph] (2022).

28. Mohapatra, R. N. *et al.* Theory of neutrinos: A White paper. *Rept. Prog. Phys.* **70,** 1757–1867. arXiv: hep-ph/0510213 (2007).

29. Donoghue, J. F., Golowich, E. & Holstein, B. R. *Dynamics of the Standard Model : Second edition* ISBN: 978-1-00-929103-3, 978-1-00-929100-2, 978-1-00-929101-9 (Oxford University Press, 2014).

30. Buras, A. *Gauge Theory of Weak Decays* ISBN: 978-1-139-52410-0, 978-1-107-03403-7 (Cambridge University Press, June 2020).

31. Peskin, M. E. & Schroeder, D. V. *An Introduction to quantum field theory* ISBN: 978-0-201-50397-5 (Addison-Wesley, Reading, USA, 1995).

32. Weinberg, S. *The Quantum theory of fields. Vol. 1: Foundations* ISBN: 978-0-521-67053-1, 978-0-511-25204-4 (Cambridge University Press, June 2005).

33. Muta, T. *Foundations of quantum chromodynamics. Second edition* (1998).

34. Gattringer, C. & Lang, C. B. *Quantum chromodynamics on the lattice* ISBN: 978-3-642-01849-7, 978-3-642-01850-3 (Springer, Berlin, 2010).

35. Kronfeld, A. S. Twenty-first Century Lattice Gauge Theory: Results from the QCD Lagrangian. *Ann. Rev. Nucl. Part. Sci.* **62,** 265–284. arXiv: 1203.1204 [hep-lat] (2012).

36. Leutwyler, H. Foundations and scope of chiral perturbation theory. *Lect. Notes Phys.* **452** (eds Bernstein, A. M. & Holstein, B. R.) 14. arXiv: hep-ph/9409423 (1995).

37. Ioffe, B. L., Fadin, V. S. & Lipatov, L. N. *Quantum chromodynamics: Perturbative and nonperturbative aspects* ISBN: 978-1-107-42475-3, 978-0-521-63148-8, 978-0-511-71744-4 (Cambridge Univ. Press, 2010).

38. Braun, V. M. *Light cone sum rules* in *4th International Workshop on Progress in Heavy Quark Physics* (Sept. 1997), 105–118. arXiv: hep-ph/9801222.

39. Colangelo, P. & Khodjamirian, A. QCD sum rules, a modern perspective (eds Shifman, M. & Ioffe, B.) 1495–1576. arXiv: hep-ph/0010175 (Oct. 2000).

40. Cabibbo, N. Unitary Symmetry and Leptonic Decays. *Phys. Rev. Lett.* **10,** 531–533 (1963).

41. Kobayashi, M. & Maskawa, T. CP Violation in the Renormalizable Theory of Weak Interaction. *Prog. Theor. Phys.* **49,** 652–657 (1973).

42. Pontecorvo, B. Mesonium and anti-mesonium. *Sov. Phys. JETP* **6,** 429 (1957).

43. Maki, Z., Nakagawa, M. & Sakata, S. Remarks on the unified model of elementary particles. *Prog. Theor. Phys.* **28,** 870–880 (1962).

44. Wolfenstein, L. Parametrization of the Kobayashi-Maskawa Matrix. *Phys. Rev. Lett.* **51,** 1945 (1983).

45. Workman, R. L. *et al.* Review of Particle Physics. *PTEP* **2022,** 083C01 (2022).

46. Ali, A. Flavor changing neutral current processes in B decays. *AIP Conf. Proc.* **300** (eds Mann, A. K. & Cline, D. B.) 437–466 (1994).

47. Wilson, K. G. Nonlagrangian models of current algebra. *Phys. Rev.* **179,** 1499–1512 (1969).

48. Buras, A. J. *Weak Hamiltonian, CP violation and rare decays* in *Les Houches Summer School in Theoretical Physics, Session 68: Probing the Standard Model of Particle Interactions* (June 1998), 281–539. arXiv: hep-ph/9806471.

49. Misiak, M. Radiative and rare semileptonic B decays. *PoS* **FPCP2010** (ed Bianchi, F.) 025 (2010).

50. Shifman, M. A. *ITEP lectures on particle physics and field theory. Vol. 1, 2* (1999).

51. Uraltsev, N. Topics in the heavy quark expansion (eds Shifman, M. & Ioffe, B.) 1577–1670. arXiv: hep-ph/0010328 (Oct. 2000).

52. Bigi, I. I. Y., Shifman, M. A., Uraltsev, N. G. & Vainshtein, A. I. Sum rules for heavy flavor transitions in the SV limit. *Phys. Rev. D* **52,** 196–235. arXiv: hep-ph/9405410 (1995).

53. Manohar, A. V. & Wise, M. B. *Heavy quark physics* ISBN: 978-0-521-03757-0 (2000).

54. Petrov, A. A. & Blechman, A. E. *Effective Field Theories* ISBN: 978-981-4434-92-8, 978-981-4434-94-2 (WSP, 2016).

55. Mannel, T. Effective theory for heavy quarks. *Lect. Notes Phys.* **479** (eds Latal, H. & Schweiger, W.) 387–428. arXiv: hep-ph/9606299 (1997).

56. Burgess, C. P. *Introduction to Effective Field Theory* ISBN: 978-1-139-04804-0, 978-0-521-19547-8 (Cambridge University Press, Dec. 2020).

57. Bharucha, A. Recent progress in decays of b and c hadrons (Dec. 2022).

58. London, D. *Anomalies in B Decays: A Sign of New Physics?* in *11th International Symposium on Quantum Theory and Symmetries* (Nov. 2019). arXiv: 1911.06238 [hep-ph].

59. Bloch, F. & Nordsieck, A. Note on the Radiation Field of the Electron. *Phys. Rev.* **52,** 54–59. https://link.aps.org/doi/10.1103/PhysRev.52.54 (2 July 1937).

60. Kinoshita, T. Mass singularities of Feynman amplitudes. *J. Math. Phys.* **3,** 650–677 (1962).

61. Lee, T. D. & Nauenberg, M. Degenerate Systems and Mass Singularities. *Phys. Rev.* **133** (ed Feinberg, G.) B1549–B1562 (1964).

62. Davidson, N., Przedzinski, T. & Was, Z. PHOTOS interface in C++: Technical and Physics Documentation. *Comput. Phys. Commun.* **199,** 86–101. arXiv: 1011.0937 [hep-ph] (2016).

63. Golonka, P. & Was, Z. PHOTOS Monte Carlo: A Precision tool for QED corrections in Z and W decays. *Eur. Phys. J. C* **45,** 97–107. arXiv: hep-ph/0506026 (2006).

64. Schonherr, M. & Krauss, F. Soft Photon Radiation in Particle Decays in SHERPA. *JHEP* **12,** 018. arXiv: 0810.5071 [hep-ph] (2008).

65. Frixione, S. *et al. Initial state QED radiation aspects for future* e^+e^- *colliders* in *Snowmass 2021* (Mar. 2022). arXiv: 2203.12557 [hep-ph].

66. Agarwal, N., Magnea, L., Signorile-Signorile, C. & Tripathi, A. The infrared structure of perturbative gauge theories. *Physics Reports* **994,** 1–120. arXiv: 2112.07099 [hep-ph] (2023).

67. Zwicky, R. Notes on QED Corrections in Weak Decays. *Symmetry* **13,** 2036. arXiv: 2205.06194 [hep-ph] (2021).

68. Mott, N. F. On the influence of radiative forces on the scattering of electrons. *Mathematical Proceedings of the Cambridge Philosophical Society* **27,** 255–267 (1931).

69. Jauch, J.-M. & Rohrlich, F. The infrared divergence. *Helv. Phys. Acta* **27,** 613–636 (1954).

70. Chung, V. Infrared Divergence in Quantum Electrodynamics. *Phys. Rev.* **140,** B1110–B1122 (1965).

71. Sommerfeld, A. *Annalen der Physik* **403,** 257–330. eprint: https://onlinelibrary.wiley.com/doi/pdf/10.1002/andp.19314030302. https://onlinelibrary.wiley.com/doi/abs/10.1002/andp.19314030302 (1931).

72. Grammer Jr., G. & Yennie, D. R. Improved treatment for the infrared divergence problem in quantum electrodynamics. *Phys. Rev. D* **8,** 4332–4344 (1973).

73. Yennie, D., Frautschi, S. C. & Suura, H. The infrared divergence phenomena and high-energy processes. *Annals Phys.* **13,** 379–452 (1961).

74. Sterman, G. F. *Partons, factorization and resummation, TASI 95* in *Theoretical Advanced Study Institute in Elementary Particle Physics (TASI 95): QCD and Beyond* (June 1995), 327–408. arXiv: hep-ph/9606312.

75. Sterman, G. F. *An Introduction to quantum field theory* ISBN: 978-0-521-31132-8 (Cambridge University Press, Aug. 1993).

76. Collins, J. *Foundations of perturbative QCD* ISBN: 978-1-107-64525-7, 978-1-107-64525-7, 978-0-521-85533-4, 978-1-139-09782-6 (Cambridge University Press, Nov. 2013).

77. Kibble, T. W. B. Coherent soft-photon states and infrared divergences. iv. the scattering operator. *Phys. Rev.* **175,** 1624–1640 (1968).

78. Kibble, T. W. B. Coherent soft-photon states and infrared divergences. iii. asymptotic states and reduction formulas. *Phys. Rev.* **174,** 1882–1901 (1968).

79. Kulish, P. P. & Faddeev, L. D. Asymptotic conditions and infrared divergences in quantum electrodynamics. *Theor. Math. Phys.* **4,** 745 (1970).

80. Doria, R., Frenkel, J. & Taylor, J. C. Counter Example to Nonabelian Bloch-Nordsieck Theorem. *Nucl. Phys. B* **168,** 93–110 (1980).

81. Andrasi, A., Day, M., Doria, R., Frenkel, J. & Taylor, J. C. Soft Divergences in Perturbative QCD. *Nucl. Phys. B* **182,** 104–124 (1981).

82. Carneiro, C. E., Day, M., Frenkel, J., Taylor, J. C. & Thomaz, M. T. LEADING NONCANCELLING INFRARED DIVERGENCES IN PERTURBATIVE QCD. *Nucl. Phys. B* **183,** 445–470 (1981).

83. Libby, S. B. & Sterman, G. F. Cancellation of Infrared Divergences in Massive Quark Potential Scattering. *Phys. Rev. D* **19,** 2468 (1979).

84. Sterman, G. F. Mass Divergences in Annihilation Processes. 1. Origin and Nature of Divergences in Cut Vacuum Polarization Diagrams. *Phys. Rev. D* **17,** 2773 (1978).

85. Sterman, G. F. Mass Divergences in Annihilation Processes. 2. Cancellation of Divergences in Cut Vacuum Polarization Diagrams. *Phys. Rev. D* **17,** 2789 (1978).

86. Taylor, J. R. SCATTERING THEORY: THE QUANTUM THEORY ON NONRELATIVISTIC COLLISIONS. (1972).

87. Greco, M., Palumbo, F., Pancheri-Srivastava, G. & Srivastava, Y. Coherent State Approach to the Infrared Behavior of Nonabelian Gauge Theories. *Phys. Lett. B* **77,** 282–286 (1978).

88. Curci, G. & Greco, M. Mass Singularities and Coherent States in Gauge Theories. *Phys. Lett. B* **79** (ed Greco, M.) 406–410 (1978).

89. Butler, D. R. & Nelson, C. A. Nonabelian Structure of Yang-Mills Theory and Infrared Finite Asymptotic States. *Phys. Rev. D* **18,** 1196 (1978).

90. Catani, S., Ciafaloni, M. & Marchesini, G. Asymptotic Coherent States and Color Screening. *Phys. Lett. B* **168,** 284–288 (1986).

91. Catani, S., Ciafaloni, M. & Marchesini, G. NONCANCELLING INFRARED DIVERGENCES IN QCD COHERENT STATE. *Nucl. Phys. B* **264,** 588–620 (1986).

92. Sudakov, V. V. Vertex parts at very high-energies in quantum electrodynamics. *Sov. Phys. JETP* **3,** 65–71 (1956).

93. Sen, A. Asymptotic Behavior of the Sudakov Form-Factor in QCD. *Phys. Rev. D* **24,** 3281 (1981).

94. Ginsberg, E. S. & Smith, J. Radiative corrections to the muon polarization in k0(mu3) decays. *Phys. Rev. D* **8,** 3887–3894 (1973).

95. Cirigliano, V., Knecht, M., Neufeld, H., Rupertsberger, H. & Talavera, P. Radiative corrections to K(l3) decays. *Eur. Phys. J. C* **23,** 121–133. arXiv: hep-ph/0110153 (2002).

96. Beneke, M., Bobeth, C. & Szafron, R. Enhanced electromagnetic correction to the rare B-meson decay $B_{s,d} \to \mu^+\mu^-$. *Phys. Rev. Lett.* **120,** 011801. arXiv: 1708.09152 [hep-ph] (2018).

97. Beneke, M., Böer, P., Toelstede, J.-N. & Vos, K. K. QED factorization of non-leptonic B decays. *JHEP* **11,** 081. arXiv: 2008.10615 [hep-ph] (2020).

98. Papucci, M., Trickle, T. & Wise, M. B. Radiative semileptonic $\overline{B}$ decays. *JHEP* **02,** 043. arXiv: 2110.13154 [hep-ph] (2022).

99. Pich, A. *Effective field theory: Course* in *Les Houches Summer School in Theoretical Physics, Session 68: Probing the Standard Model of Particle Interactions* (June 1998), 949–1049. arXiv: hep-ph/9806303.

100. Georgi, H. *Weak Interactions and Modern Particle Theory* ISBN: 978-0-8053-3163-9 (1984).

101. Buchalla, G. *et al.* B, D and K decays. *Eur. Phys. J. C* **57** (eds Fleischer, R., Hurth, T. & Mangano, M.) 309–492. arXiv: 0801.1833 [hep-ph] (2008).

102. Bjorken, J. D. & Drell, S. D. *Relativistic Quantum Mechanics* ISBN: 978-0-07-005493-6 (McGraw-Hill, New York, 1965).

103. Uraltsev, N. Heavy quark expansion in beauty and its decays. *Proc. Int. Sch. Phys. Fermi* **137** (eds Bigi, I. I. Y. & Moroni, L.) 329–409. arXiv: hep-ph/9804275 (1998).

104. Neubert, M. Heavy quark effective theory. *Subnucl. Ser.* **34** (ed Zichichi, A.) 98–165. arXiv: hep-ph/9610266 (1997).

105. Buras, A. J., Girrbach, J., Guadagnoli, D. & Isidori, G. On the Standard Model prediction for BR(B{s,d} to mu+ mu-). *Eur. Phys. J. C* **72,** 2172. arXiv: 1208.0934 [hep-ph] (2012).

106. Kruger, F., Sehgal, L. M., Sinha, N. & Sinha, R. Angular distribution and CP asymmetries in the decays $\bar{B} \to K^- \pi^+ e^- e^+$ and $\bar{B} \to \pi^- \pi^+ e^- e^+$. *Phys. Rev. D* **61.** [Erratum: Phys.Rev.D 63, 019901 (2001)], 114028. arXiv: hep-ph/9907386 (2000).

107. Ali, A., Ball, P., Handoko, L. T. & Hiller, G. Comparative study of the decays $B \to (K, K^*)\ell\ell$ in the standard model and supersymmetric theories. *Physical Review D* **61.** ISSN: 1089-4918. http://dx.doi.org/10.1103/PhysRevD.61.074024 (Mar. 2000).

108. Hambrock, C. & Hiller, G. Extracting $B \to K^*$ Form Factors from Data. *Phys. Rev. Lett.* **109,** 091802. arXiv: 1204.4444 [hep-ph] (2012).

109. Bobeth, C. *et al.* $B_{s,d} \to l^+ l^-$ in the Standard Model with Reduced Theoretical Uncertainty. *Phys. Rev. Lett.* **112,** 101801. arXiv: 1311.0903 [hep-ph] (2014).

110. Khodjamirian, A., Mannel, T., Pivovarov, A. & Wang, Y.-M. Charm-loop effect in $B \to K^{(*)} \ell^+ \ell^-$ and $B \to K^* \gamma$. *JHEP* **09,** 089. arXiv: 1006.4945 [hep-ph] (2010).

111. Khodjamirian, A., Mannel, T., Offen, N. & Wang, Y.-M. $B \to \pi \ell \nu_\ell$ width and $|V_{ub}|$ from QCD light-cone sum rules. *Physical Review D* **83.** ISSN: 1550-2368. http://dx.doi.org/10.1103/PhysRevD.83.094031 (May 2011).

112. Hiller, G. & Kruger, F. More model-independent analysis of $b \to s$ processes. *Phys. Rev. D* **69,** 074020. arXiv: hep-ph/0310219 (2004).

113. Bordone, M., Isidori, G. & Pattori, A. On the Standard Model predictions for R_K and R_{K^*}. *Eur. Phys. J. C* **76,** 440. arXiv: 1605.07633 [hep-ph] (2016).

114. Measurement of lepton universality parameters in $B^+ \to K^+ \ell^+ \ell^-$ and $B^0 \to K^{*0} \ell^+ \ell^-$ decays. arXiv: 2212.09153 [hep-ex] (Dec. 2022).

115. Buras, A. J. & Münz, M. Effective Hamiltonian for B$\to X_s e^+ e^-$ beyond leading logarithms in the naive dimensional regularization and 't Hooft–Veltman schemes. *Phys. Rev. D* **52,** 186–195. https://link.aps.org/doi/10.1103/PhysRevD.52.186 (1 July 1995).

116. Bobeth, C., Hiller, G., van Dyk, D. & Wacker, C. The Decay $B \to K\ell^+\ell^-$ at Low Hadronic Recoil and Model-Independent $\Delta B = 1$ Constraints. *JHEP* **01,** 107. arXiv: 1111.2558 [hep-ph] (2012).

117. Isidori, G., Nabeebaccus, S. & Zwicky, R. QED Corrections in $\bar{B} \to \bar{K}\ell^+\ell^-$ at the Double-Differential Level, arXiv:2009.00929. arXiv: 2009.00929 [hep-ph] (Sept. 2020).

118. Weinberg, S. *The Quantum Theory of Fields* (Cambridge University Press, 1995).

119. Jenkins, E. E., Manohar, A. V. & Trott, M. On Gauge Invariance and Minimal Coupling. *JHEP* **09,** 063. arXiv: 1305.0017 [hep-ph] (2013).

120. Bourrely, C., Caprini, I. & Lellouch, L. Model-independent description of $B \to \pi\ell\nu$ decays and a determination of $|V_{ub}t|$. *Phys. Rev. D* **79.** [Erratum: Phys.Rev.D 82, 099902 (2010)], 013008. arXiv: 0807.2722 [hep-ph] (2009).

121. Wang, Y.-M., Wei, Y.-B., Shen, Y.-L. & Lü, C.-D. Perturbative corrections to $B \to D$ form factors in QCD. *JHEP* **06,** 062. arXiv: 1701.06810 [hep-ph] (2017).

122. Bernlochner, F. U., Ligeti, Z., Papucci, M. & Robinson, D. J. Combined analysis of semileptonic B decays to D and D^*: $R(D^{(*)})$, $|V_{cb}|$, and new physics. *Phys. Rev. D* **95.** [Erratum: Phys.Rev.D 97, 059902 (2018)], 115008. arXiv: 1703.05330 [hep-ph] (2017).

123. Lange, B. O., Neubert, M. & Paz, G. Theory of charmless inclusive B decays and the extraction of V_{ub}. *Phys. Rev. D* **72,** 073006. arXiv: hep-ph/0504071 (2005).

124. Gambino, P., Giordano, P., Ossola, G. & Uraltsev, N. Inclusive semileptonic B decays and the determination of $|V_{ub}|$. *JHEP* **10,** 058. arXiv: 0707.2493 [hep-ph] (2007).

125. Bauer, C. W., Ligeti, Z., Luke, M. & Manohar, A. V. B decay shape variables and the precision determination of —V(cb)— and m(b). *Phys. Rev. D* **67,** 054012. arXiv: hep-ph/0210027 (2003).

126. Alberti, A., Gambino, P., Healey, K. J. & Nandi, S. Precision Determination of the Cabibbo-Kobayashi-Maskawa Element V_{cb}. *Phys. Rev. Lett.* **114,** 061802. arXiv: 1411.6560 [hep-ph] (2015).

127. Amhis, Y. S. *et al.* Averages of b-hadron, c-hadron, and τ-lepton properties as of 2018. *Eur. Phys. J. C* **81,** 226. arXiv: 1909.12524 [hep-ex] (2021).

128. Aoki, Y. *et al.* FLAG Review 2021, Arxiv: 2111.09849. arXiv: 2111.09849 [hep-lat] (Nov. 2021).

129. Cao, L. *et al.* First Simultaneous Determination of Inclusive and Exclusive $|V_{ub}|$. arXiv: 2303.17309 [hep-ex] (Mar. 2023).

130. Gambino, P., Jung, M. & Schacht, S. The V_{cb} puzzle: An update. *Phys. Lett. B* **795,** 386–390. arXiv: 1905.08209 [hep-ph] (2019).

131. Hiller, G. & Schmaltz, M. R_K and future $b \to s\ell\ell$ physics beyond the standard model opportunities. *Phys. Rev. D* **90,** 054014. arXiv: 1408.1627 [hep-ph] (2014).

132. Aaij, R. *et al.* Determination of the quark coupling strength $|V_{ub}|$ using baryonic decays. *Nature Phys.* **11,** 743–747. arXiv: 1504.01568 [hep-ex] (2015).

133. Detmold, W., Lehner, C. & Meinel, S. $\Lambda_b \to p\ell^-\bar{\nu}_\ell$ and $\Lambda_b \to \Lambda_c\ell^-\bar{\nu}_\ell$ form factors from lattice QCD with relativistic heavy quarks. *Phys. Rev. D* **92,** 034503. arXiv: 1503.01421 [hep-lat] (2015).

134. Aaij, R. *et al.* First observation of the decay $B_s^0 \to K^-\mu^+\nu_\mu$ and Measurement of $|V_{ub}|/|V_{cb}|$. *Phys. Rev. Lett.* **126,** 081804. arXiv: 2012.05143 [hep-ex] (2021).

135. Khodjamirian, A., Mannel, T., Offen, N. & Wang, Y. .-. $B \to \pi \ell \nu_l$ Width and $|V_{ub}|$ from QCD Light-Cone Sum Rules. *Phys. Rev. D* **83,** 094031. arXiv: 1103.2655 [hep-ph] (2011).

136. Kamali, S. New physics in inclusive semileptonic B decays including non-perturbative corrections. *Int. J. Mod. Phys. A* **34,** 1950036. arXiv: 1811.07393 [hep-ph] (2019).

137. Dassinger, B., Feger, R. & Mannel, T. Complete Michel Parameter Analysis of inclusive semileptonic $b \to c$ transition. *Phys. Rev. D* **79,** 075015. arXiv: 0803.3561 [hep-ph] (2009).

138. Grinstein, B. & Kobach, A. Model-Independent Extraction of $|V_{cb}|$ from $\bar{B} \to D^* \ell \overline{\nu}$. *Phys. Lett. B* **771,** 359–364. arXiv: 1703.08170 [hep-ph] (2017).

139. Mahajan, N. & Mishra, D. $B \to X_u \ell \nu_\ell \gamma$ and determination of non-perturbative parameters. arXiv: 2303.17372 [hep-ph] (Mar. 2023).

140. Bigi, I. I. Y., Shifman, M. A., Uraltsev, N. G. & Vainshtein, A. I. On the motion of heavy quarks inside hadrons: Universal distributions and inclusive decays. *Int. J. Mod. Phys. A* **9,** 2467–2504. arXiv: hep-ph/9312359 (1994).

141. Eichten, E. & Hill, B. R. An Effective Field Theory for the Calculation of Matrix Elements Involving Heavy Quarks. *Phys. Lett. B* **234,** 511–516 (1990).

142. Khoze, V. A., Shifman, M. A., Uraltsev, N. G. & Voloshin, M. B. On Inclusive Hadronic Widths of Beautiful Particles. *Sov. J. Nucl. Phys.* **46,** 112 (1987).

143. Georgi, H. An Effective Field Theory for Heavy Quarks at Low-energies. *Phys. Lett. B* **240,** 447–450 (1990).

144. Neubert, M. Heavy quark symmetry. *Phys. Rept.* **245,** 259–396. arXiv: hep-ph/9306320 (1994).

145. Bagan, E., Ball, P., Braun, V. M. & Dosch, H. G. QCD sum rules in the effective heavy quark theory. *Phys. Lett. B* **278,** 457–464 (1992).

146. Neubert, M. Symmetry breaking corrections to meson decay constants in the heavy quark effective theory. *Phys. Rev. D* **46,** 1076–1087 (1992).

147. Ball, P. & Braun, V. M. Next-to-leading order corrections to meson masses in the heavy quark effective theory. *Phys. Rev. D* **49,** 2472–2489. arXiv: hep-ph/9307291 (1994).

148. Ligeti, Z. & Nir, Y. Phenomenological constraints on anti-Lambda and lambda(1). *Phys. Rev. D* **49,** R4331–R4334. arXiv: hep-ph/9401246 (1994).

149. Kapustin, A. & Ligeti, Z. Moments of the photon spectrum in the inclusive B —> X(s) gamma decay. *Phys. Lett. B* **355,** 318–324. arXiv: hep-ph/9506201 (1995).

150. Gremm, M. & Kapustin, A. Order 1/m(b)**3 corrections to B –> X(c) lepton anti-neutrino decay and their implication for the measurement of Lambda-bar and lambda(1). *Phys. Rev. D* **55,** 6924–6932. arXiv: hep-ph/9603448 (1997).

151. Gremm, M., Kapustin, A., Ligeti, Z. & Wise, M. B. Implications of the B –> X lepton anti-lepton-neutrino lepton spectrum for heavy quark theory. *Phys. Rev. Lett.* **77,** 20–23. arXiv: hep-ph/9603314 (1996).

152. Aoki, S. *et al.* Heavy quark expansion parameters from lattice NRQCD. *Phys. Rev. D* **69,** 094512. arXiv: hep-lat/0305024 (2004).

153. Abdallah, J. *et al.* Determination of heavy quark non-perturbative parameters from spectral moments in semileptonic B decays. *Eur. Phys. J. C* **45,** 35–59. arXiv: hep-ex/0510024 (2006).

154. Kagan, A. L. & Neubert, M. QCD anatomy of B —> X(s gamma) decays. *Eur. Phys. J. C* **7,** 5–27. arXiv: hep-ph/9805303 (1999).

155. De Fazio, F. & Neubert, M. B —> X(u) lepton anti-neutrino lepton decay distributions to order alpha(s). *JHEP* **06,** 017. arXiv: hep-ph/9905351 (1999).

156. Alonso, R., Grinstein, B. & Martin Camalich, J. Lifetime of B_c^- Constrains Explanations for Anomalies in $B \to D^{(*)}\tau\nu$. *Phys. Rev. Lett.* **118,** 081802. arXiv: 1611.06676 [hep-ph] (2017).

157. Bagan, E., Lavelle, M. & McMullan, D. Charges from dressed matter: Construction. *Annals Phys.* **282,** 471–502. arXiv: hep-ph/9909257 (2000).

158. Bagan, E., Lavelle, M. & McMullan, D. Charges from dressed matter: Physics and renormalization. *Annals Phys.* **282,** 503–540. arXiv: hep-ph/9909262 (2000).

159. Alonso, R., Jenkins, E. E. & Manohar, A. V. Geometry of the Scalar Sector. *JHEP* **08,** 101. arXiv: 1605.03602 [hep-ph] (2016).

160. Helset, A., Jenkins, E. E. & Manohar, A. V. Geometry in scattering amplitudes. *Phys. Rev. D* **106,** 116018. arXiv: 2210.08000 [hep-ph] (2022).

161. Helset, A., Jenkins, E. E. & Manohar, A. V. Renormalization of the Standard Model Effective Field Theory from geometry. *JHEP* **02,** 063. arXiv: 2212.03253 [hep-ph] (2023).

162. Ginsberg, E. S. Radiative corrections to the k-l-3 +- dalitz plot. *Phys. Rev.* **162.** [Erratum: Phys.Rev. 187, 2280 (1969)], 1570 (1967).